SAPIENZA
UNIVERSITÀ DI ROMA

Facoltà di Scienze Matematiche, Fisiche e Naturali

Philosophy degree in Earth Science

Curriculum in Applied Sciences for the Protection of the Enviroment and Cultural Heritage
XXVIII Cycle

In situ analysis of white marble from the Mediterranean Basin by LA-ICP-MS: inferences on provenace based on trace-element profiles

Giulia PORETTI

Tutor: Dr. Caterina DE VITO

Co-Tutors: Dr. Aida M. CONTE, Prof. Alessandro BORGHI

Referees: Dr. Robert F. Martin, Dr. Pilar LAPUENTE

Ph.D Coordinator: Dr. Giovanni B. ANDREOZZI

To my beautiful family

Table of content

Introduction and Aims

White marble is a carbonate dominant metamorphic crystalline rock used for more than 5000 years (late Neolithic – Cycladic civilizations) for statuary and architectural elements. The remarkable value taken on during the history is proved by the large and continuous use of this rock in the ancient societies.

So far, numerous studies have set out to determine the provenance of white marble exploited from the main quarrying sites of the Mediterranean basins. These studies led a large number of data, which are partial and not always satisfactory from a scientific point of view.

Actually, white marble of archeometric interest is largely characterized through minero-petrographic studies and isotopic signatures, primarily carbon, oxygen and strontium.

A complete description of the geochemical composition, aimed at an exhaustive provenance study, is still missing.

The application of the Laser Ablation Inductively Coupled Plasma Mass Spectrometry (LA-ICP-MS) permits the measurement of a large number of trace elements. The scope is to improve the limited existing database on the trace-element profile of white marble.

The comparison of the concentration of these elements among different quarrying districts aims to identify geochemical markers as fingerprints of several white marble sites.

With these assumptions, one can start to go deeper into the problem, surveying all the bibliography, the state of the art and general knowledge about this rock, *i.e.,* its history, geology, geochemistry and archaeometry.

The specimens considered come from a collection of white marbles chips, collected from the past sampling campaigns of La Sapienza University of Rome and IGAG-CNR of Rome, and largely analyzed by

means of several analytical techniques in previous research works (*i.e.,* stable isotope concentrations, EPR intensities, petrographic observations).

The sampling is composed of about 120 white marble samples from nine different quarrying areas (*i.e.,* Carrara, Paros, Penteli, Afyon, Göktepe, Naxos, Thasos, Thiountas and Proconnesos) and eight archeological samples of known attribution to test the feasibility of the method.

This Ph.D. thesis is based on a multi-analytical approach and it can be divided in two phases. The first one consists of a systematic minero-petrographic characterization of a selection of the geological white marbles of known provenances, in order to identify the occurrence of minero-chemical markers discriminating different quarrying districts.

The second step provided analyses on rock samples from different quarries of the Mediterranean area and archeological samples from the Casa di Augusto (Palatine Hill) and Musei Capitolini collection by means the LA-ICP-MS. The analyses have been conducted at the Laboratory of Inorganic Chemistry of Eidgenössische Technische Hochschule (ETH) of Zurich and at the laboratory of CNR-Istituto di Geoscienze e Georisorse, U.O.S. of Pavia.

The goal of this study is to fulfill a database, gathering the more significant features of the proposed minero-petrographic and geochemical markers. The multidisciplinary collaboration among the different competences (geologists, chemists, conservation scientists) is fundamental to carry out this study, and this mutual collaboration is an integral part of the present Ph.D. thesis.

Going in more detail into the structure of the work, the present thesis provides: 1) an overview on the use of white marble throughout the centuries and civilizations, and the state of the art about previous studies of provenance focused on white marble; 2) the description of

the geological settings of the areas where the white marble considered were sampled, presenting also the history of the main quarries; 3) a brief description of the geological samples here analyzed and the experimental setup employed; 4) the results on the quarried samples; 5-6) a discussion and conclusion, with some proposals for future improvements. Finally, in the Appendix are presented the geochemical results of archeological samples.

Chapter 1

Provenance study of white marble

1. Provenance study of white marble

The study of different geo-materials used in the past represents one of the main issues in the field of cultural heritage and archaeometry, as the data can be useful for provenance attribution of an artifact.

The investigation of the ancient exchange systems is a major topic of archaeological research, since the reconstruction of trade is important for understanding economic aspects of societies and for the political systems, and for identifying the quarrying areas of the raw materials. In addition, scientific studies contribute to the identification of copies, forgeries and later restorations, and they are necessary pre-requisites in the planning of conservation and restoration works.

In this view, over the past 40 years, improvements in instrumentation in sample handling, precision and accuracy, along with advances in data reduction, involved a large number of analytical methods, which were successfully employed in archeological provenance studies of different materials. A brief review dealing with the main analytical methods and applications to archeological provenance studies was carried out by Tykot (2004). In Table 1.1 are reported the archeological materials which have been the subject of provenance studies by the scientific community.

The study of white marble and the identification of its quarry site are of great importance to scientists, archaeologists and art historians, and an in-depth scientific knowledge of the properties and provenance of marbles has become a fundamental tool to discriminate among materials (Attanasio *et al.*, 2006). The main reasons why marble arouses such interest are undoubtedly its wide application in artistic, sculptural and architectural work all over the history of Mediterranean, and its remarkable quality.

Tab. 1.1: Archaeological materials used for provenance studies (Tykot, 2004).

Lithic	Ceramic	Metal	Glass	Others
Alabaster	Pottery	Copper	Faiance	Amber
Basalt, granite, rhyolite	Other clay objects	Copper alloys	Glass	Horn
Greenstone (jadeite -nephrite)		Gold		Bitumen
Hematite-magnetite		Lead		Bone
Limestone-marble		Silver		Ivory
Obsidian				
Sandstone-quartzite				
Schist				
Soapstone (steatite - chlorite)				
Turquoise				

This “noble rock” was mostly exploited in the Graeco-Roman world, where extensive usage of marble is commonly associated with classical antiquity. Marble masterpieces are known from Greek temples, busts of Roman noblemen, and baroque figures to modern façade material (Attanasio *et al.,* 2006).

For many thousands of years, both white and colored marbles have been considered the noble material par excellence of plastic art and architecture. Marble has been highly prized materials in the arts also in other historical periods, the Italian Renaissance being the most celebrated example.

The multitude of raw material and the various techniques of creation raise several questions concerning the analysis, provenance, and restoration of the objects. Interest in the field has extended far beyond the pure art historical and stylistic approach to the artworks

and now involves a number of different aspects of marbles (Attanasio, 2003).

The provenance of marble represents an interesting issue with still some unresolved aspects, both from historical/archaeological and scientific points of view.

In the last decades, many scholars have attempted to perform provenance studies of white marble for different purposes and with different approaches.

Nevertheless, a systematic and exhaustive study of provenance of the raw material utilized for artworks or archaeological artifacts realization was still lacking. The reason may be attributed to several problems of different nature, primarily, the difficulty to collect geo-referenced rock samples, especially due to the variability within the quarrying areas. Moreover, in some cases there is a lack of precise geographical information for many specimens, or missing information about sites exploited in the past and nowadays abandoned. The last reason, possibly the most important, is the overlapping results due to the growing sets of databases.

1.1 State of Art

Scholars of different disciplines have been trying for more than a century to study of marble from various quarrying sites using optical microscopy, with moderately positive results.

Until almost the end of the nineteenth century, historical sources, stylistic analysis and macroscopic examination of materials were the principal means of identification.

The determination of provenance is more difficult and uncertain for white marble than colored marble, even with the use of much more sophisticated techniques. The problem is further complicated by the fact that not all ancient quarries have been brought to light, and the

origin of many materials, even those that are well known and frequently used, is still a mystery.

The German geologist Lepsius attempted the first scientific approach, exploring macro and microscopic features of white marble. He developed the first scientifically correct approach that can be defined as archaeometric in the strict modern sense of term, introducing the methods of petrography and in particular the microscopic study of thin sections. Lepsius published a treatise called *Griechische Marmor studien* that contains a description of marbles from various quarries in the Aegean (Lepsius, 1890). He based these descriptions on visual inspection of hand samples (color, smell of newly broken surface, degree of crystallization, etc.) and on petrographic analyses of thin sections under polarized light. The result was the provenance assignment of several important archaic sculptures in Athens with appreciable confidence.

Although petrographic analysis was the only method utilized for many years and it remains important today, a few of Lepsius's assignments are questionable or even incorrect. For instance, the American geologist Washington pointed out in 1898 several cases in which artifacts were attributed to two different and contradictory provenances in equally positive terms (Washington, 1898).

The limit of petrographic analysis and the need to support it with other analytical techniques led the scientific community to test new approaches. The first half of the twentieth century was gradually accompanied by the use of X-ray powder diffraction (XRPD), which permits the identification of mineral phases, and by spectroscopic techniques (XRF, OES, AAS, NAA) for the quantification of major and trace elements. However, no single analytical technique has proved to be conclusive if used alone, and multi-method approaches, using sequentially or simultaneously variables from several techniques, are currently considered to be the only possible way for the reliably

determining of the provenance of unknown samples (Herz and Garrison, 1998; Attanasio *et al.*, 2006).

In the early 1970s, analysis of stable isotopes of carbon and oxygen and petrographic characterization were proposed as the most powerful exhaustive approach (Craig and Craig, 1972). The isotopic compositions of carbon and oxygen measured in white marble samples from four different quarrying areas of Greece (Naxos, Paros, Mt. Pentelicon and Mt. Hymettos) were found to be remarkably different. The initial results were very promising, and encouraged many other researchers to take the same route. Over the following years, the first database was developed and detailed by Manfra *et al.* (1975), organically implemented by Herz (1987b; 1988a) and then critically evaluated by Germann *et al.* (1988). About the same time, the most important subsequent contribution was a more detailed investigation of the Carrara and Seravezza marbles (Herz and Dean, 1986). These authors also noticed the possibility of distinguishing the two sites based on isotopic data, whereas intra-site discrimination was found to be difficult.

After the above-mentioned studies, the isotopic references on marbles have been enlarged and updated several times. Moens *et al.* (1988, 1992) published a comprehensive account; they substantially implemented both the petrographic and isotopic data, producing excellent reference diagrams widely used by archaeometrists (Fig. 1.1). More recently Gorgoni *et al.* (2002) published an extensive diagram of the Greek quarries (Fig.1.2), whereas Zöldföldi and Satır (2003), Zöldföldi and Székely (2003; 2004b; 2005a; 2005b) documented the white marble quarries in Anatolia.

The increase in the number of analyzed samples from the various sites and the growing number of data collected, plotted on the usual $\delta^{18}O$ *versus* $\delta^{13}C$ diagram, gave progressively a more confused

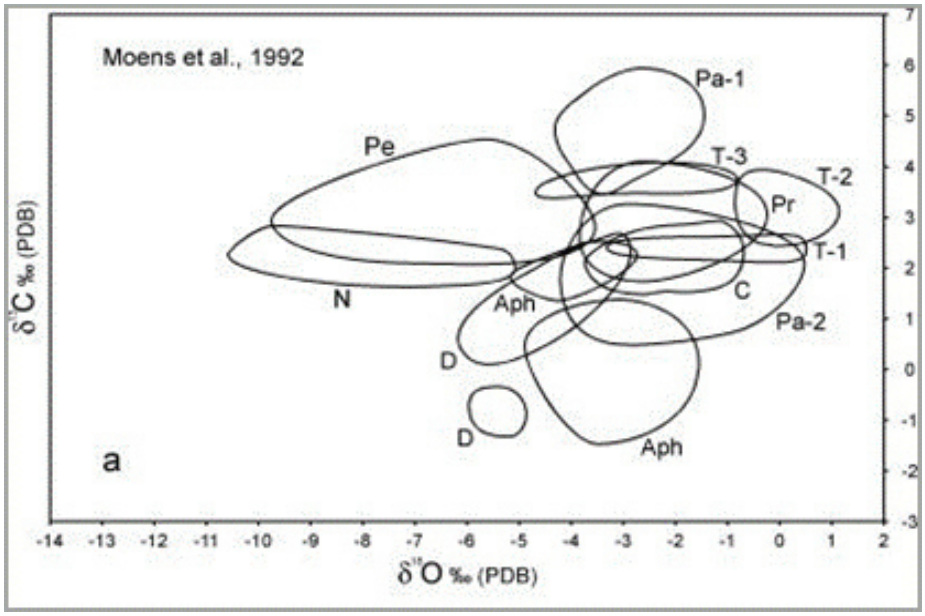

Fig. 1.1: The former isotopic reference diagram by Moens *et al.*, 1992. Legend: Aphrodisias (Aph), Carrara (C), Docimium (D), Naxos (N), Paros (Pa), Penteli (Pe), Proconnesos (Pr), Thasos (T).

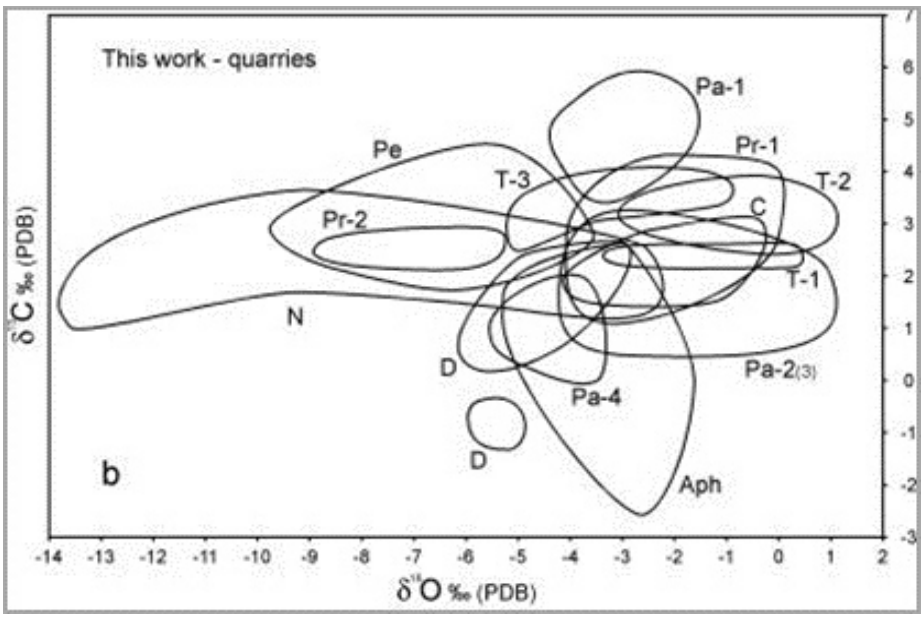

Fig. 1.2: The proposed graph result from the processing of isotopic data by Gorgoni *et al.*, 2002 and Moens *et al.*, 1992 for quarry outcrops. Legend: Aphrodisias (Aph), Carrara (C), Docimium (D), Naxos (N), Paros (Pa), Penteli (Pe), Proconnesos (Pr), Thasos (T).

framework for the growing database. The major problem of the growing number of samples led to frequent cases of the phenomenon of overlapping among different quarries, also placed in separate regions and far from each other.

For these reasons, in the last twenty years, isotopic methods have been accompanied by the use of electron, electron paramagnetic resonance spectroscopy (EPR or ESR), cathodoluminescence (CL), laser reflectance and quantitative analysis of texture.

Another early multi-disciplinary contribution, involving a combination of petrographic characteristics (average grain-size, type of crystal shape and structure, semiquantitative assessment of accessory minerals) and the determination of the Ca/Sr ratio (Chilingar *et al.*, 1967) was proposed by Lazzarini *et al.* (1980a; 1980b). Actually, temperature controls the Ca/Sr ratio, which remains unaltered in marbles (metamorphism being an essentially isochemical process) so this datum can be useful in estimating the thermic level reached by these rocks. It has been observed, in fact, that strontium levels vary considerably in some of the most important marbles of antiquity, and this has led to the attribution of provenance of numerous artefacts (Lazzarini *et al.*, 1980a; 1980b).

Finally, in 1989, Barbin and others (Barbin *et al.*, 1989; 1991; 1992) proposed the use of cathodoluminescence, with the petrographic study of the same thin section; this led to the determination of accurate cathodomicrofacies of the main marbles of antiquity. The cathodoluminescence of these stones is linked to the presence of traces of Mn^{2+}, which enhance it, and of Fe^{2+}, which reduces it. Calcite shows orange or blue luminescence, whereas the color of dolomite is red. The intensity and the distribution of these luminescences are additional parameters that can be useful to distinguish different sources of marbles (Fig. 1.3). The use of cathodoluminescence was applied in monographic studies of

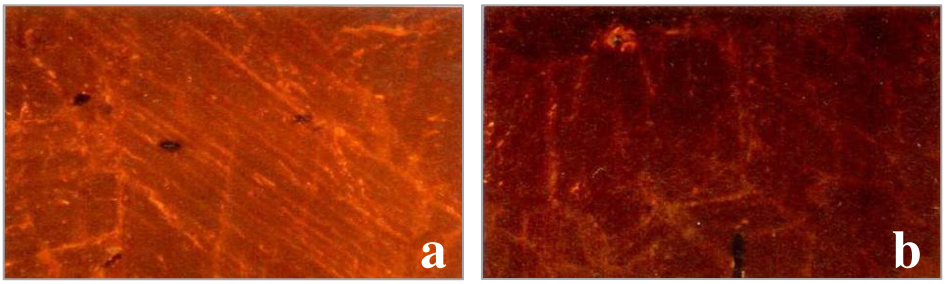

Fig.1.3: Paros-Chorodaky (Paros-2) marble with orange luminescence (a) Thassos-Aliki with orange luminescence (b). Paros marble shows a weaker luminescence than Thassos-Aliki marble. Ancient quarries have been investigated by means of cathodoluminescence (Barbin *et al.*, 1992).

important marbles, including those from Luni, *i.e.,* Carrara marble, from the Cyclades Islands, Turkey (*e.g.,* Barbin *et al.,* 1989; 1991; 1992), and marbles from Roman Hispania (Lapuente *et al.,* 2000), all of which still provide substantial help to archaeometric scientists.

An important contribution was made by Cordischi and his co-authors (Cordischi *et al.*, 1983), with the proposal to use electronic spin resonance (ESR) for traces of Mn in marbles. As the method was applied to an increasing number of marbles, the initial encouraging results were placed in another perspective by the overlapping of representative fields of isotopic data and data from other techniques (Lloyd *et al.*, 1988; Maniatis *et al.,* 1988).

Data on Electron Paramagnetic Resonance spectroscopy (EPR or ESR) allowed one to build new databases for white marbles. In the field of marble provenance, the EPR spectroscopy detects, among others, the Mn^{2+} impurity ubiquitously present in marbles.

Later, some of the most important Greek, Turkish and Italian historical quarrying sites have been studied by Armiento *et al.* (1997) and by Attanasio (1999; Attanasio *et al.,* 1999). Since then, numerous contributions have been published (*e.g.,* Maniatis and Polikreti 1998, Attanasio and Platania, 2000; 2003), but the use of EPR spectroscopy has remained relatively limited. This is partly due to the intrinsic characteristics of the method, which is not particularly suited for

quantitative determinations, and the lack of generally accepted standards for both signal, intensity and magnetic field strength. In any case, the amount of information that EPR spectroscopy provides on marble is remarkable, and since its first introduction, the database has been considerably enlarged and updated. New samples have been collected and analyzed and new, more suitable, procedures of standardization have been adopted. Furthermore, the analytical procedure has been modified and improved, particularly in the case of the petrographic or morphological variables, which were previously estimated on a qualitative basis and given as categorical variables (Attanasio *et al.*, 1999; Attanasio, 1999). The classification, based on discrimination function analysis and taking into account the new experimental results, has been optimized and validated using standard statistical techniques, as well as a set of test samples. This last point, *i.e.* the validation step, is particularly important in the development of a reliable method of classification depending upon the ability to estimate realistically its error bar.

Extension of the database to other techniques was introduced by Attanasio, where morphological variables have been included. Based on the above outline, Attanasio created an updated account of the EPR and petrographic marble database, covering all aspects of the data collected, and where it became clear that the multi-method approach is the only way forward (Attanasio, 2003). All previous studies revealed that no single analytical technique is capable of resolving the problems of provenance; frequently one of the previous reported techniques, although extremely sophisticated, will produce data that does not discriminate some of the possible provenance sites, which are instead easily distinguished by using different techniques, and vice versa. It is commonly agreed that an approach that integrates two or three different methods and measures is necessary to determine reliable attribution of provenance.

Considerable interest has been aroused by the determination of rare earths (Barbin *et al.*, 1991) carried out with various methods including NAA (*e.g.,* Meloni *et al.*, 1995), and the new Inductively Coupled Plasma-Mass Spectrometry (ICP-MS) (Green *et al.*, 2002). In agreement with Matthews (Matthews *et al.,* 1995; Matthews, 1997) and Green *et al.* (2002) the creation of a data bank for REE would be immensely useful.

With laser ablation inductively coupled plasma-mass spectrometry (LAICP-MS) have been able to determine the concentrations of trace elements, especially rare earths, of 24 samples of marble from different sites of the island of Naxos Ebert *et al.* (2010) (Fig. 1.4).

Because of the detection limits, even lower than the concentrations of the trace elements, this technique has made possible the acquisition of analytical data essential to discriminate among different mining sites and among different quarries of the same site.

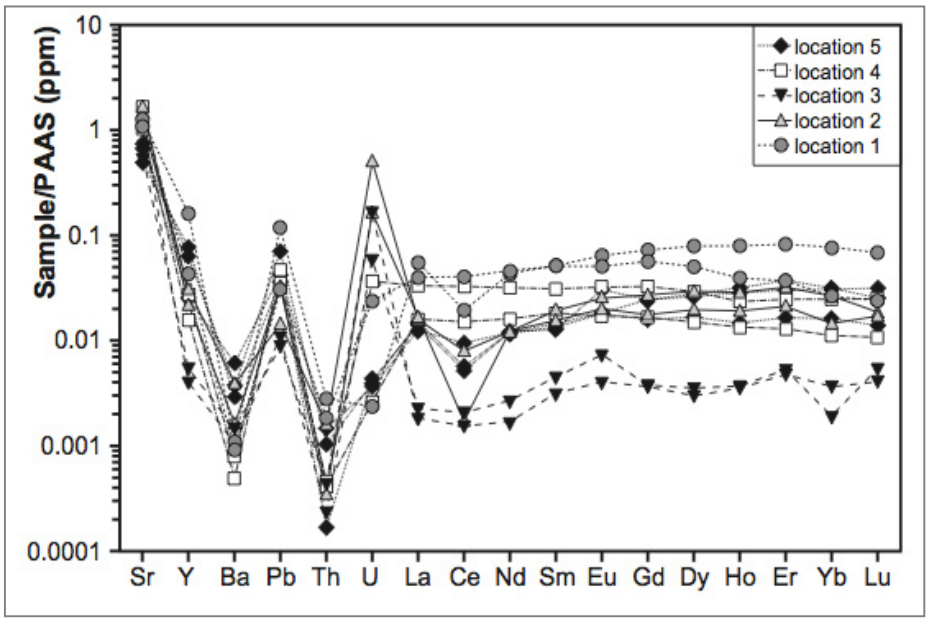

Fig.1.4: Patterns of trace element enrichment or depletion in calcite marbles from Naxos. The authors considered five different locations (displayed using differing symbols) along the central profile on Naxos. The concentrations are normalized to PAAS (Post-Archean Australian Shale) (Ebert *et al.*, 2010).

Finally, recent studies on the Turkish white marble of Göktepe highlighted a new problem (Attanasio *et al.*, 2015). The isotope values in this marble are very similar to those of white Carrara marble and show petrographic characteristics typical of fine-grained white marble (Fig. 1.5). The authors stated that the marble Göktepe can be distinguished from other white fine grain marbles only through comparison of the concentrations of trace elements, particularly those elements that replace the calcium in the lattice of calcite (Mn, Sr) (Attanasio *et al.,* 2015).

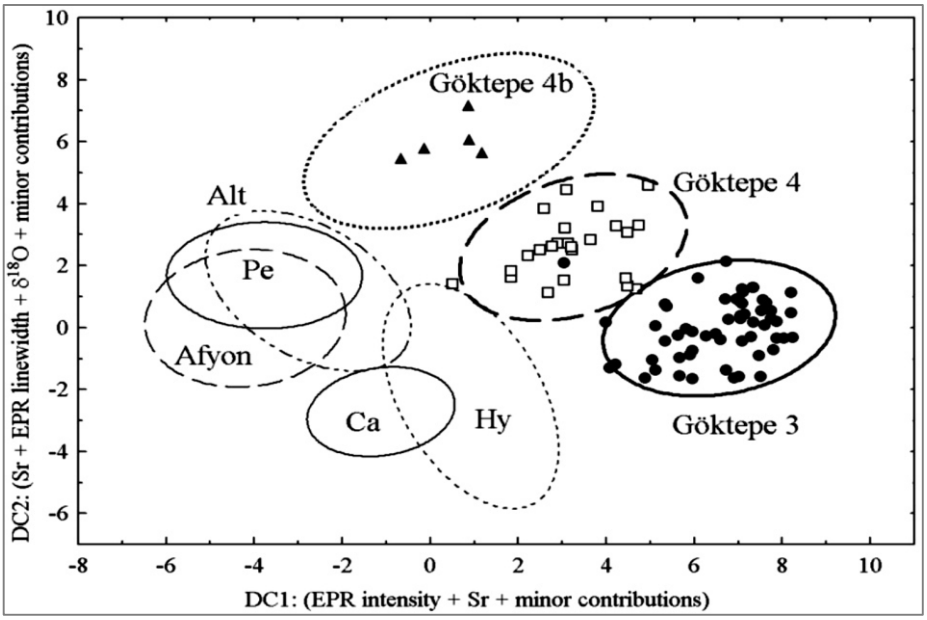

Fig. 1.5: A statistical graph of the database of fine-grained white marbles. The white Göktepe marbles fall completely outside of the region spanned by other fine-grained varieties and therefore can be identified (Attansio *et al.*, 2015).

Chapter 2

Geographical and Geological Setting

2.1 The properties and geology of marbles

The etymologic origin of the word marble derives from the ancient Greek language, its root deriving from the verb marmairo that means "*to shine*".

Petrographically the term marble has a precise and more restricted meaning: it is an originally calcareous rock that has undergone physico-chemical transformation processes referred to as metamorphism, which impart a characteristic "*saccharoidal*" texture.
Marble is the product of metamorphism of carbonate rocks. Its primary constituent is calcite ($CaCO_3$) or dolomite ($CaMg(CO_3)_2$), although many other minerals in various percentages may be present as accessory minerals, deriving from reactions of the free compounds of carbonate with those of silicates.
The project deals with a specific category of marbles, grouped under the name of *white marbles*; they are crystalline homogeneous carbonate-dominant rocks consisting almost exclusively of calcite or dolomite. The carbonate content is at least 95%, and they are therefore classified as "*pure*". Calcite is susceptible to extensive textural changes due to recrystallization. Consequently, under most environmental conditions, it undergoes only textural readjustments following solid-state re-crystallization. The metamorphism of carbonate rocks is probably an isochemical process, which takes place without any significant modifications to their chemical composition. In order to characterize and distinguish these marbles, so similar among the different quarry sites, it is necessary to have an in-depth knowledge of the geochemical properties of the specimens. Not less important are their mode of formation and the geological setting of the quarrying areas. In this context, in the following chapter, a brief description of the geographical and geological settings will be presented.

2.2 Carrara

The marbles from the Alpi Apuane, and in particular the white variety called *Carrara marble* or *Lunense marble*, are well known geological materials owing to their extensive use both as building stones and statuaries (Rutter, 1972; Casey *et al.*, 1978; Spiers, 1979; Schmid *et al.*, 1980; Schmid *et al.*, 1987; Wenk *et al.*, 1987; Fredrich *et al.*, 1989; De Bresser, 1991; Rutter, 1995; Covey-Crump, 1997). In this thesis, "Alpi Apuane marbles" indicates the Liassic marble formation cropping out in the whole Alpi Apuane area, whereas "Carrara marble" stands for metamorphic rocks exposed in the northwestern Alpi Apuane tectonic window in northern Tuscany, Italy (Fig. 2.2.1). Carrara marbles are the most intensely quarried variety of marble within the entire Alpi Apuane (Molli *et al.*, 2000).

Apuan marbles are the product of a regional metamorphic event developed under greenschist-facies conditions of originally carbonate rocks deposited in a shelf environment during Rhaetian-Liassic times (Cantisani *et al.,* 2005). Carrara marbles are part of the lower to middle Liassic carbonate platform sequence of the former Italo-Adriatic continental margin, which was deformed and metamorphosed during the Apennine orogeny (Oesterling *et al.,* 2007) (Fig. 2.2.1).

The type of sedimentation can be subdivided in two main phases: a Noric-Rhaetian phase corresponding to the shelf of the Grezzoni Formation, and a second Rhaetian Hettangian, corresponding to the carbonatic shelf, which then produced the marbles. These two phases are separated by a phase of sedimentation set in the late Rhaetian, characterized by deep climatic changes, representative of the passage from an environment of low depth to a notably deeper environment well distinguished in the area of Orto di Mt. Donna, Mt. Altissimo, M.te Corchia (Coli and Fazzuoli, 1992).

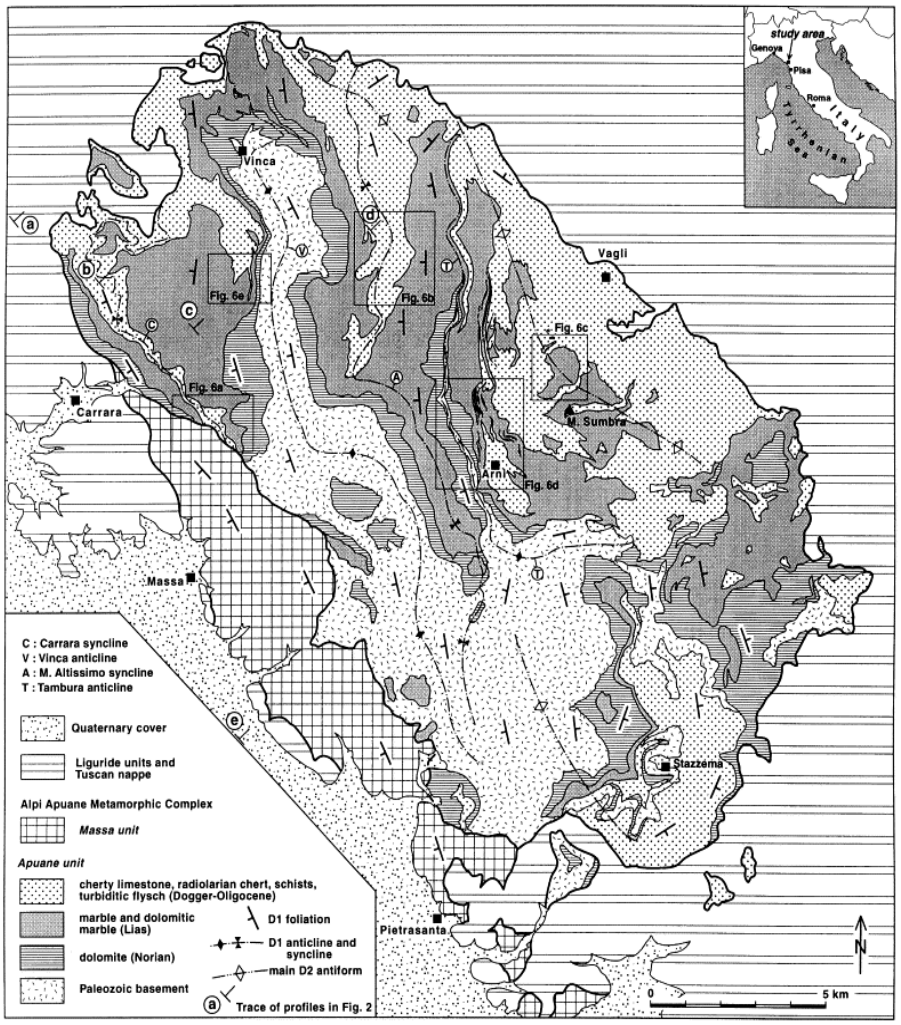

Fig. 2.2.1: Structural map of the Alpi Apuane area (Molli *et al.*, 2000).

Between late Rhaetian and Hettangian, the base of the «marbles carbonate shelf» develops covering the underlying breccias. The sedimentary basin successively becomes deeper and more differentiated. A fracture of the carbonatic shelf develops giving rise to isopic zones (Coli and Fazzuoli, 1992).

The Apuan marbles are involved in the main tectono-metamorphic events that affected the Massa and Apuane units. Starting from the Upper Oligocene, after the deposition of Pseudomacigno sandstones,

two main polyphase tectono-metamorphic events can be recognised: the main deformation event (D1) started in Late Oligocene times as part of a crustal shortening regime, dated with the K/Ar and the $^{40}Ar/^{39}Ar$ methods at 27 Ma (Giglia and Radicati di Brozolo, 1970; Kligfield *et al.*, 1986). It gave rise to kilometer-scale isoclinal folds, antiformal stack development and shear-zone formation. The second event (D2) began in the Early Miocene (12-14 Ma) as the result of crustal extension (Kligfield *et al.*, 1986) dated at 10-8 Ma. It deforms all earlier features, developing folds and shear zones (Carmignani *et al.*, 1980; Carmignani and Kligfield, 1990; Molli *et al.*, 2000). The interference between D1 and D2 events produces complex deformative structures, also recumbent folds of kilometric extension.

During the early stage of D1, regional-scale isoclinal folds were generated with inclined axial planes dipping to the SW (Fig. 2.2.2). Folding terminated in conjunction with a thermal event that caused an annealing of all dynamic microstructures. During the latter part of the D1 history, deformation was localized in discrete shear zones which overprinted the annealed microstructures (Molli *et al.*, 2000). The nappe stacking at the end of the first deformation event produced an antiformal stack geometry. The nappe stack was deformed during D2, when open folds with sub horizontal axial planes and microscale shear zones developed (Fig. 2.2.2). Folding is restricted to lithologically heterogeneous sequences such as the middle to upper Liassic cherty limestone, which is composed of alternating layers of quartzite and impure limestone. Small-scale shear zones occur mainly in the pure and homogeneous calcite marble (Carrara marble). Vergence of minor folds as well as the shear sense indicators is directed top to the SW on the SW-side of the culmination of the Alpi Apuane and top to the NE on the NE-side of the culmination (Oesterling *et al.*, 2007).

As regards the metamorphic grade, it is necessary to consider the presence, in the Apuan massif, of a metamorphic polyphasic and

syntectonic evolution marked by mineralogical associations typical of the chlorite-biotite zone of the greenschist facies (Barberi and Giglia, 1965). The occurrence of the stable association pyrophillite + quartz (Franceschelli *et al.*, 1986; 1997) indicates temperatures of 300-400° C and pressures of 3-4 kbars. The application of the calcite-dolomite geothermometer allowed to obtain different temperatures in the various zones (Di Pisa *et al.*, 1985). The marbles of the western zone display a wide range of $MgCO_3$ that corresponds to temperatures in the range 420-460 °C, those of the eastern zone show temperatures in the range 310-380 °C, whereas those of the central zone display intermediate temperatures. These variations point to an increase of the metamorphic grade inside the Apuan metamorphic complex proceeding from East toward West. The last studies related to the microstructural characteristics allow one to distinguish marbles produced according to processes of static recrystallisation, dynamic recrystallisation and remobilisation during the last stage of deformation (Molli *et al.*, 1997; Molli and Giorgetti, 1999; Molli and Heilbronner, 1999; Molli *et al.*, 2000).

Marbles with an equigranular polygonal microstructure (granoblastic or «foam» microstructure), and straight to slightly curved grain boundaries belong to the first group.

Marbles with this microstructure were found in the Western part, Middle and Eastern zone of the Apuane, with a characteristic variation of the grain size from one zone to another (250-300 μm in the western side, 80-100 μm in the eastern side). These marbles were produced during the thermal relaxation and heating realized after early D1 deformation (Cantisani *et al.,* 2005).

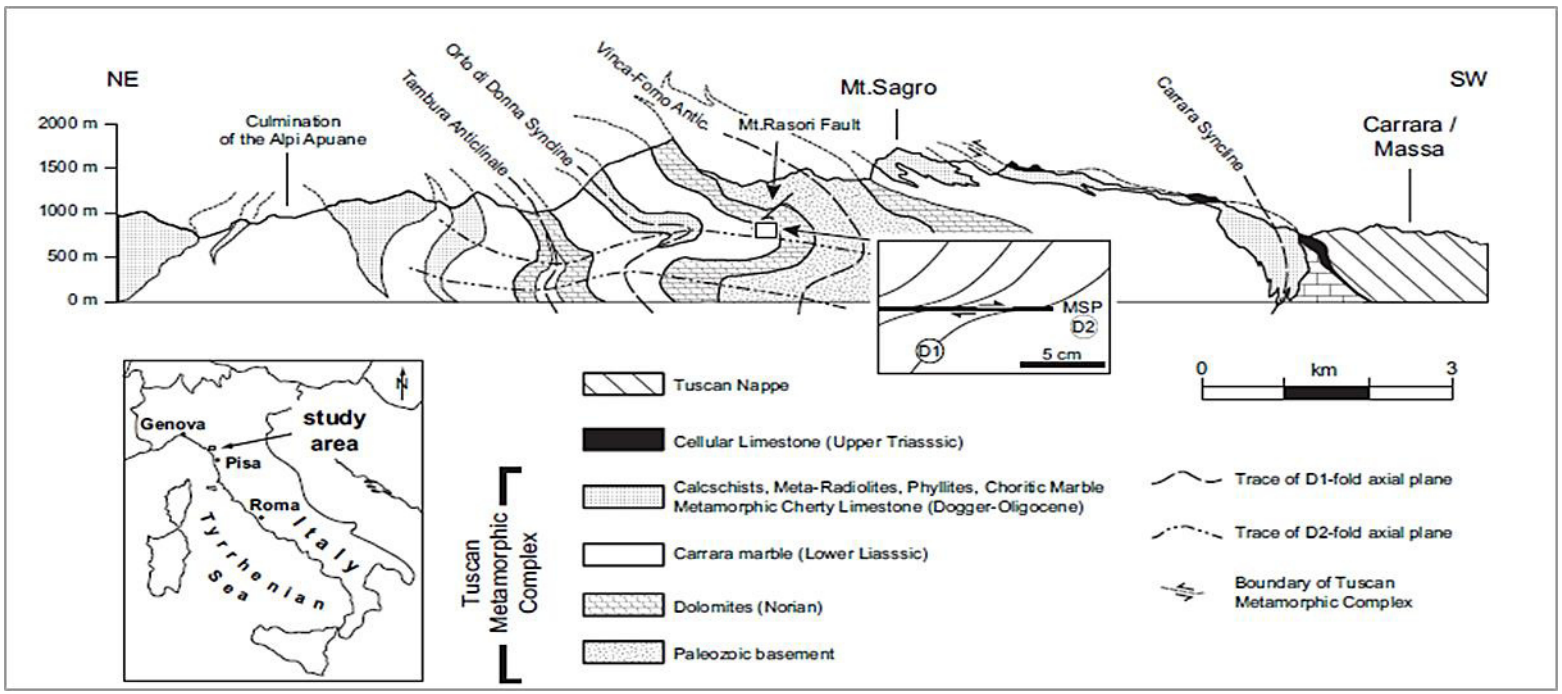

Fig. 2.2.2: Schematic geological cross-section and stratigraphic section of the Alpi Apuane tectonic window (modified after Carmignani and Giglia, 1978). The sample location is marked by the rectangular box. The details in the box show the orientation of the median shear plane (MSP) of the D2 shear zone and the S1 layering. Note that the section is oriented with NE at the left.

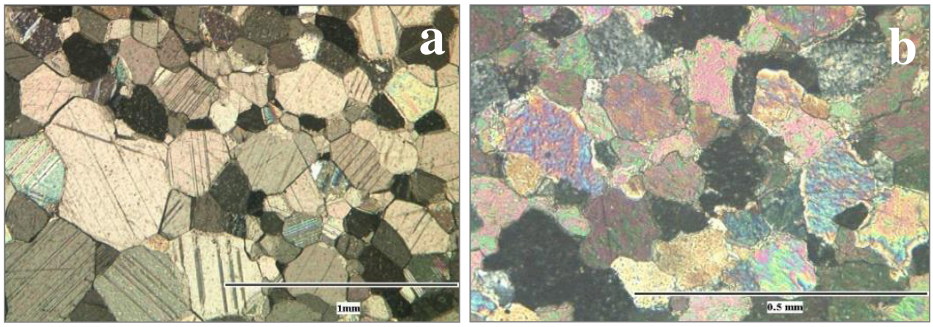

Fig. 2.2.3: a) Thin section of granoblastic marble that underwent annealing, or a late static recrystallization during stage of thermal relaxation; b) xenoblastic marbles underwent a dynamic synkinematic recrystallization. (Molli and Giorgetti, 1999).

Marbles with microstructure exhibiting strong shape-preferred orientation, coarse grains with lobate/sutured boundaries, formed during the late stage of D1 event, are considered products of the dynamic recrystallization. Also, microstructures formed during the D2 event with shape-preferred orientation, polymodal grain-size distribution, smaller grain-size (the crystals that are the relics of the preceding microstructure show a mean grain size between 150 and 200 μm, whereas those formed during the recrystallization have dimensions of 20-50 μm) and rotation of the subgrains are referred to dynamic events. The D2 event is, in fact, associated to an exhumation process in condition of retrograde metamorphism. During this event in the highest Apuan Alps levels, shear zones, millimetric to decimetric thick, develop (Carrara area), whereas in the lowest levels (Ami area), only folding occurs. The dynamic microstructures are related to high strain and high temperature, still in greenschist facies. Grain-boundary migration and recrystallization can be considered predominant in the first one (D1 event), whereas rotation recrystallization and grain-boundary are important migration in the second one (D2 event) (Catisani *et al.*, 2005) (Fig. 2.2.3).

The microstructure characterized by the consistent presence of twinning has been interpreted as produced at low temperatures in the late stage of exhumation of the metamorphic complex. This deformation is found, with different intensity, at all levels of the marble (Molli *et al.*, 2000).

2.3 Cyclades Archipelago

The Cycladic Archipelago lies in the center of the Aegean Sea in an area that is currently seismically stable, whereas the surrounding regions are characterized by an intense and active seismicity (Jackson and McKenzie, 1984; Taymaz *et al.*, 1991) (Fig.2.3.1).

Fig. 2.3.1: Map of Cyclades islands (www.pix-hd.com/gallery/greece).

The complex of the Hellenic Belt was formed by stacking of the upper crustal units within an accretionary wedge with SW-verging thrusts from the Eocene to the Late Miocene in continental Greece (Brunn *et al.,* 1976, Jacobshagen *et al.*, 1978, Bonneau and Kienast, 1982,

Doutsos *et al.*, 1993, Sotiropoulos *et al.*, 2003, Ring *et al.*, 2001, Ring *et al.*, 2007a; 2007b; Vanderhaeghe and Teyssier, 2001; Vanderhaeghe *et al.,* 2007).

After the formation of the Hellenic Belt in the Eocene, the Cycladic Islands rested upon a continental crust that was thinned to 26 km in the Oligocene and the Miocene (Vigner, 2002; Tirel *et al.*, 2004a; 2004b; Karagianni *et al.,* 2005). The Moho discontinuity is rather flat below the whole archipelago, suggesting a low viscosity of the lower crust and a high Moho temperature at the time of extension (Tirel *et al.,* 2004b). Extension started in the Late Oligocene above the subduction zone, mainly as a consequence of slab retreat (Le Pichon and Angelier, 1979; Le Pichon and Angelier, 1981; Jolivet and Faccenna, 2000).

The Cycladic archipelago is presently localized (in the external Hellenic arc, in western Turkey, in southeastern continental Greece, in northern Greece and along the North Aegean trough, which represents the extension of the dextral strike-slip North Anatolian Fault in the Aegean domain (Fig. 2.3.2).

Before the Pliocene, extension was accommodated by a series of detachments, in the footwall of which several metamorphic core complexes were exhumed (Lister *et al.*, 1984, Gautier and Brun, 1994a; 1994b).

In the Aegean Sea, the beginning of slab retreats some 30–35 Ma ago led to post-orogenic extension of the Hellenic thickened crust by a combination of backarc extension and gravitational collapse. Post-orogenic extension reworked the stack of nappes (or thrust sheet is a large sheet like body of rock that has been moved more than 2 km or 5 km above a thrust fault from its original position) and the various nappes were redistributed within the Aegean Sea (Fig. 2.3.2).

The original vertical organization of the stack of nappes was, however, generally preserved, and one can recognize the original superposition of nappes (Bonneau, 1984; Jolivet *et al.,* 2004b).

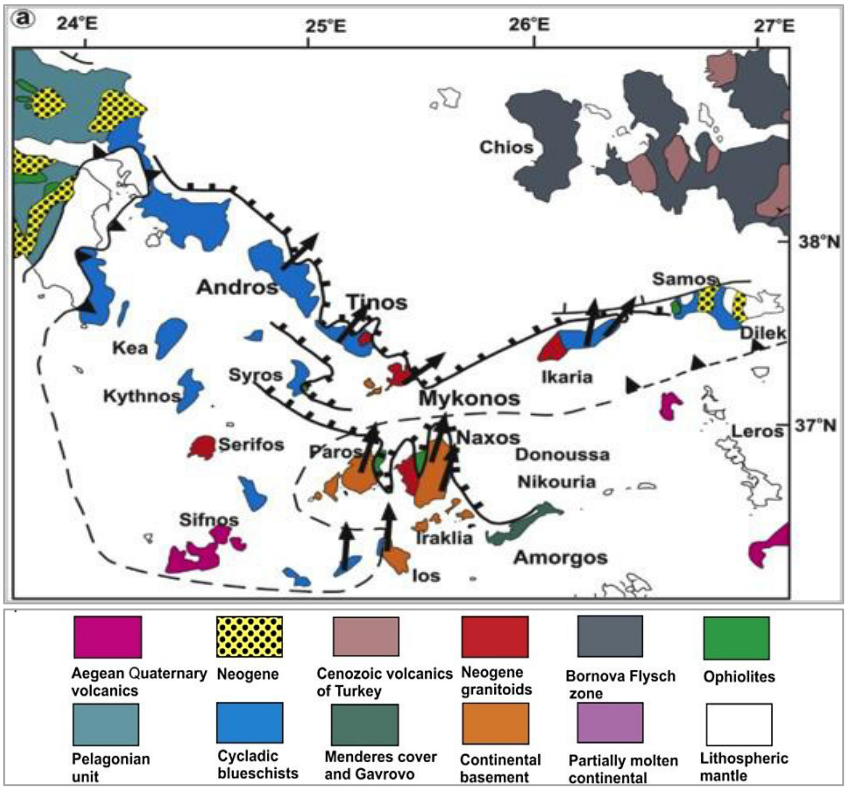

Fig. 2.3.2: Schematic geological map within the context of the North Cycladic Detachment System. The arrows indicate the sense of ductile shear in the lower plate (Jolivet *et al.*, 2010).

From top to bottom, one can recognize the following units:

1) The uppermost unit observed in the Cyclades is the Upper Cycladic Nappe, an equivalent of the Pelagonian nappe in the Hellenides. The Pelagonian nappes are thus found from continental Greece to the Cyclades and as far as Crete at the top of the edifice (Reinecke *et al.*, 1982; Bonneau, 1984; Papanikolaou, 1987).

2) The Upper Cycladic Nappe overlies the Cycladic Blueschists, a composite unit with a significant component of metabasic rocks included in metapelites and marbles (Blake *et al.*, 1981; Avigad and Garfunkel, 1991; Keiter *et al.,* 2004). Ages of the protolith range from the Triassic to the Cretaceous (Bröcker and Pidgeon, 2007). The nappe

is generally considered a lateral equivalent of the Pindos oceanic zone in the Hellenides (Bonneau, 1984). It differs from the Vardar Ocean that was located north of the Pelagonian domain and it is composed of several superposed units, including a mafic olistostrome well exposed on Syros Island (Keiter *et al.*, 2004). The Cycladic Blueschists show a complex metamorphic evolution, with an early burial in high pressure – low temperature (HP-LT) conditions (blueschists and eclogites) during the Eocene, followed by a high temperature – low pressure (HT–LP) overprint during the Oligocene and Miocene (Altherr *et al.*, 1979, Altherr *et al.*, 1982, Wijbrans and McDougall, 1986; 1988).

3) The Cycladic basement crops out on the islands of Paros, Naxos, Mykonos and Ios. Ios shows overthrusting relations between the Cycladic Blueschists in the hanging wall of a major shear zone and the basement in the footwall (Huet *et al.*, 2009). This thrust was originally interpreted as a detachment with a top-to-the-south sense of shear (Vandenberg and Lister, 1996). Radiometric ages show that top-to-the-south shear bands (thrust related in the interpretation of Huet *et al.*, 2009) were active at 35 Ma and before, and that they were replaced by top-to-the-north shears at around 25 Ma (Foster and Lister, 2009).

No evolution is observed toward HT metamorphic conditions in the Oligocene and Miocene, at variance with the nearby islands of Paros, Naxos and Mykonos, where amphibolite-facies metamorphism and anatexis are dated to the Late Oligocene–Early Miocene (Altherr *et al.*, 1982). In this case, the basement is exhumed in the core of extensional gneiss domes below the main detachments (Buick and Holland, 1989; Buick, 1991; Duchêne *et al.*, 2006; Martin *et al.*, 2006).

Syntectonic Miocene granites intrude the domes in Naxos, Mykonos, Serifos and Ikaria (Jansen, 1973; Lee and Lister; 1992; Altherr and Siebel, 2002; Grasemann and Petrakakis, 2007; Iglseder *et al.*, 2009). The brittle detachments are localized at the base of the Upper Cycladic Nappe, at the contact with the Cycladic Blueschists, in

correspondence of the basement, or the granites. Two types of detachments can be distinguished. The most common ones are those showing an Oligocene-Miocene evolution toward HT metamorphic conditions in their footwall, or at least a strong retrogression of HP–LT parageneses in the greenschist facies (Buick and Holland, 1989; Parra *et al.*, 2002; Jolivet *et al.*, 2004a; Duchêne *et al.*, 2006). They are found on the islands of Andros, Tinos, Mykonos, Ikaria, Paros and Naxos, associated with a top-to-the-north or northeast sense of shear (Faure *et al.*, 1991; Lee and Lister, 1992; Gautier *et al.*, 1993; Gautier and Brun, 1994a; Mehl *et al.*, 2007). The detachment itself is not always present, but a similar footwall evolution is observed in the western Cyclades with, however, an opposite sense of shear.

Serifos shows outcrops of the detachment and serpentinites of the Upper Cycladic Nappe in small peninsulas to the southwest and northeast of the island (Brichau *et al.,* 2009).

A top-to-the-southwest sense of shear, interpreted as extensional, is observed in a low-angle mylonite derived from a 37 Ma old intrusion. A late Miocene granitoid, dated at 8–9 Ma (Altherr *et al.*, 1982; Henjes-Kunst *et al.*, 1988), intrudes the mylonite and is also affected by a top-to-the-southwest shearing (Grasemann and Petrakakis, 2007). Kea and Kythnos also show a top-to-the-southwest sense of shear, but the Upper Cycladic Nappe is absent. They formed contemporaneously with backarc extension.

In particular, on Naxos and Paros, this unit consists of ophiolitic rocks overlaying by neritic limestones of Lower Cretaceous age (Papanikolaou, 1980; Robert, 1982), followed by a succession of Neogene clastic sediments. Stratigraphic data from Naxos and Paros (Jansen, 1973, 1977; Roeslet, 1978; Angelier *et al.*, 1978; Papanikolaou, 1980; Robert, 1982) and from the Cyclades as a whole show that shallow-water, mainly detritic sedimentation has been continuous from Lower Miocene (Aquitanian) to Upper Pliocene in this domain.

The second type of exhumation process of the nappe shows instead a good preservation of HP–LT parageneses in their footwall; the closer to the detachment, the better preserved are the eclogites and blueschists (Trotet *et al.*, 2001a; 2001b). Such detachments are found principally on the islands of Syros and Tinos (Vari detachment). They were active in the Eocene when they accommodated the exhumation of eclogites and blueschists in the subduction channel or in an extrusion wedge (Ring *et al.*, 2001; Ring and Layer, 2003; Ring *et al.*, 2007a;).

A gradient of finite extension is shown by the evolution of topography and crustal thickness from continental Greece to the Cyclades (Jolivet *et al.*, 1994). The main compressive structures of the Hellenides are preserved in continental Greece, whereas they are highly reworked by extension in the Cyclades. This gradient is associated with the maximum retrograde temperature gradient observed in the Cycladic Blueschists from Mt Olympos to Naxos and Mykonos (Jolivet and Patriat, 1999).

Along this transect, an evolution of Oligo–Miocene extensional structures is also observed, from essentially brittle structures (steep normal faults) near Mount Olympos to ductile shear zones and shallow-dipping detachments in Evia and the Cyclades.

2.3.1 Naxos

Naxos is the largest island of the Cyclades Archipelago in the Aegean Sea (Greece). It is considered as a metamorphic core complex (MCC) originating from post-orogenic extension, which resulted in an elongated a-type dome structure (Lister *et al.*, 1984.; Jolivet *et al.*, 2004) (Fig. 2.3.1.1).

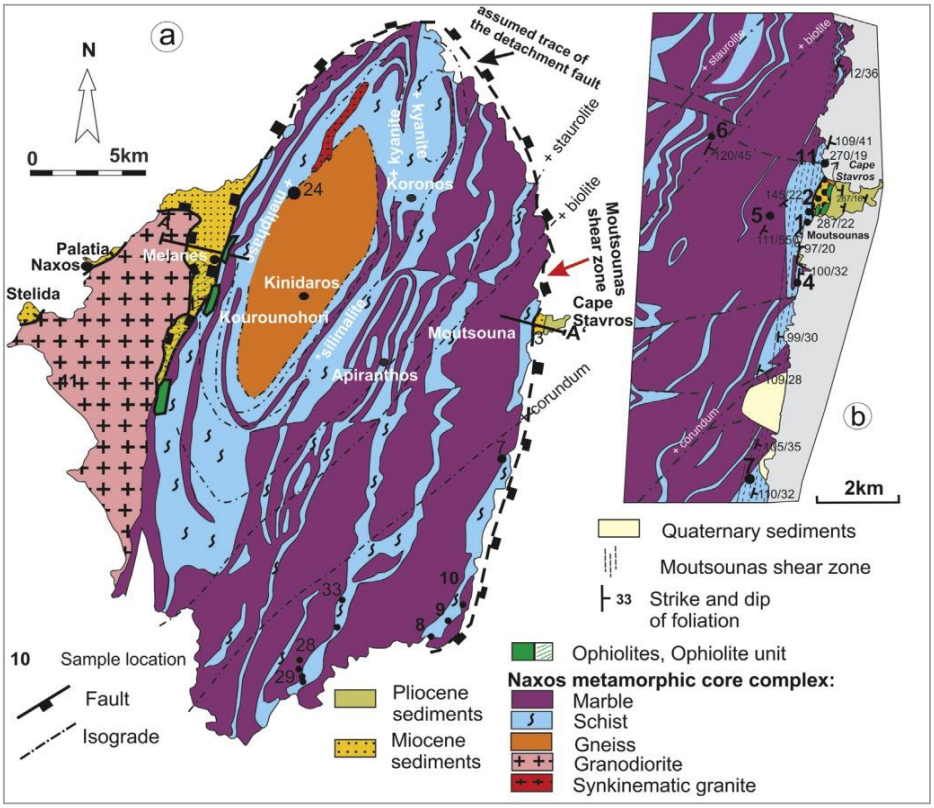

Fig. 2.3.1.1: Geological map of the Naxos MCC in the Cyclades Islands (Cao *et al.,* 2013).

The main structure of the Naxos is a migmatite-cored gneiss (MCG) dome that is structurally overlain by a ductile low-angle normal fault in the east and a steep strike-slip-type fault zone in the west, the latter located in an N-S-trending topographic depression (Cao *et al.*, 2013).

Naxos consists of a metamorphic complex in the eastern part of a Miocene granodioritic mass (Jansen, 1973; Jansen and Schuiling, 1976; Kruckenberg *et al.*, 2011).

The metamorphic complex, composed of continental basement probably of Variscan age (Altherr *et al.*, 1982; Strumpf, 1997; Reischmann, 1998), is a migmatitic gneiss dome surrounded by a sequence of metamorphic zones. It is a metasedimentary-metavolcanic sequence mainly composed of interbedded micaschists and marbles. The marbles are particularly abundant in the low-grade parts of the metamorphic terrain. In the higher-grade zone, the schists-marble sequence contains interbedded amphibolites. Small, discontinuous bands of metamorphosed bauxites occur in the marbles throughout the metamorphic complex. Two horizons of ultramafic bodies are present near the migmatite dome. All rocks were folded by a phase showing synmetamorphic lineations and fold axes oriented N15E, as appears to be a characteristic feature of many metamorphic complexes in the eastern Mediterranean.

In addition to the HP-LT (glaucophane bearing) assemblages, the medium-pressure (MP)/higher-temperature assemblages widespread in the whole Attic-Cycladic Massif, two main successive Alpine metamorphic events affected the metamorphic rocks of the middle and lower units within the Naxos MCC: a Eocene HP-LT metamorphic phase M1 and an Oligocene–Miocene Barrovian-type metamorphism M2 (*e.g.,* Andriessen *et al.*, 1979; Urai *et al.*, 1990; Keay *et al.*, 2001).

Episode M1 developed under glaucophanitic schist facies, characterized by HP (7-9 kbar) and MT (490-530 ºC).

It is related to a subduction-controlled compressional phase generating large thrusts (Forster and Lister, 2005). This tectonic phase was followed by extensional tectonics resulting in the Aegean back-arc basin (Gautier *et al.*, 1999). Exhumation and rapid uplift of lower crustal units caused the thermal dome structures (Jolivet *et al.,* 2004a;

2004b). Lower crustal rocks were brought into contact with upper crustal units via major shallow-dipping shear zones (Lister *et al.*, 1984; Urai *et al.*, 1990). It is inferred that the M1 phase has affected the whole island, but most of its record has been erased by the second phase of metamorphism M2.

The M1 phase is recorded by relics of blueschist facies minerals preserved in metamorphic rocks of southern sectors of the island (Wijbrans and McDougall, 1986; Avigad, 1998; Avigad and Garfunkel, 1991; Cao *et al.*, 2013). The $^{40}Ar/^{39}Ar$ ages of ca. 45 ± 5 Ma on white mica document an Eocene age for blueschist metamorphism (Andriessen *et al.*, 1979; Wijbrans and McDougall, 1986; 1988).

The blueschist metamorphic phase (M1) was later overprinted by a widespread Barrovian type (MP-MT) metamorphism (M2) during the Miocene, grading from greenschist facies to amphibolite facies conditions, and reaching partial melting conditions at the deepest structural levels (Jansen and Schuiling, 1976; Buick and Holland, 1989; Wijbrans and McDougall, 1988; Avigad and Garfunkel, 1991; Duchêne *et al.*, 2006; Martin *et al.*, 2006; 2008). The M2 temperature isograds reached 700° C in the center of Naxos and a MP (about 5-7 kbar) (*e.g.,* Jansen and Schuiling, 1976).

The related deformation and regional high-temperature metamorphism M2 are mainly responsible for the present rock fabric. Based on $^{40}Ar/^{39}Ar$ mineral ages, the timing of Barrovian-type peak M2 metamorphism was first estimated to have occurred between 20 and 15 Ma (Wijbrans and McDougall, 1988) and is consistent with new Rb/Sr ages for micas and garnets (Duchêne *et al.*, 2006).

External overgrowth rims on the zircon in the core migmatites have ages ranging from 19 to 14 Ma (Keay *et al.*, 2001; Martin *et al.*, 2006). Finally, Martin et al. (2006, 2008) found U-Pb zircon ages of ca. 16 Ma for the Barrovian type metamorphism. In the structurally higher metamorphic rocks, the age of MP-MT metamorphism M2 is

constrained between 27 and 19.9 Ma by $^{40}Ar/^{39}Ar$ dates of phengite dating (Wijbrans and McDougall, 1988; Cao *et al.*, 2013).

The western part of Naxos is occupied by a granodioritic intrusion with a tourmaline-rich aplitic border facies representing the latest stage of crystallization. Veins of aplitic and granodioritic composition have intruded at about 1 km wide zone of contact metamorphism of the andalusite-sillimanite type in the country rock, M3; this zone transects the metamorphic zonation of the M2 event.

Some parts of the crystalline basement of Naxos are overlain by remnants of an overthrust nappe probably coming from the north. The allochthonous rocks are mainly unmetamorphosed Oligocene-Middle Miocene sediments and minor gabbros, diabases and serpentinised peridotites; they occur in the western part of the island and in a small area on the east coast.

Another small remnant of the nappes on the east coast consists of unmetamorphosed Permian sediments. In the granodiorite, streaks of pseudotachylite were observed within the thrust-plane zone. The fourth metamorphic event, M4, is a very weak retrograde event recorded in the northwestern part of the island. It was probably related to the Late Miocene/Pliocene overthrust movements.

In conclusion, a variety of rock types can be observed on Naxos Island (Jansen, 1973; Jansen and Schuiling, 1976), and the presence of marbles is abundant (purple area in Fig. 2.3.1.1). Marbles alternate with schists in the lower metamorphic regions, and with the higher-metamorphic grade gneisses in the migmatitic central part of Naxos. The marbles form bodies of a few meters to several hundreds of meters in thickness. Intercalated with the marbles are amphibolites, metamorphic ultrabasic rocks and metabauxites, which were penetrated by granites and pegmatites. In the western part of Naxos, a large granodiorite body is exposed that intrudes the metamorphic core complex. These units are tectonically overlain by allochtonous,

non-metamorphic Tertiary sediments. The typical deformation structures in the metamorphic rocks are kilometre-scale isoclinal folds that are re-folded, both with north–south fold axes. Due to a gentle east–west compression, all structures were folded along the north–south axis and, in a last phase, in the east–west direction, leading to a structural dome. Therefore, the foliation is arching over the migmatite core. Stretching lineations that indicate the shear direction are typically north–south orientated. A complete description and an interpretation of all deformation structures on Naxos are given in Urai *et al.* (1990).

2.3.2 Paros

Paros Island has an area of 196 km^2, being the third largest Cyclades Island after Naxos (428 km^2) and Andros (374 km^2). The largest part of the Paros coast is jagged and rocky with high slopes, whereas some parts are sandy. The coastal zone is relatively flat, whereas the central part of the island is quite mountainous, with the highest peak of St. Ilias at an altitude of 771 m (Evelpidou, 2002).

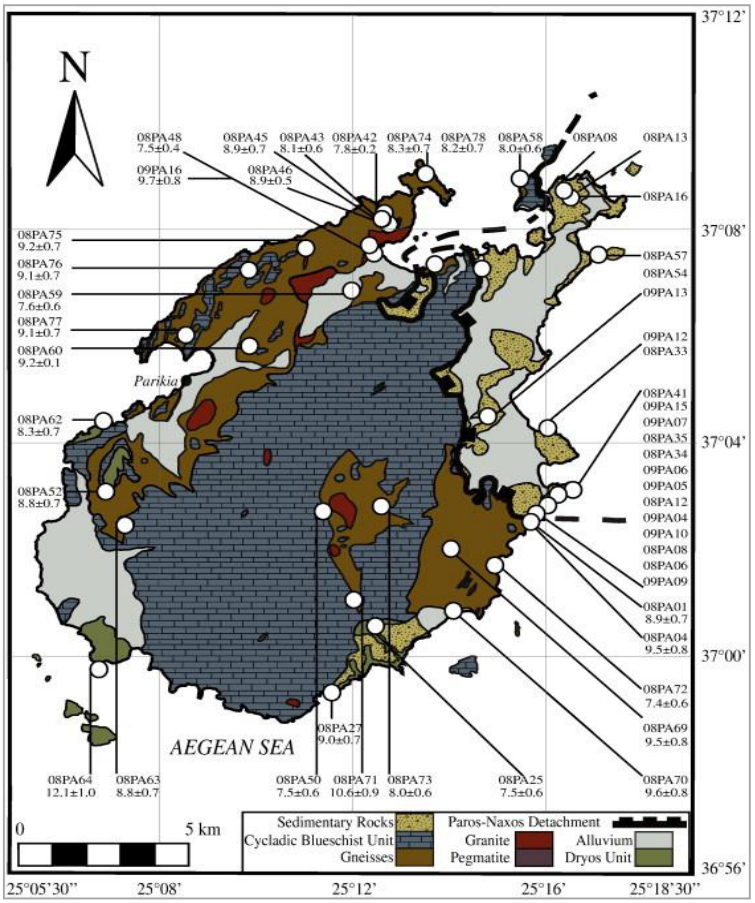

Fig. 2.3.2.1: Simplified geologic map of Paros. The dominant structural feature is the Paros–Naxos low-angle extensional detachment fault, which separates the supra-detachment basin from the metamorphic core complex (after Papanikolaou, 1996; Papp, 2007).

The main lithological formations of Paros are relatively complex and include carbonate-bearing sedimentary rocks and a gneiss-schist basement core complex; igneous rocks and quaternary sediments are present in smaller occurrences. In the basement, the greenschist type parageneses has replaced the blueschist one, due to the extensive granite intrusion. Tectonic deformations are evident through isoclinal recumbent folds, mainly with an N-S or NNE-SSW axis. All deformations, metamorphic and magmatic events of the Cyclades area ended at the Upper Miocene (Papanikolaou, 1977, 1980). Paros is unique among the central Cyclades in that it exposes a nearly complete succession of footwall crystalline rocks and hanging-wall sediments (Bargnesi *et al.*, 2013) (Fig. 2.3.2.1).

In more detail, in the footwall, the Cycladic basement rocks of Paros are composed of highly deformed Carboniferous ortho- and paragneisses (Engel and Reischmann, 1998; Robert, 1982) and less deformed, S-type granites (Altherr *et al.*, 1982). At one location in the NW of the island, basement rocks are crosscut by clearly much younger and completely undeformed rhyolitic dikes (Hannappel and Reischmann, 2005; Papp, 2007). The ortho- and paragneissic basement complex is overlain by intercalated amphibolite-facies marbles, mica schists, and amphibolites of the Cycladic Blueschist Unit (CBU). On Paros, Miocene Barrovian-style metamorphism has pervasively overprinted an earlier high-pressure signature (Gautier and Brun, 1994a; 1994b), although relict blueschist assemblages have been identified from correlative units on the neighboring island of Naxos. Overprinting relationships suggest at least three episodes of deformation, which may have developed as a continuous sequence during progressive shearing (Gautier *et al.*, 1993; Papanikolaou, 1977; Papp, 2007).

A low-angle detachment fault separates the high-grade MCC footwall from the hanging-wall sediments, which are mainly exposed

along the coast in NE Paros (Fig. 2.3.2.1). The stratigraphically lowest units of the hanging-wall block comprise a gently folded, incomplete marine sequence of uncertain provenance and tectonic origin. The base of this sequence is always a tectonic contact, and no depositional contact can be observed. The marine units are overlain by polymictic conglomerates interbedded with sandstones with variable grain size, color, and bed thickness. The lower clastic packages are capped by flat-lying Pliocene(?) limestone and travertine deposits (Dermitzakis and Papanikolaou, 1980). Although most work has focused on the neighboring island of Naxos, several geologists have investigated the Cenozoic tectonic evolution of Paros. Geochronologic data indicate Miocene heating and a thermal history similar to that of the Naxos lower-plate, based on $^{40}K/^{39}Ar$ determinations (Altherr *et al.*, 1982; Wijbrans and McDougall, 1986; 1988). Sparse apatite fission-track (AFT) data from the Paros gneisses suggest rapid cooling during the Late Miocene (~12–8 Ma) on the order of 70 ° C/Ma, and a corresponding Miocene erosion rate of ~0.3 km/Ma (Hejl *et al.*, 2003). Slip rates of 6–7 km/Ma for the low-angle detachment on Paros were calculated based on apatite and zircon fission-track and (U–Th)/He dating of crystalline rocks (Brichau *et al.*, 2006).

Early investigators interpreted the basin fill as a contraction-related, backarc clastic molasse deposit with a biostratigraphically determined depositional age of Early to Late Miocene (Dermitzakis and Papanikolaou, 1980; Papageorgakis, 1968; Papanikolaou, 1977; 1980; Robert, 1982), and some, as Middle to Late Miocene (Papageorgakis, 1968). Interpretation of the biostratigraphic data is problematic because of extensive sedimentary recycling and redeposition (Dermitzakis and Papanikolaou, 1980). More recently, some have attributed the Paros upper-plate sedimentary package to, at least in part, synextensional supradetachment basin deposits (Gautier and Brun, 1994a; 1994b; Sánchez-Gómez *et al.*, 2002). A detrital mica

$^{40}Ar/^{39}Ar$ and $^{40}K/^{39}Ar$ study of clasts in the sedimentary section on Paros revealed two distinct age populations:

1) Eocene to Late Cretaceous signature with ages between 100 and 40 Ma and

2) Middle to Late Miocene population of 16–9 Ma (Sánchez-Gómez *et al.*, 2002).

These data indicate a complex structural and exhumational–erosional history for Paros and the central Cyclades, with multiple episodes of deformation and deposition from several distinct source terranes, some of which may have been completely eroded. Fission detritus in track studies of the upper-plate sedimentary rocks on Naxos corroborate a multistage pre- and synextensional tectonic history and complex lithostratigraphy (Kuhlemann *et al.*, 2004; Seward *et al.*, 2009). Naxos and Paros upper-plate rocks may be genetically linked, as it is inferred that they share the same low-angle detachment fault (Gautier *et al.*, 1993).

2.3.3 Thasos

Thasos Island is in the northern Aegean Sea of Greece. In the extensional area of the Aegean Sea and the adjacent mainland, several metamorphic core complexes occur (Fig. 2.3.3.1). These high-relief core complexes were exhumed by a succession of ductile normal detachments, at least active from the Oligocene to the present (Lister *et al.*, 1984; Burg *et al.*, 1990; Kolocotroni and Dixon, 1991; Schermer, 1993; Avigad, 1993; Dinter and Royden, 1993; Gautier and Brun, 1994a; 1994b; Jolivet *et al.*, 1994; Wawrzenitz, 1994; Wawrzenitz and Krohe, 1998).

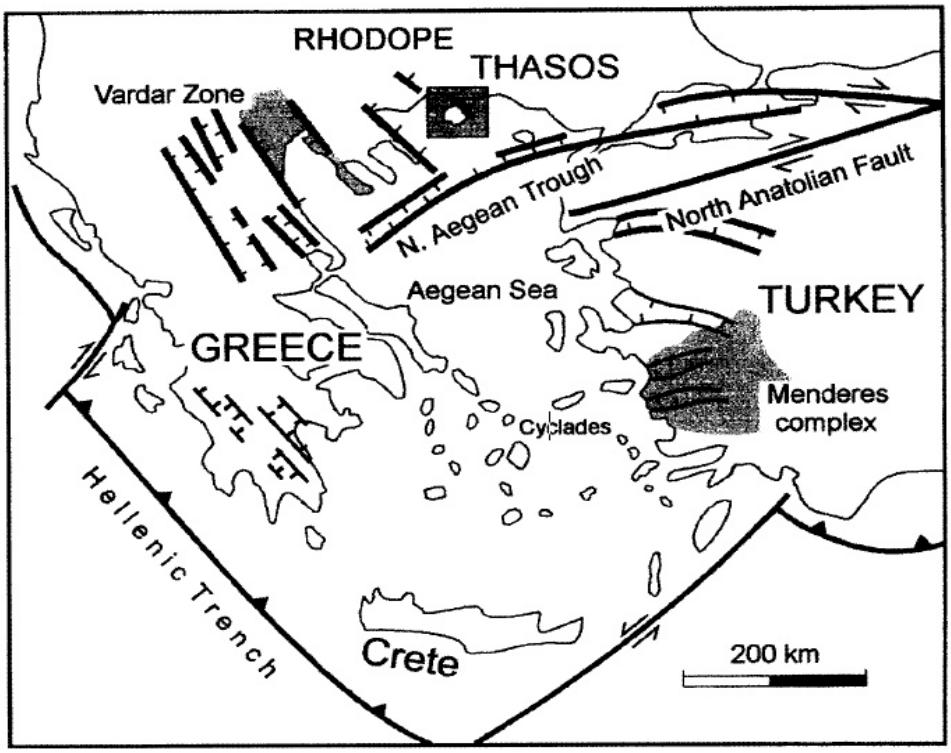

Fig. 2.3.3.1: Simplified structural map of the Aegean region showing the study area at the western extremity of the North Anatolian Transfer Fault. Thasos Island is boxed. Also shown are the Vardar Zone (suture), the Menderes Massif, and the Cyclades. Modified after Beck and Schermer (1994).

The formation of Thasos Island was controlled by two phases of deformation lasting from at least 26 Ma (Late Oligocene) until at least 13 Ma (Middle Miocene). The first phase was uniform SW-directed non-coaxial deformation and denudation of the higher part of the core complex. The second phase involved the generation of a gneiss dome by up-warping of the deeper parts of the core complex by non-coaxial polydirectional plastic flow. The morphology of the island portrays the pattern of differential movements associated with plastic and brittle increments of deformation of the crust (Wawrzenitz and Krohe, 1998).

The crustal structure of the north Aegean region (Fig. 2.3.3.1) reflects Late Cretaceous to Eocene collision of the Adriatic (Apulian) plate (may be considered as a part of Africa) with Eurasia and subsequent deformation episodes (*e.g.,* Dewey and Sengör, 1979; Papanikolaou, 1984).

In the northwestern and northeastern areas of Fig. 2.3.3.1, fundamentally different crustal evolutions are recorded:

1) The northwestern area contains the suture zone (represented by the Vardar Zone, Fig. 2.3.3.1) between the plates. This area is occupied by tectonic complexes reflecting pre-Alpine as well as Alpine sedimentary events and metamorphism.

2) The northeastern area of Fig. 2.3.3.1 (shown in more detail in Fig. 2.3.3.2), which comprises the area considered in this study, is part of the Eurasian plate. This area is essentially occupied by fault-bounded superimposed gneiss complexes representing pre-Alpine continental lithosphere, pervasively reworked by Alpine metamorphism and deformation.

The area of Fig. 2.3.3.2 comprises superimposed gneiss complexes that are more or less flat-lying. As a general trend, geochronologic ages decrease from higher to deeper levels. The eastern section of Thasos Island exposes the deepest structural levels of this area (see below). The uppermost tectonic complexes include the Vertiskos Gneiss

Complex (upper parts of the Serbomacedonian Massif; Sakellariou, 1989).

In a lower structural position, gneiss complexes occur showing in part Paleocene, but essentially Eocene Rb-Sr and K-Ar ages of biotite, white mica and hornblende and a U-Pb date of monazite from a migmatite (Harre *et al.*, 1968; Liati and Kreuzer, 1990; Jones *et al.*, 1994; Wawrzenitz, 1994; Mposkos and Wawrzenitz, 1995). These are termed the Kerdilion Gneiss Complex (lowermost tectonic unit of the Serbomacedonian Massif; Sakellariou, 1989), and Sidironero Gneiss Complex (Upper Tectonic Unit of Papanikolaou, 1984; West Thracian Gneiss Complex of Dinter *et al.*, 1995), in the western and eastern part of this section, respectively (Fig. 2.3.3.2).

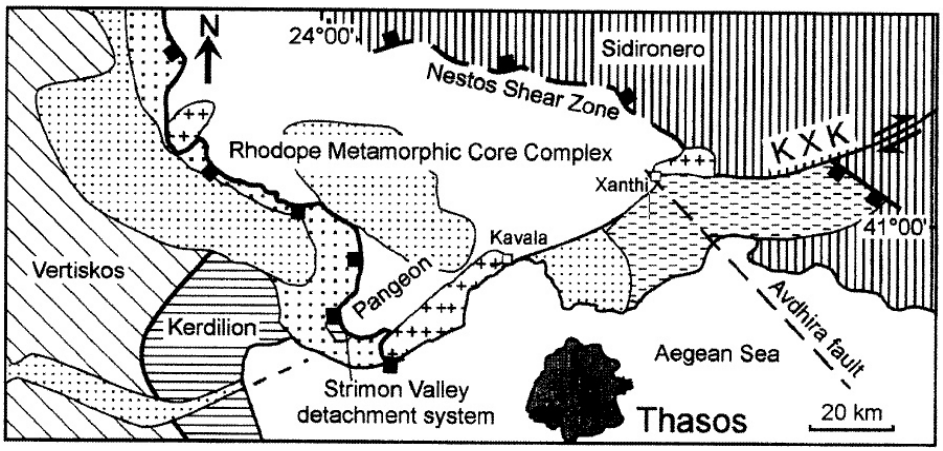

Fig: 2.3.3.2: Generalized map of northeastern Greece showing the structural setting of the S Rhodope area. Simplified and compiled after Maltezou and Brooks (1989), Sakeltariou (1989) and Dinter et al. (1995). *KXK* = Kavala-Xanthi Komofini Fault. Sedimentary basins: hatched, Eocene Oligocene (Xanthi Komofini basin to the south of the KXK); coarse stipples, Miocene sedimentary basins (supradetachment basins); fine stipples, Pliocene to Recent (post-detachment) basins. Crosses, granitoids (Vrondou in the northwest. Kavala in the south, Xanthi in the east); barbed lines, low-angle normal detachment surfaces.

The lowermost structural position is occupied by the Rhodope and Thasos Metamorphic Core Complexes (Lower Tectonic Unit of Papanikolaou, 1984) (cf. Dinter and Royden, 1993; Sokoutis *et al.*, 1993) and by parts of the eastern Rhodope. Various Rb-Sr, Ar-Ar and U-Pb dates range from the Oligocene to Miocene. The complexes consist of metapsammites, metapelites, marbles and metabasites, whose protolith ages are unknown, and of orthogneisses and metapegmatites, derived from a Palaeozoic (Variscan) magmatic suite (Wawrzenitz, 1994; Dinter *et al.*, 1995; Mposkos and Wawrzenitz, 1995). In the Rhodope Metamorphic Core Complex, in orthogneisses and metapelites, high-pressure metamorphic conditions of 14-15 kbar and 550-600 °C, suggesting Alpine crustal thickening, were followed by near-isothermal decompression (Liati and Mposkos, 1990), first to 8 kbar, and then to 4 kbar at 550 °C. During the retrograde P-T path, pervasive mylonitic foliations and stretching lineations developed, gently dipping either to the southwest or to the northeast (Dinter *et al.*, 1995).

Most parts of the metamorphic succession of Thassos Island are related to the Rhodope metamorphic core complex (Fig. 2.3.3.3).

The Thassos Island crystalline complex is made up of three superimposed tectonic units (lower, intermediate, and upper unit, Fig. 2.3.3.4b) with geochronologic ages decreasing downwards (Wawrzenitz and Krohe, 1998). These tectonic units are separated by two SW-dipping low-angle normal fault systems (Dinter and Royden, 1993; Peterek *et al.*, 1994; Wawrzenitz and Krohe, 1998).

The upper unit is considered as the hanging-wall block of the core complex and consists of Tertiary clastic sediments and non-mylonitic metamorphic rocks including biotite-plagioclase gneisses that are locally migmatic, muscovite gneisses, pegmatites and minor ultramafic bodies and marbles. High-grade gneisses and deformed pegmatoites show Eocene mica ages (about 51 Ma, see below).

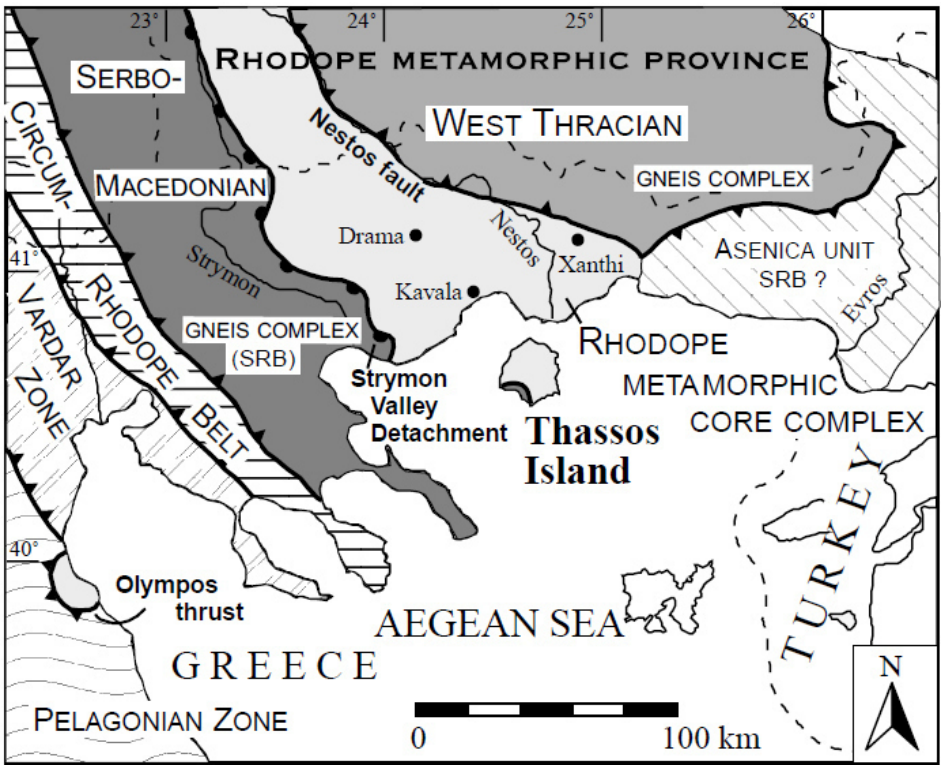

Fig. 2.3.3.3: Tectonometamorphic map of the north Aegean region (NE Greece) showing the structural setting of the south Rhodope area (simplified and compiled after Papanikolaou, 1984; Dinter, 1998; Kilias *et al.*, 1999).

These ages are similar to those of the Kerdilion Gneiss Complex on the mainland (see above), which is in the upper plate of the S Rhodope Metamorphic Core Complex (Dinter and Royden, 1993).

The intermediate and lower unit form the metamorphic core complex. Both units are made up by pervasively mylonitized paragneisses, micaschists, marbles, calc-silicates, amphibolites (cf. Zachos, 1982), and orthogneisses. In the intermediate unit, pre-mylonitic mineral assemblages locally indicating medium-grade conditions, were retrogressed to low-grade assemblages during mylonitization. Rb-Sr mica ages range between 24 and 23 Ma, which is similar to Rb-Sr ages of white mica and U-Pb ages of titanite of the

Rhodope Metamorphic Core Complex on the mainland (Del Moro *et al.,* 1990; Dinter *et al.,* 1995). In the lower unit, which forms the gneiss dome, the major phases of mylonitization still occurred during medium-grade conditions. This unit is characterized by still younger Rb-Sr white mica ages, ranging between 21 and 18 Ma. In the footwall of each detachment surface, the intermediate and lower units warp up to a mountainous relief that rises about 1200 m above sea level (lower unit) (Wawrzenitz and Krohe, 1998). Basins surrounding the island show a Miocene to Recent stratigraphic record (Sidiropoulos, 1980) and are situated on the metamorphic assemblages of the upper unit. The pre-Pliocene stages of subsidence of these basins have been inferred to be controlled by movements on low-angle detachment systems (supradetachment basins; Dinter *et al.,* 1995).

Furthermore, the metamorphic succession is dominated by massive marble complexes alternating with paragneisses, orthogneisses, and amphibolites (*e.g.,* Peterek *et al.*, 1994). In response to crustal thickening during Alpine tectonics (Dinter, 1998), the maximum metamorphic conditions were estimated of approximately 620 °C/4.7 kbar for the lower unit and 580 °C/2.4 kbar for the intermediate unit, as determined by geothermobarometric analyses of amphibole gneisses (unpublished data and recalculated data of Schulz, 1992). Penetrative shearing during crustal uplift produced a main extensional fabric overprinting older compressive structures within the metamorphic succession, under retrograde metamorphic conditions (Peterek *et al.*, 1994).

Characteristic of this process is the development of NE±SW trending mineral lineation with a top-to-SW oriented sense of shear. Rb±Sr analyses of whole-rock data and white mica constrain the onset of extensional deformation at 26 Ma and ongoing deformation at 23±24 Ma (Wawrzenitz and Krohe, 1998).

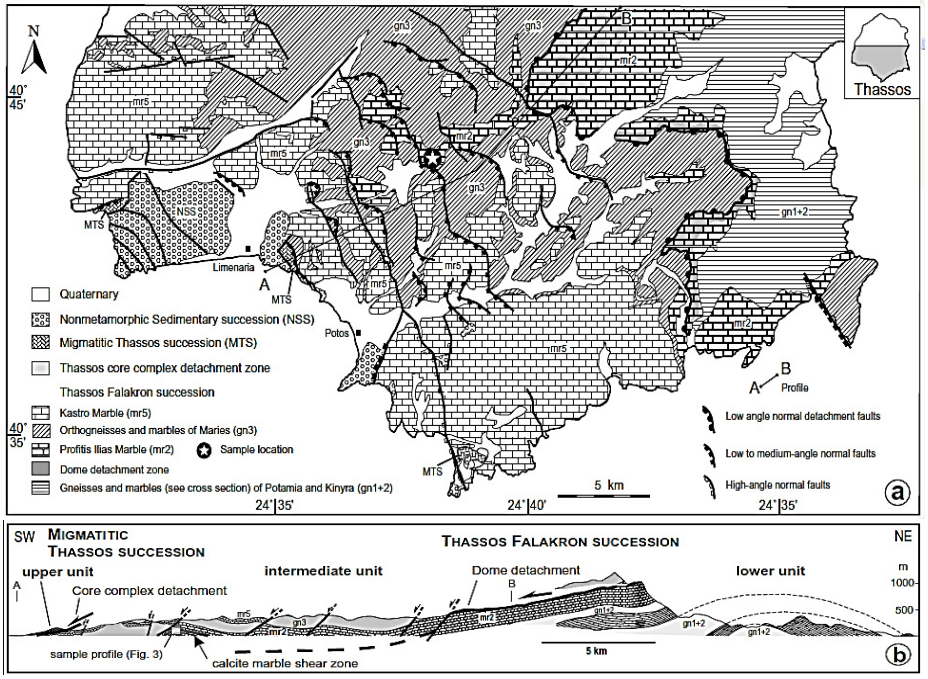

Fig. 2.3.3.4: a) Geological map of the southern part of Thassos Island, Greece; b) Geological cross-section through the Thassos island crystalline complex and geotectonic position of the investigated shear zone. (Bestmann *et al.*, 2000).

This event is considered by Wawrzenitz and Krohe (1998) to be associated with decoupling of the brittle hanging wall (Migmatitic Thassos succession) from the plastically flowing deeper crust (Thassos Falakron succession) (Fig. 2.3.3.4a). After deformation under middle crust conditions, the Thassos Falakron succession was separated into an intermediate and a lower unit during continuous uplift of the metamorphic core complex. The decoupling took place along a SW-dipping low-angle normal detachment zone (Wawrzenitz and Krohe, 1998), cutting through a massive marble complex (Profitis Ilias Marble, Fig. 2.3.3.4b).

Strain localization corresponded to decreasing P±T conditions during continuing extensional tectonics and linked to the exhumation process of the metamorphic core complex. In the pure calcite marble

complexes of the intermediate unit, this stage of deformation is recorded by several shear zones of up to 3 m thickness that are oriented parallel to the foliation plane in the host rocks (Bestmann *et al.*, 2000).

2.4 Attica

Attica is currently the wealthiest and most densely populated region of Greece. It consists of a number of interconnected plains, floored by alluvium and Pleistocene sediments, and cut off to the northwest by the great mass of Mount Parnes (Fig. 2.4.1).

Fig. 2.4.1: Map of Attica (Higgins and Higgins, 1996).

The Central Plain around Athens is bounded on the north by Mount Parnes, on the northeast by Mount Pentelicon, on the southeast by Mount Hymettos, and on the west by Mount Aigaleos. It connects with the smaller plains of Marathon on the northeast, Eleusis (the Thriasian Plain) on the northwest, and the Mesogeia on the south.

The geological structure of Attica, as in much of Greece, is dominated by a series of nappes stacked up during Alpine compressional movements. The oldest rocks in the region occur in one of the higher nappes along the northwestern borders of Attica, in the mountains of Aigaleos and Parnes. These mountains are dominantly made of Triassic limestones of the Pelagonian zone, similar to those occurring as far north as Thessaly and western Macedonia (Higgins and Higgins, 1996).

Schists and marbles of the Attic Cycladic metamorphic belt similar to those in southern Euboea and the Cycladic islands underlie the southern and eastern parts of Attica. These marbles make up Mts Hymettos and Penteli, as well as the hills around Marathon and Lavrion (Marinos, 1973).

The highest nappe is made of schists, cherts and ophiolites, which is in turn overlain by slightly metamorphosed and unmetamorphosed limestones and flysch sediments of Cretaceous to Eocene age. The uppermost part of this series is called the Athens schist (Marinos, 1973).

During the Neogene period, compressional forces associated with Alpine mountain-building ceased. Erosion and faulting produced a series of basins, which were flooded by the sea and filled with sandstones, shales, and limestones. These rocks are still in their original places of deposition, except that they have been raised above sea level by geologically recent tectonic movements.

2.4.1 Mount Pentelicon

Mount Pentelicon (1,106 m) is part of a 20 km long sector of metamorphic rocks northeast of Athens, extending past Marathon to the coast opposite Euboea, and its geologic evolution is not well understood (Higgins and Higgins, 1996).

Despite the lack of consensus over Mount Pentelicon's origin, there are aspects of the mountain's history that are in agreement by most authors. Mount Pentelicon lies in the northern section of the Attic-Cycladic geotectonic zone (Pike, 1999) (Fig. 2.4.1.1).

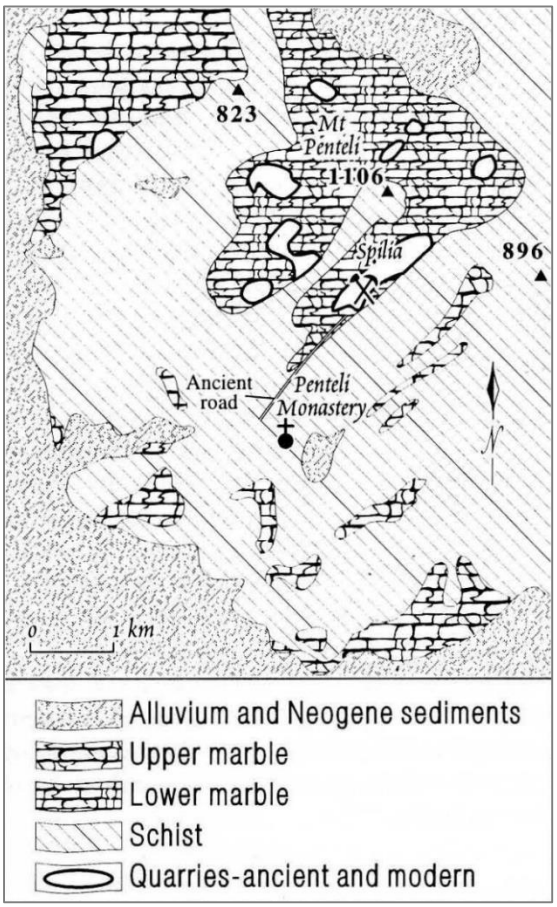

Fig. 2.4.1.1: Map of Mount Pentelicon (Higgins and Higgins, 1996).

This zone marks the southernmost of three massifs forming the Pelogonian Zone of the Hellenides mountain system (Katsikatsos *et al.*, 1986; Dürr, 1986), formed by original shallow-sea sediments that are thought to have been similar to the Bahamian style.

The metamorphic belt continues southwards in the Cycladic islands and to the east, where it merges with the Menderes massif near the Anatolian coast. The Menderes massif is geologically similar to the Attic-Cycladic metamorphic belt, but also shows some affinities with metamorphic rocks from Africa (Higgins and Higgins, 1996). It is still not clear whether the Menderes massif is a remnant of African crust or if it is simply a lateral extension of the Attic-Cycladic belt. Schliestedt *et al.* (1988) suggested that the metamorphic rocks comprising the Attic-Cycladic massif were rapidly subducted roughly 50 km during the Eocene compression of the Alpine orogeny. Soon after the burial, subduction ceased, so these marble units underwent the typical blueschist-facies metamorphism of HP-LT. Most of the major marble-producing quarries within Greece and Anatolia are located within the Attic- Cycladic / Menderes metamorphic belt.

The German geologist Lepsius (1893) described the western section of Mount Pentelicon as being composed of three autochthonous formations that were labeled Lower Marble Formation, Intermediate Schist Formation and Upper Marble Formation. Lepsius attributed to these rock formations a Precambrian age. Since then, the occurrence of numerous fossil remnants allowed one to date this marble as being Triassic-Upper Cretaceous in age (Steinmann, 1890; Negris, 1912; 1915; Kober, 1929; Marinos and Petrascheck 1956; Leleu and Neuman 1969; Papadeas, 1970; Katsikatsos *et al.,* 1986). The Upper Marble formation is 100 m thick, and the Lower Marble is estimated to have a minimum thickness of at least 500 m (Avdis, 1991). Research suggests that the current Attic topography is the result of a series of tectonic nappes related to the Eohellenic orogeny of the Eocene (Katsikatsos

1977). In particular, the Mount Pentelicum is characterized by a large–scale antiform related to a NE-thrusting direction. Avdis (1991) argued that the topography of Mount Pentelicon is the result of uplift of the autochthonous crystalline basement rocks by a long series of high-angle dip-slip faults. This interpretation, although compelling, fails to take into consideration the structural major and minor folds throughout the formation.

Since the classical antiquity, the quarries of Mount Pentelicon, together with those of Mount Hymettus, were the principal source of white marble in continental Greece. The ancient Greek and Roman Pentelic quarries of white marble are situated in the exposed upper section of the Lower Marble Formation, on the southwest limb of the primary fold.

On both mountains, there are two main marble layers: the geologically upper layer is predominantly grey, whereas the lower is predominantly white (Lepsius, 1893). Paradoxically, the lower marble is exposed near the main summit of Penteli, and the upper marble is at lower elevations. The grey color is produced by the presence of minute amounts of graphite, formed by metamorphism of plant remains in the original limestone. Some parts of the marble beds contain muscovite, which considerably reduces the resistance of the rock to weathering.

Although both white and grey marble occur on both mountains, in antiquity the best white marble was obtained from Penteli, and the best grey from Hymettos, a fact which has misled many modern authors to refer (incorrectly) to the grey as “Hymettan” and the white as “Pentelic” (Higgins and Higgins, 1996).

2.5 Turkey

Turkey consists of several continental fragments that were joined together into a single landmass in the late Tertiary. During the Phanerozoic, these continental fragments, called terranes, were separated by oceans, whose relics, ophiolites and accretionary prisms, are widely distributed throughout the Anatolia. Indeed, about 100 million years ago in the place of the Anatolia, there was a large ocean, and the various continental fragments (which make up Anatolia) were distributed on either side of this ocean or formed islands within this ocean (Fig. 2.5.1a). This ocean, called Tethys, existed at least since 350 Ma between the two large continents of Gondwana in the south and Laurasia in the north. A further complexity is that Tethys was not a single wide ocean as the present-day Atlantic, but consisted of several relatively narrow oceanic seaways separated by island arcs or continental slivers (Fig. 2.5.1a). The final closure of the Tethyan seaways and the collision between the different terranes resulted in the Alpine orogeny and the creation of Anatolia as a single landmass in the Oligocene.

In detail, the age and distribution of subduction-accretion complexes in Turkey are consistent with the existence of two Tethyan oceans, Paleotethys and Neotethys, between Gondwana and Laurasia at least since the Carboniferous (Stampfli and Borel 2002), and these partly overlapped in time (Sengör, 1979; 1987; Sengör and Yilmaz, 1981; Okay and Tüysüz, 1999; Stampfli, 2000). Although it is traditionally, for simplicity, accepted that Paleotethys was essentially a Paleozoic - Early Mesozoic ocean and that Neotethys was a Mesozoic - Early Tertiary ocean, there is no agreement on their definitions and paleogeographic locations (Bozkut and Mittwede, 2001).

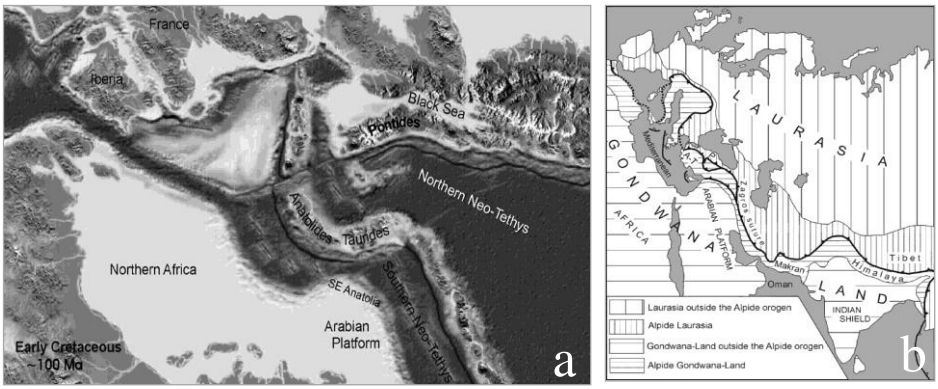

Fig 2.5.1: a) A view of the Mediterranean palaeogeography during the Early Cretaceous (110 Ma) (Aral, 2008); b) Tectonic setting of Turkey within the Alpine-Himalayan chain (modified after Şengör 1987). A-T: Anatolides-Taurides; P: Pontides (Okay, 2008).

Three separate Neotethyan oceanic basins developed: the Intra-Pontide, northern Neotethys, and southern Neotethys (Bitlis ocean or Peri-Arabic ocean). Even though the southern basin continues to survive as the eastern part of the Mediterranean Sea, an oceanic basin dating from the Triassic (Robertson, 1998) or even Late Permian (Stampfli, 2000), the other two no longer exist. The southern part of the country is now in a post-collisional phase (Sengör and Yilmaz, 1981; Sengör *et al.*, 1985; Pearce *et al.*, 1990) along the Southeast Anatolian suture, whereas areas in the west, such as the Cyprus area, are still in the early collisional phase (Robertson and Grasso, 1995).
These oceans closed diachronously. The northern branch of the Neotethyan ocean closed by final collision and suturing during the Late Paleocene-late Burdigalian, whereas northward subduction across the southern branch continued through the late Middle Miocene, and then was closed entirely during the continent-continent collision across the Arabian Plate in the south and the Anatolian Plate in the north along the Southeast Anatolian suture (Yilmaz, 1993; Elmas, 1996a; Yilmaz and Yildirim, 1996).

It is important to note that many alternative models have been proposed for the evolution of the Tethydes in Turkey, and they differ in the timing of ocean basin opening and closure, subduction polarity, and the location and number of sutures (Sengör and Yilmaz, 1981; Okay and Tüysüz, 1999; Ustaömer and Robertson, 1999; Göncüoglu *et al.,* 2000; Stampfli, 2000; Elmas and Yigtbas, 2001).

In the early years, Ketin (1966) subdivided geologically Turkey into three main tectonic units:

1) Pontides;
2) Anatolides-Taurides;
3) Arabian Platform (Fig. 2.5.1).

These tectonic units, which were once surrounded by oceans, are now separated by sutures, which mark the tectonic lines or zones along which these oceans have disappeared (Ketin, 1966).

The Pontides terrane comprises the region north of the İzmir-Ankara-Erzincan suture. They are folded and thrust-faulted during the Alpine orogeny but were not strongly metamorphosed. In contrast to the Anatolides-Taurides, they bear evidence of Variscan (Carboniferous) and Cimmeride (Triassic) orogenies during the closure of Paleotethys and its marginal basins, the Karakaya and Küre basins (Ustaömer and Robertson, 1999; Okay, 2000). The Pontides consists of three major tectonic zones (Okay, 1989), which show markedly different geological evolutions. These are the:

1) Strandja Massif;
2) İstanbul Terrane;
3) Sakarya Terrane.

The Pontic terranes were amalgamated into a single terrane by mid-Cretaceous times.

The Strandja Massif forms part of the large crystalline terrane in the southern Balkans, which also includes the Rhodope and Serbo-Macedonian massifs (Fig. 2.5.2). It is a composite orogenic belt

deformed and regionally metamorphosed during the Late Variscan (high-amphibolite facies with granitoid intrusions) and Late Jurassic - Early Cretaceous (greenschist facies) orogeneses (Okay *et al.*, 2001). The basement is made up of predominantly quartzofeldspathic gneisses intruded by Late Carboniferous and Early Permian (257 ± 6 Ma) granitoids (Okay *et al.,* 2001; Sunal *et al.*, 2006). The basement lithologies form a belt about 20 km wide extending from Bulgaria to Çatalca near İstanbul.

A sedimentary sequence of Triassic and Jurassic age lies unconformably on the Variscan basement. The Triassic series resembles the Germanic Triassic facies, with a thick sequence of Lower Triassic continental clastic rocks overlain by middle Triassic shallow marine carbonates (Hagdorn and Göncüoğlu, 2007). At around the Jurassic-Cretaceous boundary (150-155 Ma). The Strandja Massif underwent a second phase of deformation and metamorphism involving north - to northeast vergent thrusting (Okay *et al.*, 2001). Following this mid-Mesozoic orogeny, the metamorphic rocks were exhumed and then were unconformably overlain by mid Cretaceous (Cenomanian) shallow marine sandstones. In the Strandja Massif, the Late Cretaceous magmatism also produced large number of andesitic dykes, sills, small intrusions and the Demirciköy pluton with an age of ca. 78 Ma (Moore *et al.*, 1980).

The İstanbul terrane is a continental fragment 400 km long and 55 km wide on the southwestern margin of the Black Sea (Okay, 2008) (Fig. 2.5.2). It consists of a Precambrian basement and unconformably overlying Ordovician to Eocene sediments with numerous unconformities (Aydin *et al.*, 1986; Görür *et al.*, 1997; Dean *et al.*, 2000). The Precambrian basement is characterized by gneiss, amphibolite, metavolcanic rocks, meta-ophiolite and voluminous Late Precambrian granitoids (Chen *et al.*, 2002; Yiğitbaş and Yilmaz *et al.*, 1996; Ustaömer *et al.*, 2005).

The Palaeozoic rocks were deformed by folding and thrusting during the Carboniferous and are overlain unconformably by a Triassic sedimentary sequence. The Triassic series is well developed east of Istanbul and shows a typical transgressive development starting with red sandstones with basaltic lava flows, passing up into shallow marine and then into deep marine limestones and ending with Upper Triassic deep- sea sandstones and shales. In the western part of the Istanbul Zone, the Jurassic and Lower Cretaceous sequences are absent, and the Palaeozoic and Triassic rocks are unconformably overlain by Upper Cretaceous-Palaeocene clastic, carbonate and volcanic rocks. In contrast, there is a thick Middle Jurassic to Eocene succession marked by small unconformities in the eastern part of the Istanbul Zone.

The Istanbul terrane is separated from the Sakarya terrane by the Intra-Pontide suture marking the trace of the Intra-Pontide Ocean (Şengör and Yılmaz 1981). During the Carboniferous, the Intra-Pontide ocean probably formed the eastern extension of the Rheic Ocean (Okay *et al.*, 2006); it closed following the collision of the Istanbul and Sakarya terranes in the mid-Carboniferous. The different Mesozoic stratigraphies of the Istanbul and Sakarya terranes suggest that the Intra-Pontide Ocean reopened during the Triassic only to close again in the mid-Cretaceous (Okay, 2008).

The Sakarya terrane forms an elongate crustal ribbon extending from the Aegean in the west to the Eastern Pontides in the east (Okay, 2008) (Fig. 2.5.2). It consists of unmetamorphosed to variably metamorphosed rocks (mainly to greenschist facies) formed during the Late Paleozoic and the latest Triassic, intensely deformed and imbricated basement, and Jurassic to Tertiary clastic and carbonate cover rocks (Genç and Yilmaz, 1995; Yilmaz *et al.*, 1995; Elmas, 1996b; Okay and Monie, 1997). The most southerly of these zones, the Sakarya, is juxtaposed with the Anatolides along the main Neotethyan

suture zone, the Izmir-Ankara-Erzincan zone (IAEZ) (Rojay and Altiner, 1998; Göncüoglu *et al.*, 2000; Okay, 2000; Kozur *et al.*, 2000) (Fig. 2.5.3).

In contrast to the Istanbul terrane, the sedimentary sequence starts with Lower Jurassic sandstones, which rest on a complex basement. The crystalline basement of the Sakarya terrane can be broadly divided into three types (Fig. 2.5.3):

1) A high-grade Variscan metamorphic sequence of gneiss, amphibolite, marble and scarce metaperidotite (Topuz *et al.*, 2004; 2007; Okay *et al.*, 2006);
2) Palaeozoic granitoids with Devonian, Carboniferous or Permian of ages crystallization (Delaloye and Bingöl 2000; Okay *et al.*, 2002; 2006; Topuz *et al.*, 2007);
3) A low-grade metamorphic complex (the lower Karakaya Complex) dominated by Permo-Triassic metabasite with lesser amounts of marble and phyllite (Topuz *et al.*, 2007).

The Late Triassic – Early Jurassic deformation and metamorphism in the Sakarya terrane are referred to as the Cimmeride orogeny, as a result of which accretion of oceanic fragments to an active continental margin resulted in brief periods of localised deformation. In the latest Triassic and earliest Jurassic, a large oceanic plateau or large number of oceanic islands were accreted to the southern margin of the Laurasia (Pickett and Robertson 1996; Okay 2000). This accreted mafic crust, which comprises late Triassic eclogite and blueschist, along with earlier accreted trench sediments, constitute the Karakaya Complex of the Sakarya terrane (Okay, 2008) (Fig. 2.5.3).

The three Pontic terranes were amalgamated into a single plate in the mid-Cretaceous following the closure of the Intra-Pontide ocean and the opening of the Black Sea. Recent isotopic data from the eclogites and blueschists in the Central Pontides indicate that the Neo-Tethys was already subducting under the Pontides in the Early

Cretaceous (ca. 105 Ma) (Okay *et al.*, 2006). However, the magmatic arc started to develop only in the Late Cretaceous (Turonian, ca. 90 Ma) (Robinson *et al.*, 1995; Okay and Şahintürk 1997). The Upper Cretaceous magmatic arc can be traced along the Black Sea coast from Georgia to the Sredna Gora in Bulgaria.

The collision between the Pontides and the Anatolides-Taurides were delayed during the Late Palaeocene - Early Eocene. The collision was followed by uplift and extensive erosion. A new cycle of deposition and volcanism started in the Middle Eocene, which was probably related to extension associated with the opening of the Eastern Black Sea basin. The sea finally left the Pontides by the end of the Eocene, and the region has been a land area since the Oligocene (Okay, 2008).

The Anatolides and the Taurides to the south are usually treated together and, therefore, are termed the Anatolide-Tauride platform (TAP) (Sengör and Yilmaz, 1981). The Anatolide-Tauride terrane forms the bulk of the southern Turkey; in contrast to the Pontic continental fragments, it shows a Palaeozoic stratigraphy similar to the Arabian Platform, including common glacial deposits of Late Ordovician age (Monod *et al.*, 2003).

During the episodes of obduction, subduction and continental collision in the Late Cretaceous and Palaeocene, the Anatolide - Tauride terrane was in the footwall position and therefore underwent much stronger Alpine deformation and regional metamorphism than that observed in the Pontic zones. During the mid-Cretaceous, a very large body of ophiolite and underlying tectonic slices of ophiolitic mélange were emplaced over the Anatolide-Tauride terrane. The northern margin of the Anatolide-Tauride terrane underwent HP-LT metamorphism at depths exceeding 70 km under this oceanic thrust sheet.

The different types and ages of Alpine metamorphism lead to subdivision of the Anatolide Taurides into zones with different

metamorphic features, in a similar manner to the subdivision of the Western Alps into Helvetics and Penninic zones. There are three main regional metamorphic zones in the Anatolide- Taurides in the western Anatolia:

1) Tavsanli zone in the north, a belt of deformed volcano-sedimentary rocks affected by HP-LT metamorphism during the Campanian (Harris *et al.*, 1994; Okay, 1984; Sherlock *et al.*, 1999);
2) Afyon zone in the center, a Paleozoic (Devonian-Permian) to Mesozoic (Triassic-Maastrichtian) sedimentary sequence consisting mainly of metaclastic rocks and thick platform carbonates with rare metabasites, metamorphosed to the greenschist facies during Paleocene time (Özcan *et al.*, 1988; Okay, 1984; Göncüoglu *et al.*, 1996-1997);
3) Menderes Massif in the south. To the northwest of Menderes Massif there is a belt of chaotically deformed uppermost Cretaceous-Palaeocene flysch with Triassic to Cretaceous limestone blocks. The Bornova flysch zone is a chaotically deformed belt consisting of large (kilometer-scale) uppermost Triassic to Cretaceous limestone blocks within a highly tectonized and intensely sheared matrix of Maastrichtian Paleocene graywacke-shale alternations (Erdogan, 1990; Okay *et al.*, 1996) (Fig. 2.5.2).

Although the Anatolide-Tauride terrane shows a variety of metamorphic, structural and stratigraphic features, there are some stratigraphic elements common to all of these zones, which distinguish the Anatolide-Tauride terrane as a single palaeogeographic entity. These elements are: a late Precambrian crystalline basement, a mixed clastic-carbonate Palaeozoic succession, and a thick Upper Triassic to Upper Cretaceous carbonate sequence (Okay, 2008).

The Afyon Zone occupies the region between the Menderes Massif and the Tavşanlı Zone (Fig. 2.5.2). It exhibits the typical Tauride

stratigraphy with a mixed carbonate-clastic Palaeozoic series overlain by Mesozoic marbles but shows a low medium to high pressure metamorphism characterized by extensive occurrences of carpholite and local sodic amphibole (Candan *et al.*, 2005). The metamorphic rocks are tectonically overlain by an ophiolitic melange and by ophiolites. The age of regional metamorphism is not analytically determined but is stratigraphically constrained as latest Cretaceous to Palaeocene.

Southeast Anatolia forms the northernmost extension of the Arabian Platform. During the Mesozoic and Tertiary, the Arabian Platform was separated from the Anatolide-Taurides by the southern branch of the Neo-Tethys, which today is represented by the Assyrian suture (Şengör and Yılmaz, 1981). The Arabian Platform has a Pan-African crystalline basement overlain by a Palaeozoic to Tertiary sedimentary sequence. In most areas of the southeast Anatolia, only the Cretaceous and younger deposits crop out on the surface. The lower parts the sequence are exposed in several anticlines (Rigo de Righi and Cortesini, 1964). These include the Amanos mountains west of Gaziantep, the Derik and Hazro anticlines south and north of Diyarbakır respectively, and the Zap anticlines south of Hakkari. In the Zap anticline between Hakkari and Çukurca the Cambrian to Carboniferous sequence is dominated by clastic rocks, whereas the Permian to Eocene sequence consists largely of shallow marine carbonates (Perinçek, 1990).

During the Late Cretaceous and Tertiary, ophiolites, ophiolitic melanges and thrust sheets were emplaced over the Arabian Platform, which are denoted as the “Lower Nappe”. This was part of an extensive emplacement of the oceanic lithosphere over the continent extending from Antakya on the Mediterranean coast to Oman in Arabia. The continental collision with the Anatolides-Taurides occurred later during the Miocene, when a second set of allochthonous units

including the Bitlis Massif and the underlying mélange units were emplaced over the Arabian Platform. Three important allochthonous units are mapped over large areas south of the Bitlis Massif:

1) The Hakkari and Maden Complexes;
2) The Yüksekova Complex.

By the end of the Oligocene, most of the Anatolian terranes were amalgamated into a single landmass. The only exception was a narrow seaway between the Arabian Platform and the Anatolides-Taurides in southeast Anatolia. The Miocene collision between Arabian and the Anatolian plates (Şengör *et al.*, 1985; Yılmaz 1993; Robertson and Grasso 1995) eliminated this last vestige of the intact oceanic crust in Anatolia. This ushered in a new tectonic era in Turkey characterized by continental sedimentation and widespread calc-alkaline magmatism. The tectonic regime in this new phase was dominated by extension and strike-slip faulting. During the Miocene most of western and central Anatolia was the site of large lakes surrounded by swamps. Sediments to the lakes were supplied by nearby volcanoes and by uplifted ranges of older sedimentary and metamorphic rocks. The subsiding lakes were filled by a sequence of sandstone, shale, limestone, tuff, basalt and andesite. The magmatism was initially cal-alkaline with a magma composition ranging from basaltic andesite to rhyolite (Aldanmaz *et al.*, 2000; Yılmaz *et al.*, 2001). In the Late Miocene, it switched to alkaline with the generation of minor amounts of alkali basalts. The Neogene continental deposits of western Turkey comprise the world's largest borate reserves (Helvacı, 1995), as well as rich deposits of sodium sulfate, lignite and clay. The tectonic regime during the Neogene was characterized by extension and strike-slip faulting. Large low-extension faulting was creating space for the Miocene basins as well as exhuming deeply buried crystalline rocks. Recent studies have shown that some of the crystalline complexes of western Anatolia, such as the Kazdağ or Simav massifs, were exhumed

at the footwall of large low-angle normal faults (Okay and Satır, 2000; Işık *et al.*, 2004). The underlying cause of the regional extension was the southward migration of the Hellenic trench, which also led to the opening of the Aegean Sea as a back-arc basin.

The grand structure of the neotectonic phase is without doubt the North Anatolian Fault, a right-lateral strike-slip fault which extends for 1200 km from the eastern Anatolia into the Aegean Sea (Barka, 1992; Şengör *et al.*, 2005). The classical view is that the North Anatolian Fault was initiated as an escape structure following the Miocene collision between the Arabian and Anatolian plates. However, recent studies have shown that right lateral strike-slip faults with cumulative offsets of 100 km or more existed during the Oligocene in western Anatolia (Zattin *et al.*, 2005; Uysal *et al.*, 2006; Okay *et al.*, 2008). These structures were transporting continental crustal fragments into the north-south extending Aegean region, suggesting that the underlying cause of the westward translation of Anatolia was, and is still, the pull of the Hellenic subduction zone rather than the push of the Arabian Plate.

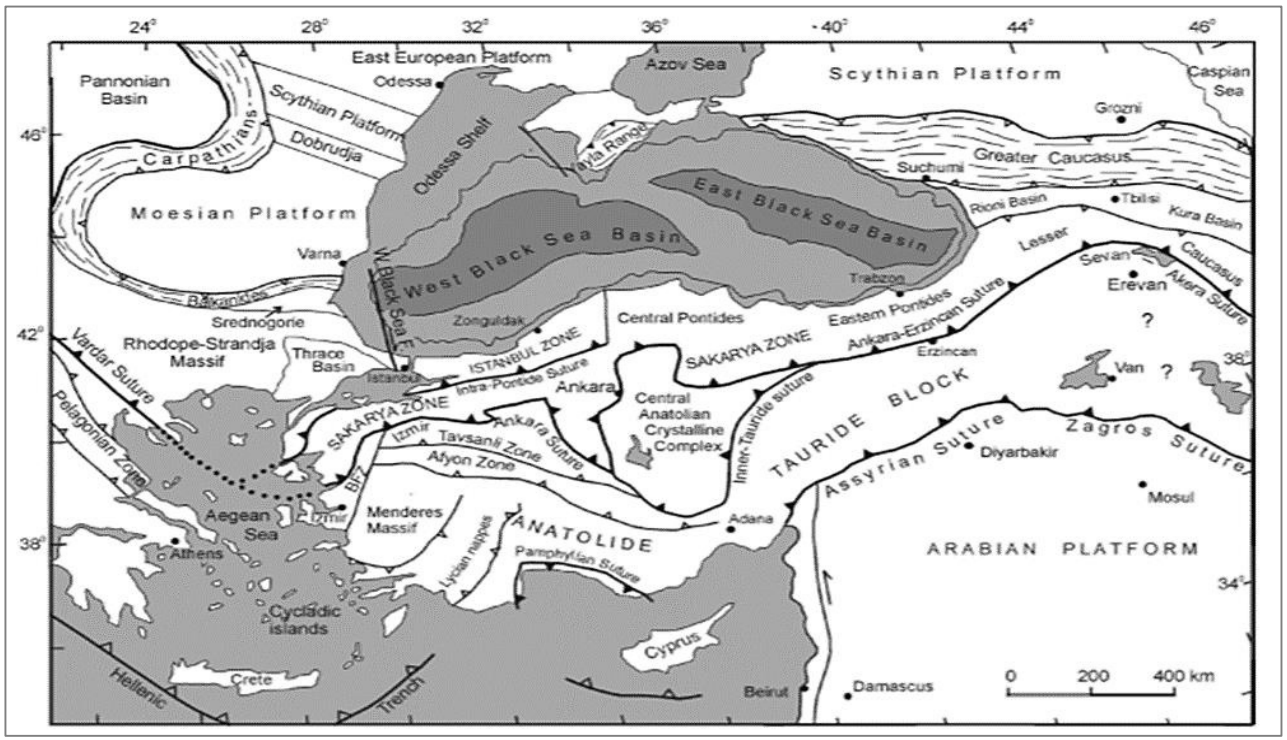

Fig. 2.5.2: Tectonic map of the northeastern Mediterranean region showing the major sutures and continental blocks. Sutures are shown by heavy lines with the polarity of former subduction zones indicated by filled triangles. Heavy lines with open triangles represent active subduction zones. The Late Cretaceous oceanic crust in the Black Sea is shown by grey tones. Small open triangles indicate the vergence of the major fold-and-thrust belts. BFZ denotes the Bornova Flysch Zone (modified after Okay & Tüysüz 1999).

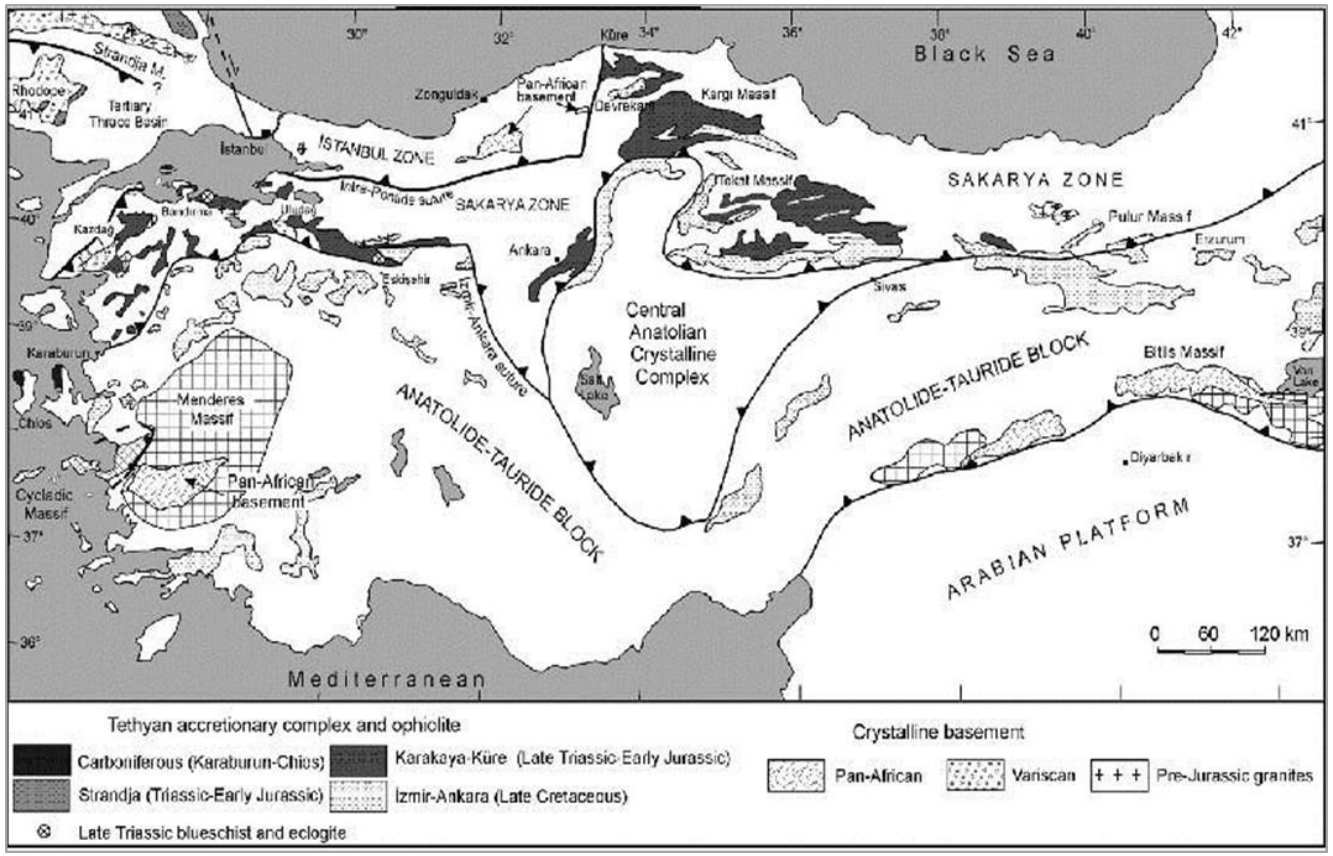

Fig. 2.5.3: Distribution of different basement types and accretionary complexes in Turkey (modified from Okay *et al.,* 2006).

2.5.1 Proconnesos

The Marmara Island (formerly called Proconessos Island) is located in the Marmara region, NW Turkey, along the western extension of the North Anatolian Fault (NAF), which reaches the Marmara Sea (Ates *et al.*, 2003). The island is located in the southwestern part of the Marmara Sea, a marine basin 275 km long and 80 km wide, in northwestern Turkey, that connects the Aegean Sea with the Black Sea (Attanasio *et al.,* 2008a).

The Marmara Sea can be regarded as the southeasterly extension of the Thrace Basin (Ergun and Ozel, 1995), which is a Tertiary basin where significant subsidence took place during the Middle Eocene (Doust and Arıkan, 1974).

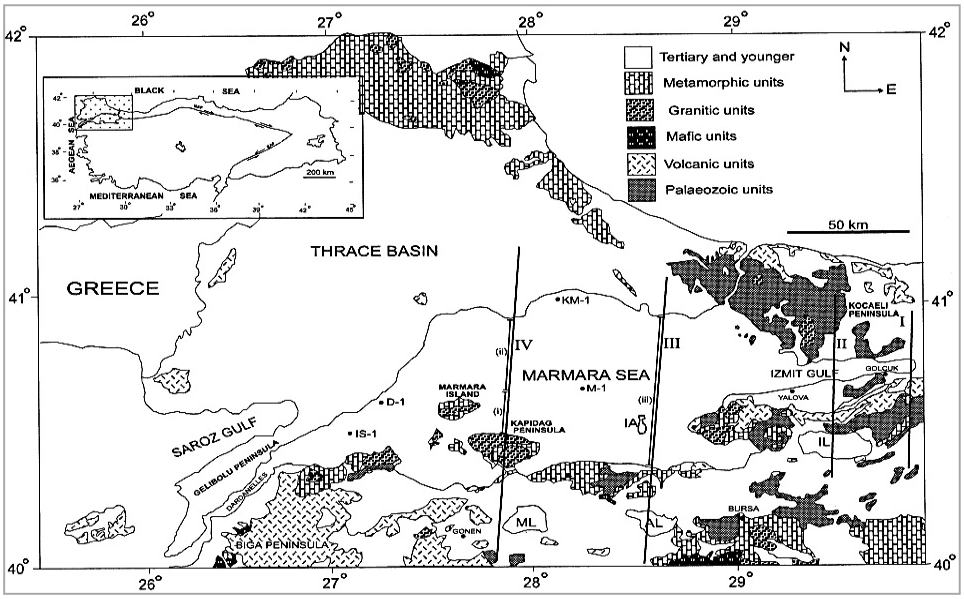

Fig 2.5.1.1: Simplified geological map of the Marmara region (Erentoz and Pamir, 1964). Profiles I through IV are explained in the text. Lines from i to iii show the extension of the Bouguer anomaly profiles obtained during seismic acquisitions. ML: Manyas Lake, AL: Apolyan Lake, IL: Iznik Lake, IA: Imralı Island, IS-1: Isıklar-1 borehole, D-1: Doluca-1 borehole, KM-1: Kuzey Marmara-1 borehole, M-1: Marmara-1 borehole.

The Thrace Basin was filled with Eocene to Lower Miocene sedimentary rocks (Turgut *et al.*, 1991).

The extension of these formations on the offshore is revealed by the Kuzey Marmara-1 (KM-1) petroleum borehole (Fig. 2.5.1.1). The northern coastal region of the Marmara Sea consists of Upper Miocene continental to lagoonal sediments which lie unconformably over the Middle Eocene and Palaeozoic formations (Okay *et al.*, 2000). Palaeozoic rocks consisting of thick sedimentary sequences extend to the Bosphorus and the Kocaeli Peninsula (Gorur *et al.*, 1997). However, the nature of the deep geologic strata in the Marmara Sea is not well known owing the lack of deep boreholes in the region. The existing boreholes in the Marmara Sea (Fig. 2.5.1.1) reach the Cretaceous and Palaeozoic overlain by the Cenozoic deposits, but they provide little information about the Pre-Tertiary formations because they stop immediately below the Tertiary units.

Nevertheless, Marmara Island, along with the Kapıdağ Peninsula and the other smaller islands on the south side of the Sea of Marmara, from part of a geologically distinctive area. A geological map of the Marmara region simplified from Erentoz and Pamir (1964) (Fig. 2.5.1.2) reveals granitic intrusions and metamorphic units on the Marmara Island. These crystalline rocks are associated with the Middle Jurassic tectonism (Wong *et al.*, 1990).

The metamorphic rocks have undergone progressive regional metamorphism under MP-HT conditions and various phases of deformation during Palaeozoic orogenesis (Aksoy, 1996). The metamorphic sequences have been intruded by Palaeogene calc-alkaline granitoids (Aksoy, 1995) as part of the magmatism that occurred during the Alpine orogeny. Petrographically, it consists of dioritic and granodioritic gneisses, commonly cut by aplite veins.

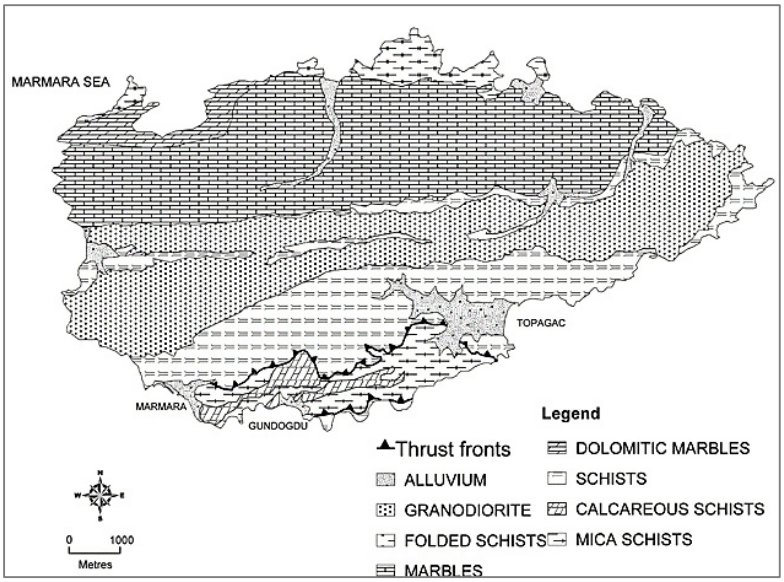

Fig. 2.5.1.2: Satellite image and geologic map of the island of Marmara. The main quarrying area around the village of Saraylar and the smaller quarries along the north-western coast are clearly visible (MDA Earthsat 1999, Earth Scan Lab) (Attanasio *et al.,* 2008).

The lower unit (Fig. 2.5.1.3) consists of the Erdek complex at the top, petrographically made of metaserpentinite, metagabbros, metabasalts and amphibolites, and the Gundogdu complex at the bottom, made of calcschists, micaschists and recrystallized carbonates (Lisans 2002). Both outcrop extensively in the south of Marmara Island. The upper unit constitutes the top Saraylar complex of metamorphosed limestone and dolomite (Lisans, 2002), that form the north-island indented coastline, and the marble formation, mainly made of coarse-grained calcitic carbonate, rarely white but in general characterized by grey stripes, which makes the Proconnesian marbles so distinctive. These marbles outcrop in the north of the island and are in tectonic contact in some cases with the schists of the lower unit, but extensively with the calc-alkaline intrusion that outcrops along the east–west direction and divides geographically the rock units of Marmara (Attansio *et al.*, 2008a) (Fig. 2.5.1.3).

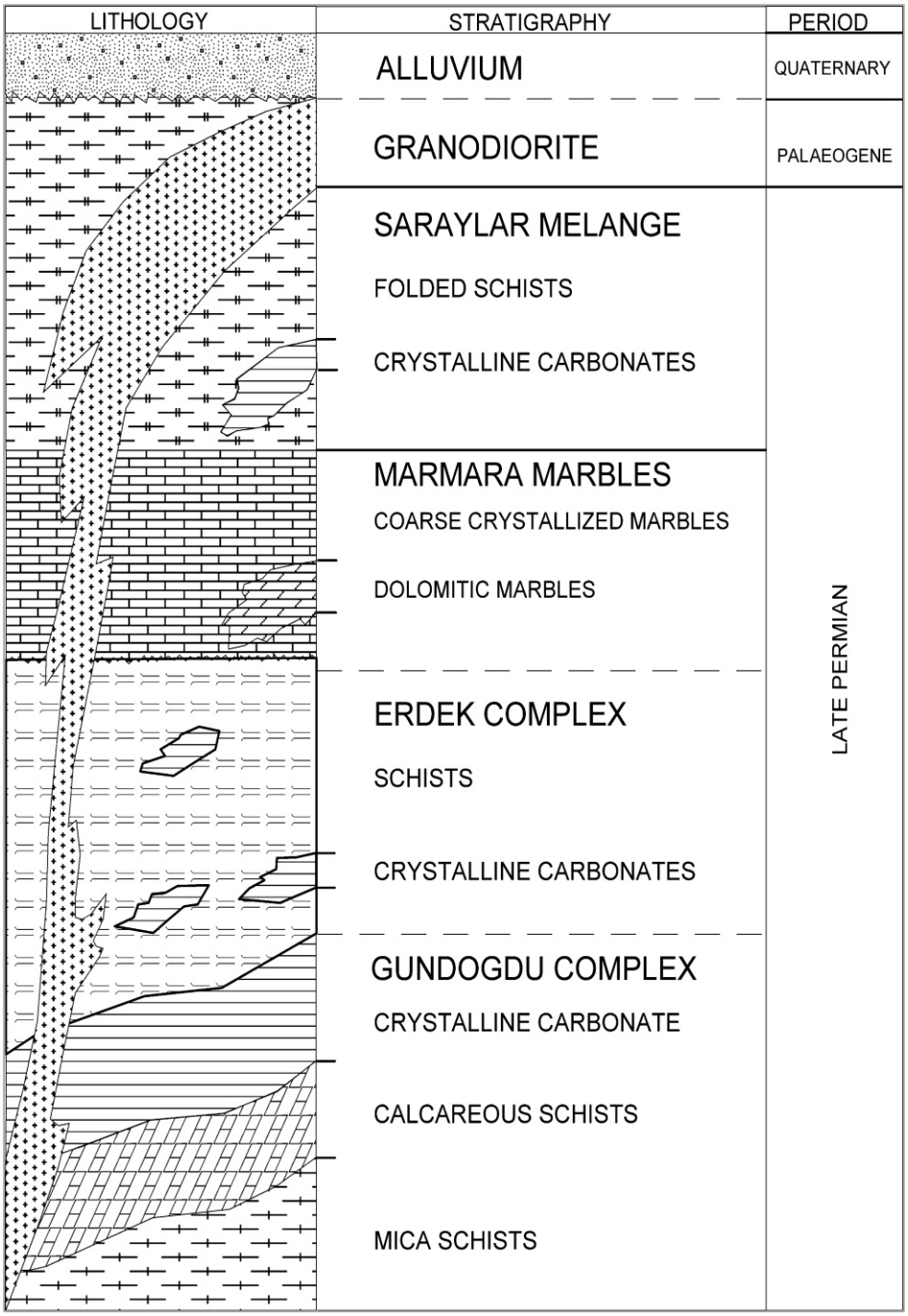

Fig. 2.5.1.3: Schematic presentation of tectonostratigraphic units and stratigraphic complexes on the island of Marmara (Attanasio *et al.*, 2008a).

Chapter 3

Materials and Methods

3.1 Geological samples

In the past, the historic quarries discussed in this Ph.D. thesis have been subject to extensive and detailed research and survey (*e.g.,* Gorgoni *et al.,* 2002; Attanasio, 2003; Lazzarini, 2004; Attanasio *et al.,* 2006; Antonelli and Lazzarini, 2015). The historical, archaeological, geological and technical aspects of these varieties of white marble, exploited since the 5th millennium BC, having been studied extensively, and in this section, the features of all the ancient quarries analyzed are presented.

The geological samples were sampled in the main districts of:

- Italy (Carrara);
- Greece (Naxos, Thassos, Paros and Pentelicon);
- Turkey (Afyon, Thiountas, Göktepe and Proconnesos).

The samples were collected from standing rock walls, both from natural outcrops and from quarry walls. Only fresh rocks were collected. The sample size was generally larger than 2 cm^3. All the geological samples belong to the collection of the University La Sapienza of the Sapienza University of Rome and IGAG-CNR of Rome (Table 3.1).

Fig. 3.1.1: Samples of Pentelic white marble.

In this section, a brief description of the exploited areas and updated information have been considered useful. The quarries descriptions include information regarding the location, number and type of samples collected.

Table 3.1: List of samples considered in petrographic and chemical analyses.

	Districts	Quarry	Samples
Carrara	Colonnata	Gioia	G5, G6, G7, G8, G16, G17, G19, G22
		Fossacava	FO1, FO3, FO7, FO8, FO9, FO10, FO11
		Calagio	CL2, CL6
	Torano	Sponda I	TR8
Naxos			CYNA70, CYNA72, CYNA75, CYNA77, CYNA78, CYNA81
Paros			CYPA3, CYPA5, CYPA11, CYPA12, CYPA14, CYPA25, CYPA26, CYPA28, CYPA67, PAROS1
Thasos		Aliki	TA1, TA5, TA6, TA7, TA8, TA22
		Mourgena	MUOR1, MOUR5
Pentelicon	Spilià (low level)	Quarries 13-15	SML1.1, SML2.4, SML13, SML14, SML33, SML42
	Spilià (high level)	Quarries 6-8	SMH1.3, SMH1.9, SMH2.18, SMH2.21
	Kokkinaras		K3, K5, K7
	Quarry I		I1-I2
Proconnesos	Altintas Yalanci Palatya	Altintaş	PRO14, PRO15, PRO17, PRO18, PRO19, PRO22, PRO25, OC994_3
	Mandira and Çamlik	Filiz	OC 13_2, OC13_4, OC13_5, OC13_6, OC13_8, OC140_1
	Silinte Harmantaş	Ancient quarry	OBG1
Afyon	Latin quarries	Bacakale Quarry I	D2A, D9A, D11A, D14A
		Roder Quarry II	D26A, D27A, D28A, D34A, D36A, D37A
		Boluk Mermer Quarry V	D38A, D39A, D40A, D43A
		Mermer Isletmesi Quaries III and IV	D59, D62, D64, D68
Thiountas		Ancient quarry of Doğanli	T3, T6, T8, T10, T13, T17, T20
Göktepe			GT1, GT2, GT4,GT5,GT6, GT7, GT8, GT9, GT10, GT11, GT12

3.1.1 Geological samples from Carrara district

The basins of Carrara marble are one of the most excavated areas in the world, with an average density of seven quarries/km^2 (Baroni *et al.,* 2010). They are located to northeast of the city and morphologically are divided into quarrying «basins» that correspond to three valleys on the western slopes of Monte Sagro (1748 m). From east to west, these basins are known as Colonnata, Miseglia, Torano basins after the names of the valleys derived from those of villages where quarry workers lived (Fig. 3.1.1.2).

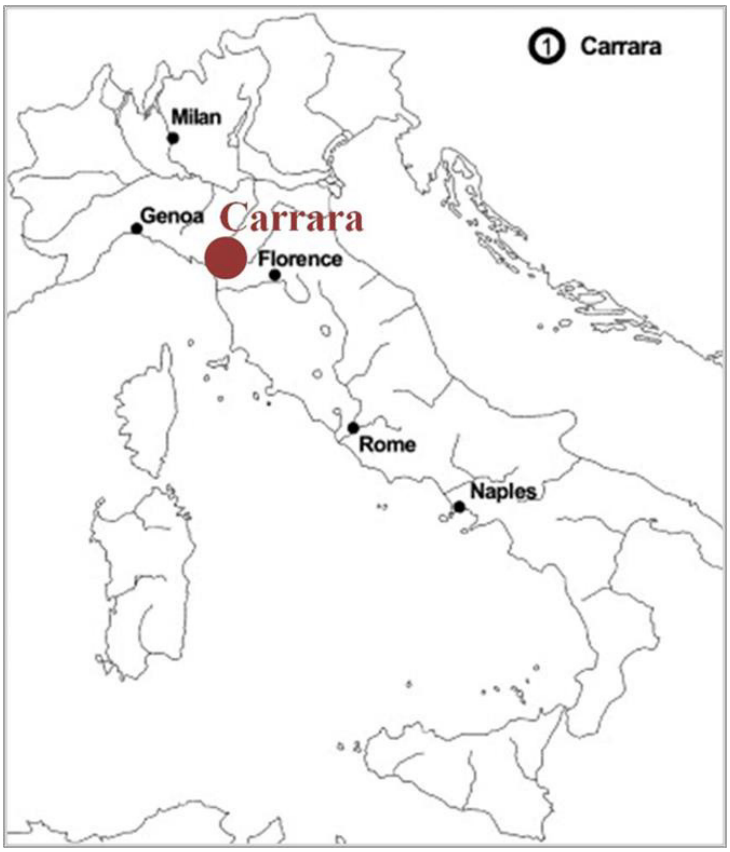

Fig. 3.1.1.1: Location of Carrara white marble districts (Capaedri *et al.*, 2004).

For the sake of clarity, many authors report the name of the fourth valley, known as the Pescina-Boccanaglia basin (Baroni *et al.,* 2010). However, the location of its exploitation and the beginning of such activity are still a subject of open debate. In the Carrara Marble Basin direct evidence of pre-Roman exploitation is not present, although this activity is testified by the occurrence of funerary sculptures (about 100 artifacts, dating back from the 6th to 3rd-2nd centuries BC) from the Etruscan settlement of Pisa and from neighboring localities (Paribeni *et al.,* 1999). Petrographic analyses of these artifacts suggest that they were produced using Carrara marble (Mannoni, 1990).

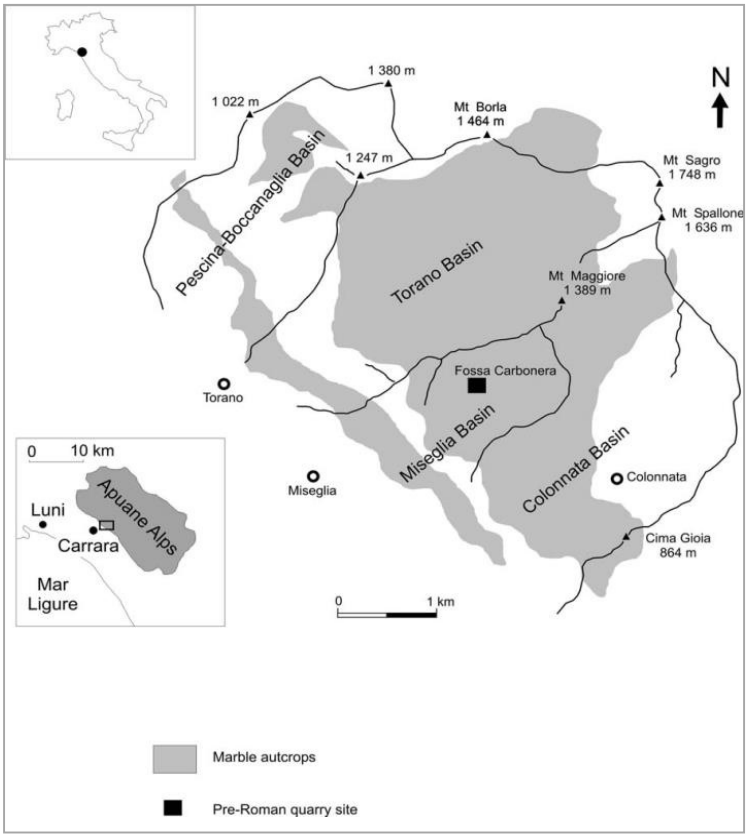

Fig.3.1.1.2: Map of the area of the Carrara quarries with the location of the four basins (Bruschi *et al.,* 2004).

For a long time, evidence concerning the beginning of marble exploitation was found at the base of marble statues in the archaeological excavation of Luni, the inscription reported ages of the past 2nd century BC. From the study of Etruscan marble artifacts, found in several localities of Northern Tuscany, emerges a quarrying activity of the marble of the Apuane Alps since pre-Roman time, even if the exact location of such exploitation is still unknown (Bonamici, 1989; Paribeni *et al.,* 1999).

On the other hand, the Roman exploitation of the Carrara Marble Basins is well known (Dolci, 1985), with abundant evidence preserved in the form of quarry cuttings, semi-manufactured stones (*e.g.,* columns and capitals) with quarry markings. Semi-manufactured items are usually found in the old ravaneti (*i.e.,* slope where debris are accumulated), progressively demolished during the modern quarrying activities.

Archaeological and literary sources document that marble exploitation started during the 2nd century BC, when the Apuane region was definitively pacified by the Romans with the subjugation of the Ligurian population. The territory then was submitted to the control of Luni, a Roman colony founded at the mouth of the Magra River in 177 BC.

Carrara marble became popular in Rome during the 1st century BC. Plinius the Elder in 48 BC was the first historian to report the use of Carrara marble in the construction of Mamurra's house. In his Naturalis Historia, Plinius speaks about the luxurious house that Mamurra, one of Caesar's commanders in Gaul, built on the Celio, and in which large columns of Luni marble were found. From the beginning of the 1st century BC to the fall of the Roman Empire, Luni marble was utilized not only in Rome and in the rest of Italy, but also in other parts of the Empire such as Gaul and the African provinces (Attanasio, 2003).

The exploitation activity is well documented until the 3rd century AD; extensive exploitation probably decreased during the following centuries and stopped during the 7th century AD (Dolci, 1985). A moderate resumption of marble exploitation is known from the 12th century, but a great revival occurred during the Renaissance (Klapisch-Zuber, 1973). Many authors report that the resumption of the exploitation started when Michelangelo was invited to visit the area by Pope Leo X, and opened the first quarry, Finocchiaja, on Monte della Cappella. This quarry was utilized on a regular basis for a number of decades by the Medici family of Florence, and then was abandoned again. It was reopened in the first half of the 19th century, and some quarries are still functioning today (Bruschi *et al.*, 2004). A period of particularly intense exploitation was during the 19th century, when the widespread use of explosives meant that up to 90% of the material that was quarried was rejected (Zaccagna, 1905).

For this reason, the rejected debris dispersed along the slopes below the quarries, locally named *ravaneto* (which means debris), and became a dominant element in the landscape of the Carrara quarries. The invasive extraction techniques were progressively abandoned, beginning in 1900 with the introduction of mechanical systems of marble cutting (*e.g.,* helicoidal iron wire) that limited the impact on the slopes and reduced the volume of rejected material (Bradley, 1991; Pandolfi and Pandolfi, 2003).

Marble production in the second half of the 19th century was less than 100,000 tonnes per year (Zaccagna, 1905), and marble was extracted from only a few dozen active quarries. Today, there are 78 active quarries, 68 of which are open-air, and ten of which are underground (Baroni *et al.,* 2010).

In conclusion, in terms of quantity and quality of production, the marble site of Carrara is certainly one of the greatest of the ancient age and still maintains this importance.

3.1.2 Geological samples from Greek quarries

Cycladic marbles, extracted mainly from the islands of Naxos and Paros, were the first to have been utilized in the Greek world, playing an important role in the development of working techniques and evolution of Greek sculpture and architecture.

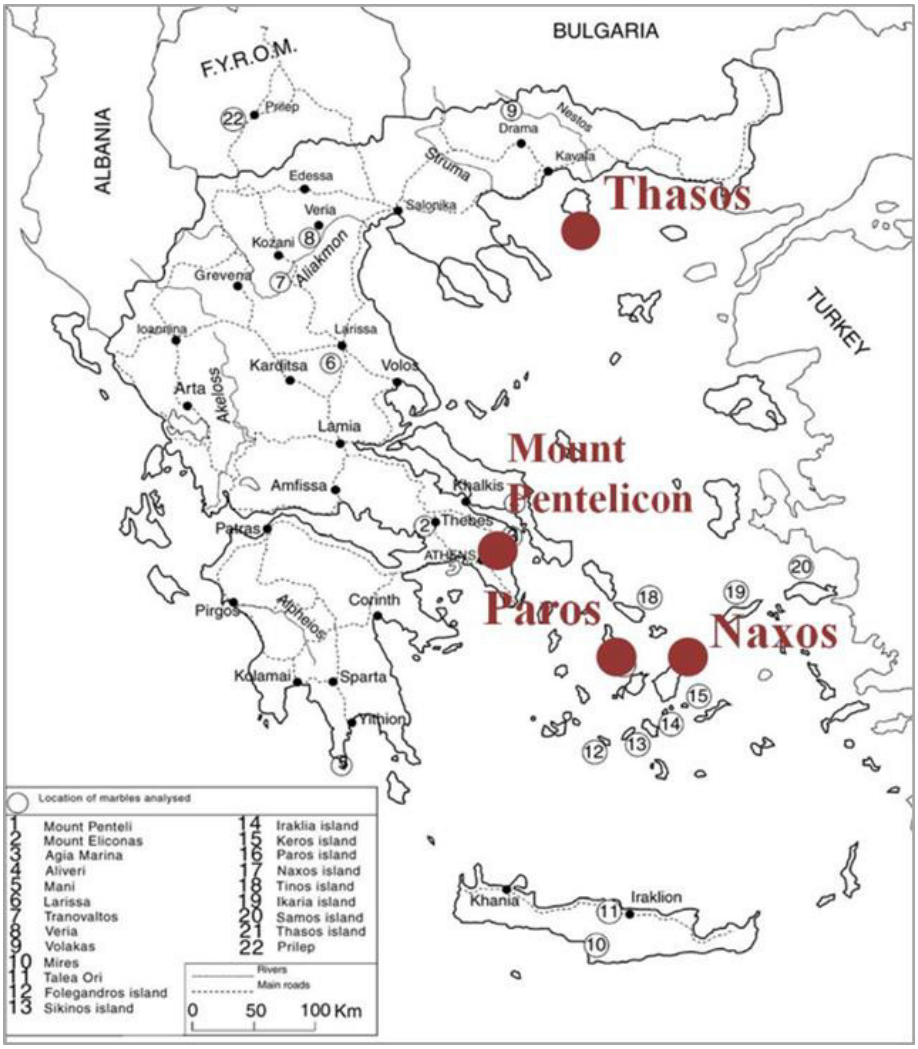

Fig.3.1.2.1: Location of Greek white marble quarries analysed (Capaedri *et al.*, 2004)

3.1.2.1 Naxos

The quarries of white marble on Naxos are mostly located in the central and northern parts of the island, especially towards the center of the island, where the purest white material was available. The regions are Melanes, Kinidaros, Apiranthos and Apollonas (Attanasio, 2003) (Fig. 3.1.2.1.1).

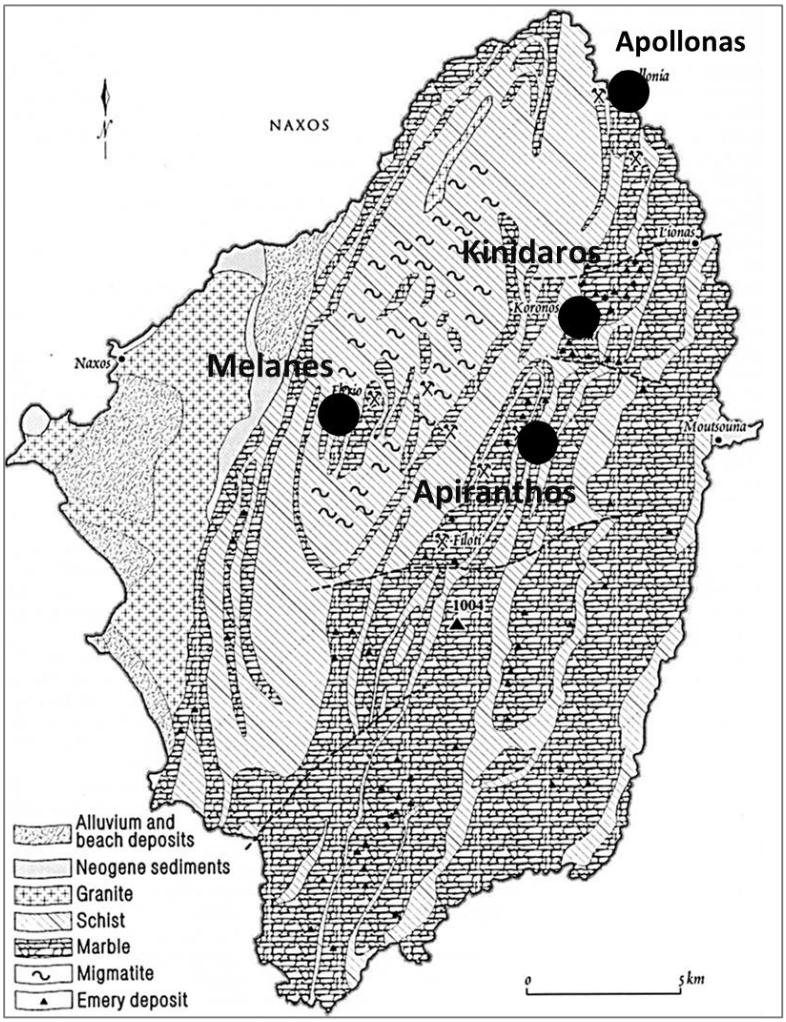

Fig. 3.1.2.1.1: Location of the quarry sites on Naxos Island (Higgins and Higgins 1996).

The main quarries were exploited since prehistoric times in a holy context (Lazzarini *et al.*, 1980b) and the first examples of figurines in marble date back to the late Neolithic period (about 4500 BC). The famous figurines of the Cycladic culture occur also in Crete and on the Greek mainland.

In the 7th century BC, the earliest large format of Greek statue was created on Naxos, and in the 6th century BC, the "Oikos of the Naxians", the first early Archaic building of religious cult on the island of Delos, had a roof of Naxian marble.

Starting from its birthplace and experimental field on the islands, Cycladic marble architecture has decisively influenced the development of the classical architecture on Attic mainland and Athens (Germann *et al.*, 1988).

Things changed in the Roman epoch, when Naxos marble, in contrast to marble from Paros, was not held in high esteem and was rarely used; as a matter of fact, it is not included in Pliny's inventory. The importance of this marble remained within Greece, and its use influenced the Archaic epoch (Attanasio, 2003).

Besides, there were also other operations in close proximity to the quarries. Findings from archaeological research indicate that near the quarries lived and prospered small societies of miners, craftsmen, and sculptors. The extracted marble was processed in workshops very near to the quarry before it was shipped to its destination (Kaliampakos and Mavrikos, 2006).

Nowadays, over approximately 300 marble quarries are currently in operation, whereas the total number of companies involved either with marble production or processing exceeds 4,500. Mainly, the modern quarries are located to the south of Kinidaros, at an altitude of several hundred meters above sea level (Kaliampakos and Mavrikos, 2006; Attanasio, 2003).

3.1.2.2 Paros

White marble from Paros Island played a great role in the Archaic epoch, similar to the other Cycladic marble, especially the Naxos marble. Parian marble was famous throughout the Greek world, and it is much renowned and has continuously consolidated and increased its reputation with time. Over the centuries, it became the white statuary marble for excellence (Attanasio, 2003).

The most important quarries on Paros are located, as for naxian sites, in the center and northern parts of the island, near Marathy, a few kilometers from the capital Paroikia (Fig. 3.1.2.2.1). The quarries are located in the two small valleys of Chorodaki and Stefani, on the slopes of Mount Marpissa.

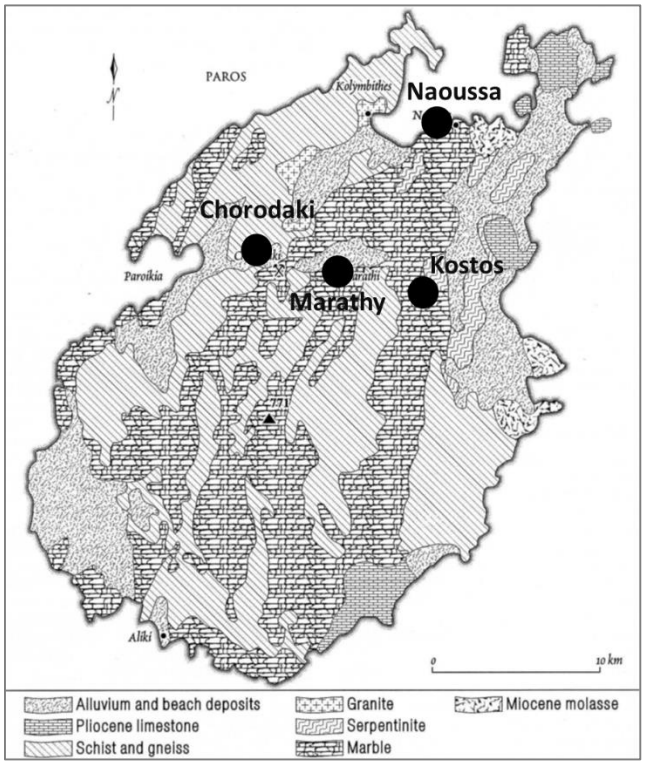

Fig. 3.1.2.2.1: Marble quarries on Paros Island (Higgins and Higgins, 1996).

On the western side of the valley, three quarries are visible, and open like amphitheatres (Fig. 3.1.2.2.2a); on the right side of the valley, there are at least four main quarries (Attanasio, 2003). They are dug into the side of the mountain, like small caves, and they extend underground at an angle of 35° for about 200 metres (Higgins and Higgins, 1996) (Fig. 3.1.2.2.2b).

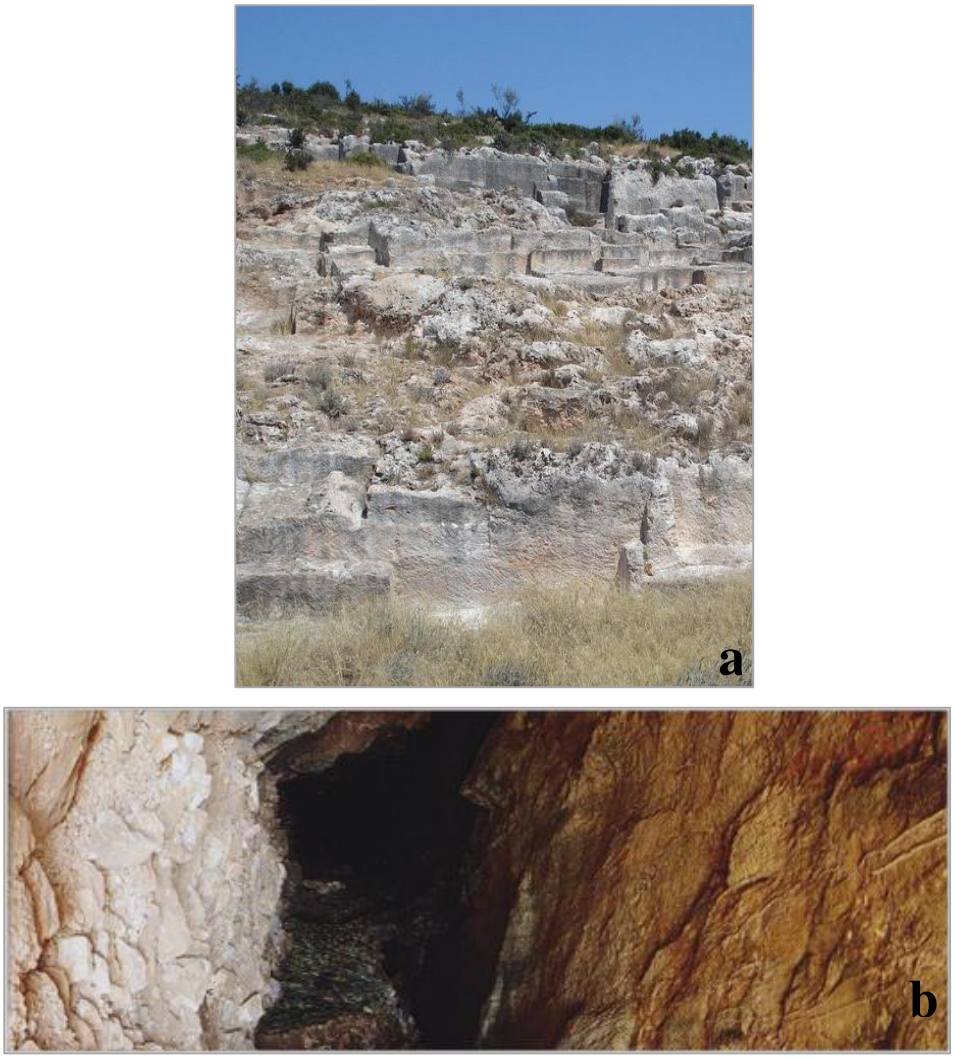

Fig. 3.1.2.2.2: a) Ancient quarry of Kleonon (http://www.greece.com/); b) Underground marble quarry, Paros (Zapheiropoulou, 1998).

Other less important sites are located near to the town of Naoussa and Kostos.

Different varieties of marbles are exploited on Paros, and the most highly esteemed is still known as Lychnites, because, as affirmed by Plinius, it was quarried in the light of a lamp (lychnos).

Parian marble, utilized since the Cycladic epoch, was soon exported to whole of the Greek world and beyond (Attanasio, 2003).

Exploitation of the marble sources on Paros and Naxos began in earnest in the 7th century BC, with the quarrying and export of large rectangular blocks to locations throughout the Aegean (Herz, 2000). By the 6th century BC, the sources of Parian lychnites had been appreciated across the Mediterranean area owing to its fine and uniform grain-size and multidirectional translucence. The demand for and economic gain from this type of marble were strong enough to sustain mining activity throughout Roman times, despite the extreme danger associated with quarrying in underground mines (Herz, 2000).

Schilardi *et al.* (2000) cited the Parian contribution to the Athenian League, which was twice that of its larger neighbor Naxos, as evidence that the revenues from the quarries were key to the economic prosperity of Paros. The authors suggested that the greatest economic evolution coincided with the greatest affluence of the island in the late 6th to early 5th century BC (Schilardi and Katsonopoulou, 2000).

Paros was also the location of the most extensive mining activity in the Cyclades during the Classical and Hellenistic periods. The wealth of Paros from the late Archaic period onward is especially visible in the construction of numerous monumental temples and altars, city walls, and harbors (Sheedy, 2000).

When Paros Island was incorporated into the Roman Empire and its quarries became Imperial property, the ownership was given to the Princeps via the Ratio Marmorum, or “Department of Marble”. The effect of this ownership was two-fold: on the practical side, it provided

a dependable and ready supply of stone for imperial construction and sculpture projects, but on the other hand it also restricted access by members of the aristocracy and impeded ostentation and competition (Pollini, 2000). This material was held in extremely high regard and used only for sculpture. Even Gnoli in his study observed that many statues of the Roman epoch have only the head in lichnite (Gnoli, 1988).

Given the quantity of known marble quarries on Paros in the Roman period and earlier, it is perhaps not surprising that there were also sculpture workshops on Paros. Several quarries of Paros, especially Spilies and Lakkoi, contained examples of partially worked artifacts, which were probably abandoned because of the defects in the stone (Schilardi *et al.,* 2000).

Some of the ancient quarries still exist, in the form of tunnels running deep into the mountainside, following the best veins.

3.1.2.3 Thasos

The Thasos Island was well known in antiquity for its white marble, known to the Romans as Marmor Thasium and to modern Italian masons as Marmo Greco Livido (Higgins and Higgins, 1996).

The peculiarity of the island is that two completely different varieties of white marble are exploited in its quarries. One of these, the more important, is the high-quality and almost pure white dolomite with medium-sized crystals; the other variety is a calcitic marble that is generally light grey in color and has large grain-size (Attanasio, 2003).

Quarries were first exploited in the 6th century BC when the temples of Thasos were constructed, and the ancient sites are all located on the east coast of the island. The earliest marble quarries were a series of small shallow pits on the westernmost peak of the Acropolis of Thasos town (Herz, 1988b; Kozelj, 1988) (Fig. 3.1.2.3.1).

Calcitic marble was exploited at Cape Phanari and Aliki sites (Fig. 3.1.2.3.1). The floors of these quarries, and many others along the coast, are presently underwater, indicating that sea level has risen since ancient times. This marble is made of very large crystals of calcite, with minor graphite coloring the grey marbles.

Aliki, on the southeastern coast, is the largest ancient quarry on the island falling among the largest quarries exploited in antiquity. By Roman times, Aliki marble was one of the most popular in the empire. Even if a rise in sea level in the 7th century AD drowned some quarries, production continued until Ottoman times.

Marble is in beds up to 300 m thick and is faintly banded (Herz, 1988b). The layers slope at about 150 towards the sea, facilitating extraction of the blocks of marble. The marble is made of calcite, with traces of graphite in the grayish bands, as well as quartz and mica.

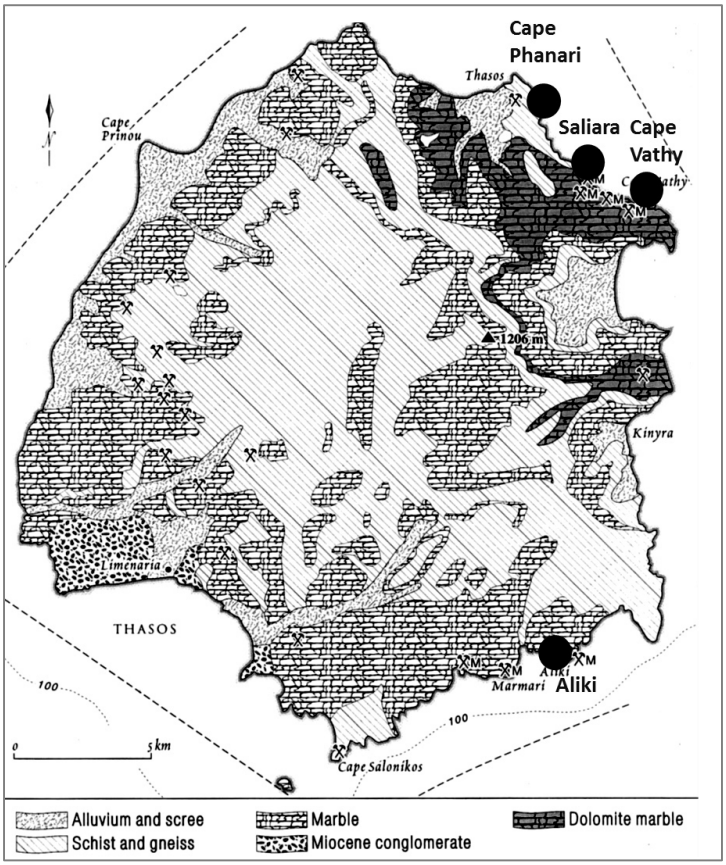

Fig. 3.1.2.3.1: Location of Thasos island and the quarry sites (Higgins and Higgins, 1996).

The dolomitic marble, instead, was exploited in the sites of Saliara and Cape Vathy, located about 10 km to the south of the capital Limenas. The ancient sites are partly destroyed by modern exploitation. Although partly submerged, some ancient quarries can be seen along the coast, containing many unfinished pieces of sculpture. The marble is made of relatively fine-grained dolomite. This is the only place in the Eastern Mediterranean where dolomitic marble was exploited in antiquity (Herz, 1988b).

Both varieties of marble, calcitic and dolomitic, were probably known from the 6th century BC, and during the same period a successful school of sculpture was established.

In the 3rd and 2nd century BC, the white marble was extensively used for new buildings in the Sanctuary at Samothrace (Higgins and Higgins, 1996).

Thasos was one of the most highly regarded sources of Greek white marble in Rome, and its quarries were part of the Imperial patrimony for a period time (Monna *et al.,* 1993); this information is not supported by all the scholars, and there are many disputes about of that (Marc, 1995). In any cases, it was economical marbles on Diocletian's edict (Giacchero, 1974), probably because it was widely available and was not valued as highly as some other varieties, such as Parian marble. There are numerous examples of the use of Thasian marble in antiquity; it was employed in numerous and very different manners, for reliefs, funeral monuments, for architectural purpose, and its use in sculpture is now documented much better (Attanasio, 2003). It was particularly in demand for sarcophagi (Higgins and Higgins, 1996).

All authors agree that the period of its greatest diffusion was in the 2nd century BC, although it continued to be exported in large quantities for at least three centuries, and it was utilized until the Byzantine epoch (Amadori *et al.,* 1998).

Nowadays, Thasos white marble is routinely exported in Europe and throughout Asia. Its main applications include sculpting, flooring, decoration and construction of monuments and buildings.

3.1.2.4 Mount Pentelicon

In classical antiquity, the quarries of Mount Pentelicon, together with those of Mount Hymettus, were the principal source of white marble in continental Greece (Attanasio, 2003).

Mount Pentelicon (1,106 m) is part of a 20-km-long sector of metamorphic rocks northeast of Athens; they are located along a crest on the southwest side of the mountain, at altitudes between 500 and 1000 metres above sea level; Mount Hymettos (1,037 m) is part of another sector of metamorphic rocks to the southeast of Athens. On both Mounts Pentelicon and Hymettos, weathering of the marble has produced a thin red soil (terra rossa) that has mostly been removed by erosion and redeposited in the valleys (Fig. 3.1.2.4.1).

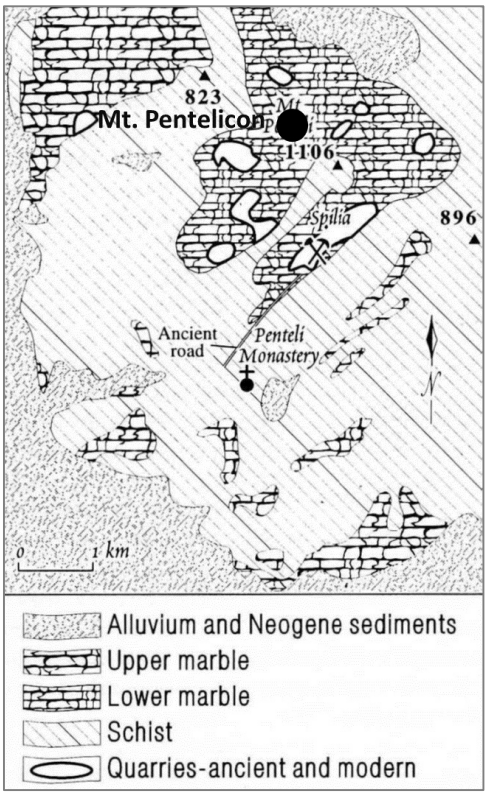

Fig. 3.1.2.4.1: Map of Mount Pentelicon (Higgins and Higgins, 1996).

Although both white and grey marble occur on both mountains, the best white marble in antiquity was obtained from Mt. Pentelicon, and the best grey from Hymettos, a fact that has led many modern scholars to refer (incorrectly) to the grey as 'Hymettan' and the white as “Pentelic”.

The precise reconstruction of the topography of Pentelic quarries is extremely difficult because excavation and destruction have taken place in subsequent epochs. In relatively recent times, however, the site has been the object of topographic studies by M. Korres (1990), and a new series of systematic sampling has led to the identification of 160 quarries, almost 30 of which show clear signs of work in the ancient times (Pike, 1999; Goette *et al.,* 1995). Quarries are located in the region of Spelia, Dionysos, Stamato Vouni, Aspra Marmare and Kokkinaras.

The existence of the quarries was already known at the beginning of the 6th century BC, but it was in the following century that the use of it became widespread, above all to supply the demand created by the impressive renewal and reconstruction projects in the age of Pericles.

The importance of the white marble from Pentelicon arises from the fact that it supplied the material for the construction of some of the most famous monuments in Athens. Its use was not confined to the famous examples of the Parthenon and the Propylaea. Other important examples include its use in the temple of Hephaestus, constructed in the same period, and in the Olympieion and the Stoá of Attalus, built is successive periods (Attanasio, 2003). It was also utilized for statues of famous sculptors as Skopas and Praxiteles.

In the Roman epoch, Pentelic marble continued to be used almost until the beginning of the 4th century AD, although it was certainly not one of the most widely used marbles in Rome, as reported by F. Corsi.

He emphasized that the quarries never became Imperial property, but they belonged to Herodes Atticus.

Even though Pentelic marble can be very pure, joints are relatively closely spaced, which restricts the maximum size of the blocks that could be extracted. This does not appear to have been a problem in classical times, but the Romans preferred to use other sources of marble for their larger pieces.

Nowadays, the modern quarries are all around the main peak of Mount Pentelicon, and have partly obliterated the ancient quarries, which lie mostly to the south of the principal summit. About 25 of them have been found situated one above the other, many linked by an ancient, paved quarry road (Pike, 1999).

3.1.3 Geological samples from Turkish quarries

The samples of Turkish white marble are from four different quarrying sites (*i.e.,* Proconnesos Island, Afyon, Thiountas and Göktepe) (Fig. 3.1.3.1).

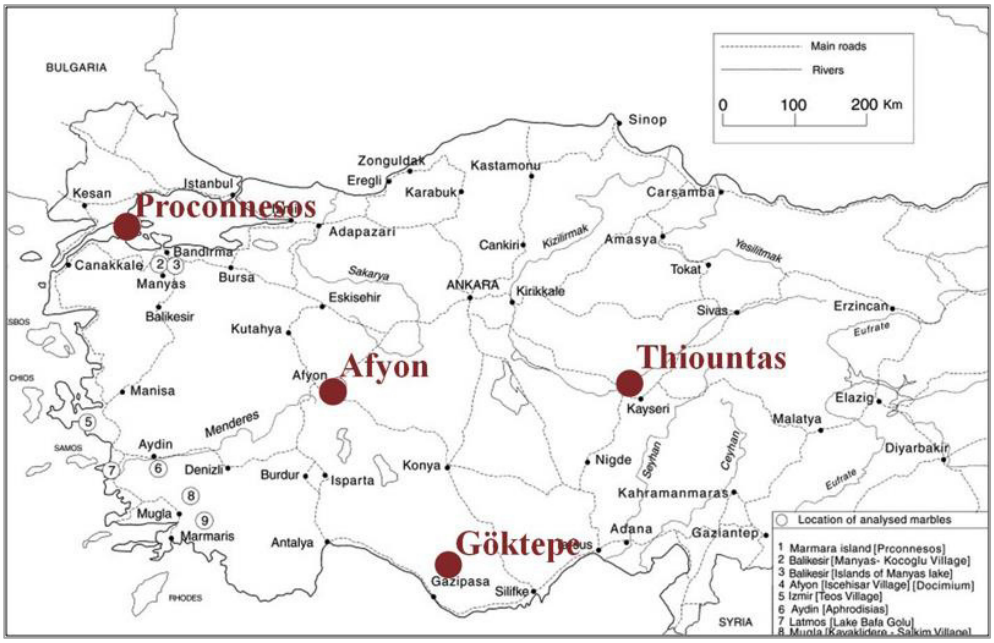

Fig. 3.1.3.1: Location of marble quarries from Turkey (Capaedri *et al.*, 2004).

3.1.3.1 Proconnesos

The marble of the Proconnesos Island, present-day Marmara, was one of the most famous and widely used marbles of the ancient world.

The quarries, occupying an extremely large area, are mostly located on the northeastern coast, near the village of Saraylar (Asgari, 1973). At least five main zones of excavation can be distinguished in the northern part of the island, proceeding from east to west, Altintas, the village of Saraylar, the localities of Çamlik and Mandira, and the zone of Silinte Harmantaş (Fig. 3.1.3.1.1).

The quarries were already known in the pre-classical epoch. This marble was probably utilized in the Artemision in Ephesus commissioned by Croesus towards the middle of 6th century BC (Monna and Pensabene, 1977). It was used most intensively from the beginning of the 1th century AD, when the quarries became Imperial property.

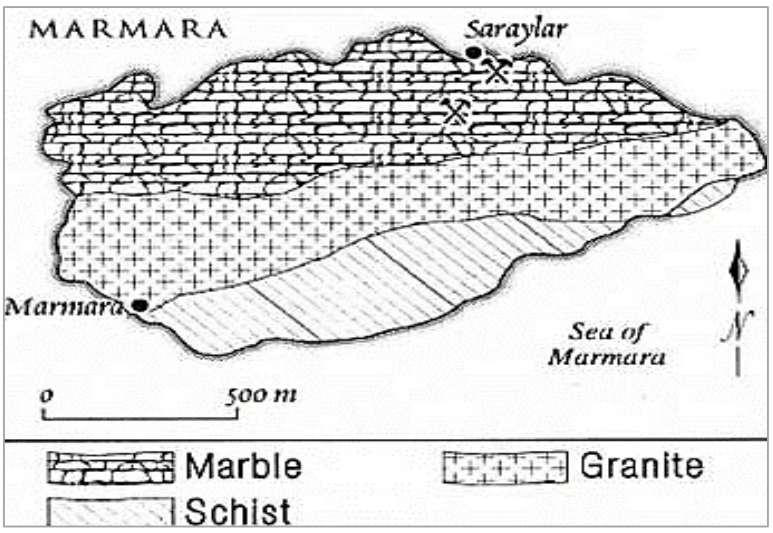

Fig. 3.1.3.1.1: Proconnesos Island and the quarry sites (Higgins and Higgins, 1996).

Its importance increased in the following centuries during the Constantinian and Justinian epochs, and for the next three centuries. Conveniently located near Constantinople, it played an important role in the construction the new Imperial capital (Attanasio, 2003).

The Proconnesos marble was known to the Romans as Marmor Proconnesium or Cyzicenum, (from the city of Cyzicus, the present-day Erdek on the southern coast of the Marmara Sea). It was very popular also thanks to the widely spaced joints allowing the extraction in large blocks. The most common type, used for architecture and sarcophagi, is coarse-grained and grayish white, with parallel bands of blue or grey. A plain bluish-white variety was used for sculpture, whereas a third variety, pure white and fine-grained, was suitable only for mosaics because it is always badly cracked (Higgins and Higgins, 1996).

During the 2nd and the 3rd centuries, Proconnesian marble was widespread all over the Imperial territory. A proof of that, in Rome it progressively superseded Luni marble, which was less easily quarried and shipped, also owing to the progressive silting of the Luna harbor (Walker, 1988). An updated study on the provenance of architectural white marble in Rome indicates that the proportion of this marble increases from less than 10% in the Flavian and Trajan-Hadrianic periods to 50% and almost 100% in the Antonine and Severan periods, respectively (Bruno *et al.*, 2002).

The quarries continued to be popular during Byzantine times and there is evidence of Proconnesian marble being used at least until the end of the 8th century AD (Attanasio *et al.*, 2008a).

The quarry districts were enormous, covering an area of more than 40 km^2, and produced high quality marble that was available in large quantities. Proconnesos marble was extremely widespread because of the immediate access to the sea from the quarries and for its convenient price (Giacchero, 1974). In addition, the extraordinary success met by Proconnesian marbles during the Roman Imperial age

was due to several different factors all of which must be taken into account to understand this phenomenon in its entirety. The quarries were conveniently located along the northern coast of Marmara Island (Asgari, 1978). For this reason, the quarrying and export of the artifacts, which could reach the ports of embarkation without excessive difficulties, were simplified to a considerable extent. Over the centuries, this gave rise to a huge exploitation and production, which definitely outclassed the marble from the Luni quarries.

Needless to say, this process was supported by the presence on the island of a large number of workers, diggers, stonecutters and sculptors who brought about a tremendous drop in the production costs of Proconnesos, one of the least expensive marbles mentioned in the price edict of the Diocletian age (Giacchero, 1974). In just a few decades, this variety undermined the production of Luna marble and, with the exception of just a few cases, caused the latter to be ousted from the market.

Nowadays, white marble from the island of Proconnesos is still quarried, and Afyon is responsible of the almost total current production of Turkish marble (Attanasio, 2003).

3.1.3.2 Afyon

Different varieties of marble were extracted at Afyon, known generically as Phrygian, Docimian or Synnadic marbles. The last one comes from the name of nearby Synada, the modern city of Suhut that is located at about 30 km south of Afyon, which was also the administrative center for the quarries (Fig. 3.1.3.2.1).

The marble quarries are located approximately 20 km northeast of Afyon, near the road to Ankara, and about 1,5 km from modern city of Iscehisar, the ancient Dokimeion or Docimium.

The large and complex marble site of Afyon comprises numerous ancient quarries. They are located along a belt that begins from the Afyon-Ankara road, near to Iscehisar, and stretches in a southeast direction for almost 10 km over a width of more than 2 km (Attanasio, 2003).

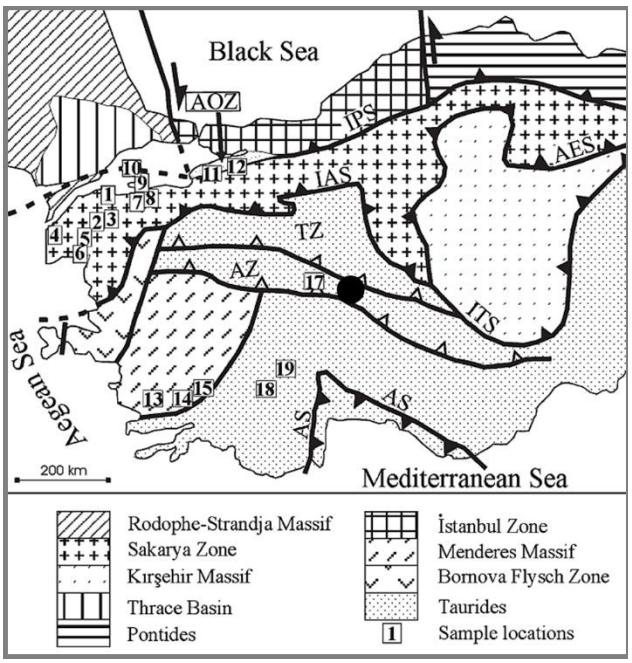

Fig. 3.1.3.2.1: Tectonic map of Turkey, red dot indicates Afyon district (Zöldföldi and Satır, 2003).

The importance of the Afyon mines is due to the fact that there is still much evidence of work having taken place in the ancient period (as semi-worked artifacts abandoned at the site bear inscriptions). Monna and Pensabene in 1977 described the history of the docimian district, its organization, and the manner in which this marble was utilized. More recently, C. J. Fant described the circumstances of the discovery of so many quarry inscriptions, summarized what they contribute to the knowledge or the history and organization of the quarry, and finally mentioned briefly some miscellaneous finds which also improve our understanding of the quarry and its output (Fant, 1984; 1987). In any case, the most exhaustive survey of the Afyon quarries is Röder's large work, published in 1971.

Afyon quarrying activity does not seem to date back to very ancient epochs. The historian Strabo was the first to mention the mines, and it is probable that intensive excavation commenced only in the Augustan age, when the quarries became Imperial property, perhaps being inherited from Augustus's son-in-law, M. Vipsanius Agrippa. Docimian marble had a wide variety of uses, from columns to wall and floor coverings, basins, sarcophagi, various types of architectural elements and also statues (Röder, 1971).

Röder (1971) divided the quarries into two main groups, Latin from the Imperial epoch and Greek from the Byzantine epoch. The Latin quarries, in turn, are divided into five sectors or districts, the most important of which is Baçakale, the largest and the most renowned quarry on the site. He calculated that from a fifth to a quarter of all the marble from the site has been extracted from this quarry and was employed mainly for constructions decreed by the Emperors that reigned during the middle of the 2nd century AD.

Currently, Docimium marble together with Proconnesus and Afyon marble, still supply almost all the marble utilized in modern Turkey (Waelkens, 1982).

3.1.3.3 Thiountas

The existence of the so-called Thiountas marble is mainly based on the discovery of numerous funeral inscriptions at Hierapolis of Phyrgia. These provide evidence of the use of this marble for sarcophagi. Many researchers have identified Thiountas marble as Hierapolis marble (Attnasio, 2003).

The location of the archaeological site, which has never been excavated, is not known precisely. It is believed to be near to the villages of Guzelpinar, about 9 km to the northeast of Hierapolis, or still farther north, near Gözler, about 23 km from Hierapolis. The white marble quarries may have been located near two villages, Doğanli and Gözler. Gözler became a completely abandoned village 20 years ago after an earthquake, and Doğanli is a modern village situated on the edge of a gorge, at the bottom of which flows the river Menderes. An ancient quarry has been located at the extreme north of the village. It is a large circular excavation, partly ancient and partly modern, surrounded by earth-covered rubble.

At the edges of the quarry and in its proximity, it is still possible to observe a pile of blocks, parts of columns and other unfinished artifacts.

Another two abandoned quarries are located just below the village, at the edge of the gorge. Other possible quarry sites can be seen on both slopes of the gorge of the Mederes as well as masses of deposited materials, both modern and ancient.

This information came from the study led by E. Schneider-Esquini on the necropolis of Hierapolis (Ramsay, 1895). Since then, the studies have been taken up by Monna and Pensabene in the 1977 and by Waelkens in 1982.

There is one quarry that is still being excavated, close to Gözler.

3.1.3.4 Göktepe

The ancient marble quarries of Göktepe, extending over an area of c. 0.5 km^2, are located in the province of Mugla, approximately 30 km north east of the provincial capital and 40 km southwest of the ancient city of Aphrodisias (Attanasio *et al.*, 2015). The Göktepe quarries were discovered in the late 1990s and first reported in 2006 by Alì Bahadir Yavuz (Attanasio *et al.*, 2008b; Attanasio *et al.*, 2009; Yavuz *et al.*, 2009) (Fig. 3.1.3.4.1).

At this site, which is relatively small compared to the other famous ancient quarries, high-quality black and white marbles exhibiting a fine or extremely fine crystal grain-size and with a compact and brilliant in color, were produced.

The white marble is present as large lenses within the black marble bed; for this reason, various shades of grey are found at the boundary between the two varieties. More often, however, the contact is quite sharp and made it possible to produce a highly characteristic, two-toned black-and-white stone that occasionally was exploited, especially in late antiquity, to obtain unusual color effects.

In antiquity, quarrying took place in four different districts at Göktepe (Fig. 3.1.3.4.2).

Districts 1 and 2, to the north, produced mainly black or in some cases, grey marble, whereas white statuary marble was quarried in districts 3 and 4. The dichromatic blocks came primarily from the southern part of the site, district 4, where the black marble surfaces again. As well as being the largest, district 3 is notable also for the presence of a large underground quarry (Fig. 3.1.3.4.2), where, as at the lychnites quarry in the valley of Marathi at Paros, the vein of highest-quality marble extended deep underground.

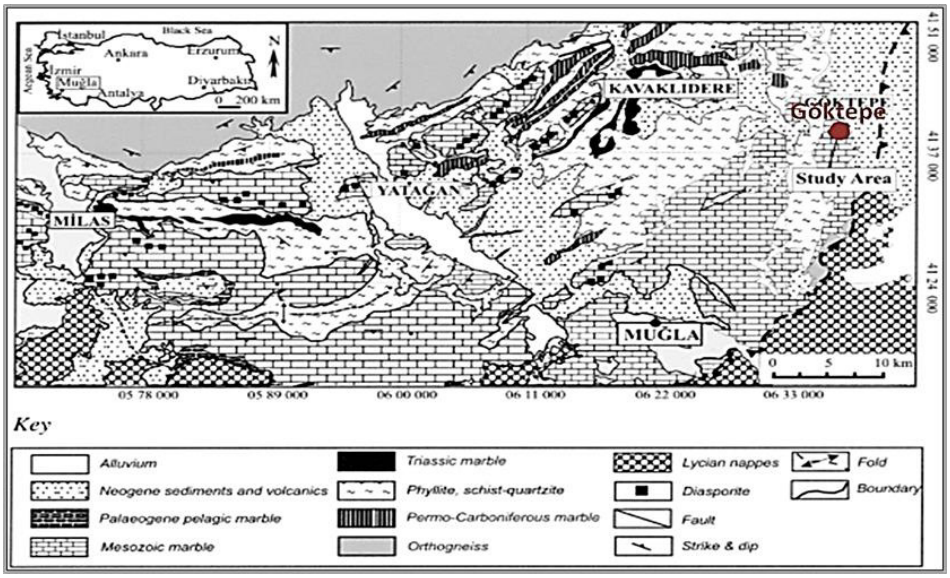

Fig. 3.1.3.4.1: A geological map of the Muğla region (Yavuz *et al.* 2005a, b).

In the case of district 3, the vein was buried beneath a thick layer of breccias. In district 4, 21 shapeless white marble blocks dressed with a medium to large punch were found. In terms of size and finish, they closely resemble the blocks of Parian marble found in the Fossa Traiana near Ostia (Pensabene *et al.*, 2000) and, like them, almost certainly were intended for sculptural use.

Two of the blocks bear quarry marks, and one of them also features a carved circular cavity made to house a lead seal, as is frequently found in the blocks of the Fossa Traiana and in many quarries known to have been under imperial control. These findings strongly suggest that, for at least part of their history, the quarries of Göktepe were under imperial administration (Attanasio *et al.*, 2012).

Nowadays, the site is completely abandoned and bears numerous traces of ancient activity. Clear traces of the heavy pick used on the fronts of the quarries and the wedge holes needed for detaching them from the bed rock, and many other traces of the presence of mining activities, have suggested that the site might have played an

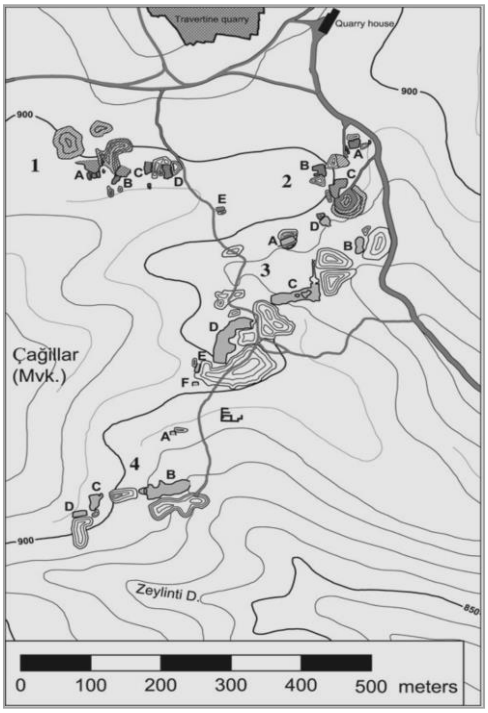

Fig. 3.1.3.4.2: Topographic sketch of the Göktepe marble site (Attanasio *et al.,* 2009).

outstanding role in the history of exploitation and use of ancient marbles (Attanasio *et al.,* 2015).

Attanasio and his team started in 2008 a program of systematic research on the properties of white marble from Göktepe and its chemical and petrographic characteristic in order to develop reliable criteria for their discrimination with respect to other macroscopically similar marbles used in antiquity (Attansio *et al.,* 2008b; Attanasio *et al.,* 2009; Attanasio *et al.,* 2012). More than 150 pieces made of white or black Göktepe marble, widespread all over the Mediterranean, have been identified (Bruno *et al.,* 2015).

According to the sculptures identified so far, the quarries were known and already active in the Augustan age at the beginning of the 1st century AD, but underwent peak exploitation in the 2nd century AD, from the Hadrianic age onwards. Apparently, a second period of peak

activity occurred in late antiquity and extended until the early 5th century AD (Attanasio *et al.,* 2015). Göktepe marble was strictly connected with Aphrodisian sculptors and their eastern style of sculpting. All the studies conducted allow to me conclude that the Göktepe white marble was among the most prized and sought-after sculptural marbles in Roman times, especially during the heyday of the Imperial age. It rivaled and partly replaced some of the most famous sculptural marbles used up to that point, such as marble from Paros, Carrara and from Afyon (Attanasio *et al.,* 2015).

3.2 Experimental setup

In this section, a brief description of instruments and of the experimental conditions used in this work is given.

Before the use of the instruments described in the next paragraphs, a preliminary characterization by means of optical microscopy was performed on petrographic sections of the rock samples (presented in Chapter 4).

3.2.1 Laser - Ablation ICP-MS

A geochemical characterization of white marble samples was performed by means of laser - ablation inductively coupled plasma – mass spectrometry (LA-ICP-MS).

In order to provide a geochemical characterization of the geological and archaeological specimens, concentrations of a large number of trace elements have been determined, including large-ion-lithophile elements (LILE), high field-strength elements (HFSE), rare-earth elements (REE) and the first-row transition elements (Sc-Cu), with a precision approaching traditional whole-rock analysis. In addition, as the scale approaches that attained by the electron microprobe, the data take into account homogeneity or heterogeneity of the chemical composition of samples. These characteristics make it a particularly attractive method for the analysis of cultural heritage materials.

The analyses have been conducted at Laboratory of Inorganic Chemistry of Eidgenössische Technische Hochschule (ETH) of Zürich and at CNR-Istituto di Geoscienze e Georisorse, U.O.S. of Pavia.

In both cases, the sample is placed in an airtight, closed ablation chamber, which was flushed with argon and helium as the carrier gas, and the laser beam is focused or imaged onto the sample surface

through a cell window. Then the material was ablated (providing irradiance sufficiently high to generate vapor, particles, and agglomerates) and transported to the plasma of the ICP-MS. The ICP serves as a separate excitation source, where the laser-generated particles are vaporized, atomized and ionized. Subsequently, ions have been extracted by the vacuum interface and guided into the mass analyzer, separated by mass-to-charge ratio and finally detected.

The two analytical instruments present a different general set-up, as presented.

LA-ICP-MS laboratory of ETH (Zürich)

The LA-ICP-MS system at ETH of Zürich, located in the Department of Chemistry and Applied Biosciences Laboratory of Inorganic Chemistry (Fig. 3.2.1.1), consists of a pulsed 193 nm Excimer laser from Lambda Physik with an energy-homogenized GeoLas optical system, coupled with a Perkin Elmer Elan 6100 DRC, and ICP quadrupole mass spectrometer. The geometry of the instrument is provided in Fig. 3.2.1.2.

Fig. 3.2.1.1: The LA-ICP-MS system at the ETH Zürich (Department of Chemistry and Applied Biosciences Laboratory of Inorganic Chemistry).

The laser energy applied on the sample was 12 J cm^{-2}, the laser frequency was 10 Hz, and the ablation aerosols were carried to the ICP-MS by He-Ar gas. The laser beam developed an 80 µm crater.

External standardization was made using the standard reference glass NIST 610, and CaO was used as the internal standard.

The lower limits of detection vary for the elements measured over a range of two or three orders of magnitude (10^{-1} to 102 $\mu g\ g^{-1}$), and the limit of detection (LOD) are controlled by a laser with 10 Hz repetition rate.

The concentrations of the following elements were measured: Li, B, Na, Mg, Al, Si, P, Cl, K, Ca, Sc, Ti, V, Cr, Mn, Fe, Co, Ni, Cu, Zn, Ga, As, Rb, Sr, Y, Zr, Nb, Mo, Cd, Sn, Sb, Cs, Ba, La, Ce, Pr, Nd, Eu, Gd, Dy, Ho, Er, Hf, W, Pb, Bi, Th, U.

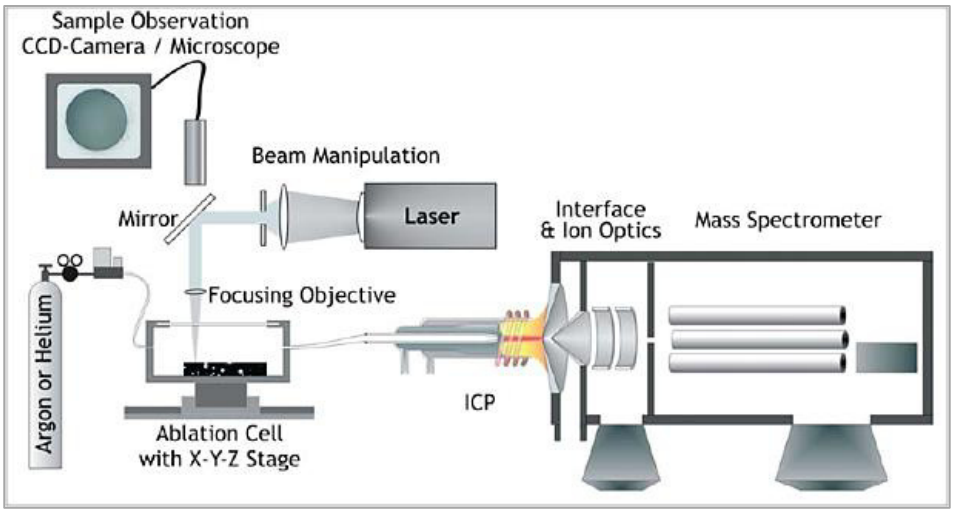

Fig. 3.2.1.2: Schematic set-up of the LA inductively coupled plasma - mass spectrometer (LA-ICP-MS), department of Chemistry and Applied Biosciences Laboratory of Inorganic Chemistry, ETH Zürich, Research Group of Prof. D. Günther.

LA-ICP-MS Laboratory of CNR-Pavia

The instrument at CNR-Istituto di Geoscienze e Georisorse, U.O.S. of Pavia consists of a Perkin Elmer SCIEX ELAN DCR-e quadrupole ICP-MS coupled with a Q-switched Nd:YAG laser source, model Brilliant (Quantel), whose fundamental emission (1064 nm) is converted to 266 nm by two harmonic generators. The spot diameter was typically 60-80 μm. Data reduction was done with the GLITTER software, using the synthetic glass NIST SRM 610 as external standard, whereas CaO was used as the internal standard for calcite.

Concentrations of the following elements measured: Li, Be, B, Na, Mg, Al, Si, P, K, Sc, Ti, V, Cr, Mn, Fe, Co, Ni, Cu, Zn, Ga, Ge, As, Rb, Sr, Y, Zr, Nb, Mo, Ag, Cd, In, Sn, Sb, Cs, Ba, La, Ce, Nd, Sm, Eu, Gd, Tb, Dy, Er, Yb, Lu, Hf, Ta, W, Au, Tl, Pb, Bi, Th, U.

Precision and accuracy (both better than 10% for concentration at ppm level) were assessed by means of repeated analyses of NIST SRM 612 and BCR-2g standards. Full details of the analytical parameters and quantification procedures were reported by Tiepolo *et al.* (2003) and Miller *et al.* (2012).

In both laboratories, five to seven measurements were performed for each sample, depending on chemical variation in the sample.

Advantages and drawbacks of the two laboratories

The first difference between the two laboratories consists in the different mode of preparation of the sample.

The first advantage encountered at ETH, Zürich, is the possibility of acquiring the measurement directly on the raw specimen surface. Conversely, at the IGG-CNR, the sample must be embedded in epoxy resin pads (blocks) with polished surface (Fig. 3.2.1.2 a, b). The possibility of carrying out *in situ* analyses, without preparation of sample, makes this methodology attractive and crucial for cultural heritage studies, where usually the amount of sample is very low. In this way, it is possible take advantage of one of the most important features of the LA-ICP-MS technique, which is the small amount of sample required owing to its sensitivity and spatial resolution.

The second difference concerns the wavelength of the laser source; that of the LA-ICP-MS at ETH is 193 nm, versus the 266 nm at CNR. Many recent studies demonstrate the great advantages of using laser with shorter wavelengths in the ablation behavior (Fryer *et al.*, 1995; Günther and Hattendorf, 2005).

Guillong *et al.* (2003) compared the transient signal for three laser wavelengths (266, 213, 193 nm) on the opaque glass standard NIST 610. The signal remained stable for more than 70 s for the 221 and 193 nm wavelengths, whereas the transient signal acquired at 266 nm shows the highest initial intensity. The signal is more unstable and decreases by approx. 70% within 70 s, as shown in Fig. 3.2.1.3.

In our cases, but also for LA-ICP-MS analyses, a constant and homogeneous ablation and aerosol transport are desirable in order to obtain high precision on elemental ratio determinations.

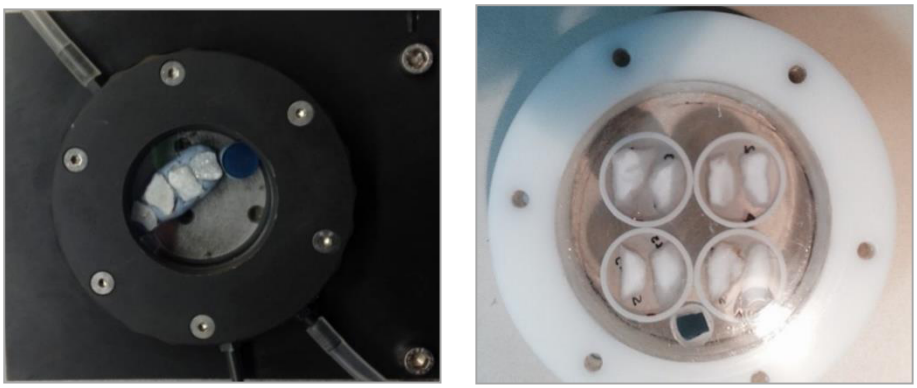

Fig. 3.2.1.2: a) The sample holder at the ETH of Zürich; b) The sample holder at the IGG-CNR of Pavia, where the specimens are embedded in resin pads.

The ICP-MS instruments, that record ion signals sequentially, like quadrupole and single-collector sector-field instruments, need stable elemental ratios over the entire ablation period to obtain accurate quantitative analysis. Besides, it has been proved that most minerals, including calcite, have increased absorption at shorter wavelengths (Jeffries *et al.*, 1998).

The last point of comparison is the limit of detection (LOD) for the samples analyzed in the two laboratories. In table 3.2.1.1-3.2.1.2, a list of the elements and their LOD are reported.

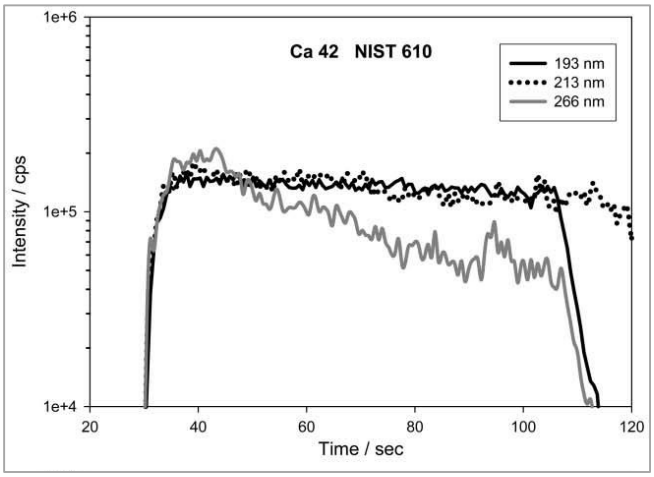

Fig. 3.2.1.3: Transient signals from NIST 610 (Guillong *et al.,* 2003).

Table 3.2.1.1: List of the elements and their LOD analyzed at the ETH Zürich (Department of Chemistry and Applied Biosciences Laboratory of Inorganic Chemistry).

Elements	LOD
K, Ca, Fe	< 10 µg/g
Cl	>100 µg/g
Li, Be, B, Na, Mg, Al, Si, P, Sc Ti, V, Cr, Mn, Co, Ni, Zn, Ga, As, Rb, Mo, Sn, Pb	<0.5 µg/g
Cu, Sr, Y, Zr, Nb, Cd, Sb, Cs, Ba, Hf, W, Bi, La, Ce, Pr, Nd, Sm, Eu, Gd, Dy, Ho, Er, Th, U	< 0.1 µg/g

Table 3.2.1.2: List of the elements and their LOD analyzed at the CNR-IGG, U.O.S. of Pavia. Precision and accuracy (both better than 10% for concentration at ppm level) were assessed by means of repeated analyses of NIST SRM 612 and BCR-2g standards.

Elements	LOD
Fe, K, Cr	1-3 µg/g
Li, Sc, Ti, Al, B, Zn, As	0.1-0.5 µg/g
Cu, Mo, Sn, Sb, W, Cd, Ga, Ni, Na, Ge, Ag, Mn, V, Rb, Sr, Zr, Cs, Ba, Gd, Pb	0.01-0.1 µg/g
Au, Bi, Y, Nb, La, Ce, Nd, Sm, Eu, Tb, Dy, Er, Yb, Hf, Ta,	0.001-0.01 µg/g
Tl, Pr, Ho, Tm, Lu, Th and U	<0.001 µg/g

3.3 Statistical treatment of data

Multivariate statistical methods are widely used in archaeometric data analysis (Baxter, 2006). The archeometric studies have to deal with the characterization of the rocks samples and the artifacts, described by many variables (*e.g.,* psych-chemical, petrographic variables) (Smith, 2002).

Multivariate statistical techniques were the methodologies most diffusely used to identify groupings among the samples on the basis of multivariate measurements, which can be clearly differentiated from each other, in order to find an archaeological classification. In this Ph.D. thesis, data have been processed by a statistic multivariate method, the principal component analysis (PCA).

The compositional data on bulk material from white marble samples using the LA-ICP-MS have been studied by means of the XLSTAT software which runs as additional component of Microsoft Excel.

In this study, statistical analysis was performed on concentration matrix of the 50 elements of about 120 samples (both rock samples and archaeological samples).

3.3.1 Principal component analysis (PCA)

The PCA is a way of identifying patterns in data, expressing the data in such a way as to highlight their similarities and differences. It belongs to unsupervised learning method techniques, namely the object is often to identify previously unknown structure in the data (Baxter and Buck, 2000; Baxter, 2006). The aim is to discover pattern, such as grouping, in the data without prior knowledge of what the pattern might be. It is a particular instance of a multidimensional scaling (MDS) method.

The method measures the dissimilarity between cases in a data matrix. Considering *k* as the number of variables (petrographic features or chemical elements) and *n* as observations (samples), after log transformation, Euclidean distance is chosen as the measure of dissimilarity between cases. In detail, PCA is based on the variance of variables that reduces the number of the variables considering only those that maximize the difference between samples. This method allows to define the anomalous samples (*i.e.,* outlier) respect to the others (Baxter, 1999) and to define how variables, in this case how chemical elements, influence the differences between samples. It calculates orthogonal linear combinations of the auto-scaled variables, by using the correlation matrix, based on the maximum variance criterion. Such linear combinations are called principal components scores and loadings the coefficients of the linear combinations. The PCA considers an X data matrix with *n* rows (samples) and *p* columns (chemical elements in our case) with the aim to create new variables low in number that conserves most of the total variance. From X data matrix the principal components are calculated according to the maximum variance criterion, *i.e.* each successive component is an orthogonal combination of the original variables such that it covers the maximum of the variance not accounted for by the previous

components. Each of principal components can describe a percentage of variance in the system. Usually, if there is a strictly correlation between variables, the first two or three principal components are able to describe the majority of the variance of system (Baxter, 1999).

The plot of the projection of the objects onto the first two or three principal components axes is a linear projection of objects onto the two or three dimensional subspace that conserves most of the total variance (score plot). The coefficients, by which the original variables must be multiplied to give the new parameters, are referred to as loadings. The numerical value of the loading of each variable on a given principal component shows how much the variable has in common with that component. Therefore, the loading plot of the variables onto the two-dimensional subspace, defined by the first two principal components, displays the correlation between the old variables (chemical elements) and these PCs.

In the score plot, the samples are represented by points and the outlier are located at the extreme of the plot, as results of the maximization of variance along the new axes since the distance between samples is inversely proportional between each other. The outlier influences the results, so it is usually deleted and the statistical analysis is carried out again on the new set of data (Baxter, 1999).

In conclusion, the advantage of using the PCA is that in a set of data of high dimension the patterns can be hard to find and PCA is a powerful tool for analyzing data. The other main advantage of PCA is that once you have found these patterns the data are compressed, *ie.,* by reducing the number of dimensions, without much loss of information (Smith, 2002).

Chapter 4

Results

4.1 Optical Microscopy (OM)

Representative samples for each district of the main eight quarrying areas, *i.e.,* Carrara, Greece and Turkey, have been chosen. The marble samples were thin sectioned for petrographic examination. The thin sections were observed under a polarizing microscope (Olympus BX4) to highlight the most significant petrographic features useful for differentiating the ancient white marble from different source areas, as widely reported in archaeometric studies (*e.g.,* Herz and Prichett, 1953, 1955; Weiss, 1954; Renfrew and Springer, 1968; Young and Ashmole, 1968; Moens *et al.,* 1988; Lapuente *et al.,* 2012; Lazzarini *et al.,* 1980a; Antonelli *et al*., 2014a; 2014b; Pensabene *et al.,* 2012; Columbu, 2014; Antonelli and Lazzarini, 2015).

Preliminary petrographic analyses were applied to discriminate groups and subgroups of samples. For the sake of clarity, the petrographic description below regards two/three samples of the different variety of marble considered in the present study. Thus the aim of the datasheet made for each marble is to describe the main petrographic features and to compare them with the information reported in the previous studies.

Microscopy analysis in thin section of rock samples

The main features noted are briefly described below, highlighting those indispensable to characterize samples of white marble from the various quarry sites.

For each thin section, the following mineralogical and petrographic features have been observed:

- Fabric (homeoblastic/heteroblastic; isotropic/anisotropic) and microstructure;

- The maximum grain-size (MGS);
- Grain-boundary shapes (GBS);
- Accessory minerals.

The maximum grain-size allows one to divide the white marble specimens in two subgroups, from 1) fine - to very fine-grained white marble (MGS < 2 mm) 2) medium - to coarse-grained marble (MGS > 2 mm).

These characteristics are reported in Tab. 4.1.1 (fine-grained marble) and Tab. 4.1.2 (coarse-grained marble).

Carrara

The thin sections of white marble from Carrara are representative of the two districts, Colonnata (Gioia, Fossacava) and Torano (Sponda I).

All samples are characterized by a homeoblastic fabric, formed by a polygonal mosaic of small (Fossacava, Gioia) to very small (Torano) calcite crystals, showing a well-developed equilibrium texture (Fig. 4.1.1). Grains are of nearly isometric shape (no evident grain-shape orientation), and without of preferred crystallographic orientation.

The calcite crystals usually present straight to slightly curved boundary shapes, and triple points are commonly developed (Fig. 4.1.2).

Optical evidence of plastic deformation is almost completely absent and only represented by thin e-twins (Cantisani *et al.,* 2005), which appear to be related to a late stage of low-temperature deformation.

With uncrossed polars, the FO3 sample appear less limpid than samples from Gioia and Torano, possibly due to a relatively high content of fluid inclusions (Fig. 4.1.3).

The maximum grain-sizes attain 0.7-0.8 mm (G7, G17), 0.5 mm (FO3) and 0.5 mm (TR8).

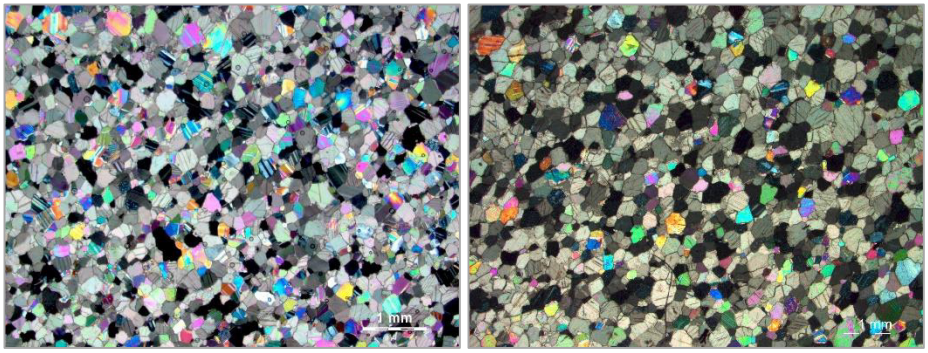

Fig. 4.1.1: Carrara samples show a homeoblastic fabric, formed by a polygonal mosaic of small (Fossacava, Gioia-G7) to very small (Torano-TR8) calcite crystals. a) TR8 sample, crossed pol.; b) G7 sample, crossed pol.

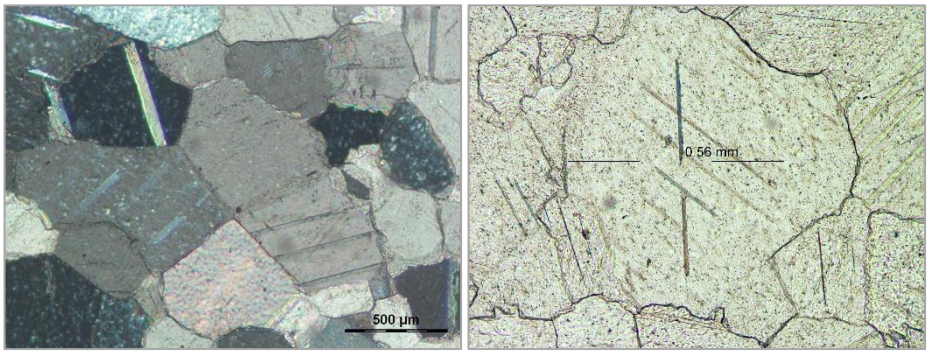

Fig. 4.1.2: a) The calcite crystals usually show straight to slightly curved boundary shapes and triple points (sample G7, crossed pol.; b) MGS= 0.56 mm (FO3 sample, uncrossed pol.).

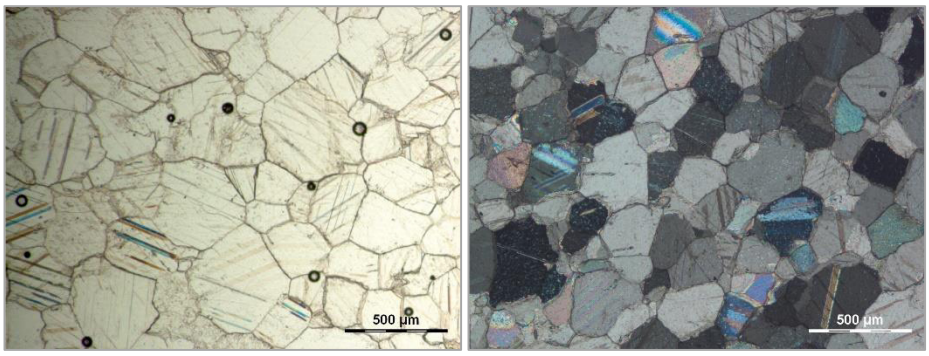

Fig.4.1.3: with uncrossed polars, samples from Gioia quarry (G7, G17) and Torano (TR8) appear more limpid than samples from Fossacava quarry. a) Sample G7 (uncrossed pol.); b) G17 sample (crossed pol.).

Paros

Parian white marble is characterized by a core and mantle structured with relatively small-strain free grains surrounding relics of large, strained grains (with kink bands, subgrains or undulose extinction).
All samples show a fine grain-size, a heteroblastic fabric and an isotropic texture (Fig. 4.1.4).
The calcite crystals usually present irregular boundaries from curved to sutured; in some cases, it is still possible observe the triple points among the relict crystals (Fig. 4.1.5).
In this marble, has various accessory minerals have been observed, such as white mica, quartz and amphibole. The white mica has been observed as an inclusion as well as at the edge of the calcite crystals (Fig. 4.1.6).
Parian white marble presents a marked heteroblastic fabric, and the maximum grain-size ranges from 2.4 to 3.1 mm. Nevertheless, it is considered a fine-grained marble because rare crystals (MGS up to 3 mm) are surrounded by smaller crystals with a maximum grain-size ranging from 0.3 to 0.9 mm.

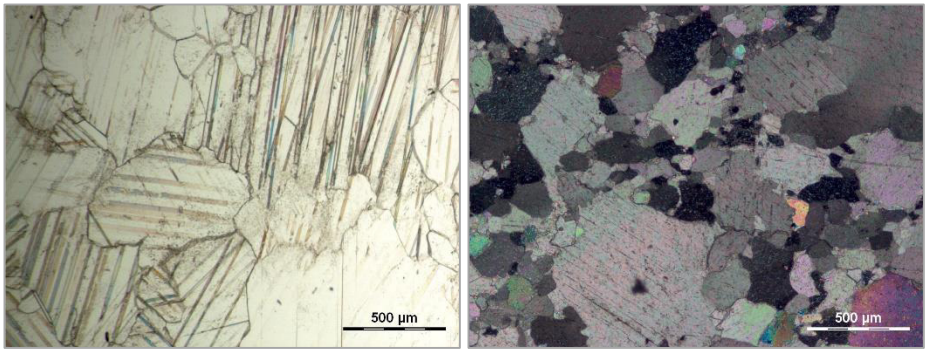

Fig. 4.1.4: Fine grain-size, heteroblastic fabric and isotropic texture. This marble shows a core and mantle microstructure, with relatively small strain-free grains surrounding relics of large, strained grains. a) CYPA67 sample (single pol.); b) PAROS1 sample (crossed pol.).

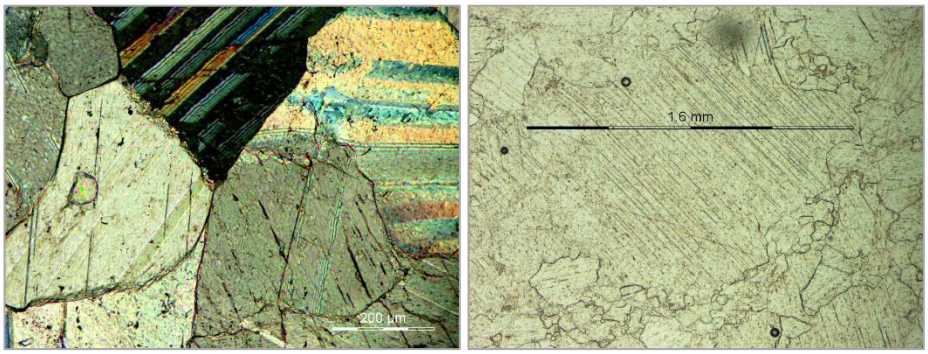

Fig. 4.1.5: a) A detail of showing triple-point microstructure (CYPA 5 sample, crossed pol.); MGS=1.6 mm (PAROS1 sample, single pol.).

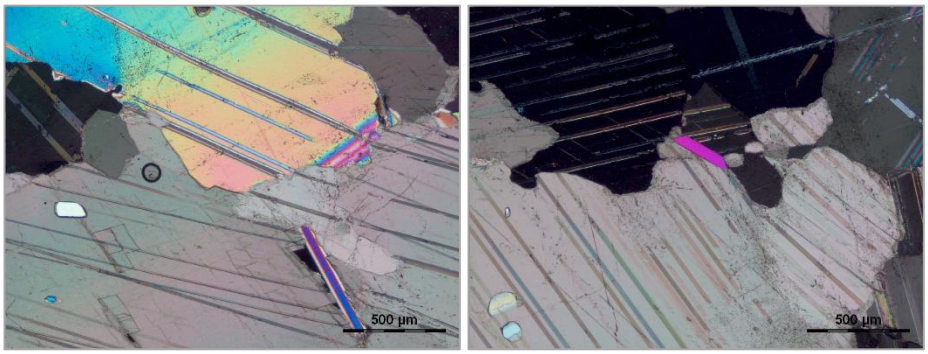

Fig. 4.1.6: a-b) White mica inclusion. The white mica has been observed as inclusion as well as at the edge of the calcite crystals (CYPA 67 sample, crossed pol.).

Pentelic marble

Thin sections of the Pentelic white marble show a fine to medium grain-size, slightly heteroblastic fabric, and an isotropic texture (Fig. 4.1.7).

As distinct from Carrara, pentelic white marble has a xenoblastic fabric, typical of marble that has been affected by deformation during metamorphism.

The calcite crystals show satured to embayed shapes, and triple points are quite absent. Calcite has very irregular boundaries, not seen in the other specimens described so far.

Samples from Spilià in the upper level quarry contain a white mica, whereas while samples from the lower level quarry contain quartz (Fig. 4.1.8).

The maximum grain-sizes range 0.8-1 mm (Spilià low and high level quarry 6-8 and 13-15), to 1.1 mm (Quarry I).

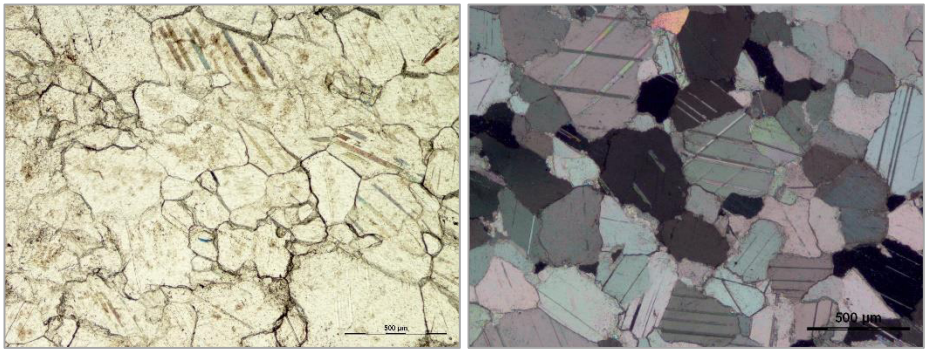

Fig. 4.1.7: Pentelic specimens show a xenoblastic fabric. a) SMH 1.3 sample, single pol.; b) I2 sample, crossed pol.

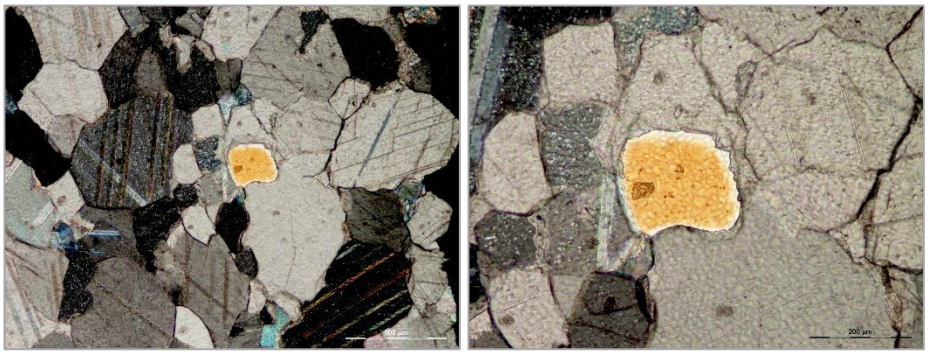

Fig. 4.1.8: a) Sample of Pentelic marble that shows quartz as an accessory mineral. a-b) Detail of SMH 1.3 sample, crossed pol.

Afyon

The Afyon white marble is characterized by a heteroblastic fabric and a marked xenoblastic microstructure related to dynamic recrystallization, recognized by variable grain-sizes and grain-boundary shapes from slightly curved or embayed to lobate (Fig. 4.1.9; Fig. 4.1.10).

The earlier granoblastic structure still visible was reworked. Among the crystals the disequilibrium contact is evident.

The maximum grain-sizes range from 0.9 mm (Bacakale quarry –D9a) to 2.3 mm (Roder II quarry).

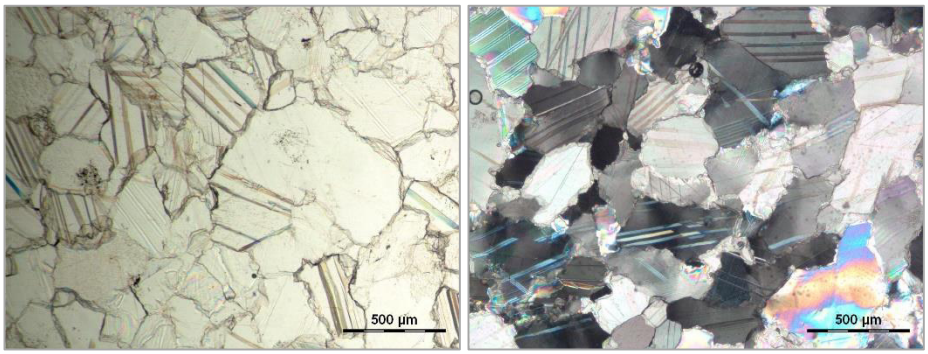

Fig.4.1.9: Afyon white marble is characterized by a heteroblastic fabric and a marked xenoblastic microstructure. a) D9a sample uncrossed pol.; b) D9a sample, crossed pol..

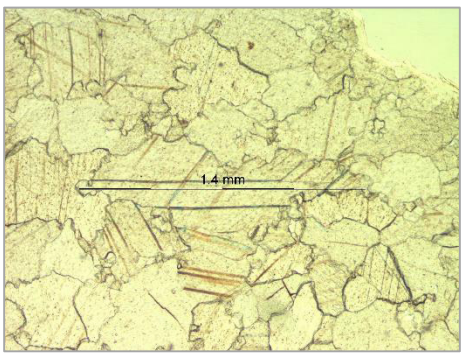

Fig.4.1.10: MGS= 1.4 mm. D27a sample, uncrossed pol.

Naxos

Naxian white marble shows a heteroblastic fabric and an isotropic texture.

The microstructure is xenoblastic and in some cases a mortar microstructure has been observed (Fig. 4.1.11).

The crystals boundaries are irregular from curved to sutured.

The maximum grain-sizes of the observed samples range from 3 to 3.5 mm (CYNA 72-75-78 samples).

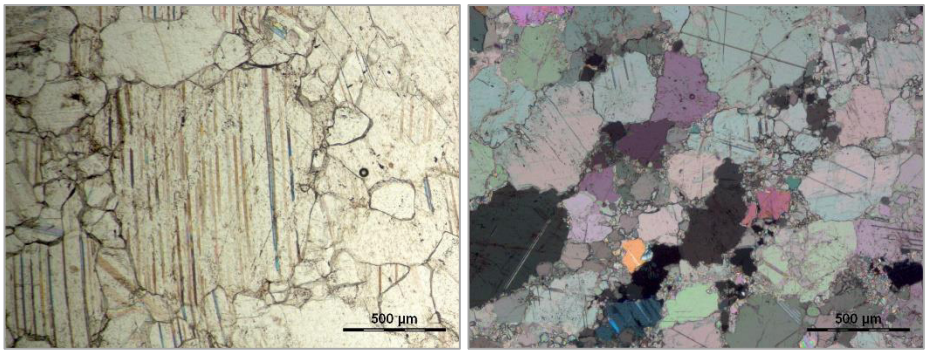

Fig. 4.1.11: The microstructure is xenoblastic; in some cases, this marble presents a mortar microstructure. a) CYNA72 sample, uncrossed pol.; b) CYNA75 sample, crossed pol.

Thasos

The samples of Thasian marble considered in this study are:

- Calcitic marble from the Aliki quarry (TA1);
- Dolomitic marble from yhe Mourgena quarry (MOUR2, MOUR5).

In both cases, Thasian specimens show a heteroblastic fabric and an isotropic texture (Fig. 4.1.12) characterized by a mosaic, generally lineated and stressed microstructure (Fig. 4.1.13).

The calcite crystals boundaries are from curved to sutured, some crystals show triple-point junctions (Fig. 4.1.14).

The maximum grain-size ranges from 5 mm for calcitic sample (TA1) and from 0.9 mm to 1.5 mm in dolomitic samples from the Mourgena quarry.

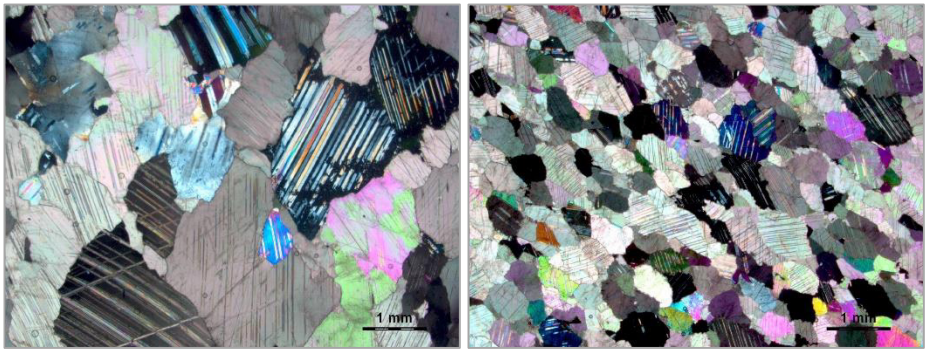

Fig. 4.1.12: Thasian calcitic (TA1) and dolomitic (MOUR2, MOUR5) marble present a heteroblastic fabric and an isotropic texture. a) TA1 sample at crossed pol; b) MOUR2 sample, crossed pol..

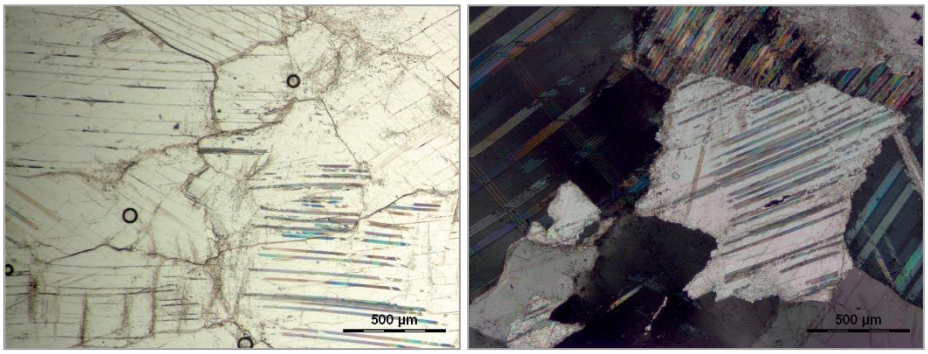

Fig. 4.1.13: Thasian samples present a mosaic, often lineated and stressed microstructure. a-b) TA1 sample, uncrossed pol. and crossed pol.

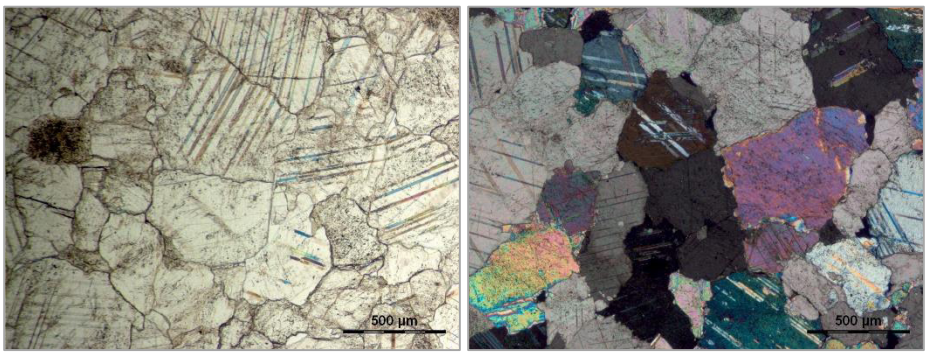

Fig.4.1.14: Triple points junction are still visible. a) MOUR2 sample, uncrossed pol.; b) MOUR5 sample, crossed pol..

Thiountas

Thiountas white marble shows a heteroblastic fabric and an isotropic texture (Fig. 4.1.15).
The mortar microstructure is marked by large relict crystals of medium to coarse grain-size, surrounded by relatively small strain-free grains (Fig. 4.1.16).
The boundaries vary from curved to sutured.
The maximum grain sizes range from 3 to 3.7 mm.

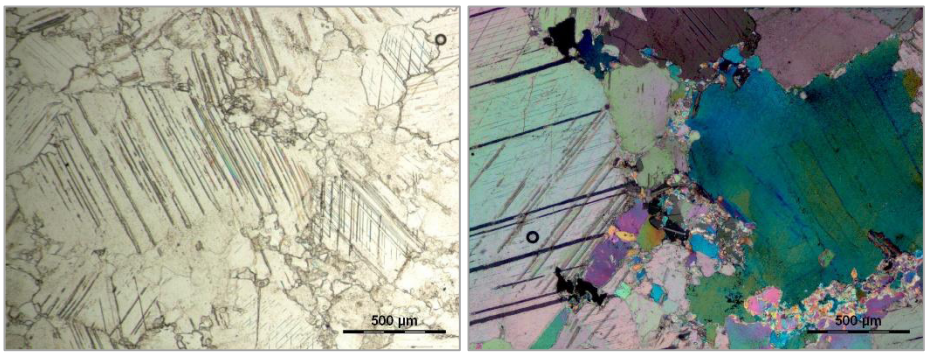

Fig. 4.1.1.5: Thiountas marble has a heteroblastic fabric and an isotropic texture. a-b) T13 sample at uncrossed and crossed pol.

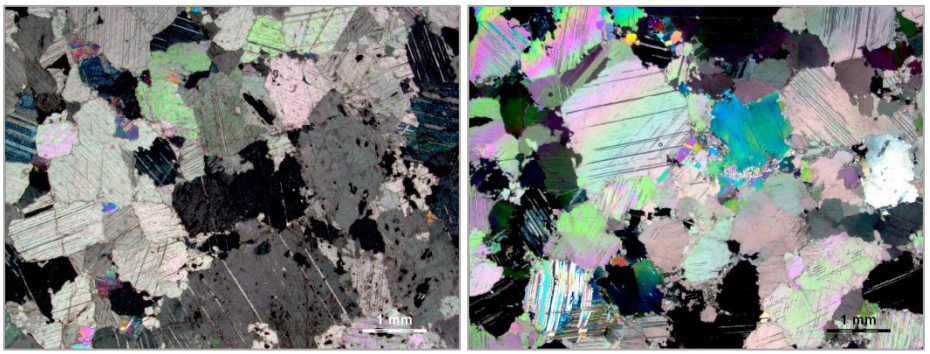

Fig. 4.1.16: These specimens present a mortar microstructure, large relict crystals of medium to coarse grain-size are surrounded by relatively small strain-free grains. a) T6 sample at crossed pol; b) T13 sample at crossed pol.

Proconnesos

Proconnesian white marble shows a heteroblastic fabric and an isotropic texture. It is characterized by a xenoblastic microstructure with, in some cases small crystals of new formation surrounding large relict crystals (Fig. 4.1.17).
The boundaries are marked by an irregular curved to sutured crystals of calcite (Fig. 4.1.18).
The maximum grain-sizes range from 2 to 4 mm (Filiz quarry OC 13/2, OC 13/5) and 2.6 mm (Altintas quarry).

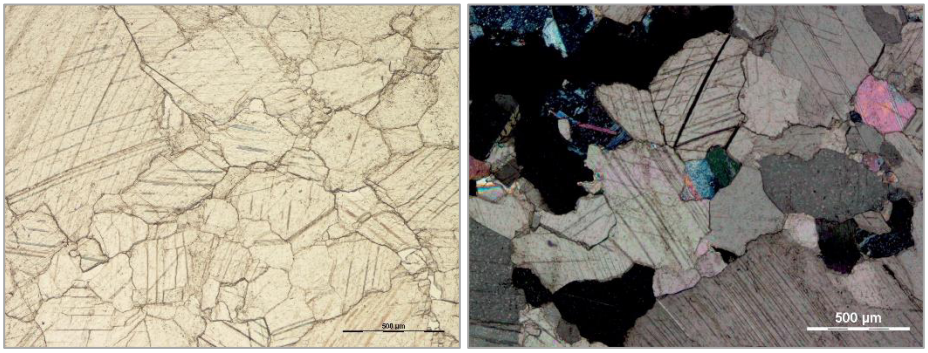

Fig. 4.1.17: Proconnesian marble has a heteroblastic fabric and an isotropic texture. It is characterized by a xenoblastic microstructure with, in some cases, small crystals of new formation surrounding large relict crystals. a-b) OC13/2 sample, uncrossed and crossed pol.

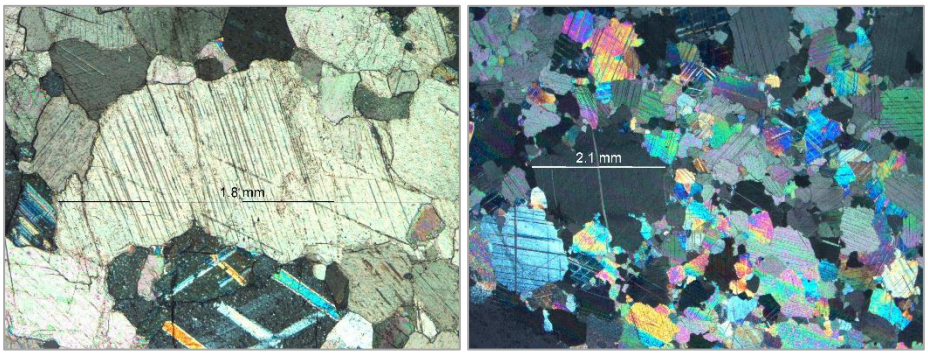

Fig. 4.1.18: Proconnesian marble is characterized by a xenoblastic microstructure with in some cases small crystals of new formation surrounding large relict crystals. a) OC13 sample at crossed pol.; b) PRO17 sample at crossed pol.

Tab. 4.1.1: Microscopic features observed in representative specimens of fine-grained white marble.

White marble	Quarry	Texture	Fabric type	Microstructure	Crystal boundaries	MGS (mm)
Carrara	Gioia (G7)	HO	Isotropic	Polygonal with triple points	Straight to slightly curved	0.7 0.1
	Gioia (G17)	HO	Isotropic	Polygonal with triple points	Straight to slightly curved	0.8 0.2
	Fossacava (FO3)	HO	Isotropic	Polygonal with triple points	Straight to slightly curved	0.5 0.2
	Sponda I (TR8)	HO	Isotropic	Polygonal with triple points	Straight to slightly curved	0.5 0.3
Paros	CYPA5	HE	Isotropic	Mortar	Curved to sutured	2.4 0.32
	CYPA67	HE	Isotropic	Mortar	Curved to sutured	3.1 0.3
	PAROS1	HE	Isotropic	Mortar	Curved to sutured	1.9 0.2
Penteli	Splià low level SML1.1	Slight HE	Anisotropic	Irregular granoblastic,	Curved to embayed	0.8 0.1
	Splià low level SML13	Slight HE	Isotropic	Irregular granoblastic	Curved to embayed	1 0.2
	Splià high level SMH1.3	Slight HE	Anisotropic	Irregular granoblastic	Curved to embayed	0.9 0.1
	Quarry I (I2)	Slight HE	Slight anisotropic	Irregular granoblastic	Curved to embayed	1.1 0.07
Afyon	Bacakale (D9a)	HE	Isotropic	Xenoblastic	Lobate	1.3 0.25
	Roder II (D27a)	HE	Isotropic	Xenoblastic	Lobate	2.3 0.2

Tab. 4.1.2: Microscopic features observed in specimens of coarse-grained white marble.

White marble	Quarry	Texture	Fabric type	Microstructure	Crystal boundaries	MGS (mm)
Naxos	CYNA72	HE	Isotropic	Xenoblastic	Embayed	3.3 0.2
	CYNA75	HE	Isotropic	Xenoblastic	Embayed	3 0.2
	CYNA78	HE	Isotropic	Xenoblastic	Embayed	3.5 0.3
Thasos	TA1	HE	Isotropic	Xenoblastic	Curved to sutured	5 0.8
	MOUR2	HO/HE	Isotropic	Xenoblastic	Curved to sutured	1.5 0.2
	MOUR5	HO/HE	Isotropic	Xenoblastic	Curved to sutured	0.9 0.2
Thiountas	T6	HE	Isotropic	Mortar	Curved to sutured	3.7 0.3
	T13	HE	Isotropic	Mortar	Curved to sutured	3 0.2
Proconnesos	Altintas (PRO17)	HE	Isotropic	Xenoblastic	Curved to sutured	2.6 0.2
	Filiz (OC/2)	HE	Isotropic	Xenoblastic	Curved to sutured	2 0.3
	Filiz (OC/13)	HE	Isotropic	Xenoblastic	Curved to sutured	4 0.25

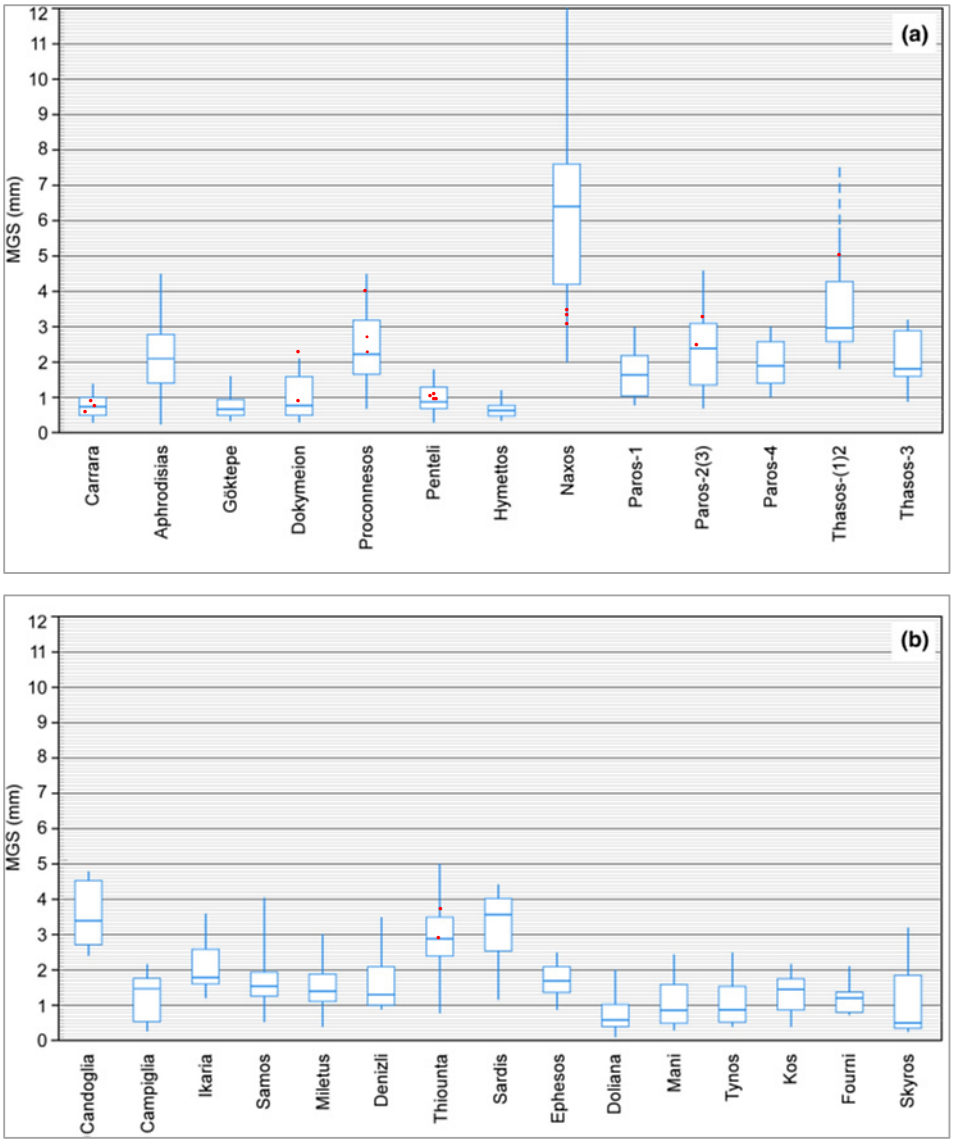

Fig.4.1.19: The updated reference maximum grain-size (MGS) shown as box bars of carbonate grains of the samples analyzed in Antonelli and Lazzarini (2015).
a) The 10 chief white marbles used in classical times.
b) The 15 most important ‘‘minor’’ Mediterranean marbles used in antiquity.
Boxes comprise 70 % of the total values; the ends of the lower and upper whistlers represent the minimum and maximum values, respectively. The bar inside a box is the median value for the MGS reported in Antonelli and Lazzarini (2015). The red dots indicate the MGS of the samples analyzed in this present work and summarized in Table 4.1.1 and 4.1.2.

4.2 Chemical analysis of the marble samples

In the previous section, marble specimens were characterized by means of optical microscopy, and according to their microstructures, the white marbles from Italy, Greece and Turkey have been divided in two main groups, *i.e.,* fine-grained and mid-coarse-grained white marbles, and from this point on, they will be treated separately.

In this section are reported trace-elements analyses of white marble specimens, using laser ablation - inductively coupled plasma - mass spectrometry (LA-ICP-MS). For each sample, the concentration of 47 elements at the ETH of Zurich and 54 elements at the IGG-CNR of Pavia, was measured as shown in Tab. 4.2.1.

In the multi-elemental diagrams selected trace elements are reported on the basis of an accurate observation of the detection limits for the analytical instruments and the dimension of the error comparable with the data. The dataset, subdivided according to ionic potential (charge/size ratio), are: Rb, Ba, K, Sr (large-ion lithophile elements, LILE), Th, U, Nb, Ta, Zr, Hf, Ti, (high-field-strength elements, HFSE), and La, Ce, Pr, Nd, Sm, Eu, Gd, Tb, Dy, Ho, Er (rare-earth elements, the REE) and Y.

The trace-element concentrations have been reported using different kinds of bivariate and multi-elemental plot. One of these is the chondrite-normalized multi-element diagram, the so-called spider diagram, widely used in petrology, which turned out to be very useful in our case study.

The normalized multi-element diagrams are based upon a grouping of elements that are incompatible with respect to a typical mantle mineralogy, and they are an extension of the chondrite-normalized REE diagrams in which other trace elements are added.

Tab. 4.2.1: Trace elements detected at the two laboratories (ETH of Zurich and IGG-CNR laboratory of Pavia).

Common elements	Detected elements at the ETH Zürich	Detected elements at the IGG-CRE- UOS Pavia
Li, B, Na, Mg, Al, Si, P, K, Sc, Ti, V, Cr, Mn, Fe, Co, Ni, Cu, Zn, Ga, As, Rb, Sr,Y, Zr, Nb, Mo, Cd, Sb, Cs, Ba, La, Ce, Nd, Eu, Gd, Dy, Er, Hf, W, Pb, Bi, Th, U	Cl, Pr, Ho, Sn	Be, Ge, Ag, In, Sm, Tb, Lu, Yb Ta, Au, Tl

In the spider diagrams, the systematic variation in trace elements is illustrated by plotting the log of their relative abundances, which are calculated by dividing the concentration of each trace element by its concentration in a set of normalizing values, such as those in chondritic meteorites.

Trace-element concentrations in rocks are usually normalized to a common reference standard, and in our case, their concentrations have been normalized to chondrite values given by Sun and McDonough (1989) or to chondrite values given by Taylor and McLennan (1985) for REE +Y diagram. The elements are subdivided in different group based on their ionic potential, because elements with the same ionic charge and size show very similar geochemical behavior (Fig. 4.2.1).

The first group, on left of the diagram, is represented by the LIL elements (Rb, Ba, K, Sr), with the ionic potential <2.0 (large cations of small charge), followed by the HFS (Th, U, Nb, Ta, Zr, Hf, Ti) and REE elements (La, Ce, Pr, Nd, Sm, Eu, Gd, Tb, Dy, Ho, Er) plus Y, with the ionic potential >2.0 (small highly charged cations).

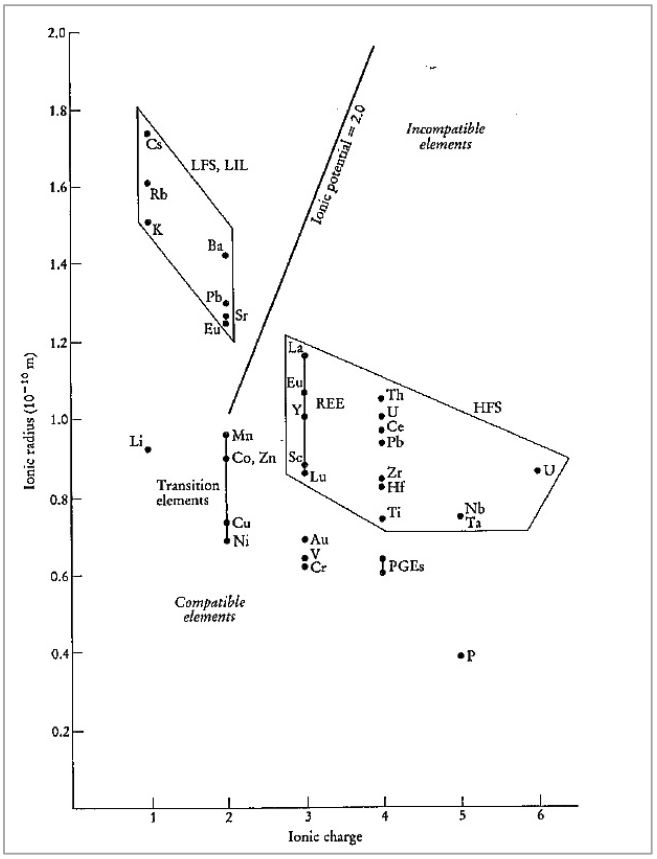

Fig. 4.2.1: Plot of ionic radius vs ionic charge for trace elements of geological interest. An ionic potential subdivides the incompatible elements, trace elements that display a preference the melt when the Earth's mantle is melted. An ionic potential (charge/size ratio) of 2.0 distinguishes LIL elements from HFS elements (Rollinson, 1993).

Moreover, the REE elements are further ordered according to on their atomic number.

The low-atomic-number members of the series are termed the light rare-earths (LREE), those with the higher atomic numbers, the heavy rare-earths (HREE), and less commonly, the middle members of the group, Sm and Ho, are known as middle REE (MREE) (Rollinson, 1993).

In this thesis, concentrations of all REE elements were established, however, some of them are invariably found to be below

the detection limits. For this reason, the following traces were considered: La, Ce, Nd (LREE), Eu, Gd, Dy (MREE) and Er, Y (HREE). The trace-earth elements considered in white marble in this dissertation are divided in the following way: La, Ce, Nd (LREE), Eu, Gd, Dy (MREE) and Er, Y (HREE). The bivariate diagram, presented in the results section, reports the LREE *vs* MREE+HREE concentrations, being the best way to discriminate among the areas of active quarrying

The multi-element diagrams contain a heterogeneous mix of trace elements or just a group of these; they are characterized by peaks reflecting the different behavior of distinct groups of trace elements. They will be discussed on the basis of the different patterns behaviors of the groups of elements measured, including their distribution and the different concentrations of the elements in the samples of white marble.

Furthermore, the trends on chondrite-normalized REE diagrams, usually referred to as REE "patterns", and the shape of the REE distributions are really important. Frequently, the plotted position of Ce and Eu lies off the general trend defined by the other elements, and may define Ce or Eu anomaly. If the plotted composition lies above the general trend, the anomaly is defined as being positive; where the anomalous composition lies below the trend, it is negative. The anomalies may be quantified by comparing the measured concentration with an expected concentration, interpolating obtained interpolating the normalized values of the elements La and Pr for Ce* and Sm and Gd for Eu*, according to the formula $Ce^*=\sqrt{LaN \times PrN}$ and $Eu^* =\sqrt{SmN \times GdN}$ where N=chondrite normalized, recommended by Taylor and McLennan (1985).

The ratio Ce/Ce* and Eu/Eu* is a measure of the anomaly. A value of greater than 1.0 indicates a positive anomaly, whereas a value of less than 1.0 is a negative anomaly.

The aim of this section is to find which elements or groups of elements can discriminate among different sites of quarrying of white marble.

The geochemical data are reported in Appendix C.

4.3 Trace-element abundances in fine-grained white marble

4.3.1 Carrara

Specimens of white marble from Alpi Apuane were sampled in four quarries, located in two different basins on the western slopes of Monte Sagro, near Carrara city, *i.e.,* Gioia, Fossacava, Calagio (Colonnata district) and Sponda I (Torano district).

In Fig. 4.3.1.1 is reported the chondrite-normalized multi-elemental diagram, in which the first group of trace elements is represented by LILE. Marble from both districts is enriched in Ba and in Sr, whereas the concentrations of Rb and K are too scattered, mainly due to the different detection limits of the instrument of the two laboratories. In particular, samples analyzed at the ETH, Zürich (continuous line), have concentrations of Rb and K higher than those analyzed at the IGG of Pavia (dashed line).

For the HFS elements, the patterns of two basins are similar, but with highly variable concentrations. The marble is enriched in U, Ta and Hf and depleted in Th, Nb, Zr and Ti. The positive Hf anomaly seems to discriminate better among the quarries; Fossacava (orange line) and Calagio (garnet line) have the lowest content, whereas Sponda I (yellow line) has intermediate values, and Gioia (red line) has the highest content.

Both HFSE and LILE have nearly the same patterns, with similar distribution, thus limiting the discrimination of Colonnata and Torano marbles; however, a clear separation is evident considering the concentration of REE, which discriminate Torano marble for its high REE content.

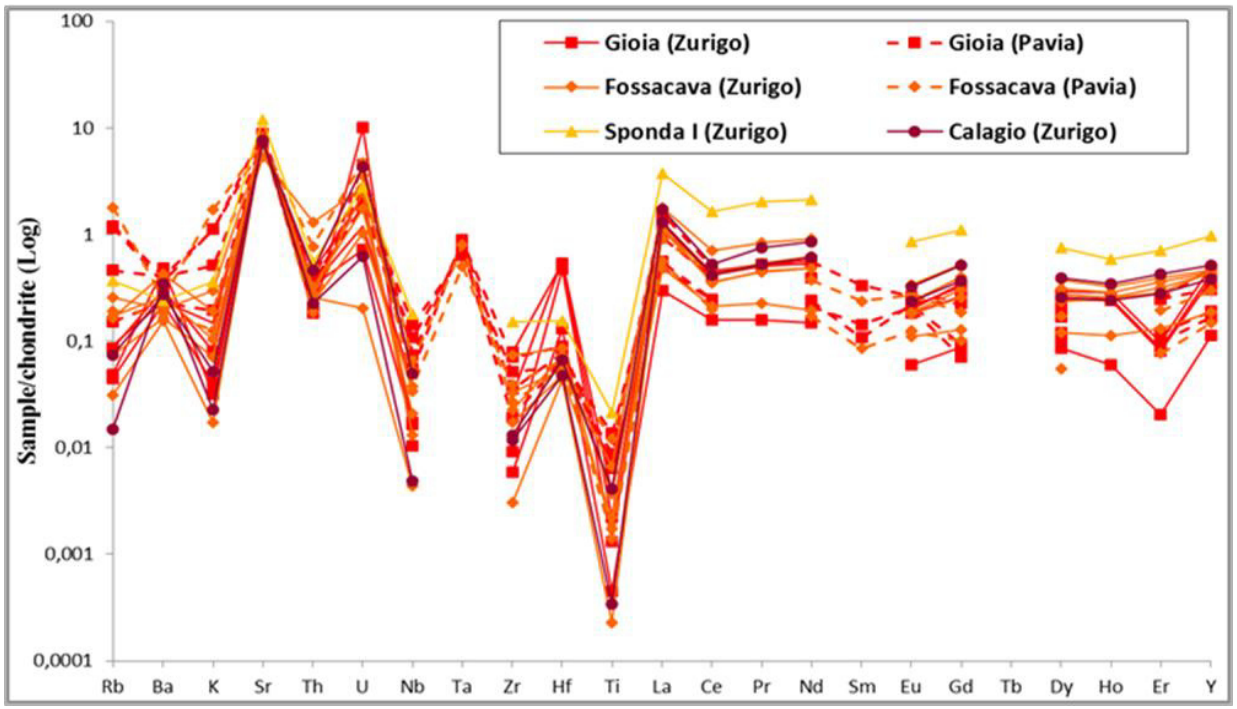

Fig. 4.3.1.1: Patterns of trace elements in calcite are given for white Carrara (Italy). The two districts are displayed using differing symbols and colors: red line for the Gioia quarry, orange line for the Fossacava quarry, garnet line for the Calagio quarry and yellow line for the Sponda I. Moreover, continuous lines are for samples analyzed at the ETH of Zürich, whereas dashed lines are for those analyzed at the IGC-CNR Pavia. The concentrations are normalized to chondrite (Sun and McDonough(1989)).

As shown in detail in the chondrite-normalized REE patterns (Fig. 4.3.1.2), the Sponda I specimen (Torano district) is characterized by a marked enrichment in REE respect to the Colonnata samples. Moreover, within the Colonnata basin, the Calagio quarry displays a more homogeneous distribution of REE than Gioia and Fossacava quarries, which have more scattered values, as illustrated in Fig. 4.3.1.3. The Gioia samples, analyzed at the ETH of Zürich, show a sharp negative Er anomaly. In addition, both districts show a slight negative anomaly for Ce, with an average value for Colonnata of 0.5 (for all the quarries) and for Torano of 0.6. Contrast, the Eu*N values are different not only for the two districts, but also whitin the Colonnata district, with Gioia 1.6 and Fossacava 1.3, respectively.

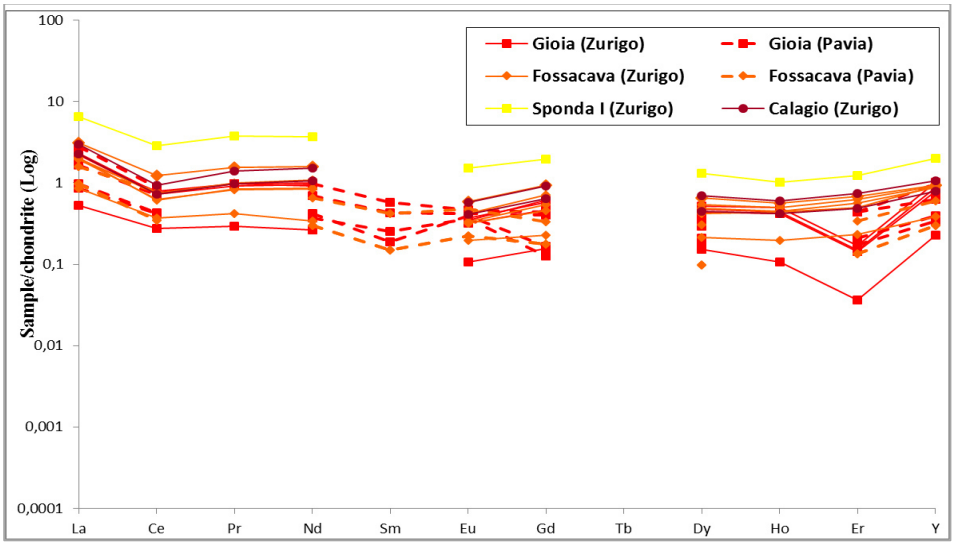

Fig. 4.3.1.2: Patterns of REE + Y in calcite for Carrara (Italy) white marble. The two districts are displayed using differing symbols and colors: red line for the Gioia quarry, orange line for the Fossacava quarry, garnet line for the Calagio quarry and yellow line for the Sponda I. Continuous lines are for samples analyzed at the ETH of Zürich, whereas dashed lines are for those analyzed at the IGC-CNR Pavia. The concentrations are normalized to chondrite (Taylor and McLennan (1985)).

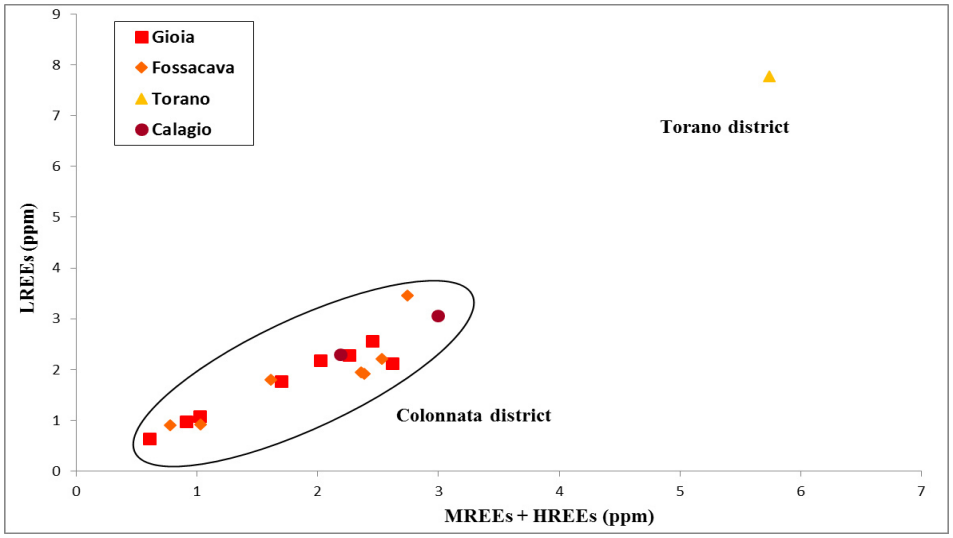

Fig. 4.3.1.3: MREE + HREE *vs* LREE diagram of Carrara marble. The REE concentrations discriminate the two different districts. Torano marble has the highest content compared to Colonnata marble. The LREE enrichment seems to be quite linear.

In the following binary plots, some of the geochemical features observed in the former diagrams have been highlighted. In this way the elements or groups of elements are more useful for a characterization of the quarrying areas.

In Figure 4.3.1.4, the HFSE content is plotted against contents of the REE. The Torano sample has the highest content for both groups, whereas samples from the Colonnata district form a distinct group.

Lastly, if the REE content is compared with Fe + Mn content (Fig. 4.3.1.5), the two regions fall in a completely separate region of the diagram. REE content of sample from the Torano district are the highest.

The different trace elements observed in TR8 sample from Torano district underlines the necessity to evaluate a greater number of specimens.

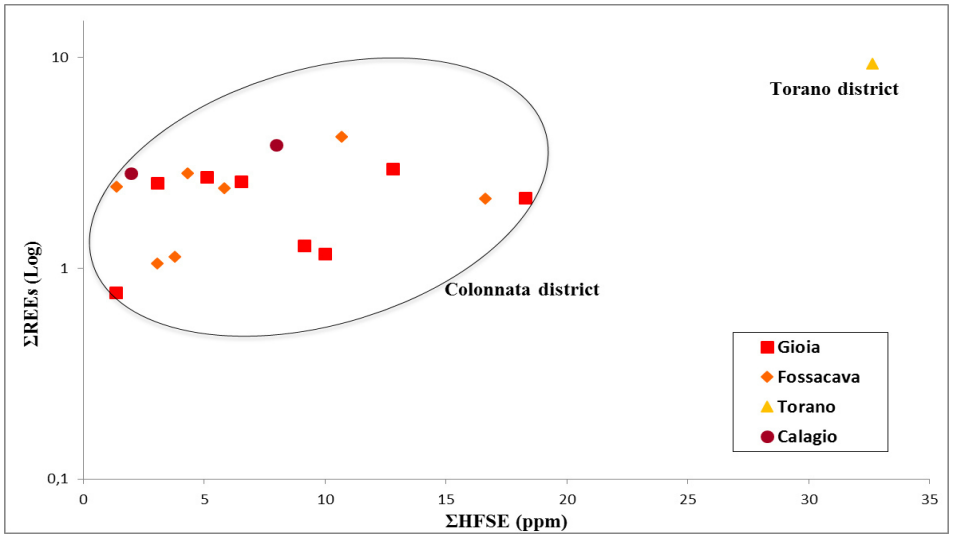

Fig. 4.3.1.4: Sum of REE *vs* sum of HFSE diagram. The Torano district has high HFSE content, the Sponda I sample (yellow triangle). The Colonnata district has a heterogeneous content which limits discriminations among the quarries.

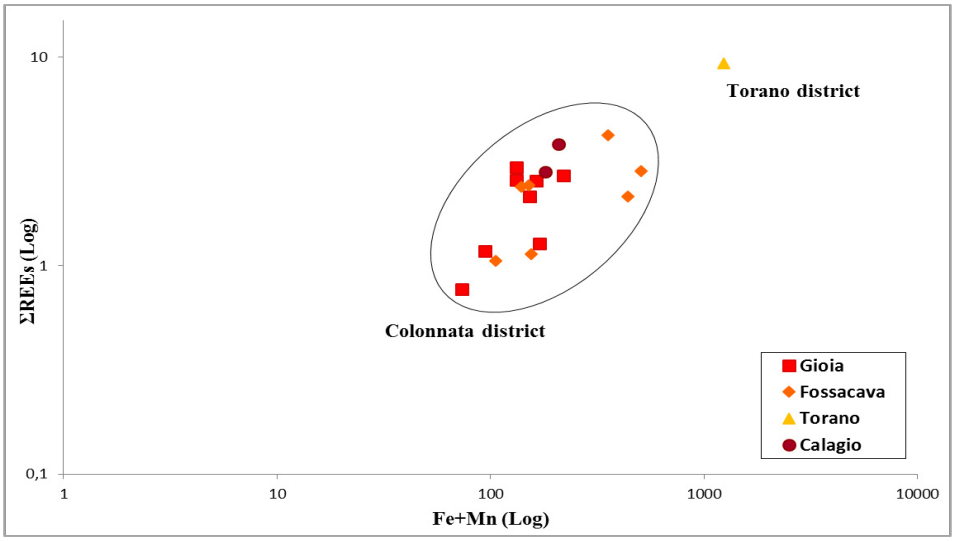

Fig. 4.3.1.5: Fe+Mn *vs* REE diagram. The Carrara marble shows different concentrations between the two districts of Colonnata and Torano. The Torano district (yellow triangle) has a high enrichment in Fe and Mn and high content of REE.

4.3.2 Paros

The samples of white marble from Paros come from two different quarries, located in the inner area of the island and active the since pre-classic period. The samples of these two quarries were called Paros and PAROS1 (light blue line), respectively.

In effect, samples of the two marble quarries are different in terms of trace-element enrichment, as showed by chondrite-normalized multi-elemental diagram (Fig. 4.3.2.1). Seven samples identified as Paros (dark blue line) are characterized by a low variability in the whole patterns. The LIL elements show positive anomalies for Ba and Sr and negative for Rb and K. Only one sample has higher concentrations.

The HFSE element patterns are similar to those of Carrara marble, being enriched in U and Hf and depleted in Th, Nb, Zr and Ti, even though some samples display scattered concentrations.

Concerning the REE + Y, Paros specimens have a wider range of trace concentrations, albeit keeping similar patterns of distribution, especially for one sample (CYPA3) that is particularly enriched in REE. In addition, a sharp negative Ce anomaly has been observed.

Sample PAROS1 is characterized by high concentrations of Rb, Ba, K. It has an opposite behavior with respect to that of samples from Paros; the patterns of LILE are typical and exclusive for this district (Fig. 4.3.2.1).

The HFSE patterns in PAROS1 are similar to Paros, but with a significantly high content of Th and U.

In addition, PAROS1 sample is characterized by low REE content.

The multi-elemental diagram for the REE and Y confirms the differences between Paros and PAROS1, allowing one to recognize two separate groups (Fig. 4.3.2.2). In fact, with respect to Paros, it has no sharp negative Ce anomaly (value of Ce anomaly is 0.8 in

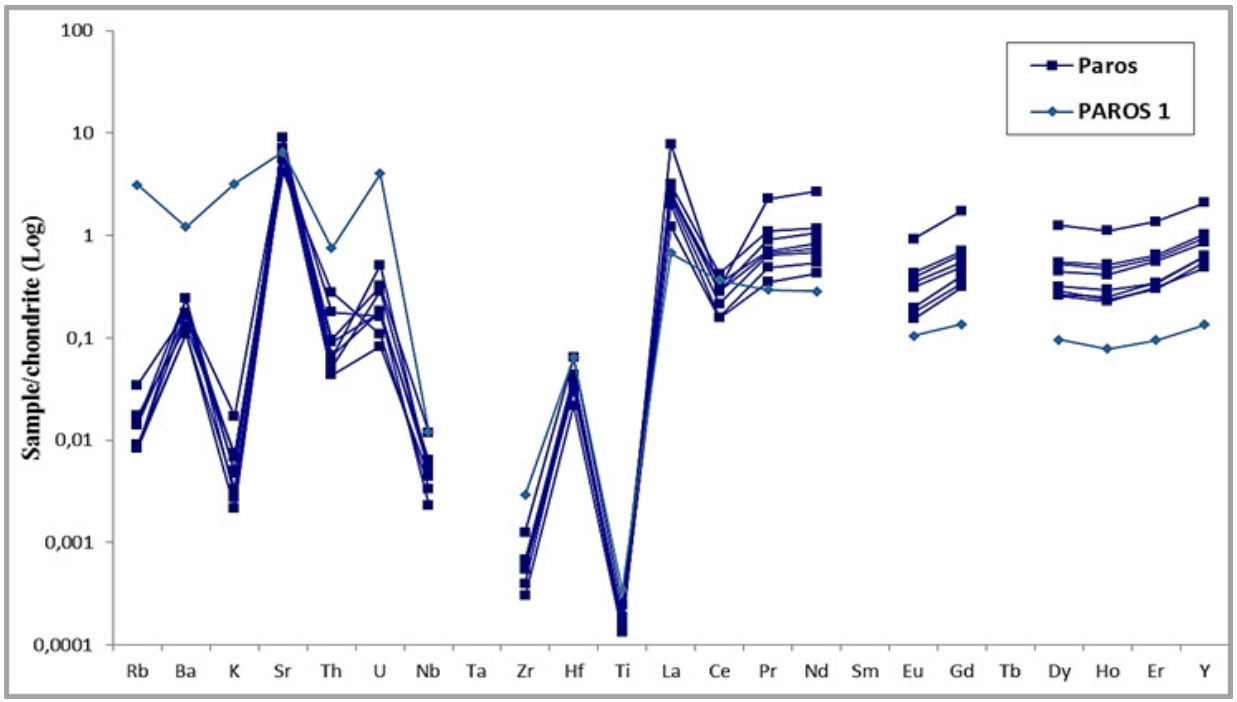

Fig. 4.3.2.1: Patterns of trace elements in Paros white marble. The two districts are displayed using differing symbols and colors: dark blue line for Paros quarry, light blue line for PAROS1 quarry. All samples were analyzed only at the ETH of Zürich and were represented by a continuous line. The concentrations are normalized to chondrite (Sun and McDonough (1989)).

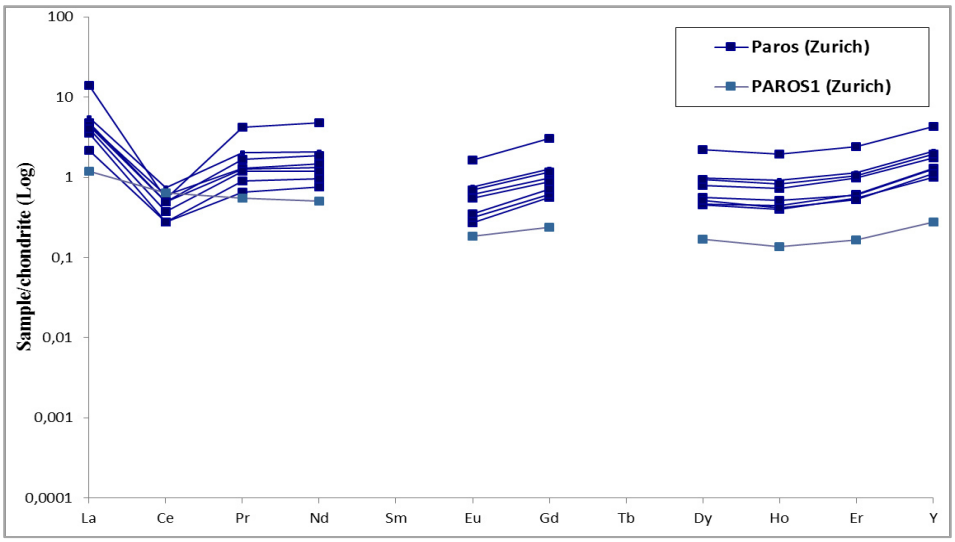

Fig. 4.3.2.2: Patterns of REE + Y in calcite for white fine-grained Paros marble. Samples represented by dark blue line are from Paros quarry, and by light blue line are from PAROS1 quarry. The concentrations are normalized to chondrite (Taylor and McLennan (1985)).

PAROS1, whereas it varies in the range 0.07 to 0.2 in the seven samples of Paros).

The sample of PAROS1 is characterized by a low content of REE, particularly for MREE and HREE, whereas the concentrations of the LREE are similar them of Paros (Fig. 4.3.2.3).

In Fig. 4.3.2.4, the Paros samples are separated from PAROS1 again by a high concentration of the REE, whereas the concentrations of HFSE are similar for both localities.

However, as observed in the multi-element diagrams above reported, the content of LILE and REE seem to separate better between Paros and PAROS1 marbles. Indeed, the diagram LILE vs REE + Y (Fig 4.3.2.5), there is evidence of two separate clusters due to the different concentration of these traces. Only sample CYPA3 from Paros is completely separate from other specimens for a high enrichment in REE.

Moreover, the samples of these two localities fall in two separate groups also if one considered the content of REE and Y *vs* Fe+Mn. In Fig. 4.3.2.6, two distinct groups are evident also for the high concentration of Fe and Mn in PAROS1.

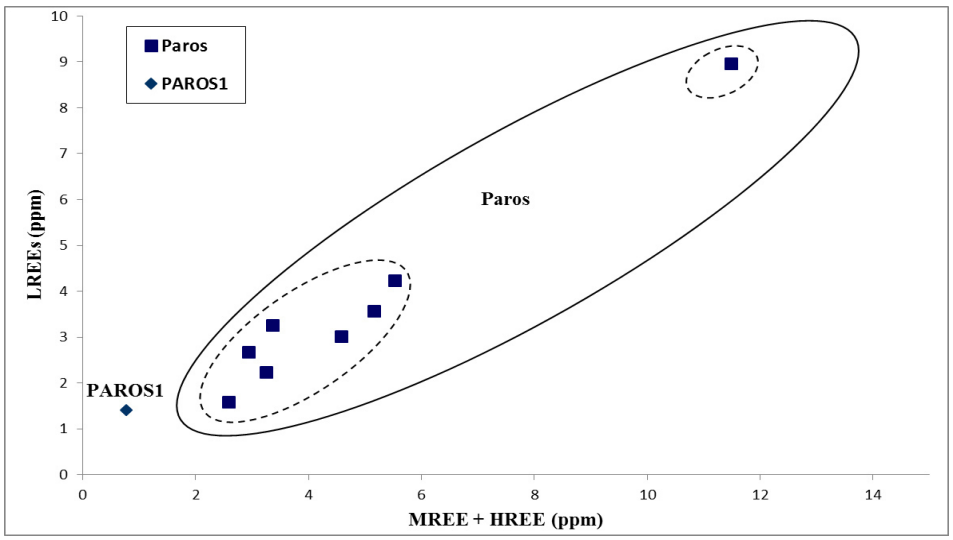

Fig. 4.3.2.3: LREE *vs* ΣHREE diagram. PAROS1 (light blue rhombus) is characterized by low content of REE, whereas Paros samples (dark blue square) are characterized by higher REE concentrations. The Paros samples are divided in two subgroups, mainly on the basis of HREE enrichment.

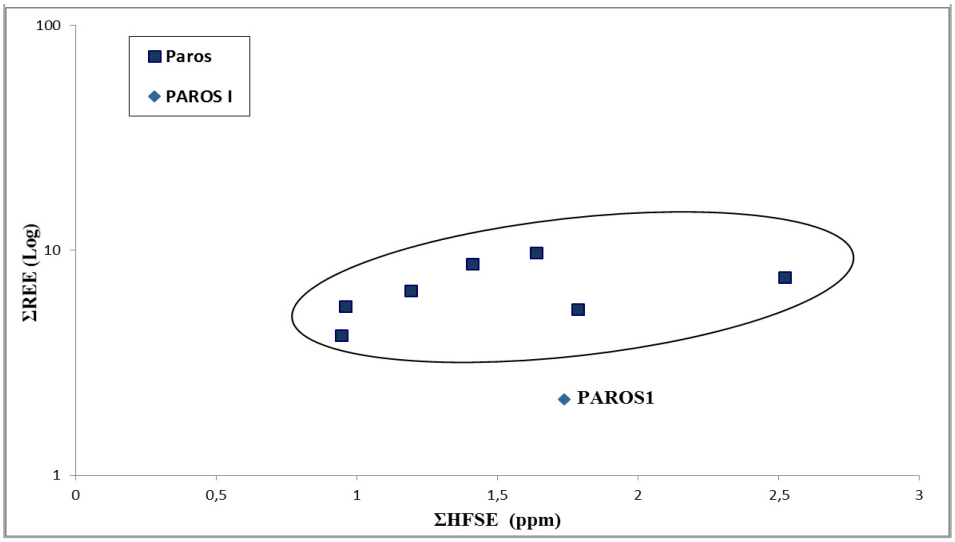

Fig. 4.3.2.4: Σ HFSE *vs* Σ REE diagram. Sample PAROS1 (light blue rhombus) has an intermediate value of HFSE concentration (1.7 ppm) compared to Paros samples (dark blue square), where the content of both elements fluctuate from 1 to 2.5 ppm.

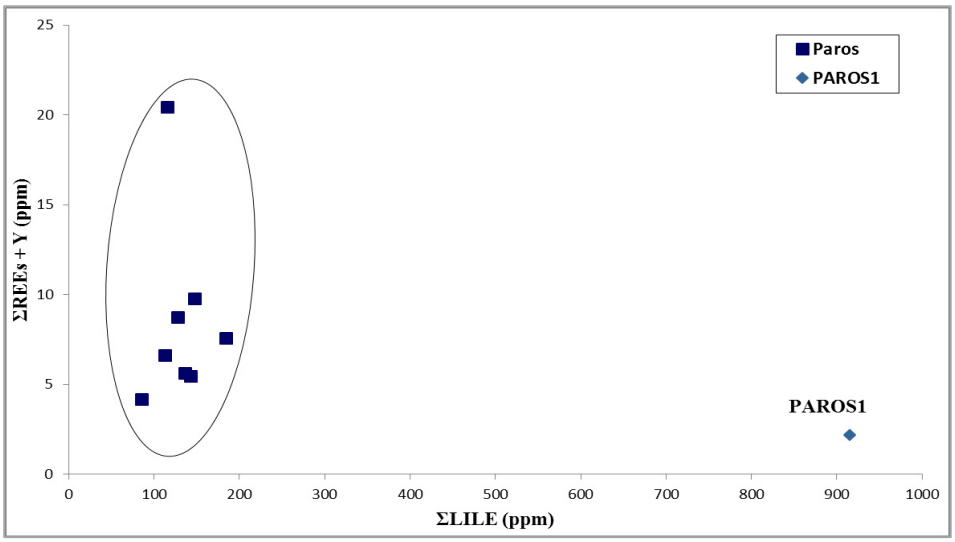

Fig. 4.3.2.5: Σ LILE *vs* Σ REE + Y diagram. Paros samples (dark blue square) have lower content of LILE than PAROS1 sample (light blue rhombus).

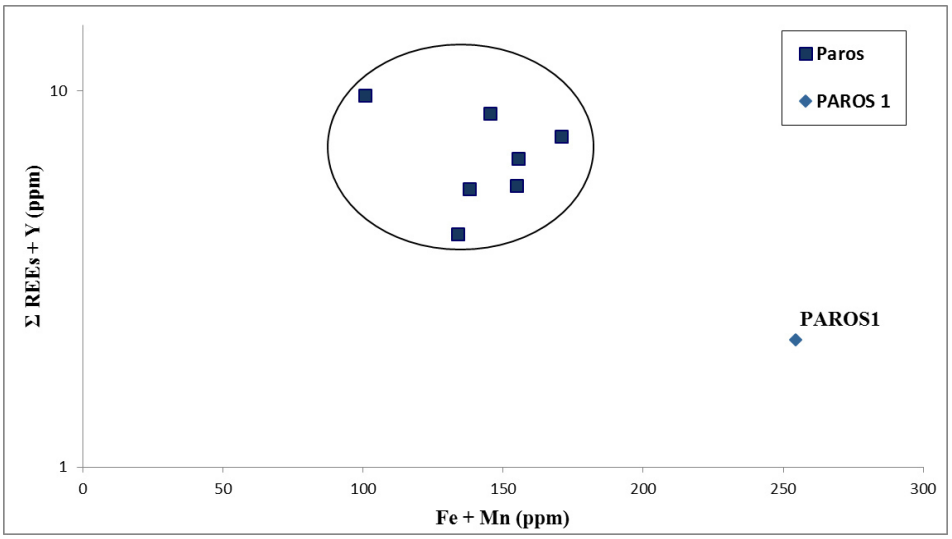

Fig. 4.3.2.6: Fe+Mn *vs* Σ REE diagram. Content separates the two samplings. PAROS1 (light blue rhombus) has a higher content of Fe + Mn than those of Paros (dark blue square).

4.3.3 Pentelic marble

The quarries of white marble of Mount Pentelicon are located in the region of Spilià, Kokkinaras, and Quarry I. The Spiliá region is divided into two quarries called Spiliá upper level (quarry 13-15) and Spiliá lower level (quarry 6-8), respectively.

The multi-elemental diagram, shown in Fig. 4.3.3.1, highlights for the LILE the usual enrichment in Sr and in Ba, seen in the previous districts, with Ba concentration really scattered. Rubidium and K have similar patterns, and the content is lower for the samples analyzed at the ETH respect to those analyzed at IGG-CNR, the same behavior as shown for the K content in the Carrara samples.

The HFSE patterns of Pentelic marble are similar to Carrara and Paros samples, having an enrichment in U, Ta and Hf, and a depletion in Th, Nb, Zr and Ti. The content of U varies not only within the same district, but also within a single quarry. The concentration of HFS elements seems to discriminate the white marble of different quarrying area, especially for the Quarry I samples, which show depletion in HFSE, whereas the Spilià district has the highest content. Moreover, as observed for Paros marbles, the concentrations of HFS elements are very scattered when compared to LIL elements.

These three regions show a different concentration values for the REE, in particular, Quarry I is very well discriminated respect to the other quarries by the significant low content in all REE and Y. All specimens are characterized by a negative Ce anomaly, more pronounced in Kokkinaras district (Ce* 0.3), weak or absent in Quarry I (average Ce* 0.7). The Spilià district has Ce* intermediate, varying from 0.6 in the upper level quarries to 0.5 in the lower level.

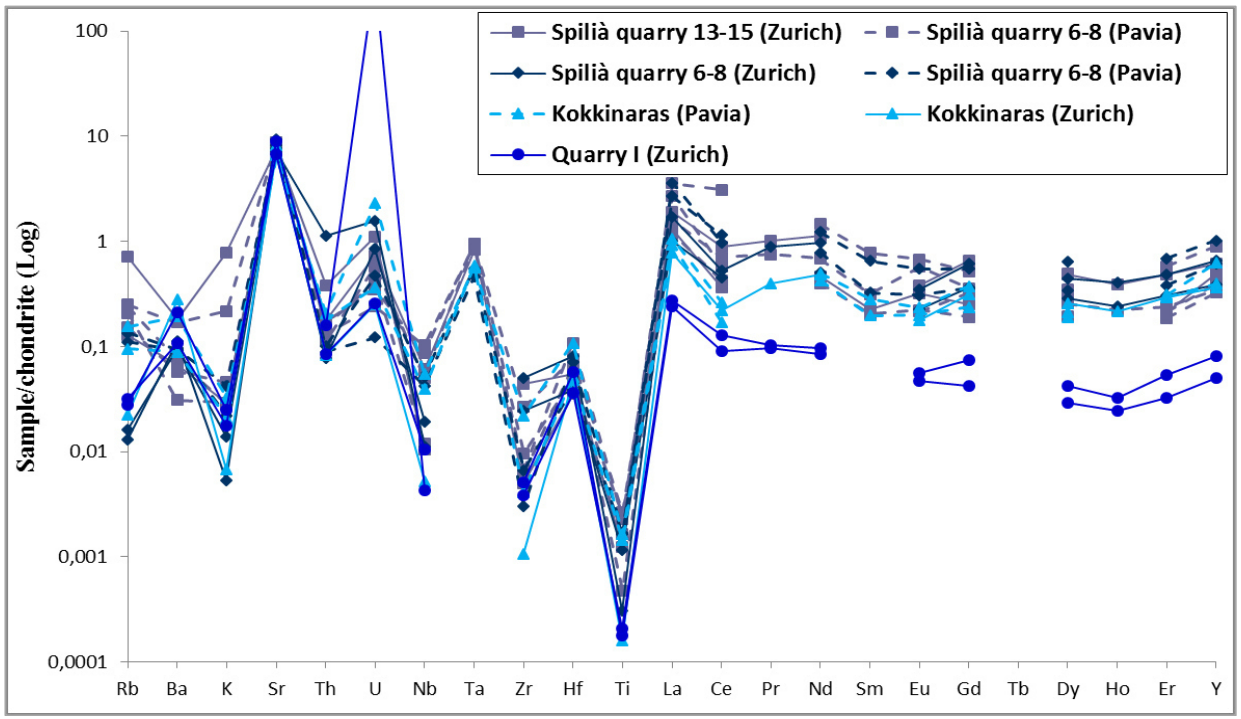

Fig. 4.3.3.1: Patterns of trace elements in Pentelic white marble. Three districts are considered and represented by different shade of blue and symbols: for the Spilià district, a lilac line characterizes the high level of the quarry face (quarry 13-15), a dark blue line for the low level (quarry 6-8); a light blue line for Kokkinaras, and a bright blue line for Quarry I. In addition, continuous lines are for samples analyzed at the ETH of Zürich, whereas dashed lines for those analyzed at the IGC-CNR Pavia. The concentrations are normalized to chondrite (Sun and McDonough (1989)).

In more detail, as shown in Fig. 4.3.3.2, the Spilià districts (Quarry 13-15, Quarry 6-8) have the highest content of REE, differing from Quarry I which, conversely, has the lowest content, with a significant depletion in the HREE (Dy, Ho and Er); the Kokkinaras district (bright blue) has intermediate values for the LREE. The concentrations of MREE and HREE are close to samples from Spilià, accounting the overlapping of the lines. Such differences are highlighted in Figure 4.3.3.3, where Quarry I lies at the bottom left of the diagram owing to its lowest content of all REE. Kokkinaras samples have a lower content of LREE compared to those of Spilià and a similar content in MREE and HREE.

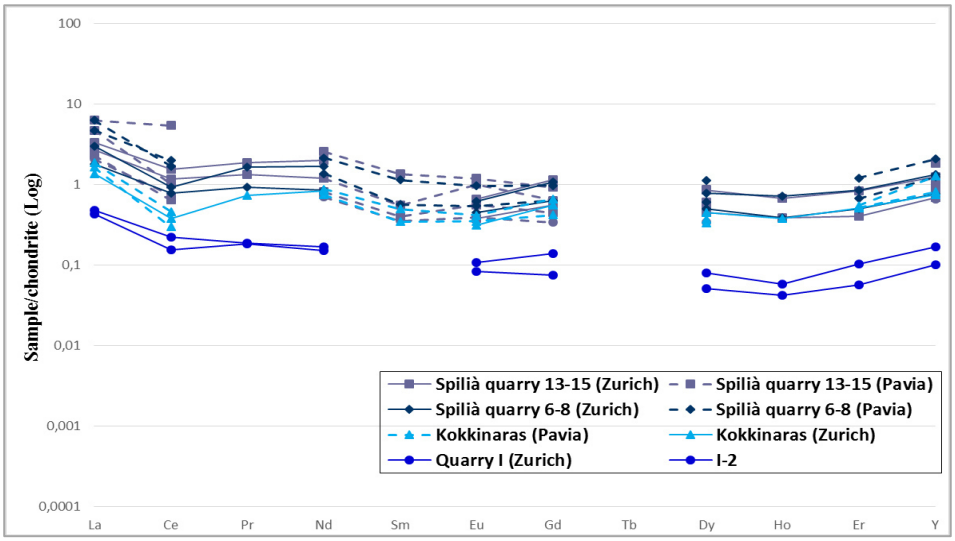

Fig. 4.3.3.2: Patterns of REE + Y in Pentelic marble. As described for the diagram above, the Spilià district is displayed by a lilac line for the high level of the quarry face (quarry 13-15) and a dark blue line for the low level (quarry 6-8); a light blue line for Kokkinaras and a bright blue line for Quarry I. The concentrations are normalized to chondrite (Taylor and McLennan (1985)).

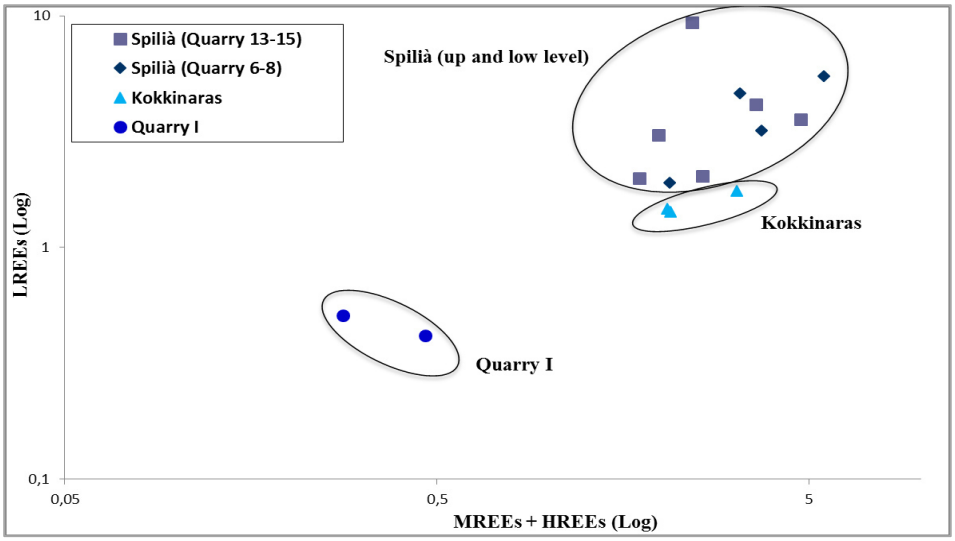

Fig. 4.3.3.3: Σ HREE vs Σ LREE diagram. REE content is different in marble from Quarry I (bright blue dot) district to Kokkinaras (light blue triangle) and Splià (lilac square and dark blue rhombus) districts. Quarry I has the lowest REE content while Kokkinaras has intermediate values among Spilià and Quarry I.

Among trace elements, the REE discriminate Pentelic districts, especially on the basis of Ce and Eu content (Fig. 4.3.3.4). Indeed, white marble samples from different sites form well defined clusters, *i.e.,* the marble from Spilià quarries has a high content of Ce, the Kokkinaras samples present an intermediate content of both elements, and the Quarry I samples fall in a separate cluster owing to its very low content in Ce and Eu.

In Figure 4.3.3.5, the comparison between the content of HFSE and REE + Y was used to discriminate among districts: however, they have similar concentrations and patterns, resulting in difficulties to discriminate the different quarrying areas on the basis of these traces, even though the content of HFSE in marble from Quarry I is lower than the others.

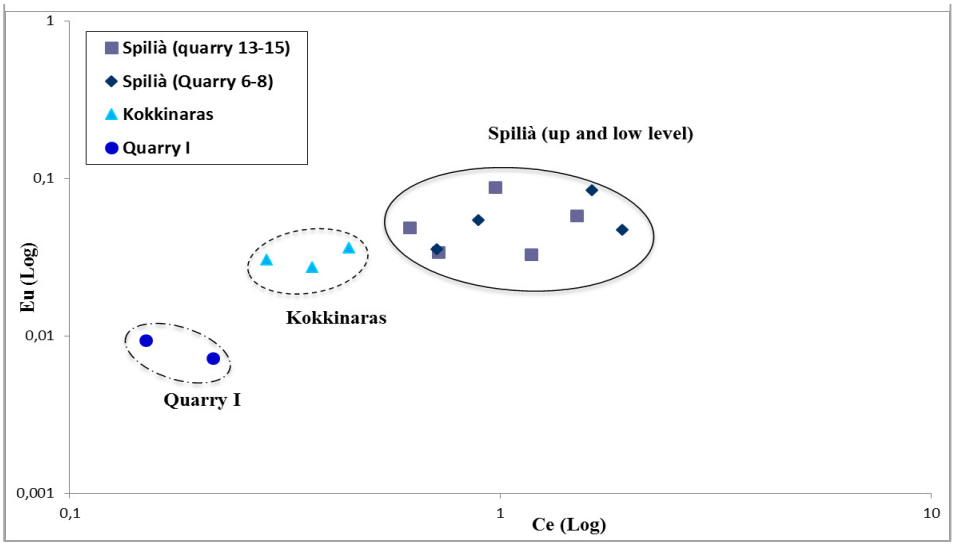

Fig. 4.3.3.4: Diagram of Ce (LREE) *vs* Eu (MREE) content in calcite allows one to separate distinctively the three districts. A progressive enrichment in Ce and Eu has been observed from the lowest content in Quarry I (bright blue circle), Kokkinaras (light blue triangle) and then in Splià (lilac square and dark blue rhombus).

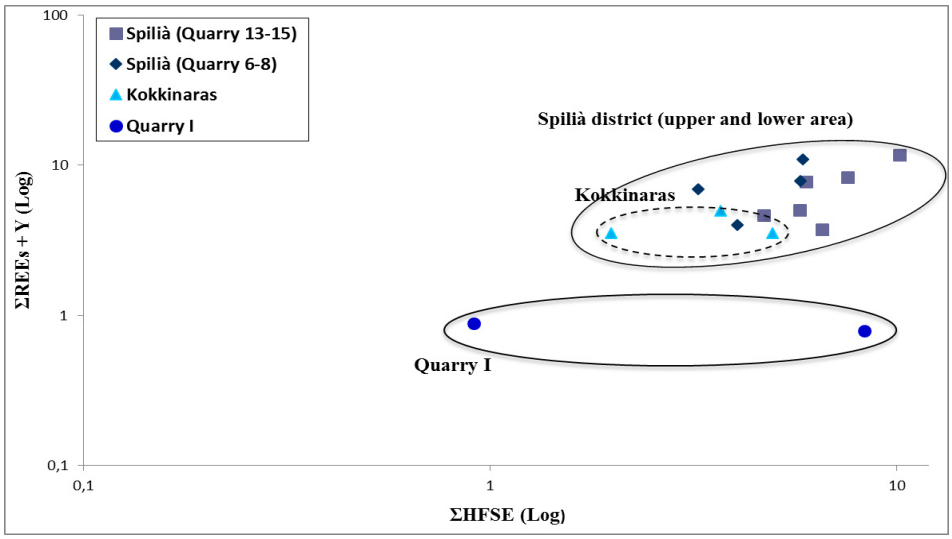

Fig. 4.3.3.5: Diagram of Σ REE *vs* Σ HFSE content. Concentrations of these two groups of trace elements are similar; one sample from Quarry I (bright blue circle) has a significantly lower content in HFSE, and Kokkinaras (light blue triangle) and both Spilià specimens (lilac square and dark blue rhombus) form a separate group owing to the enrichment in REE.

Calcite of Pentelic marbles are enriched in Fe and Mn, with values comparable to Carrara samples. In Fig. 4.3.3.6, all specimens have an extremely variable range of concentrations, and only two samples of the Kokkinaras site have a lower content compared to Spilià and Quarry I districts.

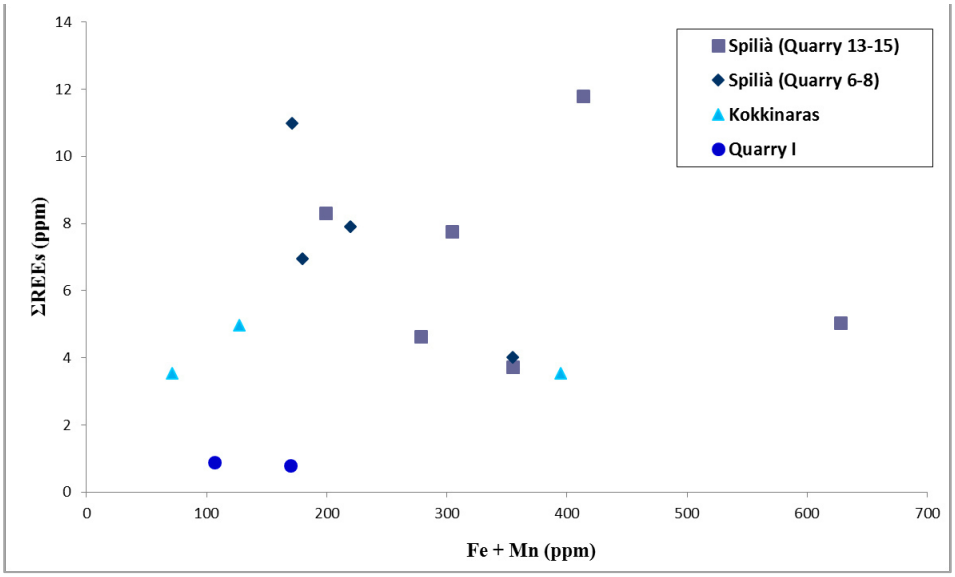

Fig. 4.3.3.6: Fe+Mn vs Σ REE diagram. The three districts are characterized by a comparable value of these elements, making it impossible to discriminate Kokkinaras from Quarry I and Spilià districts.

4.3.4 Afyon marble

The white marble from Afyon, active since Roman period, is known as “Latin quarries”. In particular, the samples are from Bacakale (dark green line), Roder (bright green line), Boluk Mermer (light green line) and Mermer Isletmesi (deep green line) quarries.

In the spider diagram (Fig. 4.3.4.1), among LILE and HFSE, Ba, Sr, U, Ta, Hf have positive anomalies and K, Th, Nb Zr, Ti negative anomalies, as previously observed in samples from Paros. The content of Rb is lower in samples analyzed at the ETH with respect to those analyzed at Pavia, as already observed in marble specimens reported above.

The concentrations of LIL and HFS elements are heterogeneous, although the distribution patterns are similar. A first discrimination among the quarry sites from Afyon can be made on the basis of Ba and Rb content. Indeed, Bacakale quarry has the lowest content in Ba and Rb (Fig. 4.3.4.1); the Roder quarry has an intermediate content and, Boluk Mermer and Mermer Isletmesi have the highest values. In addition, all specimens have a wide range of concentrations for Sr, not seen in marble from other sites.

The REE patterns are quite similar in marble samples from all Afyon districts, and, although the samples are characterized by a wide range of concentrations within quarries, some differences are remarkable among the districts. Boluk Mermer and Bacakale (except one sample D43a) have the highest concentrations in REE and Y, whereas Mermer Isletmesi quarry has the lowest concentrations (Fig. 4.3.4.2). Moreover, Mermer Isletmesi has a negative anomaly with an average value 0,7 for Ce*, while for the other three regions, the negative anomaly has average values slightly lower, ranging from 0,5 to 0,6.

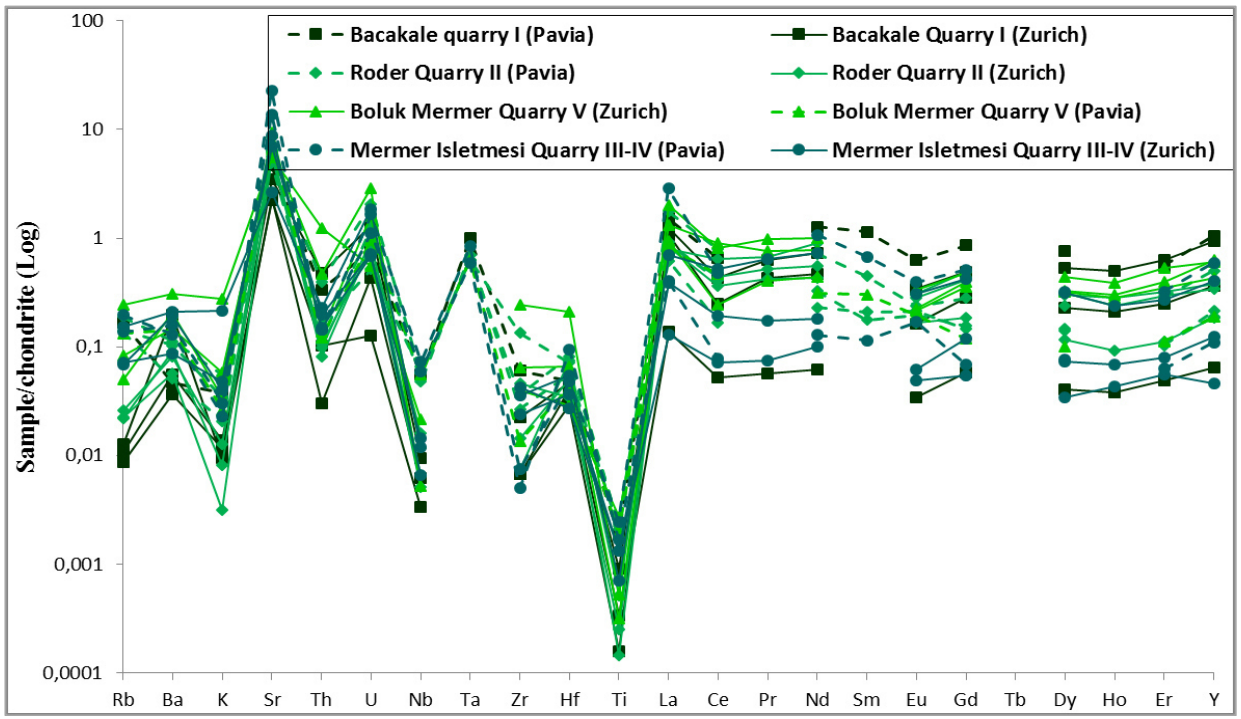

Fig. 4.3.4.1: Patterns of trace elements in the Afyon white marble. Samples are represented by using different shades of colors and symbols: Bacakale (dark green line), Roder (bright green line), Boluk Mermer (light green line) and Mermer Isletmesi (deep green line) quarries. In addition, continuous lines are for samples analyzed at the ETH of Zürich, whereas dashed lines are for those analyzed at the IGC-CNR Pavia. The concentrations are normalized to chondrite (Sun and McDonough (1989)).

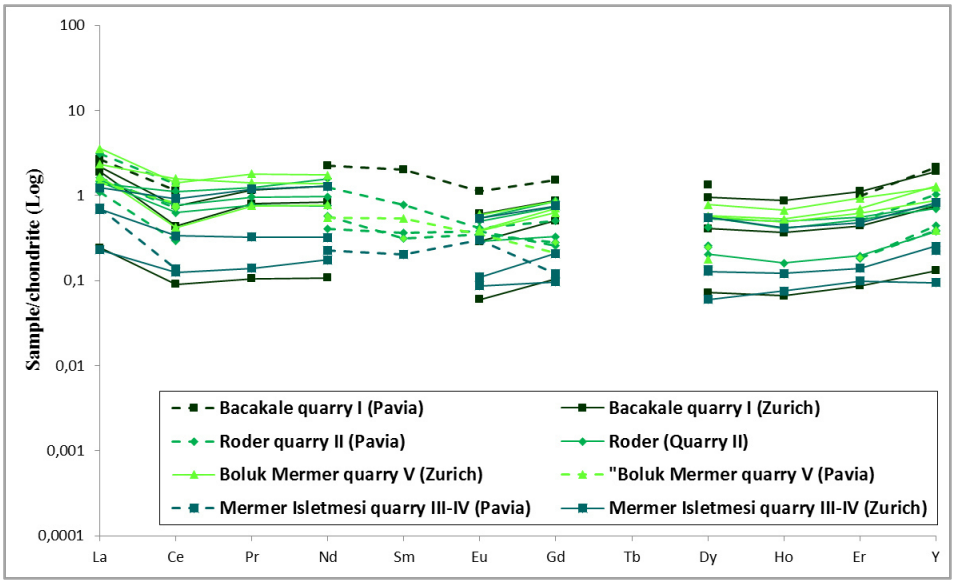

Fig. 4.3.4.2: Patterns of REE + Y in white Afyon marble from four different sites of extraction: Bacakale (dark green line), Roder (bright green line), Boluk Mermer (light green line) and Mermer Isletmesi (deep green line). Continuous lines refer to samples analyzed at the ETH of Zürich, whereas dashed lines for those analyzed at the IGC-CNR Pavia. The concentrations are normalized to chondrite (Taylor and McLennan (1985)).

In the bivariate diagram (Fig. 4.3.4.3), the marble samples from Bacakale and Mermer Isletmesi quarries present a positive correlation between LREE and MREE + HREE. Those from the other two quarry sites (Roder and Boluk Mermer) are characterized by enrichment in both the MREE and HREE. The clusters of marbles from different districts from Afyon commonly overlap, thus resulting in difficulties to discriminate among the several quarry sites; however, some considerations above reported remain valid.

Contrary to the quarrying areas treated up to now (i.e., Carrara, Paros and Penteli), where fine-grained marble was quarried, the Afyon marble have a similar content of HFSE and REE +Y so that, as shown in Fig. 4.3.4.4, the samples from the sites overlap each other.

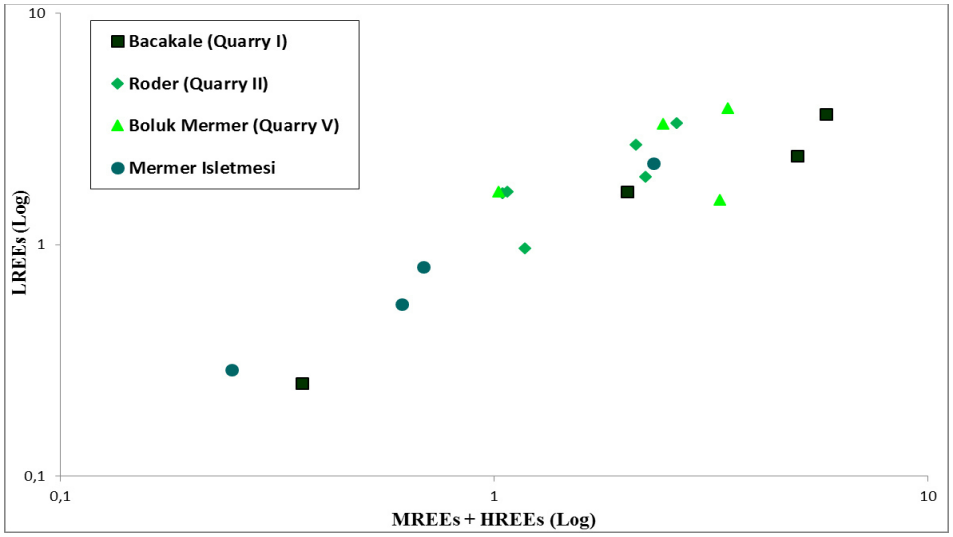

Fig. 4.3.4.3: Σ MREE + Σ HREE *vs* Σ LREE diagram.

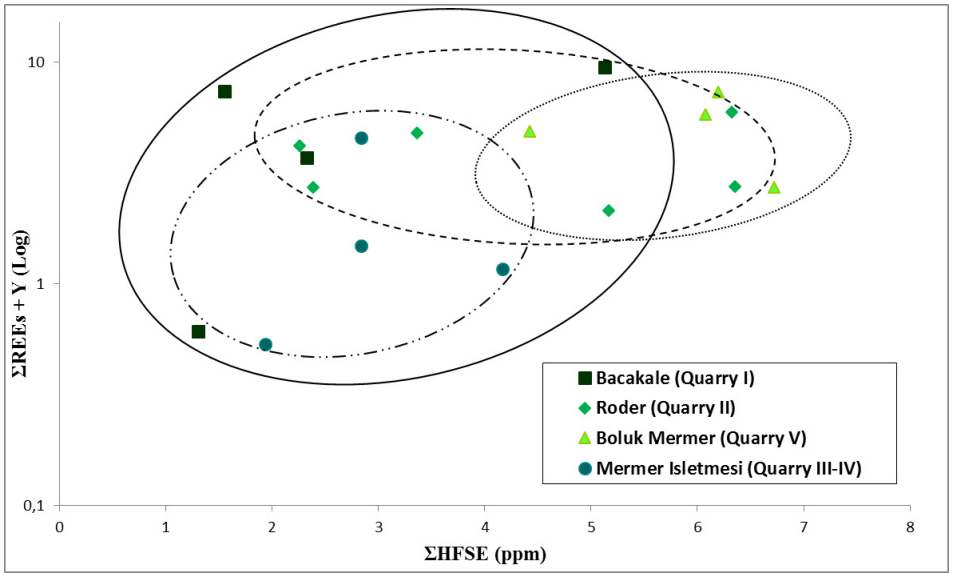

Fig. 4.3.4.4: Σ HFSE *vs* Σ REE diagram. The content of these trace elements is extremely heterogeneous in all specimens. The Quarry of Boluk Mermer (light green triangle) together with three samples of Roder have a higher content in HFSE, whereas two samples of Bacakale (dark green square) have an enrichment in REE.

In the plot in Fig. 4.3.4.5, a comparison of the content in Fe + Mn *vs* Σ REE + Y brings out the same issues faced so far, where effectively samples from the same quarries fall quite close, forming different clusters. These groups, however, are not maintained and tend to overlap when all the districts are plotted together.

So far, this white marble does not show similar trace elements content and patterns for all specimens analyzed, in particular for the REE and Sr. Indeed, in the diagram Sr *vs* REE+ Y (Fig. 4.3.4.6), Bacakale and Mermer Isletmesi samples fall in two distinct groups, whereas, Roder and Boluk Mermer quarries fall together in a separate cluster.

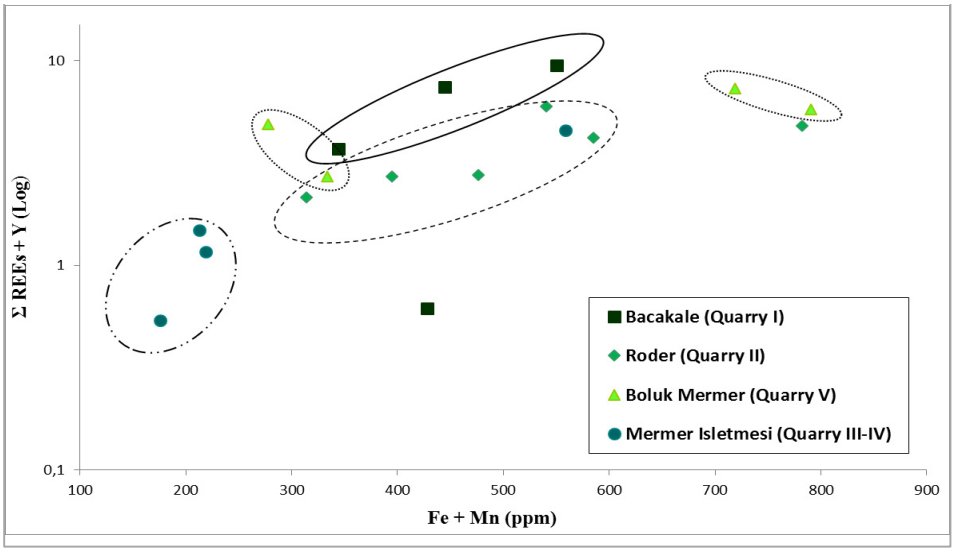

Fig. 4.3.4.5: Fe+Mn *vs* Σ REE diagram. The three districts have a wide range for Mn+Fe content, making it impossible to discriminate the districts; Mermer Isletmesi (deep green circle) has the lowest content (except for one sample), whereas Boluk Mermer (light green triangle) has a broader range of concentrations (from 280 to 790 ppm).

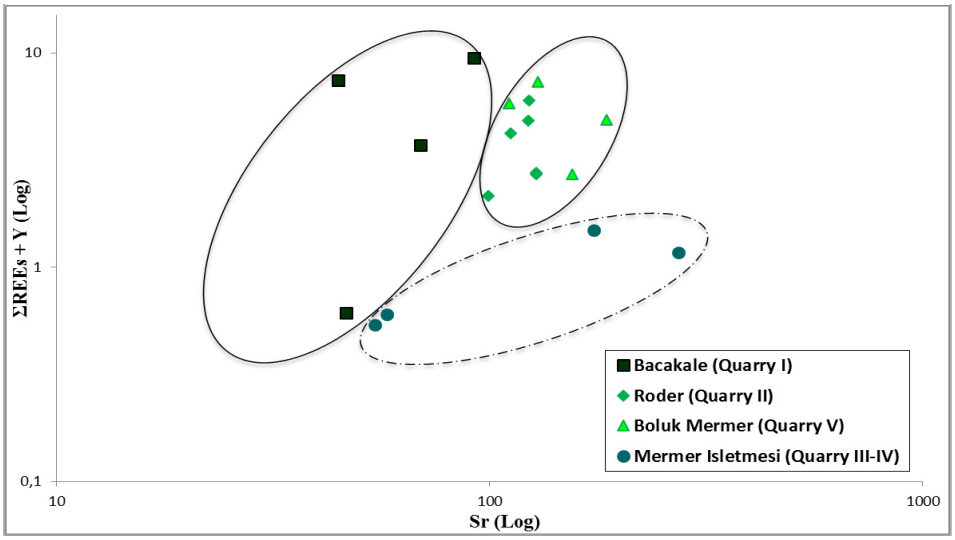

Fig. 4.3.4.6: Sr content *vs* Σ REE+ Y. Three separate groups are formed; Quarries of Mermer Isletmesi are characterized by a depletion in REE but a higher content of Sr, compared to Bacakale (dark green square). Regions of Roder and Boluk Mermer form a unique group with intermediate values.

4.3.5 Göktepe marble

The marble specimens from Göktepe were sampled in a single quarry and analyzed only at the laboratory of ETH (Zürich).

In Figure 4.3.5.1, the multi-elemental diagram shows a variable content of LILE, except for Sr. The patterns of Rb, Ba and K are very scattered, and their low content is close to the detection limit of the analytical technique used.

The HFSE show similar concentrations for what concerns a depletion of Th, Nb, Zr, Ti and enrichment in U and Hf. Only two samples have high concentrations of HFSE, in particular those of U, Nb and Zr.

The REE distribution is heterogeneous for all Göktepe samples, but at the same time helpful to characterize this marble. Indeed, the calcite in Göktepe marble presents a negative Ce anomaly, with Ce* values from 0.3 to 0.6. In addition, a marked negative Y anomaly has been observed, except for two samples (GT2 and GT3).

The spider diagram (Fig. 4.3.5.2) highlights that the marble from this quarry has a very low content in REE when compared to those from other quarrying areas previously presented.

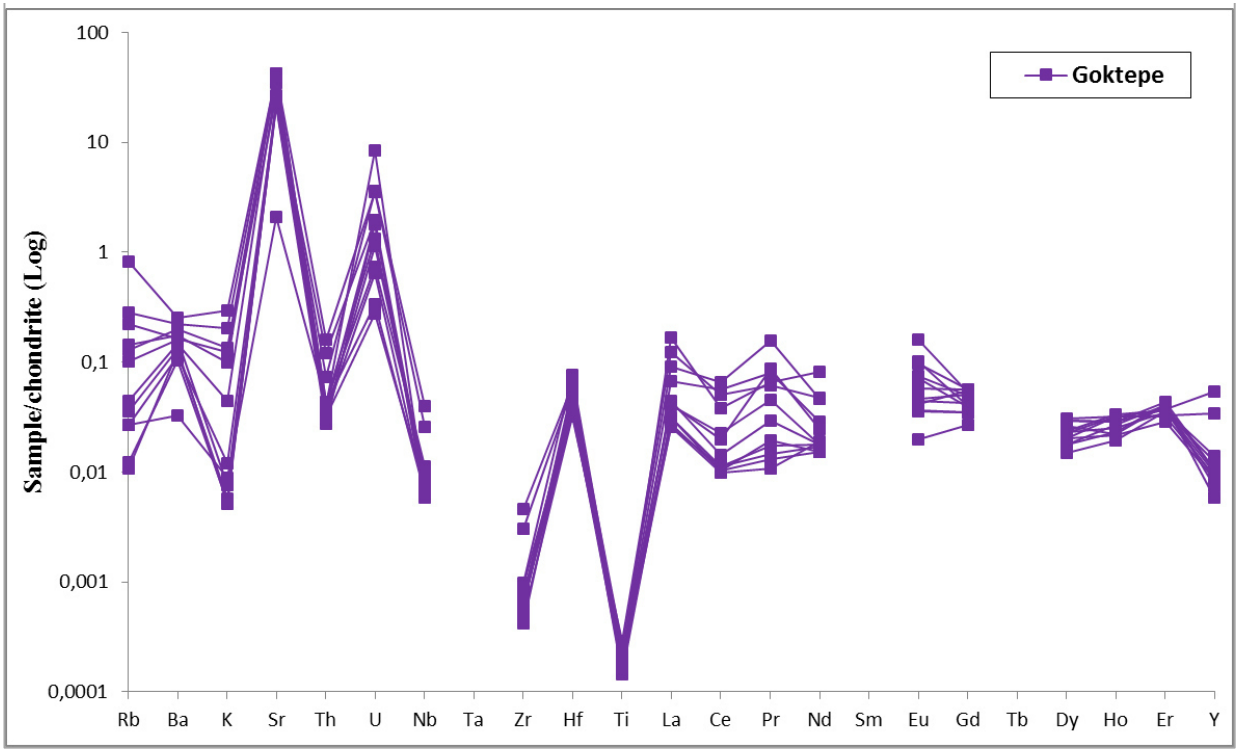

Fig. 4.3.5.1: Patterns of trace elements in white Göktepe marble. The concentrations are normalized to chondrite (Sun and McDonough (1989)).

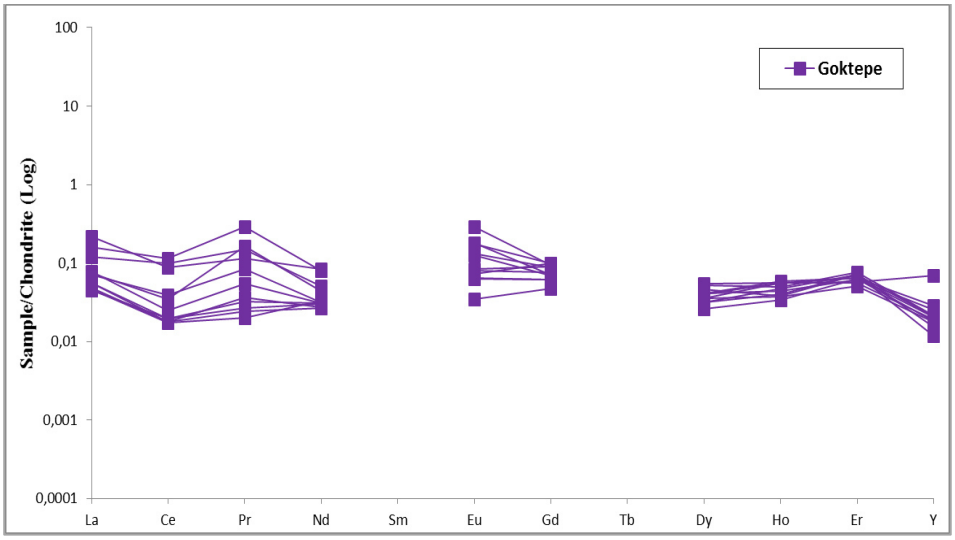

Fig. 4.3.5.2: Patterns of REE + Y in white Göktepe marble. The concentrations are normalized to chondrite (Taylor and McLennan (1985)).

The low REE content is more evident in Fig. 4.3.5.3, where the range of concentrations is reported. Although this group of trace elements varies over a short range of concentrations, it is interesting to observe the formation of two groups due to a different increasing of HREE *vs* LREE. Some specimens show a slight enrichment in LREE.

Figure 4.3.5.4 shows that the content of HFSE in Göktepe marble is comparable to that of REE, having both groups of elements concentrations lower than 1 ppm.

The concentrations of Fe and Mn in Goktpe marble are similar to marble from other quarrying sites, and also similar among different samples (Fig. 4.3.5.5).

Although the trace-element content in Göktepe marble is the lowest encountered so far, the Fe + Mn concentration is fairly similar to the other sites, and also similar among the samples (Fig. 4.3.5.5).

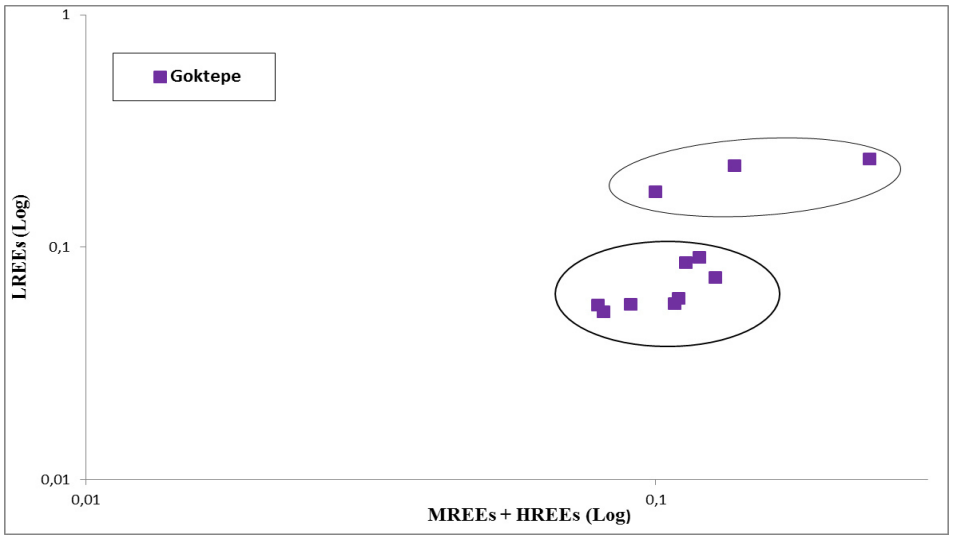

Fig. 4.3.5.3: Σ MREE + Σ HREE *vs* Σ LREE diagram. The different content of LREE separates Göktepe samples into two subgroups.

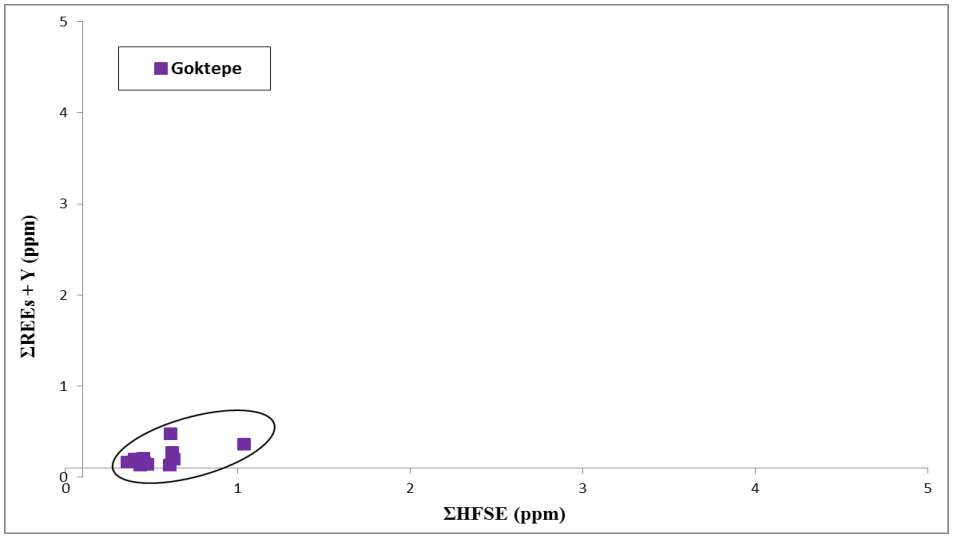

Fig. 4.3.5.4: Σ HFSE vs Σ REE + Y content in calcite of Göktepe marble. Samples have a low content of HFSE too with values comparable with those of the Σ REE. The range of values of HFSE fluctuate from 0,3 to 1 ppm, whereas for the REE it is even more lower, from 0,1 to 0,4 ppm.

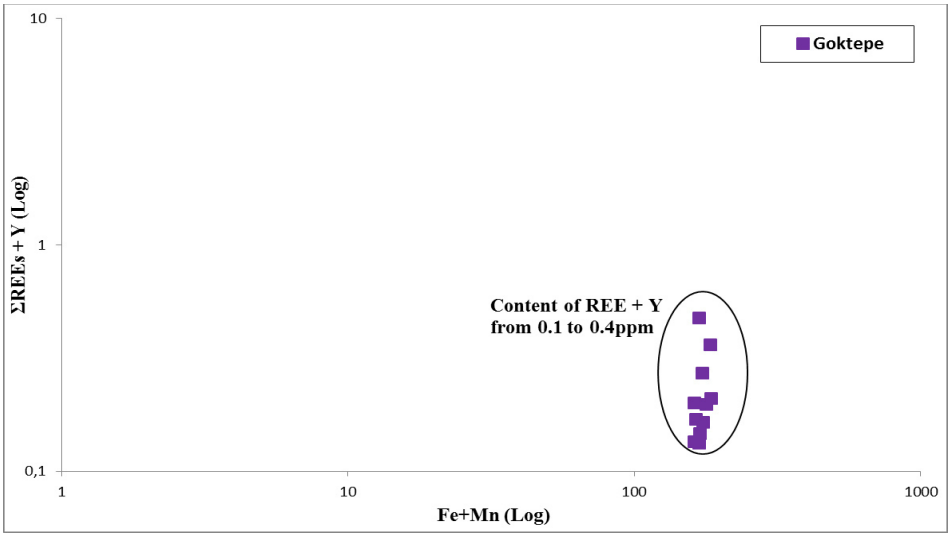

Fig. 4.3.5.5: Fe + Mn *vs* Σ REE diagram.

4.4 Trace-element abundances in coarse-grained white marble

4.4.1 Naxos

The white marble of Naxos, exploited since prehistoric times, was the earliest known white lithotype used in the Greek world. The quarries of this area are mostly located in the central and northern parts of the island (Chapter 3, Fig. 3.2.1.1).
The samples available for this project consist of a unique sampling set, grouped under the name of “Naxos-CYPA”.

The Naxian marble samples are enriched in Sr and Ba among the LILE and in U and Hf among the HFSE, and depleted in Rb, K and in Th, Nb, Zr and Ti (Fig. 4.4.1.1). Three samples show a higher depletion in Nb and Zr, forming a separate group from the remaining three samples. The chondrite-normalized multi-elemental diagram shows almost homogeneous LILE and HFSE patterns. Conversely, the REE elements, distinguish two main groups of Naxian specimens (Fig. 4.4.1.2. All samples are enriched in La and Ho and depleted in Dy. A negative Er anomaly has been observed for the samples with high content of REE, whereas the other three samples show a scattered content. The two groups are also characterized by different patterns of Ce and enrichment in Y. The average value for Ce anomaly (Ce*) is 0.4 (CYPA70, CYPA72 and CYPA81) and 0.8 (CYPA75, CYPA77 and CYPA78), respectively.

The REE enrichment of white Naxian marble is shown in Figure 4.4.1.3. One group (*i.e.,* CYPA75, CYPA77 and CYPA78) has the highest content in REE with enrichment in medium and heavy REE, whereas the second group has an enrichment of both elements.

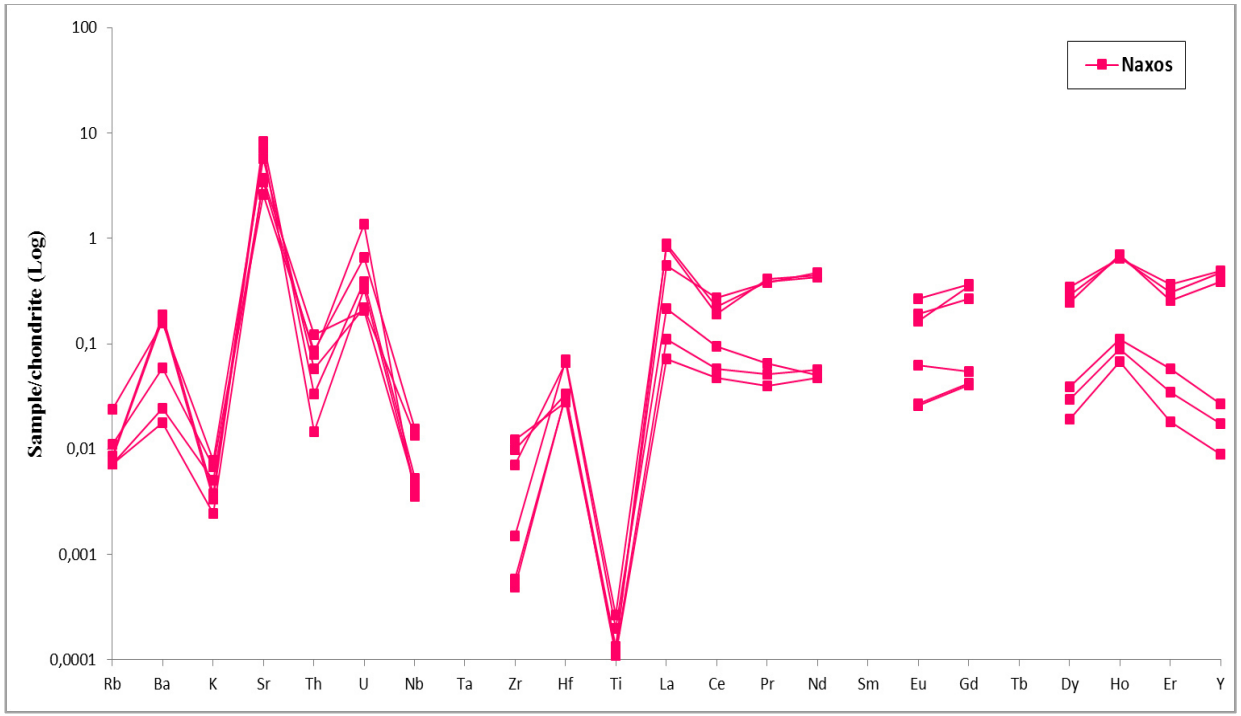

Fig. 4.4.1.1: Patterns of trace elements white marbles from Naxos. The concentrations are normalized to chondrite (Sun and McDonough, (1989)).

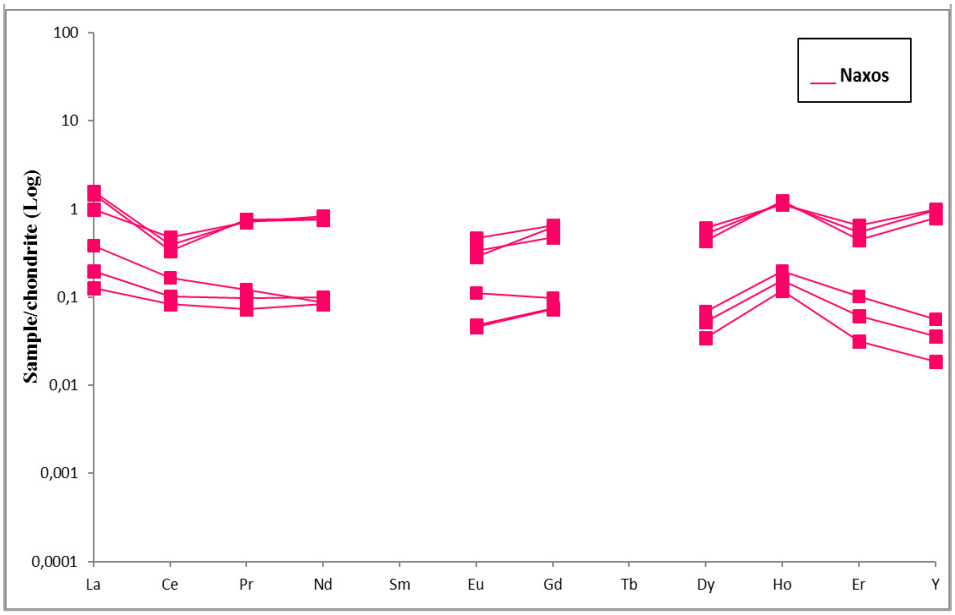

Fig. 4.4.1.2: Patterns of REE + Y in samples of white marble from of Naxos. The content of REE and Y and their patterns divide the samples in two main groups. The LA-ICP-MS data are normalized to chondrite (Taylor and McLennan (1985)).

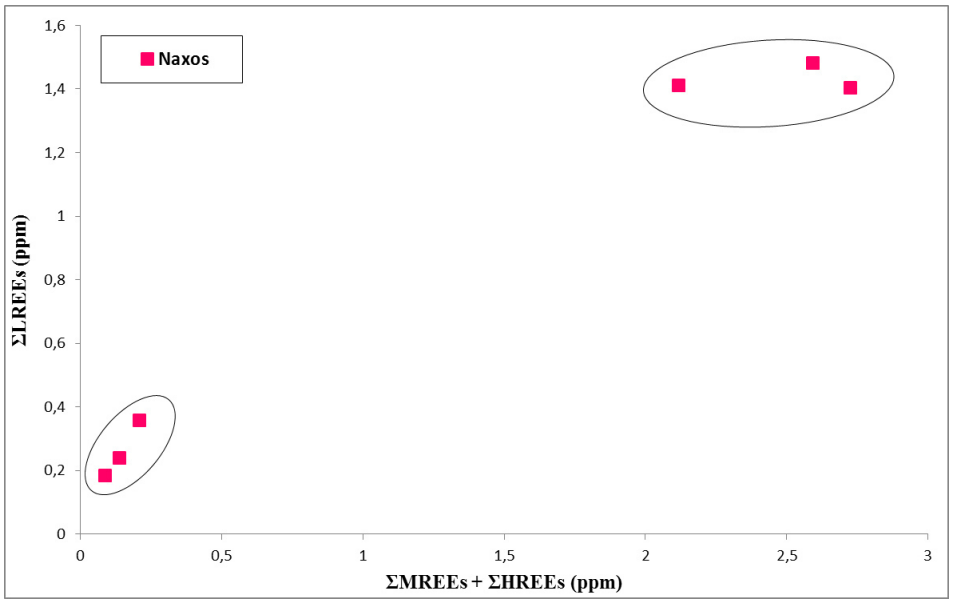

Fig. 4.4.1.3: Σ LREE *vs* Σ HREE content in marble samples for the two groups. One of these shows a high enrichment in MREE and HREE.

The three samples with the lowest content in REE are also characterized by the lowest content in HFSE (mainly due to the depletion of Zr and Nb), confirming that part of the sampling has a depletion in all trace elements (Fig. 4.4.1.4).

Moreover, all samples have similar Fe+Mn content, as shown in Fig. 4.4.1.5. The two separate clusters are discriminated only on the basis of REE content.

The various trends observed in the samples from Naxos can be explained by the occurrence of three different sites of extraction *i.e.,* Melanes, Kinidaros, Apiranthos Apollonas (Chapter 3, § 3.2.1).

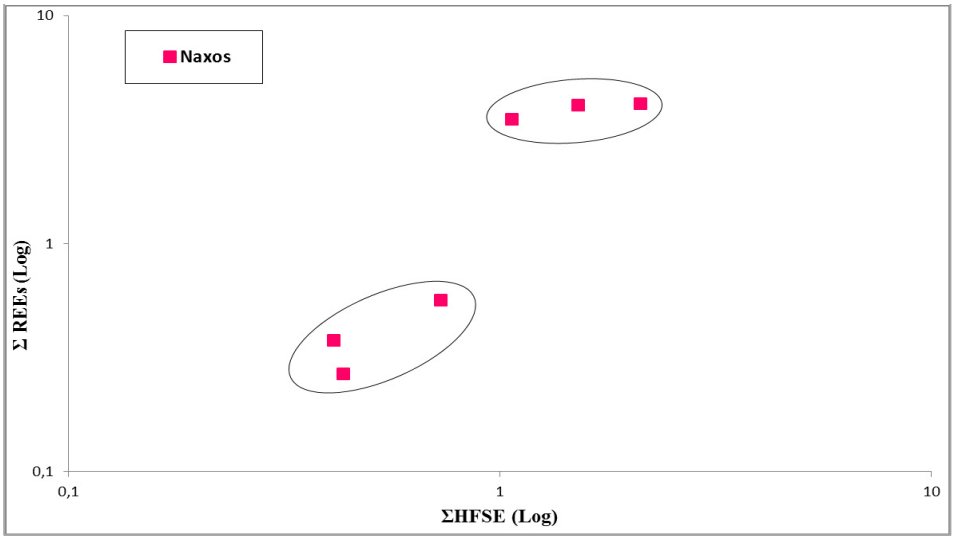

Fig. 4.4.1.5: HFSE *vs* Σ REE + Y diagram. The content of trace elements shows highlights that the three samples with the lowest content in REE are also characterized by a lowest content in HFSE. The samples on the right (at the top of the diagram) have the sum of HFSE in the range 1- 2 ppm; those on the bottom left, from 0.4 to 0.7.

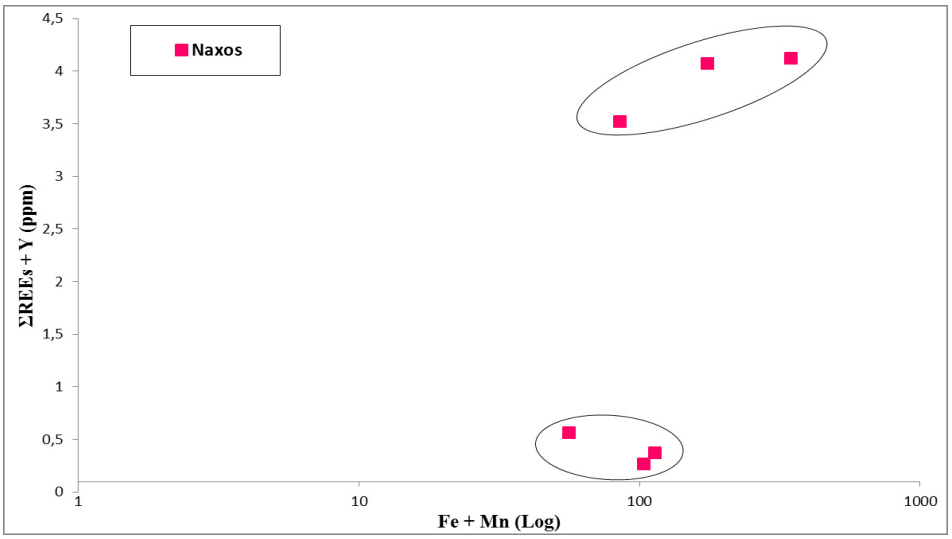

Fig. 4.4.1.6: Fe + Mn *vs* Σ REE+Y diagram. The Fe and Mn content of calcite in the Naxian marbles is similar for all the specimens analyzed, whereas the sum of REE allows one to distinguish two subgroups.

4.4.2 Thasos

Since ancient times, two varieties of white marble have been exploited in the island of Thassos. The Mourgena (orange line) quarry produces a high quality, almost pure white dolomite marble with medium-sized crystals, and the second one, Aliki (brown line), is a white calcitic marble with coarse grains. Even though the two sets of marbles are easily recognizable by means of petrographic analysis, LA-ICP-MS analysis has been conducted also on dolomite marble.

In the multi-elemental diagram (Fig. 4.4.2.1), calcitic crystals are characterized by an enrichment in Ba and Sr and a depletion in K (LIL elements), and show a really scattered content of Rb. The calcitic marbles from Aliki have similar LILE patterns to those from Murgena, excluding only one sample that has a lower Ba content.

Both districts have a similar HFSE patterns, showing a positive Hf anomaly and negative Nb and Ti anomalies. Th, U and Zr have a wide range of concentrations (Fig. 4.4.2.1).

The Aliki samples have a trace-element content higher than the dolomitic marble from Mourgena.

The two groups have different patterns and content of REE elements. Indeed, Aliki has the highest content of REE, apart from Ce, which displays a sharp negative anomaly (Ce* average anomaly is 0.2) not observed in samples from Mourgena (Ce* average anomaly is 1.1).

In detail, the chondrite-normalized REE + Y diagram (Fig. 4.4.2.2) highlights the fact that the Aliki marble specimens present a positive La anomaly and a negative Ce anomaly. Instead, the marble samples from Mourgena are characterized by a weak negative Ho anomaly. The calcite mrbleis is richer in REE than the dolomitic marble, mainly in LREE (Fig. 4.4.2.3).

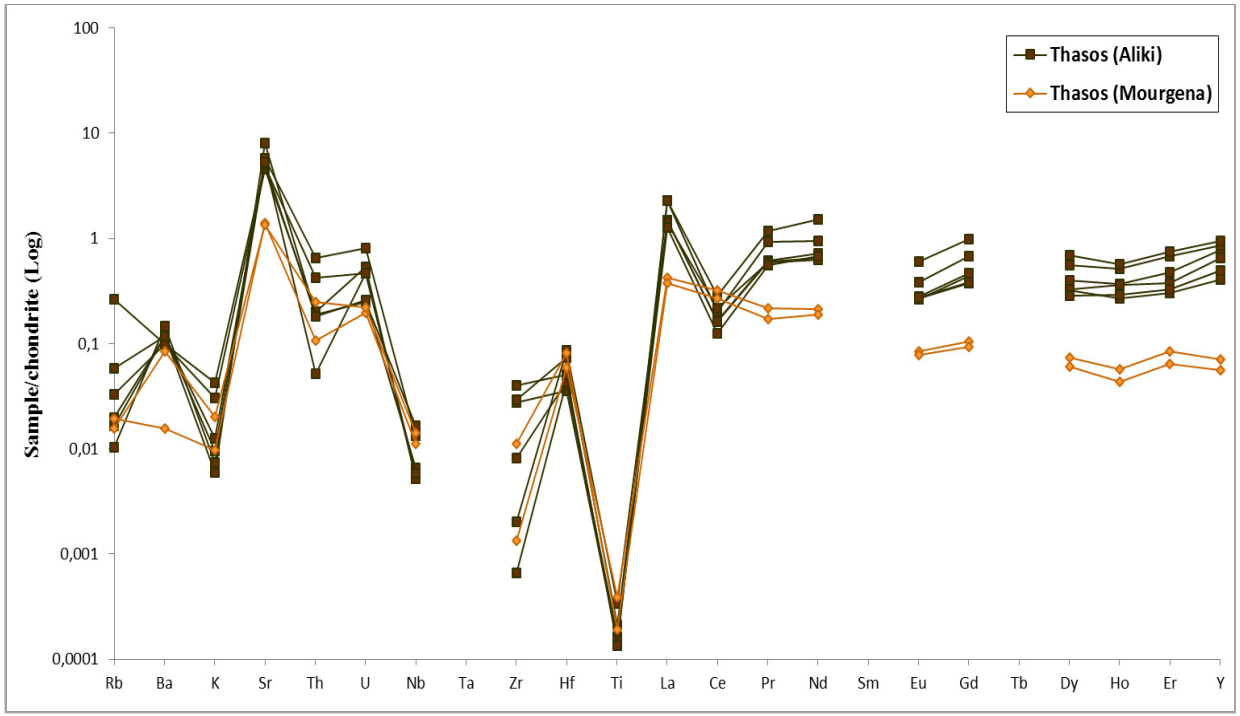

Fig. 4.4.2.1: Patterns of trace elements in Thasos marble. The LA-ICP-MS data are normalized to chondrite (Sun and McDonough (1989)).

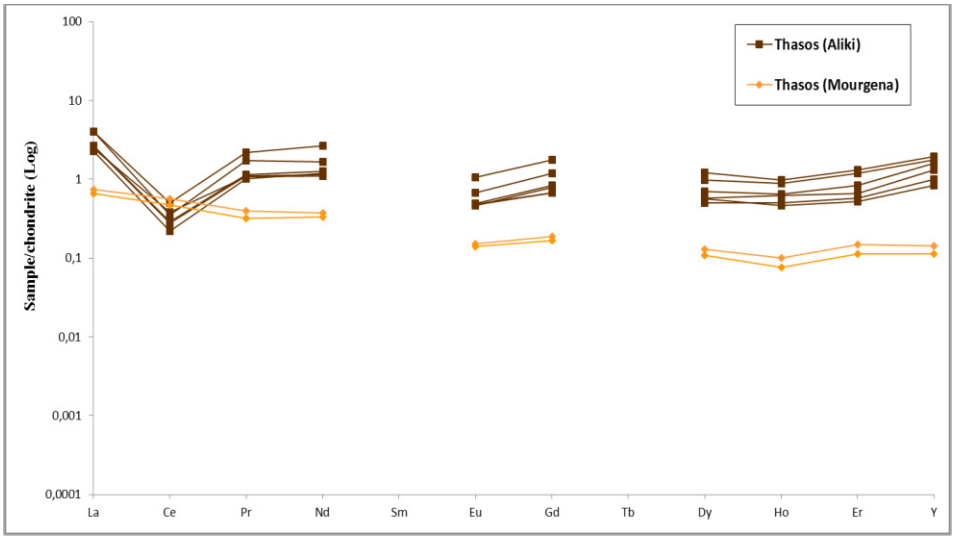

Fig. 4.4.2.2: Patterns of REE + Y in calcite marble from Thasos. The LA-ICP-MS data are normalized to chondrite (Taylor and McLennan (1985)).

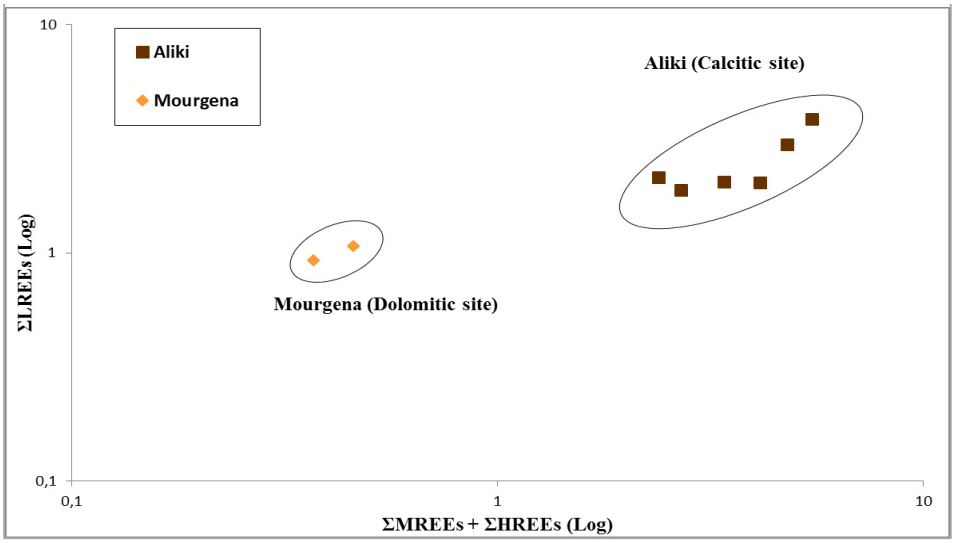

Fig. 4.4.2.3: Σ LREE *vs* Σ MREE + Σ HREE diagram. The samples from the Aliki district are richer in REE than those dolomitic marble from Mourgena, showing high enrichment in LREE.

The HFSE *vs* sum of REE plot highlights the lowest and similar concentrations of trace elements in the Mourgena marble, whereas the Aliki samples shows a wider range of concentrations. The two clusters are separate and distinct (Fig. 4.4.2.4)

On the contrary, samples of dolomitic marble are enriched in Fe + Mn, with a higher content than calcitic marble from Aliki (Fig. 4.4.2.5).

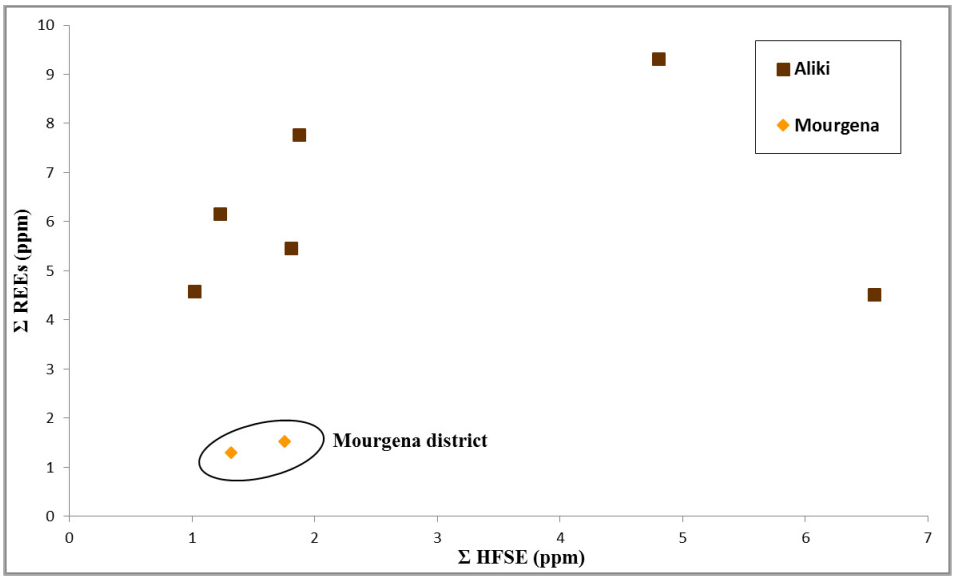

Fig. 4.4.2.4: Σ HFSE *vs* Σ REE diagram. Samples from the Mourgena district forms a separate cluster as they have low and similar concentrations of both groups of trace elements, whereas Aliki samples shows wider range of values.

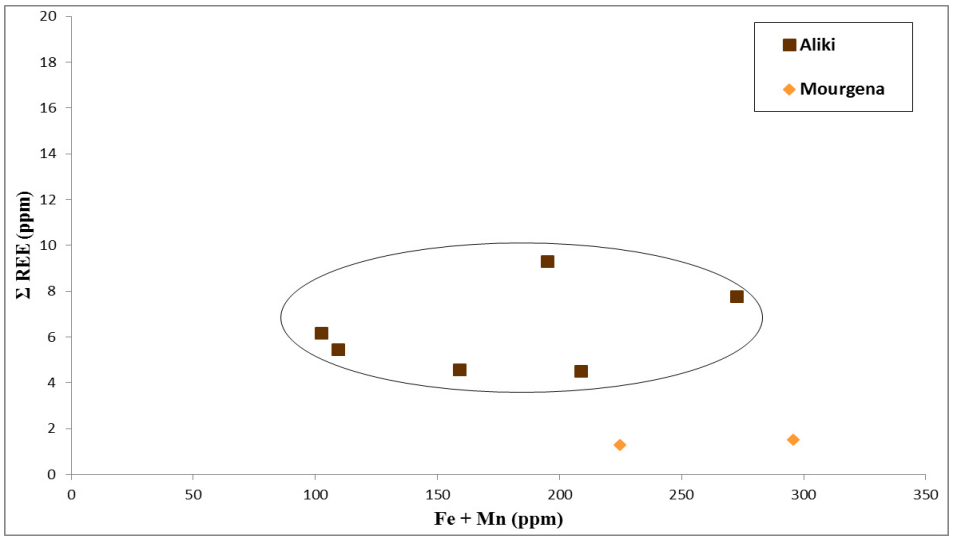

Fig. 4.4.2.5: Σ REE *vs* Fe + Mn diagram. Samples from the Mourgena district are enriched in Fe + Mn compared with samples from Aliki district.

4.4.3 Thiountas

Thiountas is a quarrying area of white marble of minor importance as it was mentioned only in some funeral inscriptions, testifying that Thiountas marbles were used locally and only for the needs of the nearby Roman towns. All the specimens treated below are from the quarry of Doğanli.

The samples are enriched in Sr and Ba, and depleted in Rb and K, having the same LILE patterns are previously observed in Naxian marble. The patterns of HFS elements are characterized by U and Hf positive anomalies and Th, Nb, Zr and Ti negative anomalies (Fig. 4.4.3.1).

The six samples have rather homogeneous concentrations for all the trace elements, except for one sample (*i.e.,* T3), which shows a higher concentration for Rb, Ba, K and U.

The REE patterns are more heterogeneous compared to those of the other traces.

In the chondrite-normalized REE patterns diagram (Fig. 4.4.3.2), all specimens are characterized by a sharp positive Er anomaly and a marked negative Y anomaly. The content is similar for all Thiuountas specimens, with almost comparable enrichment for light REE as well for medium and heavy REE (Fig. 4.4.3.3).

The HFSE *vs* REE diagram shows that Thiountas specimens of marbles are strongly enriched in HFS elements, and the content of one sample has an order of enrichment of four times respect to the others (Fig. 4.4.3.4).

Moreover, the Fe and Mn content of samples is quite similar (Fig.4.4.3.5).

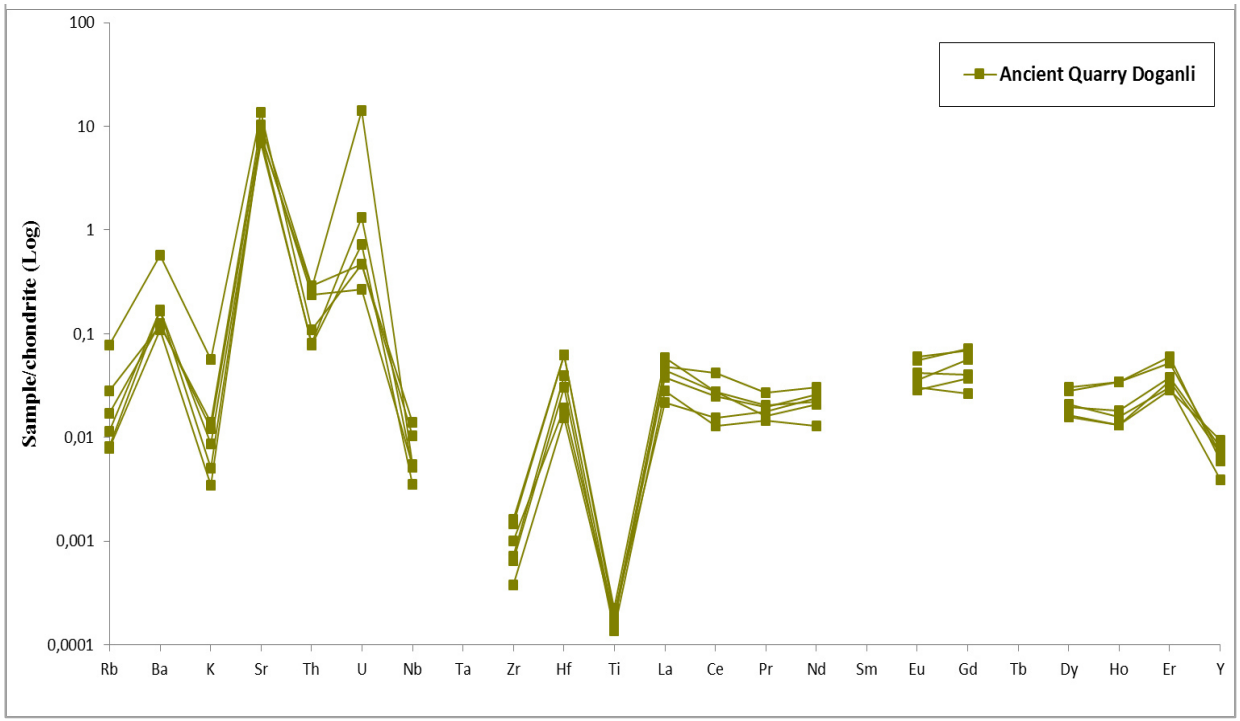

Fig. 4.4.3.1: Patterns of trace elements in calcite marble for Thiountas. The LA-ICP-MS data are normalized to chondrite (Sun and McDonough (1989)).

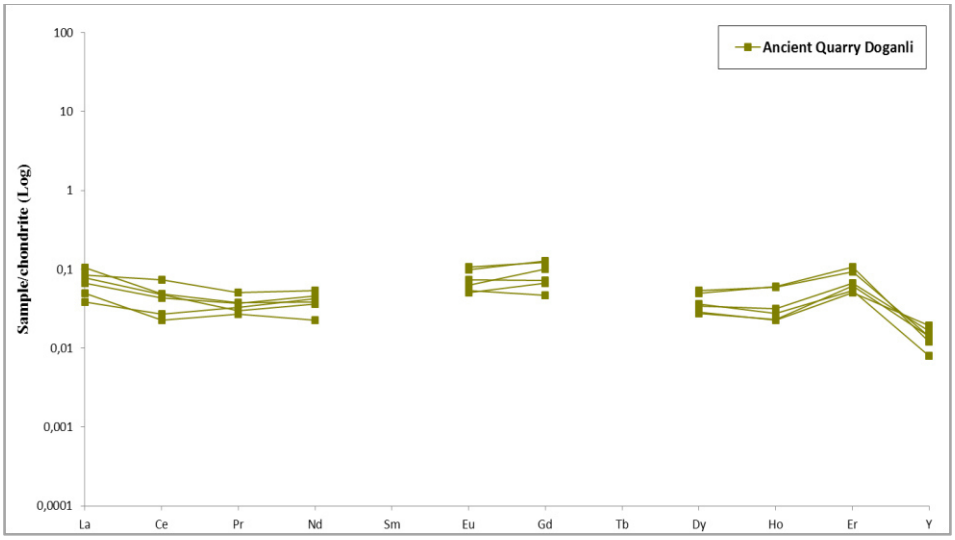

Fig. 4.4.3.2: Patterns of REE + Y in calcite marble from Thiountas. The LA-ICP-MS data are normalized to chondrite (Taylor and McLennan (1985)).

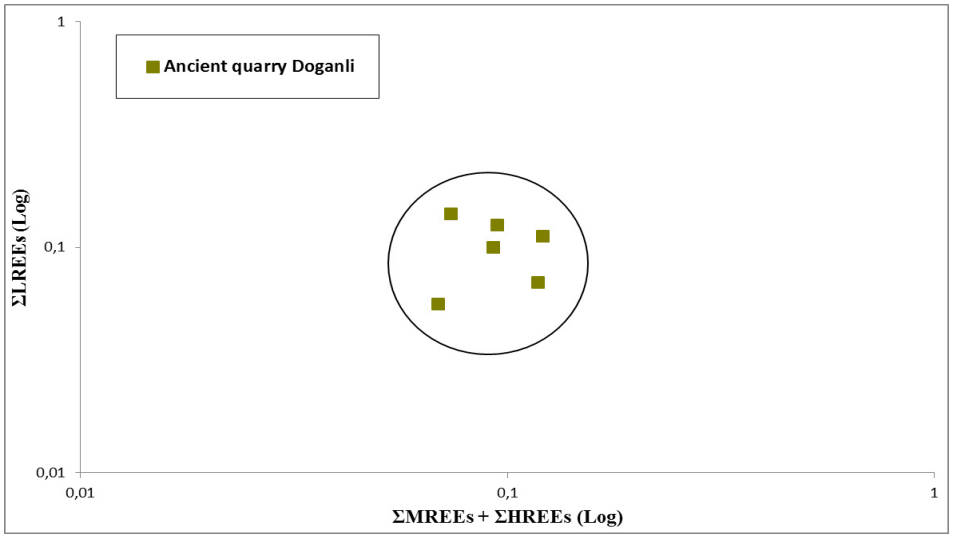

Fig. 4.4.3.3: LREE *vs* MREE + HREE diagram of Thiountas marble. The samples form a unique group, having similar REE contents.

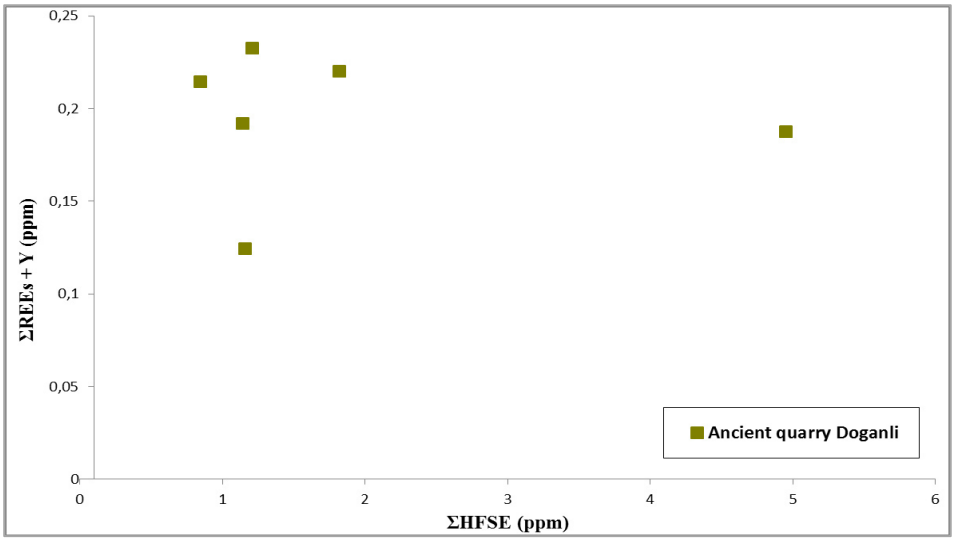

Fig. 4.4.3.4: HFSE vs Σ REE diagram. The Calcite marble from Thiountas is enriched in HFS elements, and one sample has an order of enrichment of about four times respect to the other five samples.

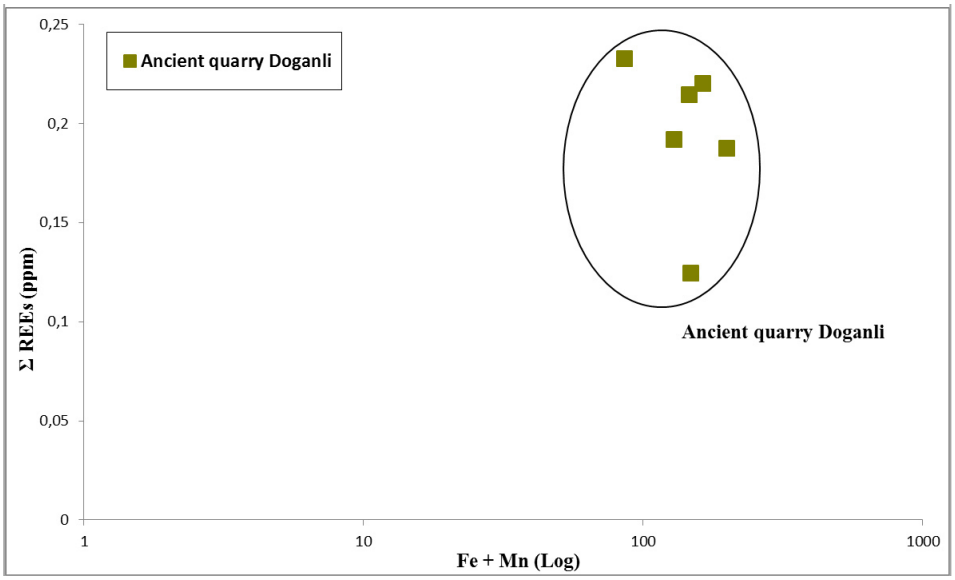

Fig. 4.4.3.5: Σ REE vs Fe + Mn diagram. The marble samples from Thiountas are similar in their content of these traces.

4.4.4 Proconnesos

The Proconnesian white marble was the most famous and widely used lithotype in classical antiquity. Its quarries occupy an area of more than 40 km^2 and are located in the northern part of the island, near the village of Saraylar; from west to east, specimens were exploited at Altintantas, Saraylar area (samples from ancient quarry of Filiz) and Harmantas (Fig. 3.1.3.1.1, Chapter 3)

In Figure 4.4.4.1, all samples show a marked enrichment in Sr, whereas the other LIL elements, i.e., Rb, Ba, and K, are scattered, causing the overlap of samples from the different extraction sites.

The HFSE patterns are similar, and all specimens are enriched in U and Hf, and depleted in Th, Nb, Zr, widely in Ti. Some samples from Altintas and Filiz show a higher content in U, Zr and Ti.

The REE patterns are scattered and the concentrations differ among samples; in particular, the LREE have a wider range. In detail, La is enriched in all samples; a positive Er anomaly occurs in samples from Filiz and Alitintas. The Ce anomaly is very variable from sample to sample. The samples with the highest values of REE are from Hermantas and OC140/1 (Fig. 4.4.4.2).

The different content of the REE allows a distinction of three different clusters. Harmantas and Filiz districts have the lowest concentrations of REE, with a slight enrichment in LREE, whereas sample OC140 has the highest content. The samples from all sites are enriched in LREE compared to MREE and HREE (Fig. 4.4.4.3).

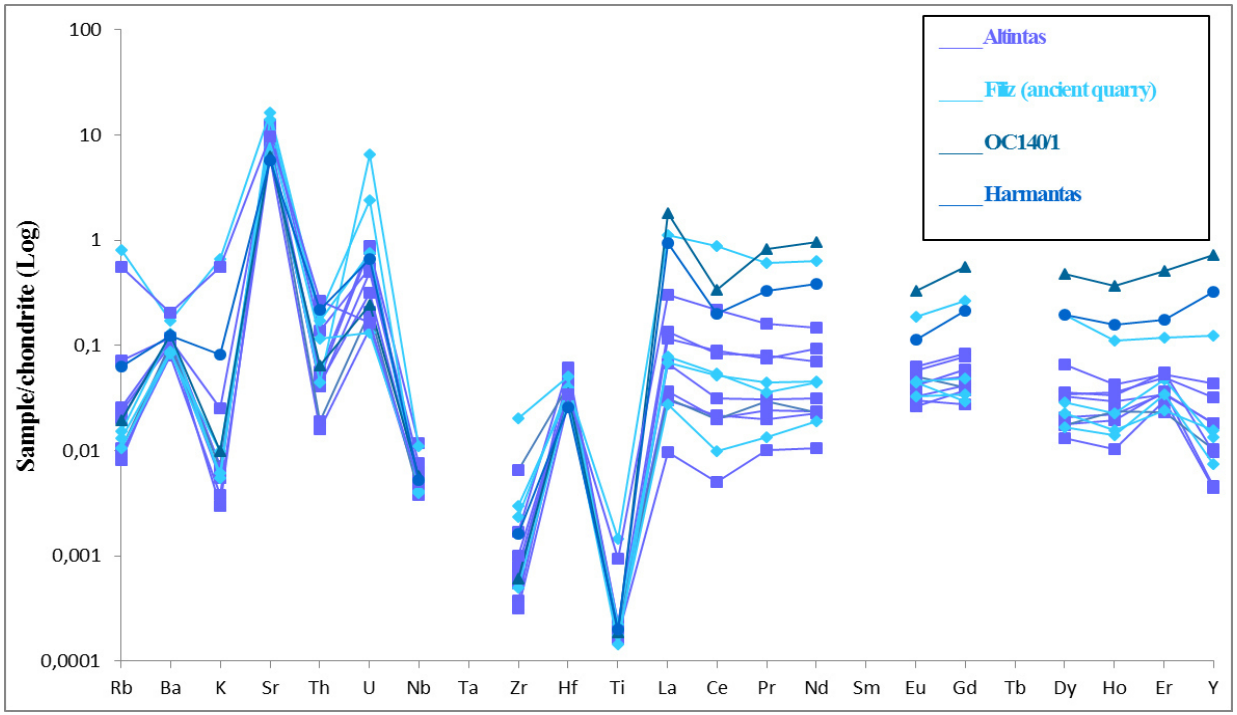

Fig. 4.4.4.1: Patterns of trace elements in white coarse calcite marble from Proconnesos. The four districts are displayed using different symbols and colors: lillac line for Altintas quarry, azure line for Filiz quarry, dark blue line for OC/140 quarry and bright blue line for Harmantas. The LA-ICP-MS data are normalized to chondrite (Sun and McDonough (1989)).

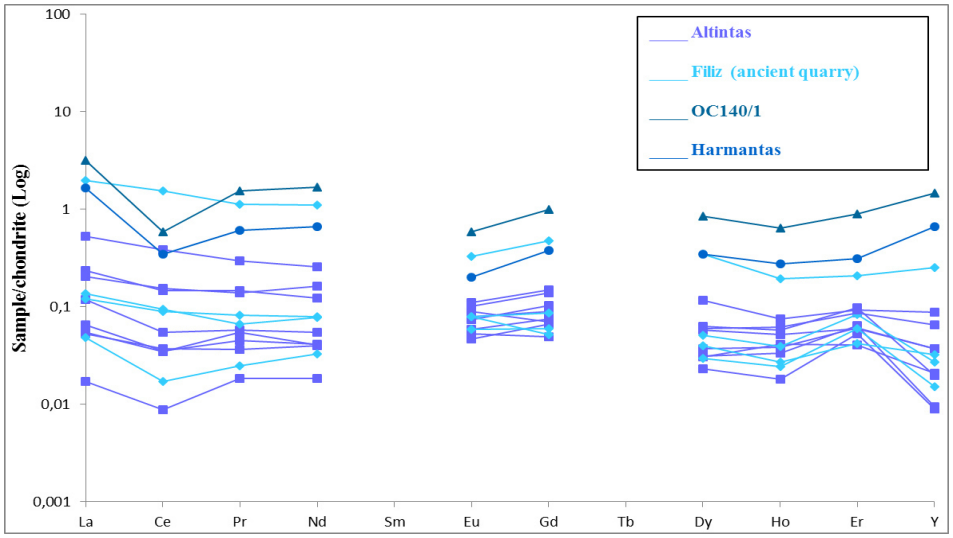

Fig. 4.4.4.2 Patterns of REE + Y in white calcite marble from Proconnesos. The four districts are displayed using different symbols and colors: lillac line for Altintas quarry, azure line for Filiz quarry, dark blue line for OC/140 quarry and bright blue line for Harmantas. The LA-ICP-MS data are normalized to chondrite (Taylor and McLennan (1985)).

In the last two diagrams (Fig. 4.4.4.4; Fig. 4.4.4.5) the content of HFS elements and the content of Fe + Mn is similar for all specimens. The clusters, formerly found, are observed again owing to the different enrichment in the REE.

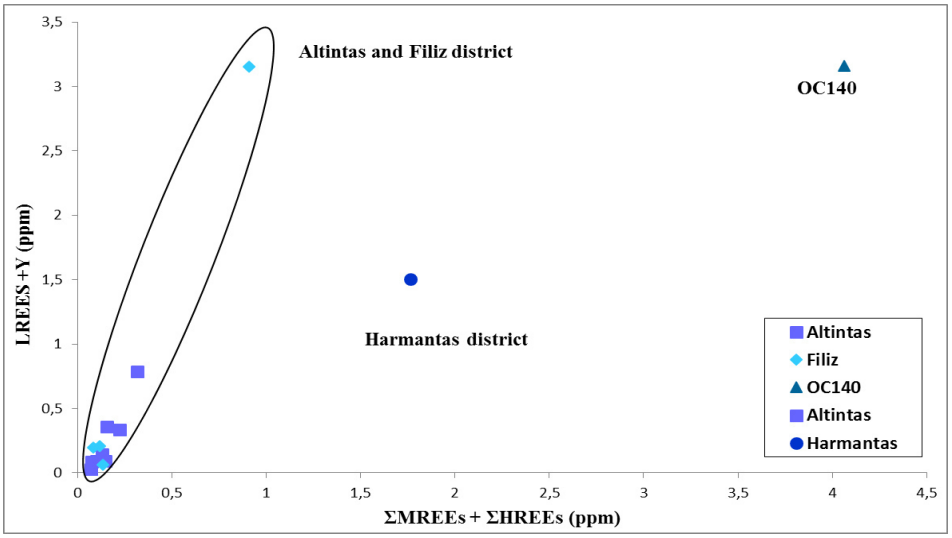

Fig. 4.4.4.3: Σ LREE vs Σ MREE + Σ HREE diagram for Procennesos marble. The four districts are displayed using different symbols and colors: lillac square for Altintas quarry, azure rhombus for Filiz quarry, dark blue triangle for OC/140 quarry, and bright blue circle for Harmantas.

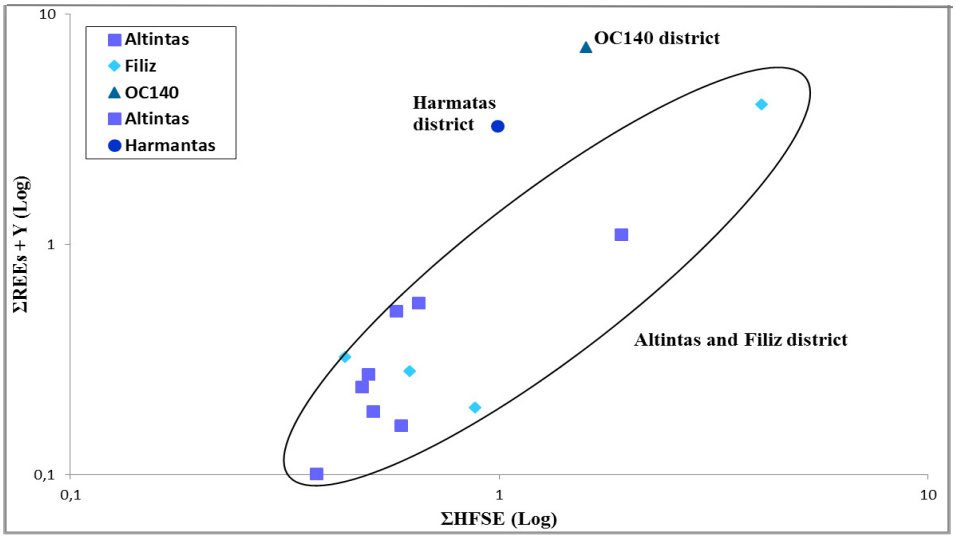

Fig. 4.4.4.4: Σ HFSE vs Σ REE + Y in calcite marble from Proconnesos. The four districts are displayed using different symbols and colors: lillac square for Altintas quarry, azure rhombus for Filiz quarry, dark blue triangle for OC/140 quarry, and bright blue circle for Harmantas.

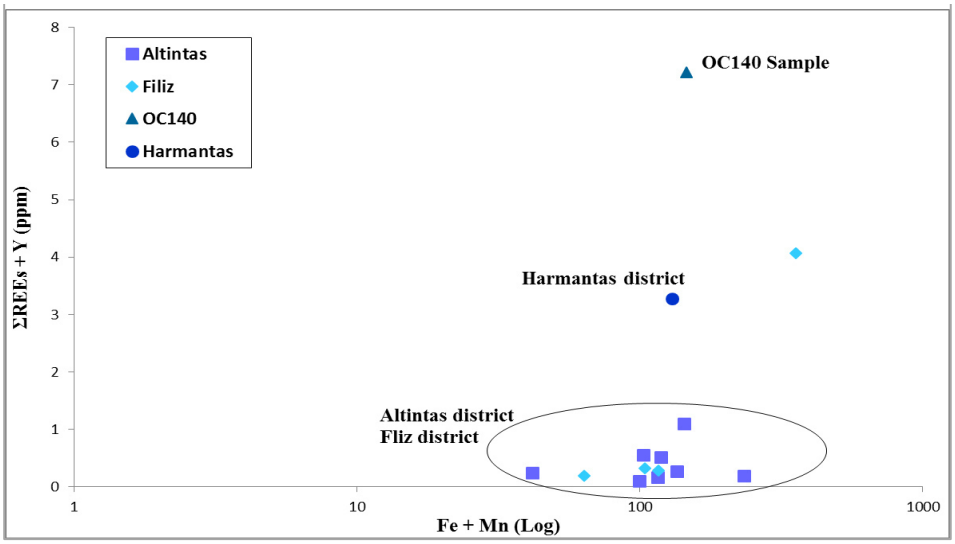

Fig. 4.4.4.5: Fe + Mn *vs* REE + Y in calcite marble from Proconnesos. The four districts are displayed using different symbols and colors: lilac square for Altintas quarry, azure rhombus for Filiz quarry, dark blue triangle for OC/140 quarry, and bright blue circle for Harmantas.

Chapter 5

Discussion

5 Discussion

The discussion chapter has been divided into three sections: 1) Use of petrographic analysis as a discriminant tool, 2) Trace elements as markers for provenance attribution, and 3) Evolutionary scenario for provenance attribution of white marble.

5.1 Use of petrographic analysis as discriminant tool

The examination of marble in thin sections under the petrographic microscope is probably the oldest technique involved in investigations of provenance. Nowadays, petrographic analysis remains the first step in any scientific multi-analytical approach, as it permits one to describe the maximum grain-size, texture and types of boundary of the carbonate crystals of marble, which are useful parameters for their distinction.

Many authors have described petrographic features, updating the reference database of the most important Mediterranean sites of quarrying (*e.g.,* Gorgoni *et al.*, 2002, Lazzarini, 2004; Attanasio *et al.,* 2006; 2009; 2015; Antonelli and Lazzarini, 2015).

Below, the main features of the marble occurrences studied here are discussed and compared with the results of literature (*e.g.,* Herz and Prichett, 1953; Weiss, 1954; Herz, 1955; Renfrew and Springer Peacy, 1968; Young and Ashmole, 1968; Moens *et al.,* 1992; Lapuente *et al.,* 2000; 2012; Lazzarini*et al.,* 1980; Antonelli *et al.* 2003; 2014a, 2014b, 2015; Pensabene *et al.,* 2012; Antonelli and Lazzarini 2013a; 2013b; 2015; Columbu, 2014). In Table 5.1 are reported the observations of previous studies, and in Table 5.2, the findings of this thesis (c.f. chapter 4.1).

Four characteristic microstructures have been observed: 1) polygonal (Carrara), 2) lineated (Pentelicon), 3) mosaic (Thasos) and 4) mortar (Proconnesos, Naxos, Thiountas) (Table 5.2).

In detail, Carrara specimens (*e.g.,* Colonnata and Torano districts) have calcite crystals structured in a mosaic of crystals, with quite straight boundaries, and triple points (*i.e.,* points resulting from the junction of three substantially linear borders at around 120°), which define a polygonal fabric (Table 5.2). Various authors have observed analogous features in Carrara marble (*e.g.,* Gorgoni et *al.,* 2002; Lazzarini 2004; Cantisani *et al.,* 2005; Lapuente *et al.,* 2012b; Attanasio *et al.,* 2015) (Table 5.1). According to Cantisani *et al.,* (2005), this microstructure is typical of marble that has reached a stable metamorphic equilibrium at a given temperature and generally suffered a late static recrystallization without oriented pressure, *i.e.,* an isotropic texture.

The white marble from the Pentelic presents a heteroblastic (HE) texture with slight foliation along with flecks of white mica, commonly arranged in trains, and dolomite as the main accessory phase (Table 5.2). Unlike the Carrara samples, the anisotropic texture of the Pentelic marble is produced by oriented stress-pressure, and under the microscope, it is visible as a lineated fabric (*i.e.,* at produced by arrangement of deformed shape grains) and deformation (strain) in the calcite crystals that show micro-folding and bent twin lines.

The Parian marble is characterized by a heteroblastic mosaic of calcite crystals (Table 5.2), containing as accessory minerals a white mica and quartz.

The Afyon samples present a heteroblastic texture with a xenoblastic microstructure (Table 5.2). Unlike what was observed by Lapuente *et al.,* (2012b), the microstructure of the samples here studied does not show a strained fabric (Table 5.1).

In this study, it was not possible to examine thin sections of Göktepe samples, as the fragments were too small to be able to obtain representative thin sections. From the literature, the Göktepe marble has a texture that varies from homeoblastic (HO) to partly heteroblastic, having a polygonal mosaic fabric. A large number of calcite crystals show straight boundaries and triple points (Attanasio *et al.,* 2015).

Proconnesian marble shows a mortar-heteroblastic fabric with calcite crystals deformed by polysynthetic twins. These petrographic features are quite typical of white marble specimens from Marmara Island (Turkey) (*e.g.,* Gorgoni *et al.,* 2002; Lazzarini, 2004).

In addition to the microstructural features, the boundaries of the crystals reflect the deformation relationships during a tectonic-metamorphic event that generated marble crystallization.

Calcite crystals of the Carrara samples present, in the most of the cases, straight boundaries with triple points due to an equilibrium texture reached during a late-postkinematic stage of metamorphism. On the contrary, sutured boundaries of strongly interlocked crystals are testimony of synkinematic conditions reached during a metamorphic event in a deformation phase. All samples considered (*i.e.,* Paros, Pentelicon, Afyon, Naxos, Thasos, Thiountas, Proconnesos, and Göktepe based of literature data) present mixed features (from straight to curved, curved to embayed and from embayed to sutured), testifying an incomplete tectonic-metamorphic re-equilibration with respect to their metamorphic history (Table 5.2).

Following Lapuente *et al.*, (2012), the specimens were divided into two groups based on Maximum Grain Size (MGS) parameter:

- Very fine (MGS<0.7 mm) to fine (MGS< 2 mm) marbles: Carrara, Pentelicon, Paros Afyon and Göktepe.
- Medium-coarse (MGS>2 mm) marbles: Naxos, Thasos, Thiountas and Proconnesos.

All these petrographic characteristics play an important role if samples of marble, apparently very similar, are investigated for provenance purpose. Actually, these features allow one to do a first discrimination (*e.g.,* Carrara samples present an HO and polygonal microstructure, whereas Afyon have a HE and xenoblastic microstructure, even if the results of petrographic analysis prove to be complex and not always exhaustive.

Tab. 5.1: Literature data on the main petrographic features of the specimens of marble studied.

	Fabric type	*Texture*	*Microstructure*	*Crystal boundaries*	*Literature references*
Carrara	HO	Isotropic	Polygonal with triple points	Straight/curved	Gorgoni *et al.,* 2002; Lazzarini 2004; Cantisani *et al.,* 2005 Lapuente *et al.,* 2012;
Paros	HE/HO	Isotropic	Mosaic	Curved, embayed	Gorgoni *et al.,* 2002; Lazzarini 2004; Lapuente *et al.,* 2012; Antonelli and Lazzarini, 2015;
Pentelicon	HE/HO	Isotropic/ Anisotropic	Lineated, in some cases regular mosaic	Curved, embayed	Gorgoni *et al.,* 2002; Lazzarini 2004; Lapuente *et al.,* 2012; Antonelli and Lazzarini, 2015;
Afyon	HE/HO	Isotropic	Mosaic with strained crystals	Embayed, sutured	Gorgoni *et al.,* 2002; Lazzarini 2004; Lapuente *et al.,* 2012; Antonelli and Lazzarini, 2015;
Göktepe	HO/ slightly HE	Isotropic	Mosaic to polygonal with some triple points	Curved and straight	Lapuente *et al., ,*2012; Antonelli and Lazzarini, 2015;
Naxos	HE	Isotropic	mosaic, with strongly strained crystals, in some cases lineated	Embayed	Gorgoni *et al.,* 2002; Lazzarini 2004; Antonelli and Lazzarini, 2015;
Thasos (Aliki)	HE	Isotropic	Mosaic, generally lineated and stressed	Curved to sutured	Gorgoni *et al.,* 2002; Lazzarini 2004; Antonelli and Lazzarini, 2015;
Thiountas	HE	Isotropic	Granoblastic with interlocking subgrains	From curved to sutured	Brilli *et al.*, 2015
Proconnesos	HE	Anisotropic	Mortar	Sutured / embayed	Gorgoni *et al.,* 2002; Lazzarini 2004; Antonelli and Lazzarini, 2015;

Tab. 5.2: The main microscopic features of the marble samples considered MGS average values.

	Fabric type	*Texture*	*Microstructure*	*Crystal boundaries*	*MGS (mm)*
Carrara	HO	Isotropic	Polygonal mosaic	Straight, curved	0.6
Paros	HE	Isotropic	Mortar	Curved, embayed	2.5
Pentelicon	slightly HE	Anisotropic	Irregular granoblastic, lineated	Curved, embayed	0.95
Afyon	HE	Isotropic	Xenoblastic, mosaic	Embayed, sutured	1.8
Naxos	HE	Isotropic	Xenoblastic, mortar	Embayed	3.3
Thasos	HE	Isotropic	Xenoblastic	Curved to sutured	5
Thiountas	HE	Isotropic	Mortar	Curved, satured	3.35
Proconnesos	HE	Isotropic	Xenoblastic	Sutured, embayed	2.9

5.2 Trace elements as markers for provenance attribution

The concentrations of trace elements in almost pure white marble depend on the processes that the protolith underwent during the metamorphic events. These processes influence the incorporation of trace elements in carbonate protolith during deposition and subsequent processes of diagenesis, dolomitization and metamorphism, giving important information about the geological history of a given lithotype.

In this thesis different groups of elements were investigated, with particular attention to common substitutions of calcium in calcite *i.e.,* magnesium, strontium, manganese and iron, and to a lesser extent, barium.

The content of REE, HFSE and LILE shows different concentrations among the Mediterranean white marble sources and seem to be the better geochemical markers (c.f. Chapter 4).

The element with the highest concentration is *magnesium* (Fig. 5.1).

The coarse-grained specimens all show similar Mg content, except for three samples from the Filiz quarry from Proconnesos Island (OC 13/4; OC 13/6; OC 994/3) and one sample from Thasos Island (TA6).

Similar abundances of Mg have been observed also in fine-grained marble, with the only exception being varieties of marble from Carrara. The Italian marble shows the highest concentration of Mg (0.04‰-0.065‰), and this element seems to be a good marker to describe this quarrying source.

Strontium also occurs in high concentrations, varying from 54 ppm in Afyon samples to 837 ppm in Göktepe samples (Fig. 5.1). The high Sr content and its variation among the varieties of white marble depend on genesis of the rock. Marble, usually generated from

marine carbonate rocks, underwent metamorphic events of various intensity. Thus, the concentration of Sr depends on those processes that exercise an influence on its incorporation in the carbonate protolith. Strontium is able to replace calcium in view of its ionic radius and valence (it is a member of the alkaline earth metals, Group IIA; ionic radius in octahedral coordination is 1.18 Å, Calcium ionic radius is 1 Å). Consequently, it is a dispersed element in many minerals, *e.g.,* calcium carbonate, and can form strontianite ($SrCO_3$).

Among the coarse-grained specimens of marbles, the Turkish specimens (*i.e.,* Thiountas and Proconessos) have higher concentrations of Sr than those from Greece (*i.e.,* Naxos, Thasos) (fig. 5.1).

The fine-grained marbles exhibit similar concentrations of Sr, except for the Göktepe samples. As shown in fig. 5.1, the white variety of Göktepe marble is well discriminated from the other specimens on the basis of its Sr content, which varies from 420 to 830 ppm. The specimens of fine-grained marble have a heterogeneous and higher content of Sr in the Pentelic and Afyon specimens than those from Carrara and Paros; the Göktepe marble has the highest concentrations of Sr (Fig. 5.1).

Another common substitute of calcium in calcite crystals is *manganese*. It presents variable abundances among the specimens considered.

The specimens of coarse-grained marble from Naxos and Thasos (Greece) have a higher content of Mn than those of Thiountas and Proconnesos (Turkey). Exactly the opposite behavior was observed for the Sr content, highlighting a negative correlation between Sr and Mn.

The high Sr and low Mn concentration in Göktepe samples was also observed by Attanasio *et al.,* (2015) in white and black varieties. These authors compared their results with those of Carrara,

Hymettos, Pentelicon and Afyon, observing the lowest Mn/Sr ratio in the Göktepe samples.

Trace-element concentrations in the Göktepe samples suggest that its original protolith may have been aragonite, an orthorhombic polymorph phase of Ca carbonate. The small cations as Mn (Mn ionic radius is 0.67 Å (low spin) and 0.83 Å (high spin)) tend to be expelled. At standard temperatures and pressures, aragonite is thermodynamically unstable and slowly this phase transforms into calcite, the polymorphous stable at this *PT* conditions. However, calcite preserves the distinctive trace composition typical of Göktepe white marbles.

In agreement with the results of Attanasio *et al.* (2015), the results of the present work confirm that Göktepe marble is distinct from the other important historical fine-grained marble sources (*i.e.,* Afyon, Paros and Pentelicon) on the basis of the content of Sr and Mn. In the diagram showing Sr content *vs* Mn/Sr (Fig. 5.2), samples of Göktepe marble are clearly discriminated from other fine-grained specimens.

It is worthy of note that among coarse-grained marbles the two Turkish sites (*i.*e., Thiountas and Proconnessos) are distinguished from the Greek marbles (*i.e.,* Naxos and Thasos) by their lower Mn content, particularly the Proconnessos specimens (Fig. 5.2).

The results on Mn content are in agreement with those of Attanasio *et al.,* (2008a) and also with the updated geochemical database of about 400 Proconnesian geological samples and artifacts (Attanasio *et al.,* 2008a). The low content of Mn is a distinctive signature of Proconnesos marble, as confirmed also by the low EPR intensity, a property associated with the low concentration of paramagnetic Mn^{2+} impurities.

The results on the content of *iron* are similar among the quarrying areas considered (Fig. 5.3), having averages between 13.5 ± 15 ppm

in coarse-grained marbles and in the range of 211 ± 65 ppm in fine-grained marble. In particular, the fine-grained marble from Göktepe has the most homogeneous content of Fe (160-179 ppm).

Another group of elements here considered are the radioactive U, Th and Pb elements (c.f. chondrite-normalized incompatible trace element patterns, Chapter 4). In the chart boxes of Fig. 5.4 are reported the concentrations of U, Pb and Th of the coarse - and fine-grained marbles.

The *uranium* content is very low and varies of an order of magnitude within both the coarse - and fine-grained varieties. These variable concentrations of U among the different sites may reflect the change of oxygen fugacity condition during calcite growth as this element has two dominant oxidation states (U^{6+} and U^{4+}) under geological conditions. This variability is in agreement with the significant U variations existing among 24 specimens from ten different Naxian localities reported by Ebert *et al.* (2010).

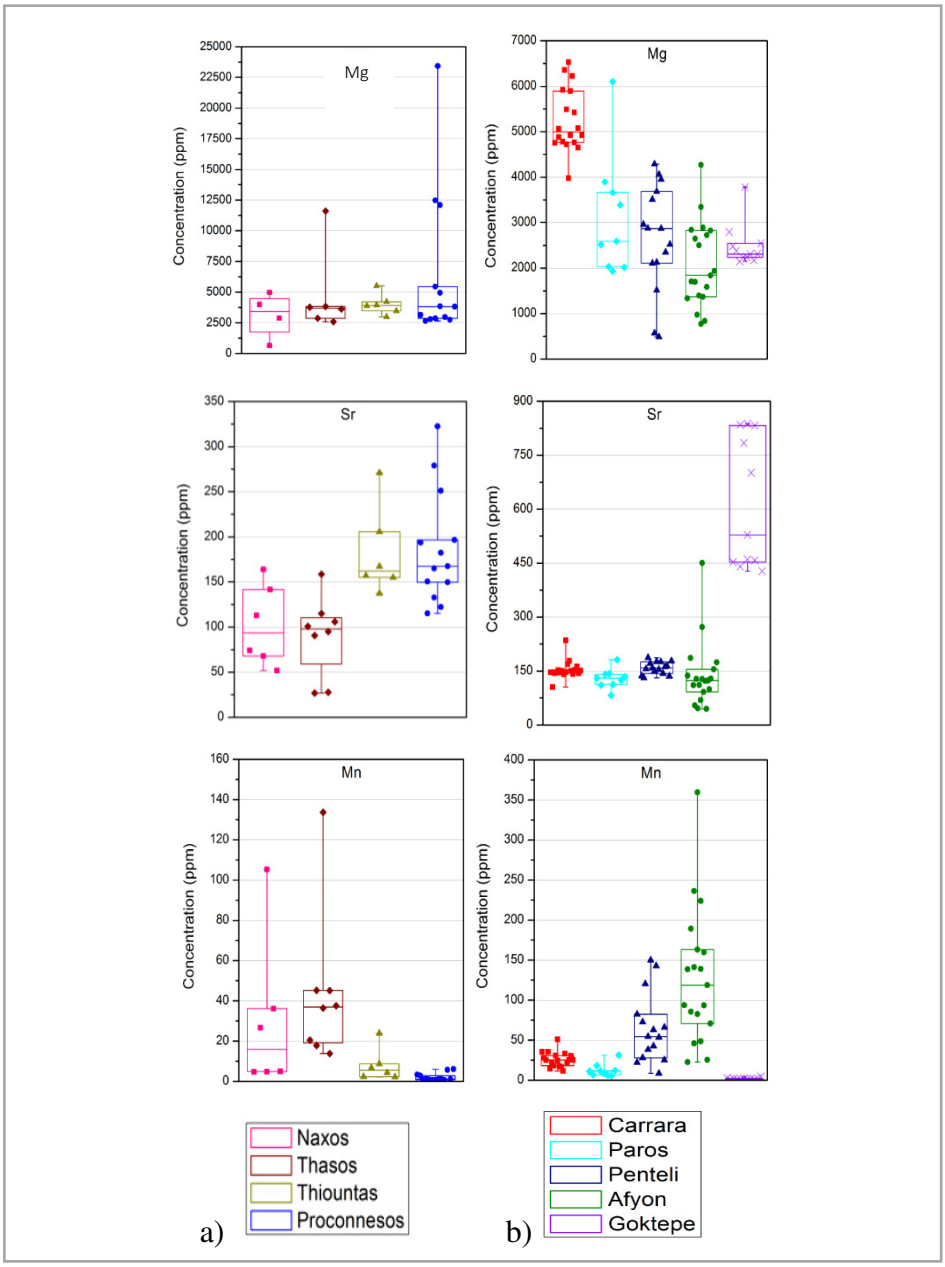

Fig. 5.1: Trace-element contents in white marble from various quarries: a) Mg, Sr and Mn contents in white coarse-grained marbles (expressed in ppm); b) Mg, Sr and Mn contents in white fine-grained marbles (expressed in ppm). Each point represents an average of five spot LA-ICP-MS measurement for each sample, and the box charts represent the dispersion of the experimental points; the median and the two percentile values are 0.25 and 0.75.

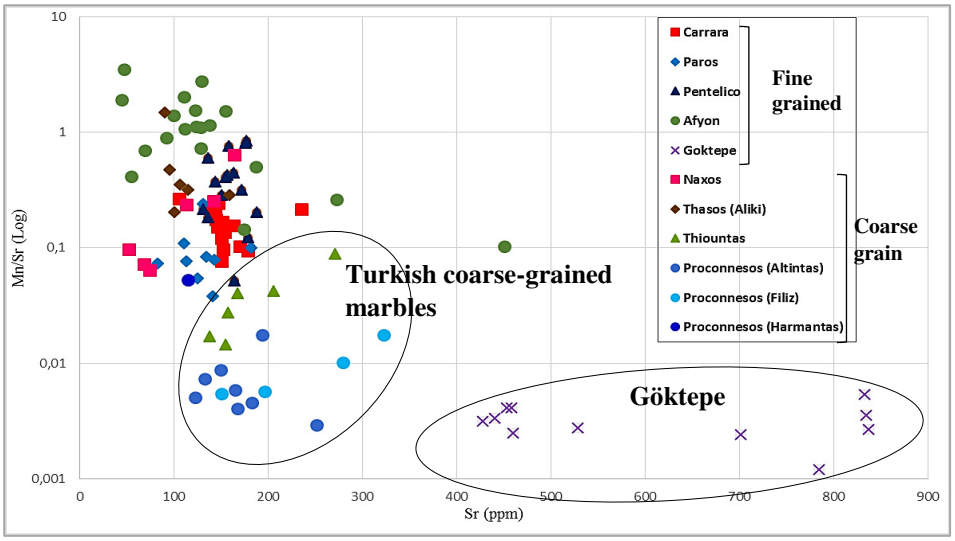

Fig. 5.2: Sr *vs* Mn/Sr in fine - and coarse-grained marbles. The highest content of Sr occurring in Göktepe samples (purple cross symbol) allow one to separate this quarrying site from the other white marbles districts.

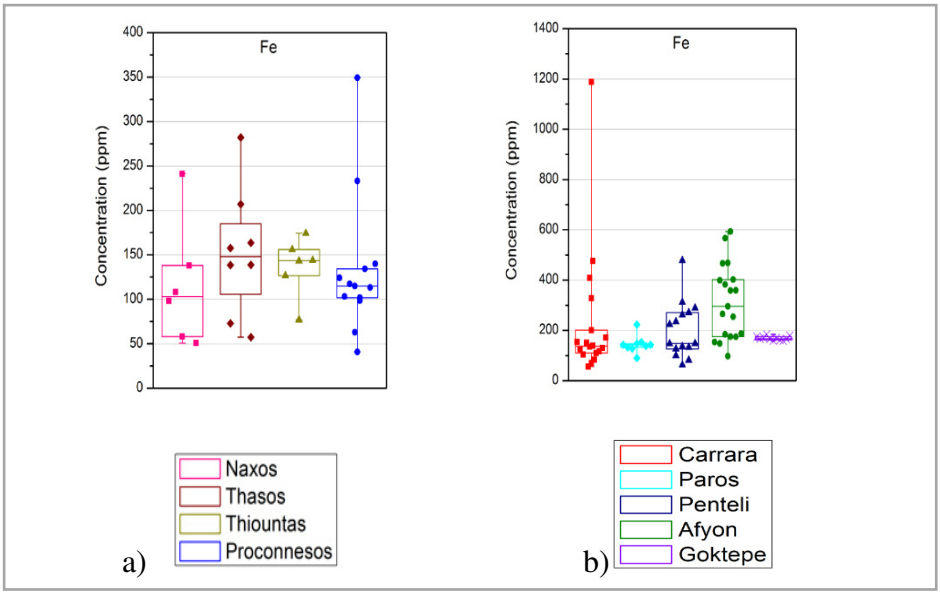

Fig. 5.3: Variability of Fe in white marble: a) Fe content in white coarse-grained marbles (expressed in ppm); b) Fe content in white fine-grained marbles (expressed in ppm). Each point represents an average of five spot LA-ICP-MS measurement for each sample, and the box charts represent the dispersion of the experimental points; the median and the two percentile values are 0.25 and 0.75.

The Göktepe samples are characterized by the lowest Pb content (0.04-0.4 ppm), whereas the other samples of fine-grained marble have higher levels and a wide range of concentrations, especially the Pentelic and Afyon specimens.

The coarse-grained specimens from Proconnesos are characterized by a homogeneous and low Pb content (Fig. 5.4), similar to the Naxos specimens; the content of Pb in the other varieties of marble range from 0.4 to 1.5 ppm, excluding three samples (*i.e.,* Thasos TA1, TA22; Thiountas T3) which have higher content, up to 3 ppm.

The content of Th in coarse-grained samples varies from 0.005 to 0.02 ppm, thus causing an overlap of the data among the different quarry sites. The fine-grained marbles, *i.e.,* Carrara, Paros, Pentelicon and Afyon, have a slightly higher Th content, with values from 0.01 to 0.03 ppm, whereas the Göktepe marble has the lowest content of Th (0.002-0.01 ppm).

In summary, the contents of U, Pb and Th are too similar among the samples of white marble of various Mediterranean sites. The use of these elements alone does not allow one to identify the sources. The only two sites that appear consistently grouped in these elements are Göktepe, with the lowest concentrations, and Carrara, with the highest Th content.

Recently, the concentrations of some trace-element in white marble have been measured mainly using the neutron activation analysis (NAA). A comparison between trace-element data acquired in this thesis, using the LA-ICP-MS with those of previous studies has been done with the aim to enlarge the existing trace-element database useful for provenance investigations of the Mediterranean quarries.

Mello *et al.* (1988), in a review of previous studies (Mello, 1983; Oddone *et al.*, 1985; Genova *et al.*, 1986), proposed a discrimination of marble samples from different source areas (*i.e.,* Carrara,

Proconnesos, Aphrodisias, Paros Pentelicon and Naxos) by means of NAA, coupled with a statistical analysis (Fig. 5.5). These authors identified a number of trace elements useful for provenance purpose. One of the most effective markers was found to be Y, along with Th, Sc and Cs).

These results must be considered preliminary in view of the limited number of the analyzed samples, but equally interesting for our common aim of finding compositional markers. In Fig. 5.5, Mello *et al.* (1988) reported the NAA results of trace elements and also the different marble sources form distinctive groups based on the provenance of extraction.

Here, Sc, Y, Ce, Th are considered on the basis of their concentrations and patterns. The content of *yttrium* in coarse-grained marble separates the Greek marble, with high and wide range of concentrations, from the Turkish occurences. In detail, the Naxian samples are split into two groups, and the Thasian specimens have the highest values of this element (Fig. 5.6). The Turkish marbles have low concentrations (except for two Proconnesian samples from the Filiz OC 13/4 and Harmantas quarries OC/140).

Samples of fine-grained marble show a similar content of Y, except for the white marble from Göktepe, which is characterized by the lowest content of Y, about of an order of magnitude lower than in the rest of the dataset.

The content of *cesium* in white marble is very similar in all specimens (*i.e.,* fine-grained and coarse-grained marbles), with concentrations that vary from 0.002 to 0.01 ppm (except for few Göktepe samples with content up to until 0.1 ppm).

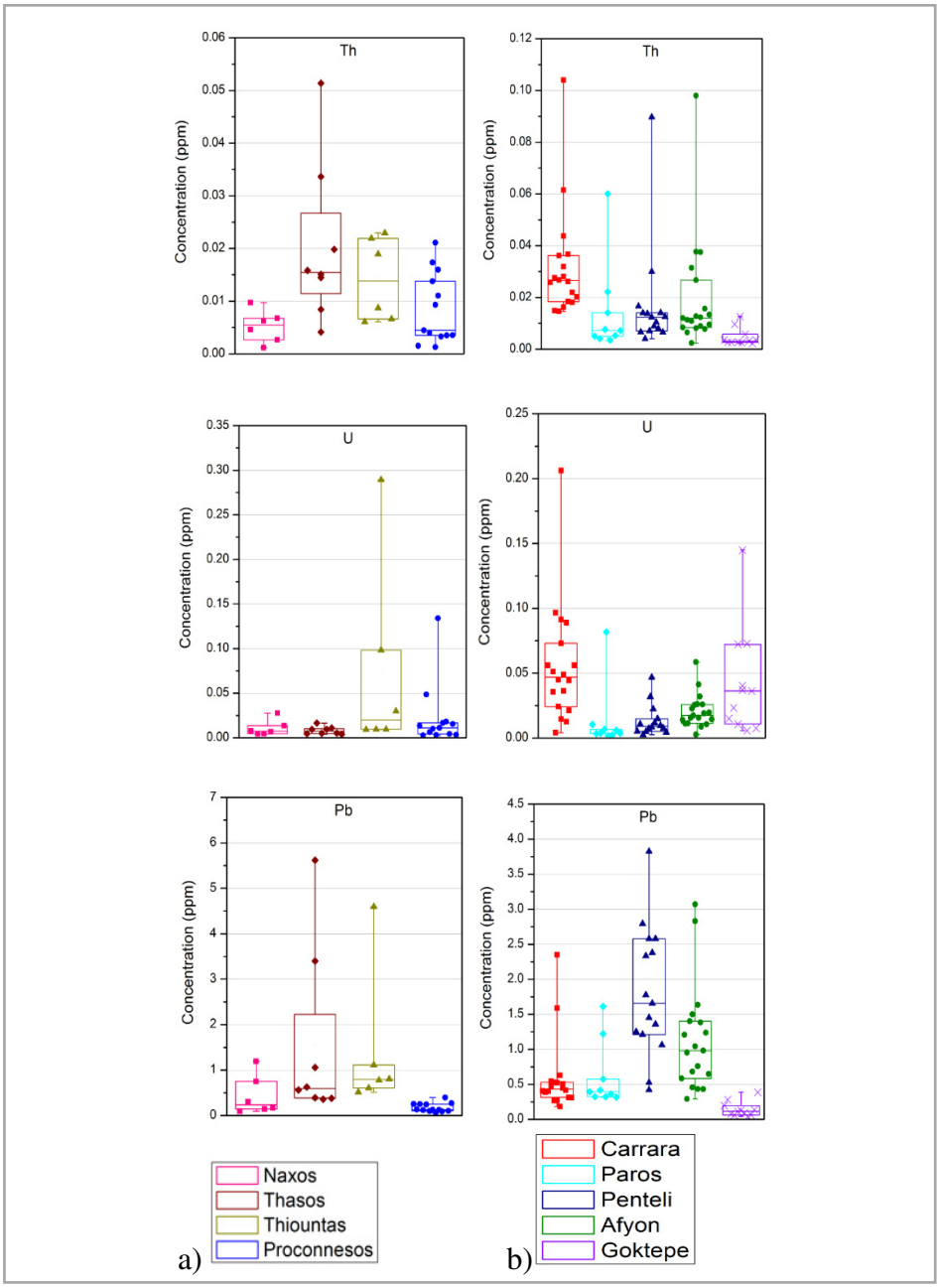

Fig. 5.4: Radioactive element behaviors of different quarries: a) Th, U and Pb content in white coarse-grained marble (expressed in ppm). B) U and Pb content in white fine-grained marble (expressed in ppm). The U content for Quarry I sample was eliminated in the chart. Each point is an average of five spot LA-ICP-MS measurement for each sample, and the box charts represent the dispersion of the experimental points: the median and the two percentile values 0.25 and 0.75. The bars join the maximum values.

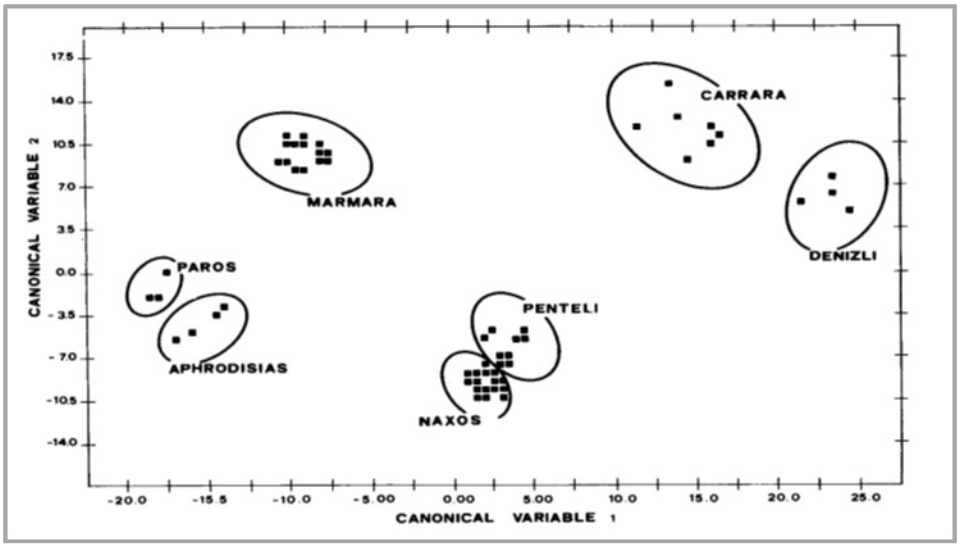

Fig. 5.5: The chart represents the various quarries in the plane of the first two canonical variables considered in the study conducted by Mello *et al.* (1988).

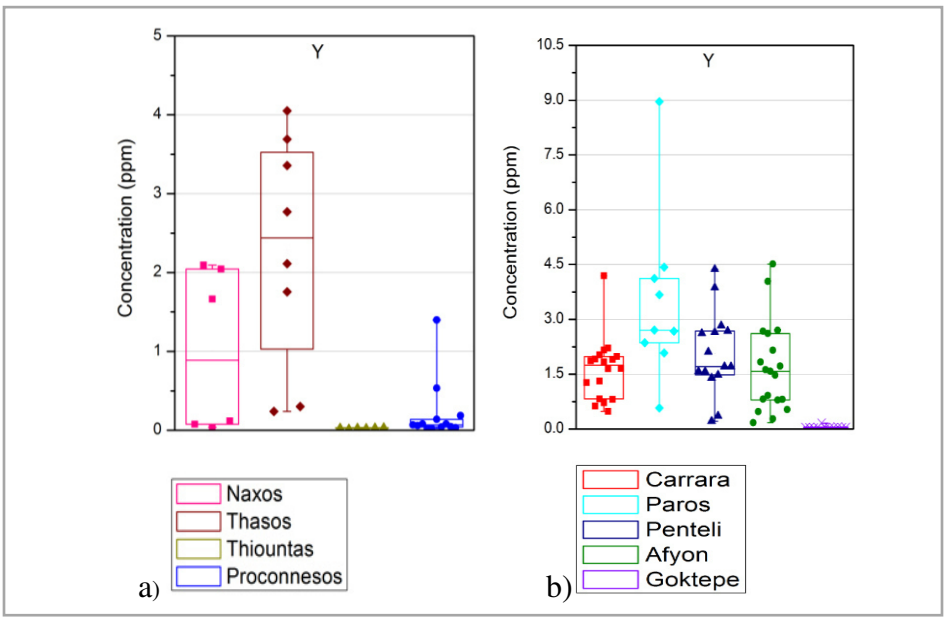

Fig. 5.6: Y content in white marbles: a) Y content in white coarse-grained marbles (expressed in ppm); b) Y content in white fine-grained marbles (expressed in ppm). Each point is an average of five spot LA-ICP-MS measurement for each sample, and the box charts represent the dispersion of the experimental points: the median and the two percentile values 0.25 and 0.75. The bars join the maximum values.

Although the concentrations of s*candium* are higher than that of Cs, the content does not vary among the samples from different quarry sites.

Finally, the concentrations of Sc, Y, Ce, Th were plotted together using the principal component analysis (PCA) in order to compare the different grouping with those of Mello *et al.* (1988) (c.f. paragraph 3.3.1). In our case (Fig. 5.5), the white marble specimens are divided in fine - and coarse-grained groups, using two different charts; samples from Proconnesos and Afyon, however,are not considered as they have high intra-quarry variability.

The PCA chart (Fig. 5.7) shows that Sc, Y, Ce and Th may be useful to discriminate between the two Greek sites, Naxos and Thasos. The Thiuontas samples form a separate group, but the span of Naxos samples on the principal component F1 axis makes it difficult to separate the samples of these two sites. Mello *et al.* (1988) reported two separate groups for Proconnesos (also called Marmara) and for the Naxos specimens.

In the case of the fine-grained samples, the Göktepe specimens are completly separated from the other three sites. In contrast to the finding of Mello *et al.* (1988), the Carrara specimens overlap part of the samples from Paros and Pentelic (Fig. 5.8). However, the Parian marble seem to confirm a quite good discrimination on the basis of Sc, Y, Ce and Th.

An important update on the database of trace-element concentrations in white marble was made by Matthews (1997) by means of the NAA, comparing his new data with those reported in a previous work (Matthews *et al.*, 1995). The goal of the work of this group was to establish a database of contents of trace elements in 183 samples of white marbles from eight quarry sites (*i.e.,* Aphrodisias, Carrara, Dokimeion, Ephesus, Paros, Pentelicon, Proconnesus, and Thasos). In his conclusions, Matthews (1997)

stated that a combination of different variables derived from trace-element analyses, coupled with multivariate statistical analysis, provides a very effective tool for provenance attribution of marble. However, the white marble from some quarries has a relatively large spread in the concentrations reported in Table 5.3, requiring one to increase the number of samples from various Mediterranean sources, but also from a single quarry site.

More than ever, this statement highlights the necessity of supplementing the database with new data. The possibility of comparing the NAA data with those from LA-ICP-MS may be a fundamental step for the future, where a database of white marble contains all the chemical results on these important lithotypes.

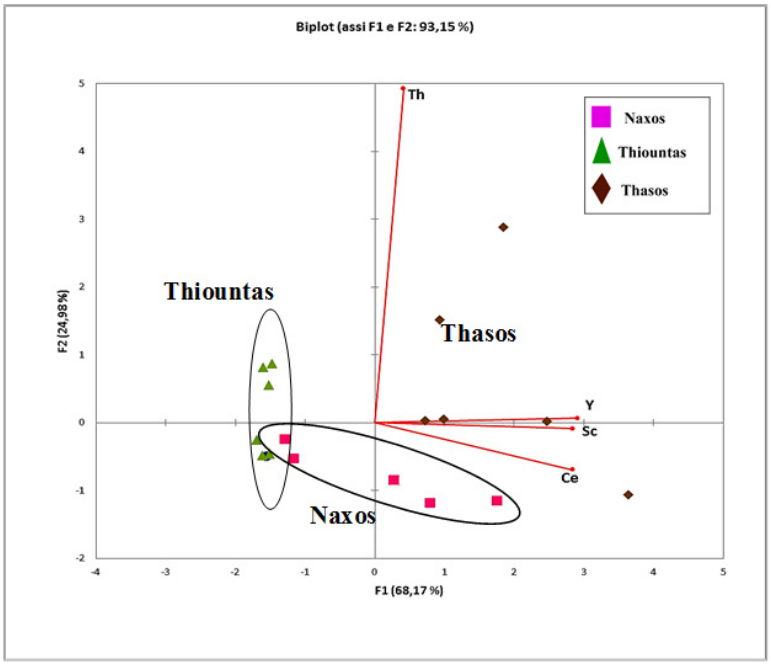

Fig. 5.8: The PCA chart of coarse-grained samples (Naxos, Thasos and Thiuontas).

In Table 5.3, the LA-ICP-MS data for each quarry site are reported and compared with those of Mello (1988) and Matthews (1997); the contents of trace elements reported in this thesis are comparable with those of literature.

Moreover, the contents of trace elements in white marble reported by Matthews *et al.* (1995) are more homogeneous, and thus useful as discriminant markers (*i.e.,* U, Cr, Rb, Fe, Cs, Ce, Sc, La, Eu, Th, Co, As, Sb, Hf). For this reason, these elements, along with the same elements examined here, were plotted using the PCA analysis approach.

The PCA plot of trace elements in coarse-grained marbles (Fig. 5.9) shows that, for these elements, the Thasian marble is the more homogeneous among the considered specimens, falling in a separate cluster, whereas the Naxian samples form at least two clusters.

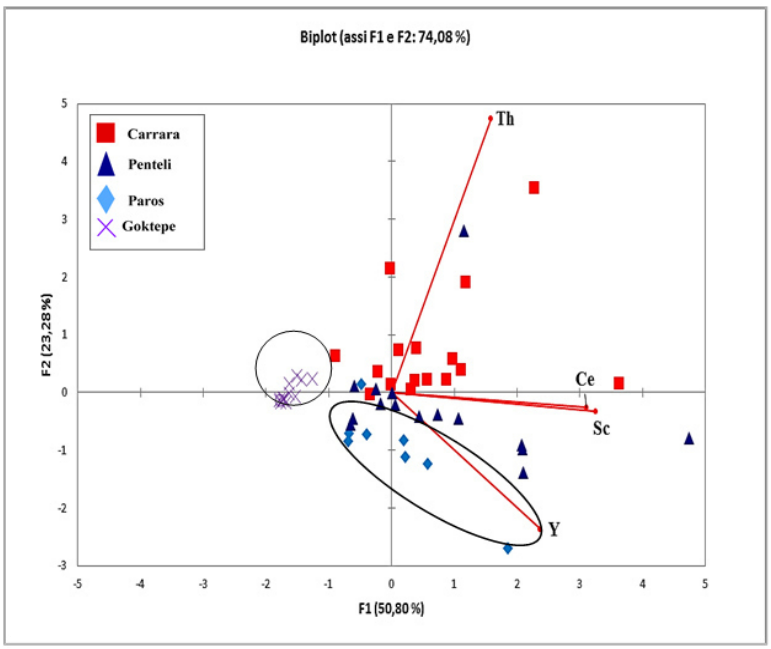

Fig. 5.9: The PCA chart of fine-grained samples from Carrara, Paros, Pentelicon and Göktepe.

Proconnesian marble is the most scattered among the coarse-grained specimens, followed by the Thiountas marble (Fig. 5.9).

Concerning the fine-grained samples (Fig. 5.10), the Göktepe samples form a quite separate cluster, far from samples of the other quarry sites. Afyon and Pentelicon samples are spread all over the plot, reflecting a great heterogeneity in the level of concentrations of these elements.

Although Paros and Carrara specimens are superimposed by Afyon and Pentelic samples, they show a greater homogeneity than those of the other two districts (*e.g.,* Pentelicon and Afyon). The only exception concerns the sample on the top of the chart (PAROS1), which plots far from the others.

These last two PCA charts of Fig. 5.9 and 5.10 include the majority of trace elements discussed above. The most important result concerns the Thasian marble, which falls completely separate from the other coarse-grained marble sources and from the other Greek marble from Naxos.

As for the fine-grained marble, Göktepe maintains its unique character among the quarries, whereas Paros, Pentelic and Afyon marbles are in part superimposed.

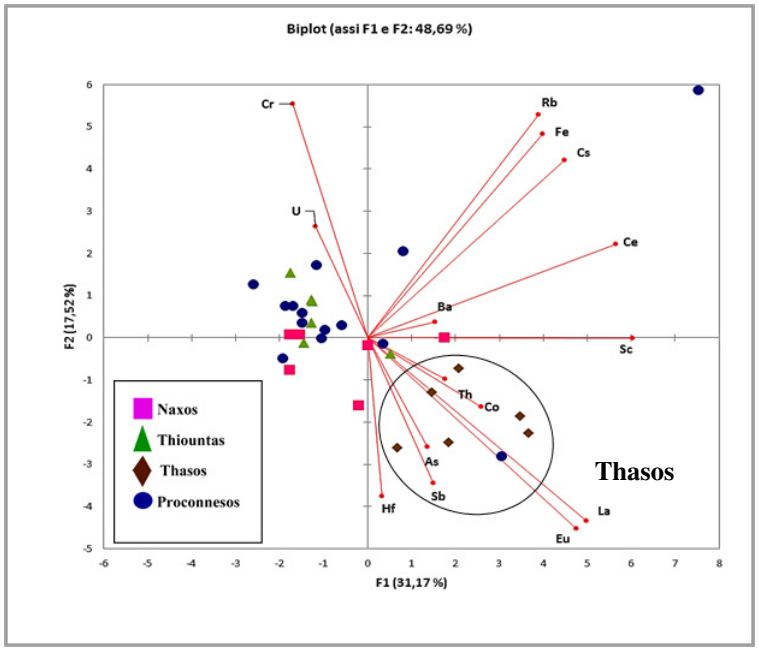

Fig: 5.9: PCA chart of the LA-ICP-MS trace-element concentrations in coarse-grained marble.

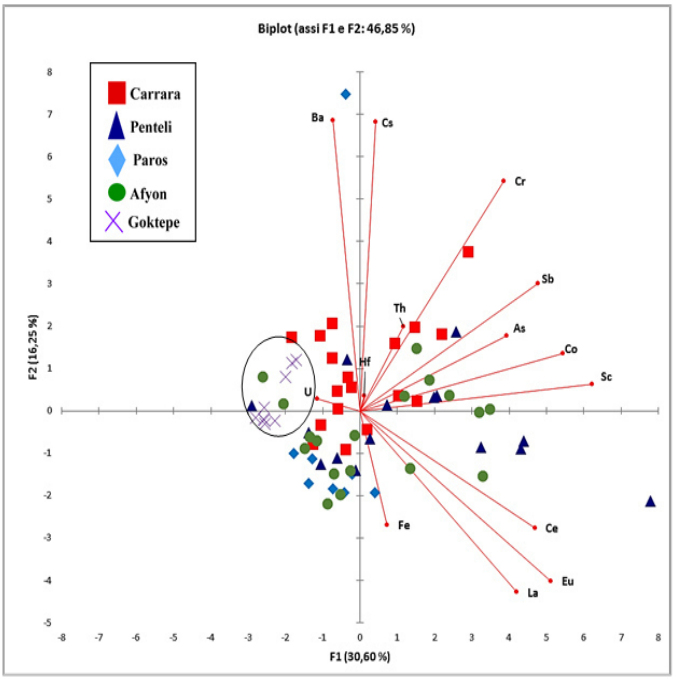

Fig: 5.10: PCA chart of the LA-ICP-MS trace-element concentrations in fine-grained marble.

Tab.5.3: Summary of NAA results obtained from quarry samples published by Matthews (1997), Mello *et al.* (1988) and compared to LA-ICP-MS results in the present study.

			Carrara	Paros	Pentelicon	Proconessos	Thasos	Naxos
Sc	*Matthews (1997)*	Mean	0.41	0.1	0.07	0.04	0.2	-
		s.d.	0.4	0.04	0.07	0.04	0.2	
	Mello et al., 1988	Mean	0.11	5.16	2.32	13.71	-	3.65
	Present study (LA-ICP-MS)	Mean	0.2	0.1	0.2	0.09	0.2	0.07
		s.d.	0.1	0.05	0.2	0.09	0.08	0.05
Cr	*Matthews (1997)*	Mean	2.74	1.8	0.8	2.7	1	-
		s.d.	1.57	0.9	0.3	2	0.6	
	Mello et al., 1988	Mean	1.28	12.63	3.52	13.95	-	5.75
	Present study (LA-ICP-MS)	Mean	1.7	0.6	1.5	2	0.8	0.8
		s.d.	0.7	0.08	0.7	0.7	0.2	0.2
Co	*Matthews (1997)*	Mean	0.3	0.09	0.3	0.5	0.5	-
		s.d.	0.2	0.05	0.4	0.1	0.4	
	Mello et al., 1988	Mean	0.12	1.71	0.71	3.55	-	0.74
	Present study (LA-ICP-MS)	Mean	0.5	0.04	0.8	0.05	0.06	0.04
		s.d.	0.6	0.01	0.7	0.01	0.01	0.01
As	*Matthews (1997)*	Mean	0.1	0.1	0.2	-	0.6	-
		s.d.	0.2	0.07	0.2		0.08	
	Mello et al., 1988	Mean	-	-	-	-	-	-
	Present study (LA-ICP-MS)	Mean	0.2	0.2	0.5	0.1	0.1	0.08
		s.d.	0.2	0.1	0.5	0.01	0.06	0.03

Rb	*Matthews (1997)*		-	-	-	-	-	-
	Mello et al., 1988	Mean	14.8	5.0	4.1	3.4	-	5.5
	Present study (LA-ICP-MS)	Mean	0.2	0.009	0.1	0.07	0.04	0.006
		s.d.	0.3	0.005	0.1	0.1	0.06	0.004
Sb	*Matthews (1997)*	Mean	0.1	0.2	0.3	0.1	0.15	-
		s.d.	0.1	0.15	0.2	0.06	0.2	
	Mello et al., 1988	Mean	0.007	0.12	0.07	0.033	-	0.48
	Present study (LA-ICP-MS)	Mean	0.03	0.02	0.04	0.025	-	0.02
		s.d.	0.01	0.004	0.02	0.02		0.005
Cs	*Matthews (1997)*	Mean	0.1	0.75	0.07	0.06	0.06	-
		s.d.	0.1	0.01	0.03	0.01	0.2	
	Mello et al., 1988	Mean	0.031	0.16	0.08	0.03	-	0.2
	Present study (LA-ICP-MS)	Mean	0.01	0.003	0.01	0.007	0.006	0.003
		s.d.	0.01	0.001	0.006	0.01	0.004	0.001
Ba	*Matthews (1997)*		-	-	-	-	-	-
	Mello et al., 1988	Mean	38.2	51.3	43.1	48.8	-	93.5
	Present study (LA-ICP-MS)	Mean	1.9	1.1	0.2	0.9	0.8	0.7
		s.d.	0.6	0.35	0.45	0.2	0.1	0.5

La	*Matthews (1997)*	Mean	1.8	1.35	0.8	0.2	1.5	0.3
		s.d.	1.5	1.2	0.4	0.3	0.9	0.2
	Mello et al., 1988	Mean	6	37.5	6	16.8	-	8.3
	Present study (LA-ICP-MS)	Mean	0.8	2	1	0.2	1.1	-
		s.d.	0.5	1.3	0.7	0.35	0.3	
Ce	*Matthews (1997)*	Mean	1.95	0.7	1.01	0.2	0.7	-
		s.d.	1.7	0.4	0.7	0.2	0.4	
	Mello et al., 1988	Mean	8.37	41.2	9.7	20.4	-	8.6
	Present study (LA-ICP-MS)	Mean	0.7	0.45	1.1	0.2	0.3	0.2
		s.d.	0.5	0.15	0.7	0.4	0.1	0.2
Sm	*Matthews (1997)*	Mean	0.35	0.1	0.1	0.07	0.3	-
		s.d.	0.3	0.06	0.08	0.05	0.2	
	Mello et al., 1988	Mean	0.3	3.2	0.9	2.1	-	0.9
	Present study (LA-ICP-MS)	Mean	-	-	-	-	-	-
		s.d.						
Eu	*Matthews (1997)*	Mean	0.1	0.05	0.04	0.04	0.07	-
		s.d.	0.06	0.03	0.02	0.05	0.03	
	Mello et al., 1988	Mean	0.1	1	0.2	0.5	-	0.2
	Present study (LA-ICP-MS)	Mean	0.04	0.05	0.05	0.01	0.005	0.02
		s.d.	0.02	0.04	0.03	0.01	0.02	0.01

Tb	*Matthews (1997)*	Mean s.d.	0.06 0.05	0.03 0.02	0.02 0.01	0.02 0.01	0.03 0.02	-
	Mello et al., 1988	Mean	-	-	-	-	-	-
	Present study (LA-ICP-MS)	Mean s.d.	-	-	-	-	-	-
Yb	*Matthews (1997)*	Mean s.d.	0.2 0.2	0.1 0.1	0.1 0.05	0.03 0.04	0.2 0.1	
	Mello et al., 1988	Mean	0.1	1	0.03	0.3		0.03
	Present study (LA-ICP-MS)	Mean s.d.	-	-	-	-	-	-
Lu	*Matthews (1997)*	Mean s.d.	0.03 0.03	0.03 0.02	0.01 0.009	0.01 0.007	0.03 0.02	
	Mello et al., 1988	Mean	0.02	0.1	0.03	0.03		0.02
	Present study (LA-ICP-MS)	Mean s.d.	-	-	-	-	-	-
Hf	*Matthews (1997)*	Mean s.d.	-	-	-	-	-	
	Mello et al., 1988	Mean	0.2	0.2	0.2	0.07		0.2
	Present study	Mean s.d.	0.04 0.05	0.01 0.003	0.02 0.007	0.01 0.003	0.015 0.006	0.01 0.005

Th	*Matthews (1997)*	Mean	0.15	0.08			0.07	-
		s.d.	0.15	0.06	-	-	0.07	
	Mello et al., 1988	Mean	0.06	1.3	1.6	0.1		1.7
	Present study	Mean	0.03	0.009	0.02	0.008	0.02	0.005
	(LA-ICP-MS)	s.d.	0.02	0.006	0.02	0.006	0.01	0.003
U	*Matthews, 1997*	Mean	0.2	0.03	0.02	0.09		
		s.d.	0.2	0.02	0.1	0.05		
	Mello et al., 1988	Mean	0.04	0.04	0.002		0.04	
	Present study	Mean	0.005	0.45	0.02	0.01	0.01	
	(LA-ICP-MS)	s.d.	0.003	1.7	0.03	0.004	0.009	

Rare-earth elements

In the result chapter (c.f. chapter 4), the REE in white marble (*i.e.,* La, Ce, Pr, Nd, Eu, Gd, Dy, Ho, Er) show homogeneous intra-district concentrations, and above all, the patterns of distribution seem to be characteristic of the various quarry sites.

REE abundances in fine-grained marble

The chondrite-normalized REE + Y diagram for white fine-grained marble is reported in Fig. 5.11.

The Afyon and Pentelic varieties have heterogeneous REE concentrations within specific quarries, overlapping the other samples in the spider diagram. For that reason, the fine-grained samples, exclude the Afyon and Pentelic samples, are reported in Fig. 5.12.

Göktepe and Paros show a negative Ce anomaly. It is is more marked in the Parian samples (Ce* 0.2). A negative Er anomaly is observed in the Göktepe marble and in the Gioia quarry at Carrara. The Göktepe marble differs from the others in having a positive Pr anomaly. The samples of fine-grained marble seem to be characterized by more similar absolute concentrations of the REE than those of coarse-grained marble. The main differences are the general depletion in REE in the Göktepe samples, and a slight HREE enrichment in the Paros samples.

Green *et al.* (2002) reported interesting geochemical results of ICP-MS analyses of 17 chips of fine-grained marble from the Paros quarries and 13 scraped samples from some sculptures of the Museum of Fine Arts in Boston. These authors observed similarities between the two Parian quarries in terms of trace-element content, particularly among the transition elements; thus demonstrating the impossibility to discriminate sample from these quarries.

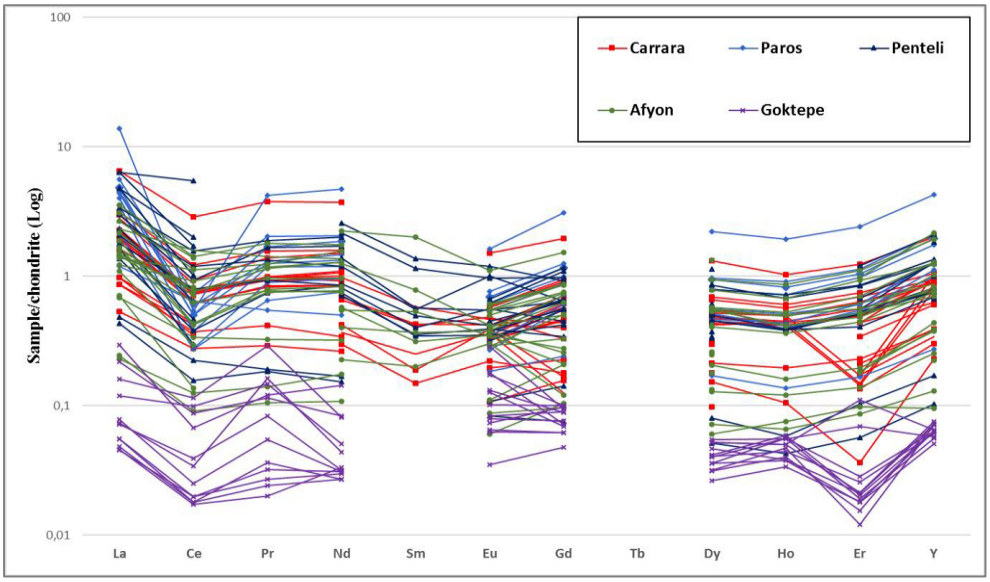

Fig. 5.11: The chondrite normalized REE + Y diagram of all fine-grained marble specimens from Carrara, Paros, Pentelic, Afyon and Göktepe sites.

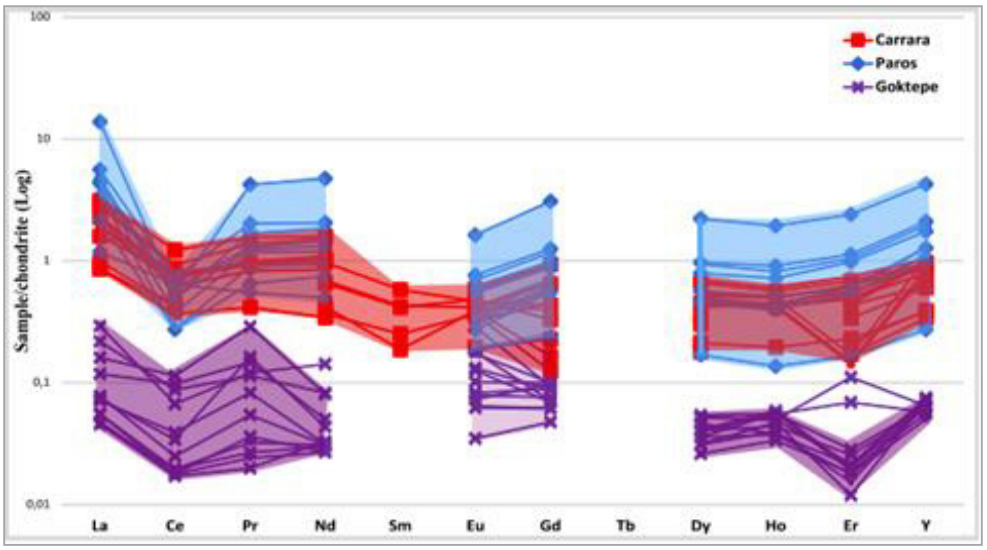

Fig. 5.12: The chondrite-normalized REE + Y diagram of fine-grained marble specimens from Carrara, Paros and Göktepe, leaving out those from Mt. Pentelicon and Afyon.

Starting from the study of Green *et al.* (2002), here are also considered the different amount of the sum of the REE and the contribution of LREE (*i.e.,* La, Ce, Pr, Nd) and HREE (*i.e.,* Eu, Gd, Dy, Ho, Er).

The samples of fine-grained marble show more similar REE concentrations in all quarries than those of coarse-grained lithotypes. The most distinct marble is from Göktepe variety. The marble from this quarry area are characterized by the lowest concentrations of REE and limited variability of both the LREE and HREE (Fig. 5.17). In Fig. 5.13, the Göktepe specimens falls in a separate cluster at the left bottom with respect to the other samples (*i.e.,* Carrara, Paros, Pentelicon and Afyon), these being characterized by higher REE content.

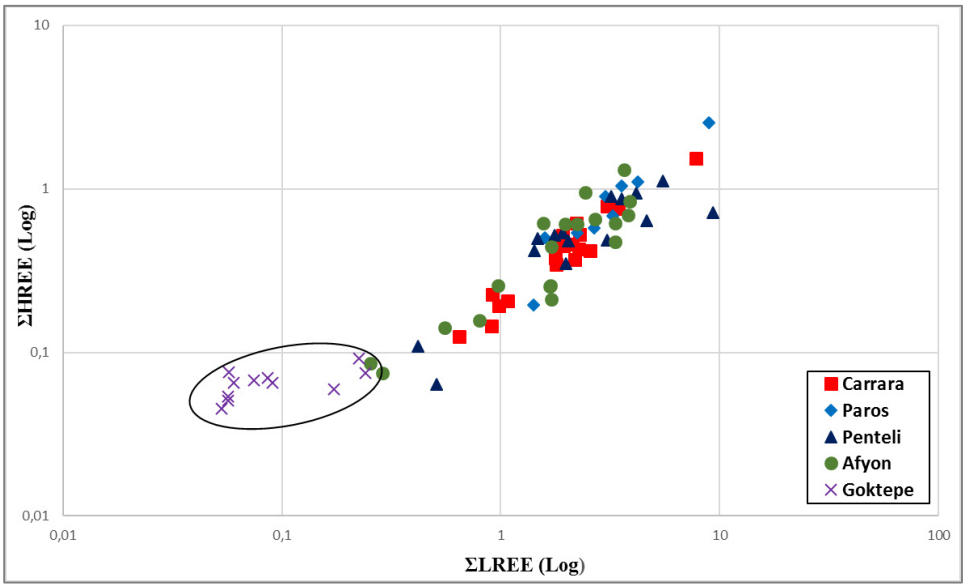

Fig. 5.13: LREE *vs* HREE content in fine-grained marbles. The Goketepe samples have the lowest concentrations of REE. The specimens of other quarries producing fine-grained white marble (*i.e.,* Carrara, Paros, Pentelicon and Afyon) are not separated, as the concentrations of REE is very similar.

REE abundances in coarse-grained marble

All coarse-grained samples of marble are plotted in the chondrite-normalized REE + Y diagram (Fig 5.14), resulting in significant differences among samples. Indeed, the marble sample from Naxos, Thasos and Thiountas can be discriminated on the basis of their absolute concentrations and patterns of REE. The Proconnesian specimens are characterized by a low content of Mn and a great heterogeneity in the REE, also within intrasite, which causes an overlap with other samples; for this reason, the Proconnesian marble does not treated with the other marble samples in Fig. 5.15.

The Thasian calcitic samples are characterized by a marked negative Ce anomaly (Ce* 0.2); a sharp positive Ho anomaly characterizes the Naxian specimens, and a positive Er anomaly is observed only in the Thiountas specimens. Both Thasian and Naxian samples present a Y enrichment. Finally, the Thiountas marble shows a marked depletion in Y, a characteristic also observed in samples from Filiz and Altintas quarries (Proconnesos samples), excluding two samples (OC 13/4 and OC/140).

In terms of absolute concentrations, the most important differences observed are the depletion of the LREE and HREE in the Thiountas samples and their enrichment in marble from Thasos.

The chart box of Fig. 5.17 highlights the fact that the coarse-grained samples are split in two different groups. The Turkish samples have the lowest concentrations of REE (*i.e.,* Thiountas and Proconnesos), whereas the sum of the REE is high and heterogeneous in both Greek samples (*i.e.,* Naxos and Thasos); the enrichment includes both the LREE and HREE.

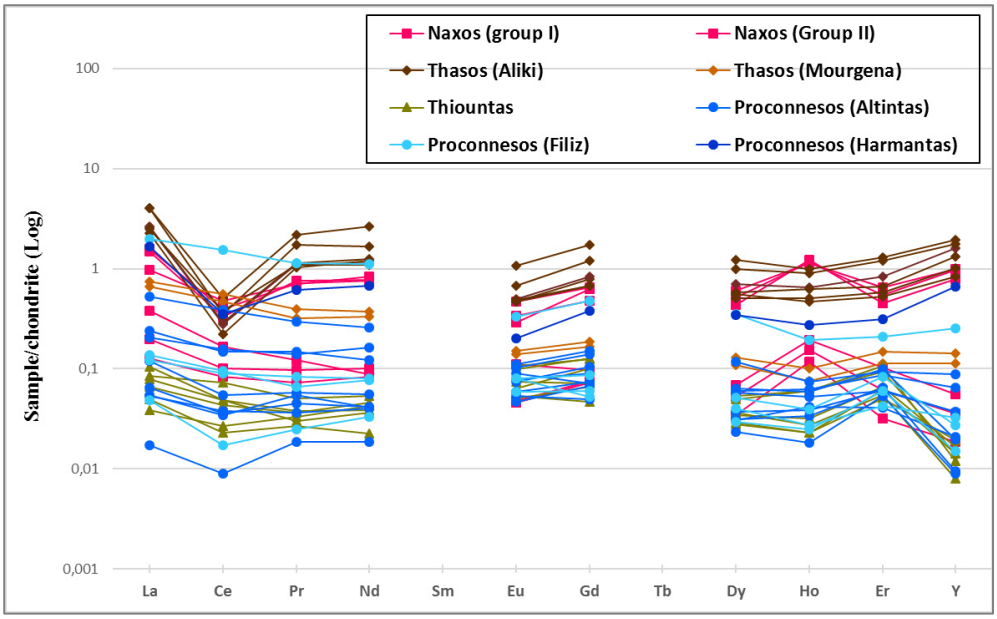

Fig. 5.14: The chondrite-normalized REE + Y diagram for coarse-grained marble specimens.

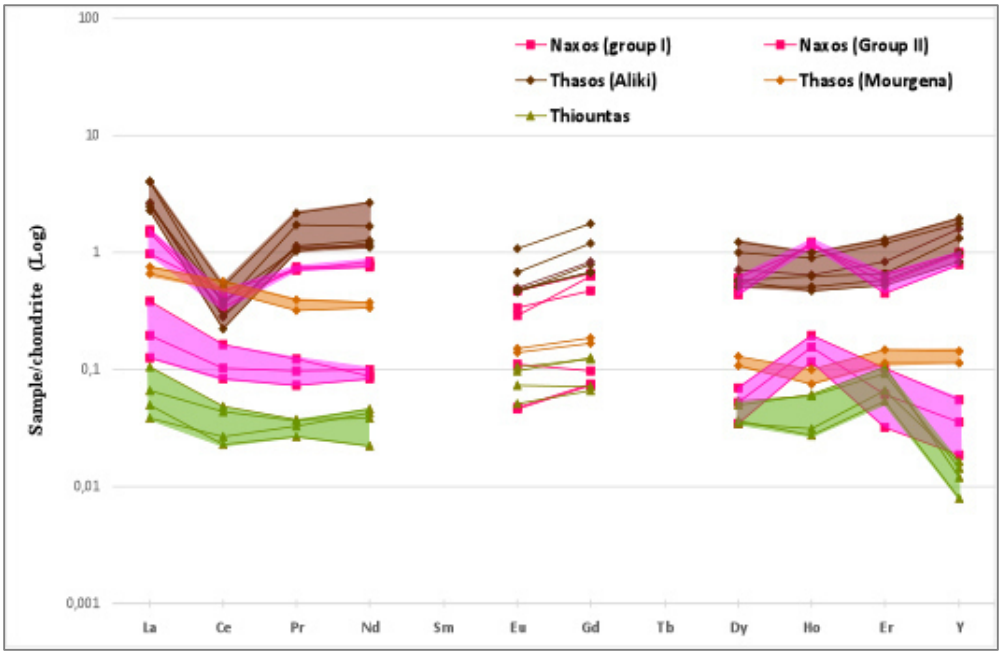

Fig. 5.15: The chondrite-normalized REE + Y diagram for coarse-grained marble specimens without Proconnesian specimens.

In the LREE *vs* HREE diagram (Fig. 5.16), the Thiountas specimens form a group well separated from those of Thasos and Naxos. Some of the Proconnesian samples overlap those of Thasos and Naxos, whereas the remaining samples, with low contents of the LREE and HREE overlaps the Thiountas specimens.

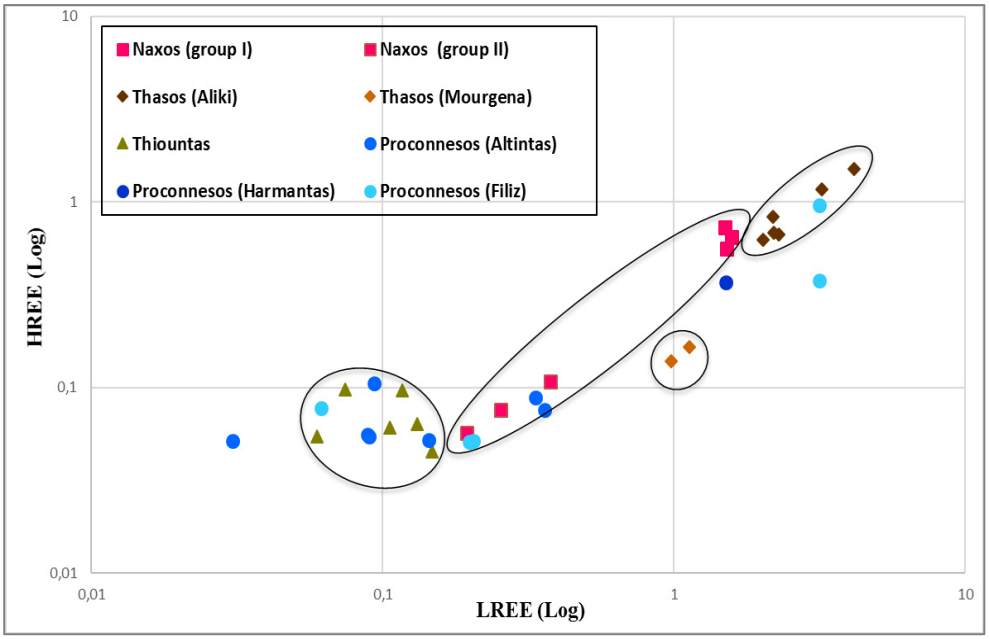

Fig. 5.16: LREE *vs* HREE diagram for coarse-grained marble. The Thiountas specimens are separated from those of Thasos and Naxos based on low LREE content. Proconnesian marbles plot apart from samples of the other quarry sites, having the widest range of concentrations for both LREE and HREE.

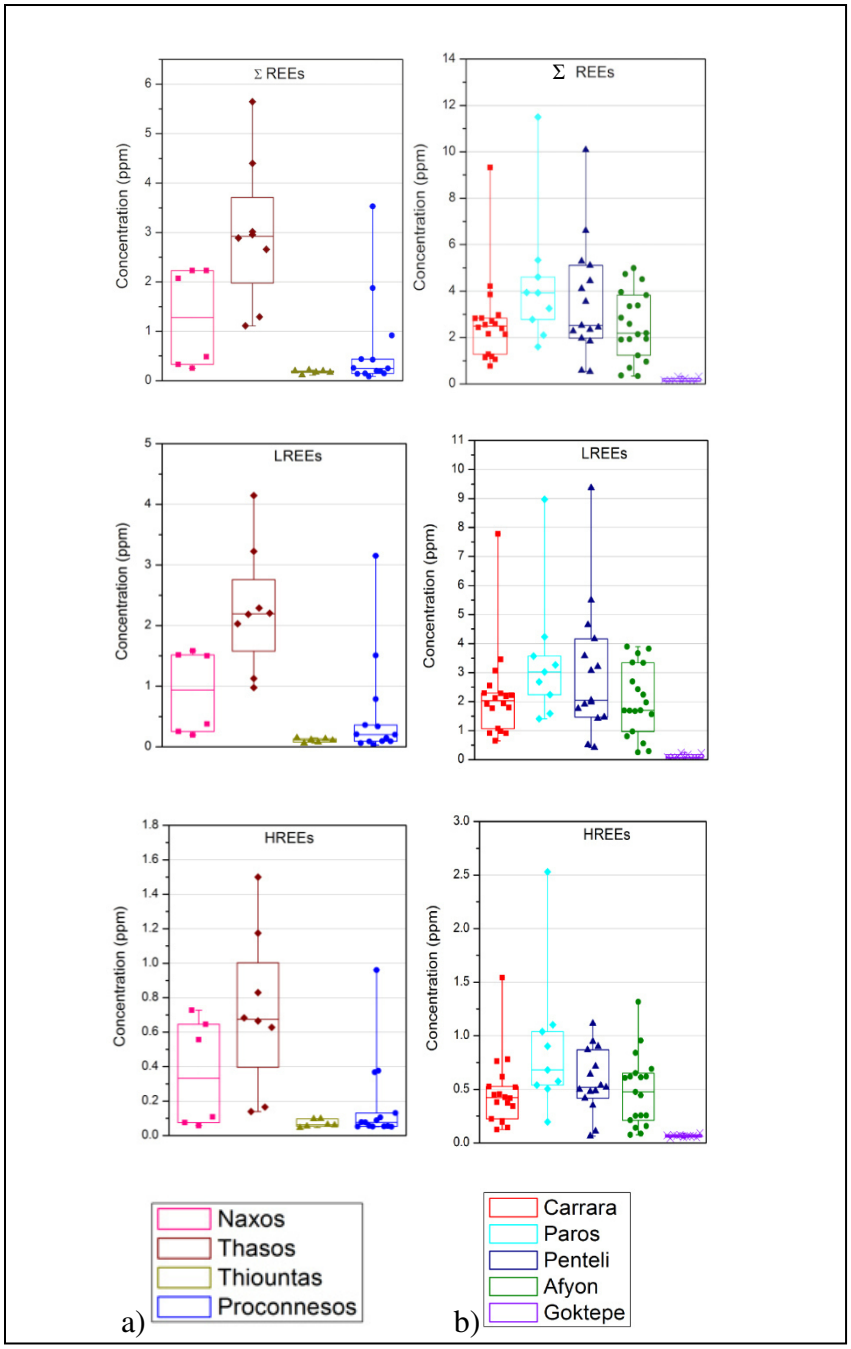

Fig. 5.17: Sum of REE, LREE and HREE content in coarse-grained (a) and fine-grained (b) samples of marble (expressed in ppm). Each point is an average at list of five spot LA-ICP-MS analyses for each sample. The box charts represent the dispersion of the experimental points: the median and the two percentile values 0.25 and 0.75, respectively.

5.3 Evolutionary scenario for provenance attribution of white marble

In recent decades, the provenance attribution of white marble has been dealt with by means of geochemical studies, which involved a complex evolutionary scenario.

From the first approaches based on isotopic results (Craig and Craig 1972; Manfra *et al.,* 1975) up to the more recent published works (Herz 1985, 1988; Gorgoni *et al.*, 2002 and references therein; Lazzarini *et al.*, 2002; Lazzarini and Antonelli, 2003; Tykot and Ramage, 2002; Attanasio *et al.*, 2006; 2009; 2015; Bruno *et al.*, 2002; Pentia *et al.*, 2002; Capedri *et al.*, 2004; Pike, 2009; Szekly and Zoldfoldi, 2009; Varti Matarangas *et al.*, 2009), the growth of the isotopic databases have revealed controversial results. Indeed, when the data are plotted all together, the overlap of different quarry sites is striking. In other words, the main drawback encountered is the great overlap among samples from the various sites of extraction.

In Table 5.4 and 5.5, the results of $\partial^{18}O$ and $\partial^{13}C$ values and the relative standard deviations acquired by Attanasio *et al.* (2003; 2006) on the same samples as those involved in this thesis are reported. The standard used to refer both carbon and oxygen isotope compositions of marbles is a calcite fossil, the rostrum of a belemnite, extracted from the Pee Dee Formation located in South Carolina (USA), commonly called the PDB standard (Attanasio, 2003; Attansio *et al.,* 2006).

Table 5.4: $\delta^{18}O$ values of all samples considered in this Ph.D. thesis, previously analyzed using a mass spectrometer by Attanasio *et al.* (2006).

		$\delta^{18}O$	Average $\delta^{18}O$	St. Dev. $\delta^{18}O$
Carrara	Torano	-0.46; -2.27	-1.55	0.61
	Fossacava	-1.30; -1.86	-1.62	0.22
	Calagio	-0.90; -1.18	-1	0.12
	Gioia	-0.94; -2.40	-1.68	0.35
Pentelicon	Quarry I	-4.96; -6.52	-5.67	0,79
	Kokkinaras	-4,32; 5,97	-5,36	0,66
	Spilià Quarry 13-15 l.l.	-4,49; -8,26	-6,32	1,09
	Spilià Quarry 6-8 h.l.	-4,48; -8,47	-7,46	0,9
Thasos	Aliki	-0.06; 0.62	-0.07	0.28
Afyon	Bacakale	-3.17; -7.08	-5.11	1.01
	Roder II	-2.43; -3.93	-3.32	0.38
	Boluk Mermer	-2.32; -7.51	-3.73	1.52
	Mermer Isletmesi	-3.11; -7.69	-5.27	1.35
Thiountas		-2.86; 4.84	-3.58	0.71
Proconnesos	Altintas	0.92; -6.40	-2.89	1.36
	Filiz	-1.39; -3.60	-2.35	0.75
	Harmantas	-0.63; -1.83	-0.97	0.37

Table 5.5: $\delta^{13}C$ values for all samples considered in this Ph.D. thesis, previously analyzed using a mass spectrometer by Attanasio *et al.* (2006).

		$\delta^{13}C$	Average $\delta^{13}C$	St. Dev. $\delta^{13}C$
Carrara	Torano	2.05; 2.50	2.29	0.18
	Fossacava	1.89; 2.48	2.13	0.19
	Calagio	1.81; 2.14	1.94	0.16
	Gioia	1.06; 2.44	2.03	0.30
Pentelicon	Quarry I	1.95; 2.98	2.60	0.56
	Kokkinaras	2.17; 2.54	2.36	0.13
	Spilià Quarry 13-15 l.l.	2.40; 3.79	2.78	0.36
	Spilià Quarry 6-8 h.l.	2.29; 2.70	2.51	0.12
Thasos	Aliki	2.92; 3.20	3.07	0.13
Afyon	Bacakale	-1.44; 1.99	0.36	1.00
	Roder II	1.78; 2.78	2.45	0.24
	Boluk Mermer	1.98; 3.08	2.46	0.30
	Mermer Isletmesi	0.42; 2.82	1.83	0.84
Thiountas		1.43; 2.23	1.78	0.25
Proconnesos	Altintas	-0.48; 3.24	2.52	0.74
	Filiz	1.95; 2.90	2.40	0.30
	Harmantas	2.39; 2.62	2.52	0.10

Fine-grained marble

One of the most controversial topics concerns the discrimination of the fine-grained marble from Carrara, Pentelicon and Afyon. In particular, the problem emerges where the isotopes of carbon and oxygen are involved in provenance studies. Indeed, the plot of Fig. 5.18, obtained by the combination of the isotopic data of the Herz database (1987a) with that of Attanasio *et al.* (2006), highlights some advances and drawbacks emerging from these studies. Although the plot underlines the homogeneity (limited dispersion of $\delta^{18}O$ and $\delta^{13}C$ values) and a good discrimination of Carrara marble from the less homogeneous Pentelic marble, the very wide area spanned by Afyon variety overlaps the isotopic composition of marble samples from Carrara and Mount Pentelicon.

Moreover, petrographic observations from literature and those reported here indicate that Carrara marble can be distinct on the basis of some typical features. These rock samples present a homeoblastic fabric and polygonal microstructure, with crystal having a straight to slightly curved boundary. In contrast, the Afyon samples have a heteroblastic fabric and xenoblastic microstructures, with crystals having a sutured and embayed boundary (Table 5.2). In addition, Carrara and Afyon samples can be distinguish on the basis of the different spectroscopic intensities (*e.g.,* EPR analyses reported in Attanasio *et al.,* 2006).

The most relevant difference obtained in this thesis is that Carrara marble is characterized by the high content of Mg (Fig. 5.19), which allows one to discriminate samples from this site and the other fine-grained specimens (*i.e.,* Paros, Pentelicon, Afyon and Göktepe).

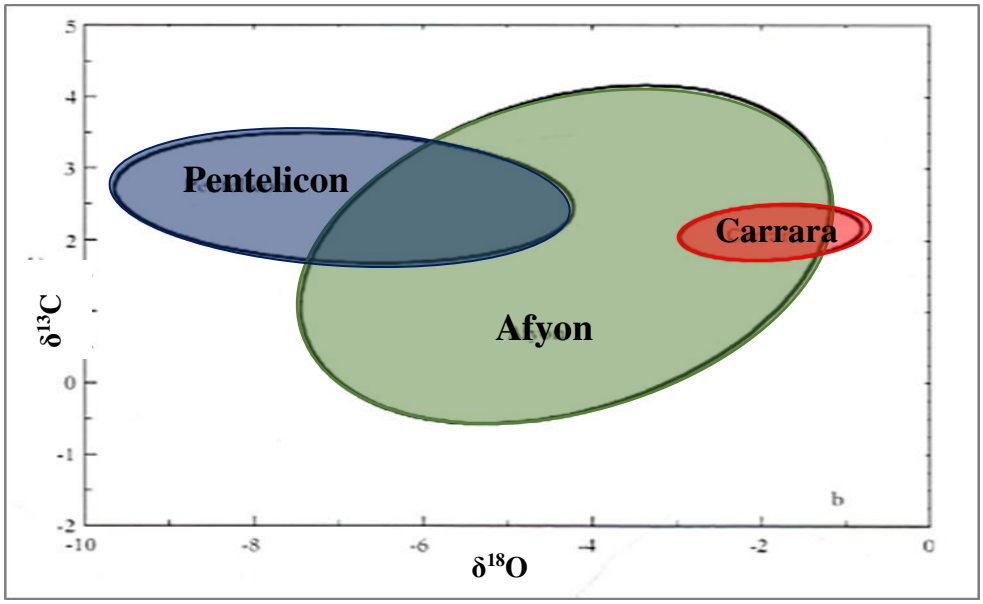

Fig. 5.18: Standard presentation of isotopic data of Carrara, Afyon and Pentelic samples and probable ellipse (90% probability). These data were obtained by the combination of Norman Herz' (1987a) database with that of Attanasio *et al.* (2006). The graph shows the level of isotopic discrimination for the three fine-grained marble varieties, the wide spanned area of Afyon samples overlaps the samples of the other two sites, apparently separated (Attanasio *et al.,* 2006).

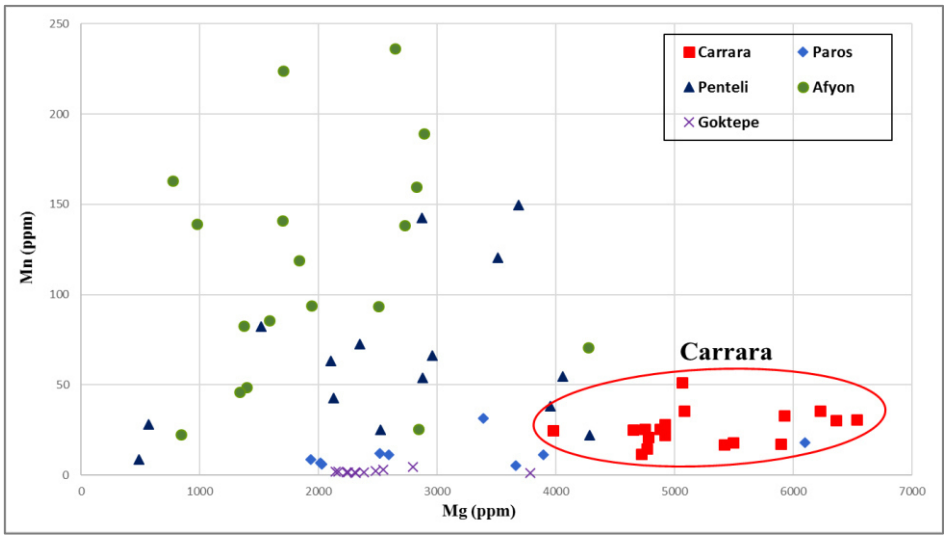

Fig. 5.19: Mg *vs* Mn content in fine-grained specimens (data from this Ph.D. thesis).

In terms of discrimination and thus provenance attribution, Carrara marble presents homogeneous features (*i.e.,* isotopic values, similar microstructure and MGS), facilitating the assignment of unknown marble of archaeological interest. However, with the data reported above, it remains difficult to discriminate samples on an inter-district basis (Attanasio *et al.,* 2006).

The LA-ICP-MS data demonstrate that the novelty for Carrara marbles is related to the intra-site discrimination. Indeed, the district of Colonnata (*i.e.,* Gioia, Fossacava and Calagio quarries) has a lower REE content than those from the Torano district (c.f. chapter 4 fig. 4.3.1.2).

Besides, Colonnata intra-site discrimination may be conducted observing the patterns of these elements as Gioia quarry specimens show a marked negative Er anomaly.

One of the main archaeological problems concerns the discrimination of Pentelic from Afyon marble. These two varieties present similar and rather high EPR intensities and carbon isotopic values; samples of Afyon marble are too heterogeneous, and overlap the data for Pentelicon (Attanasio, 2003; Attanasio *et al.,* 2006). About the Pentelic district, this marble shows highly marked intra-site superimposition of the isotopic values (Fig. 5.21). This variety of marble manifests a considerable enlargement of the provenance field due to the increase numbers of samples, particularly towards more negative $\delta^{18}O$ values, as reported in previous studies (Craig and Craig, 1972; Herz, 1985; Gorgoni *et al.,* 2002; Attanasio, 2003; Attanasio *et al.,* 2006).

In this thesis, the specimens from Pentelicon and Afyon show different petrographic features. The Pentelic specimens show an anisotropic texture, mainly foliated with an irregular granoblastic microstructure, whereas Afyon marble is isotropic with a xenoblastic microstructure (Table 5.2).

Observing the spider diagram in Fig. 5.20, samples of Afyon and Pentelic marble have similar REE concentrations; however, the Greek specimens present a more marked Ce and Sm negative anomaly.

The REE +Y diagram in Fig. 5.22 shows that Quarry I from Pentelicon is characterized by the lowest content of these elements, whereas the samples of the Kokkinaras quarry show a depletion in LREE compared to Spilià (from high - and low-level quarries). A stronger Ce anomaly of Kokkinaras samples (Ce* 0.3) than the others of Spilià, quite absent in Quarry I (Ce* 0.7) provides another discriminating feature.

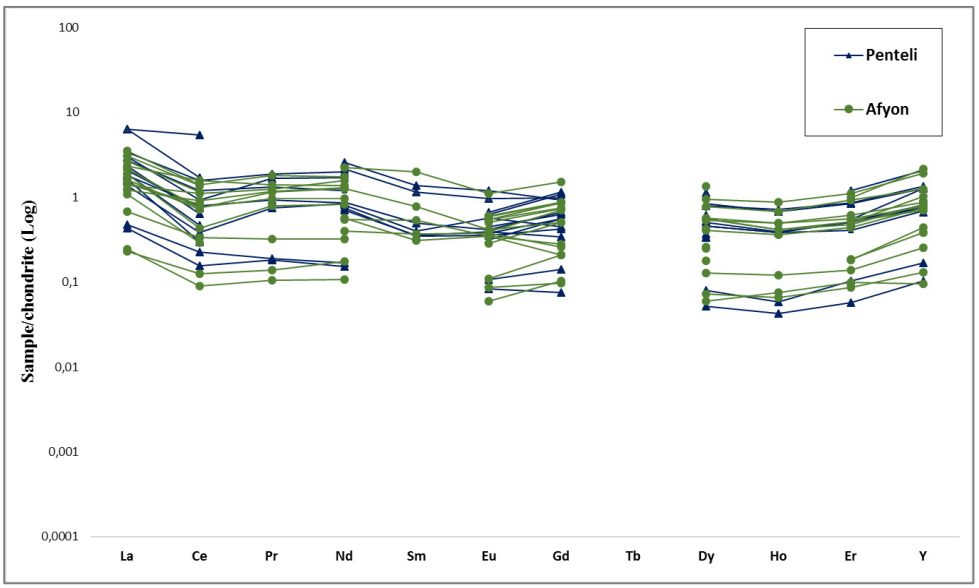

Fig. 5.20: The chondrite-normalized REE + Y diagram for fine-grained specimens of marble from Pentelic and Afyon.

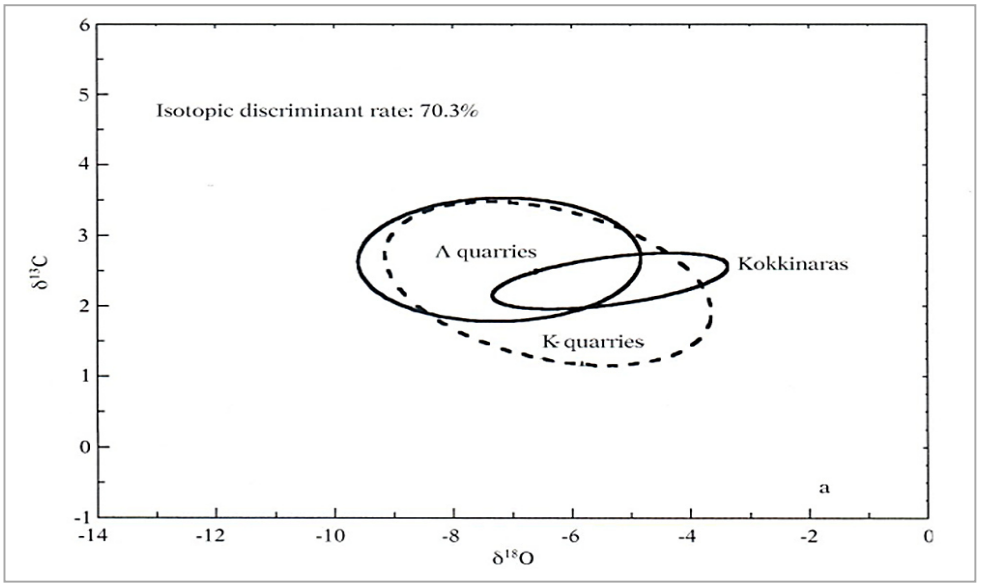

Fig. 5.21: Plot of Pentelic marble categorized by districts (Λ quarries include samples from Spilià (from low - and high-level quarries); K quarries include samples from Quarry I. The three districts of Pentelic marble show intra-site superimposition of the isotopic fields.

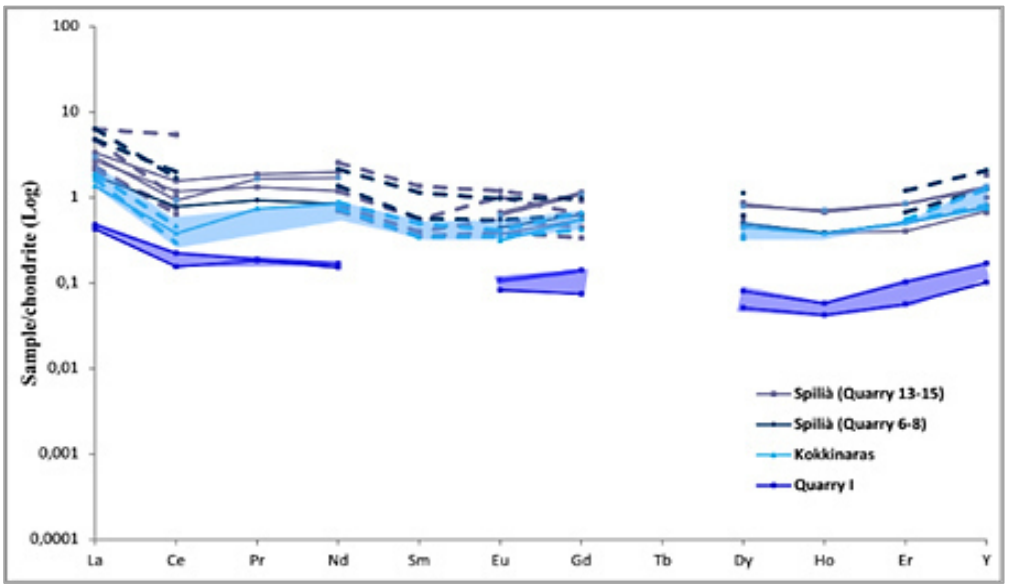

Fig. 5.22: The chondrite-normalized REE + Y diagram for the Pentelic districts, Spilià high - and low-level quarries, Kokkinaras quarry and Quarry I.

In summary, on the basis of isotopic data and some traces, the most strongly discriminated variety among the fine-grained marble samples is that of Göktepe. Indeed, Attanasio (2015) discriminated the samples of Göktepe marble from those of Carrara on the basis of Sr content and carbon and oxygen isotopes. Conversely, the results of this thesis demonstrate that the LA-ICP-MS data of Göktepe marble are more complex, showing for the first time the occurrence of numerous trace elements (at low concentrations) useful to discriminate such marble from other occurrences of fine-grained marble from Carrara, Paros, Pentelicon and Afyon. Indeed, the Göktepe marble is characterized by the highest content of Sr and the lowest levels of Mn and REE, and a Y and Er negative anomaly.

Moreover, some patterns of the REE (Ce and Sm negative anomaly) can be useful in solving the problematic attribution of provenance for Pentelic and Afyon marbles.

Table 5.6: The main important features of the fine-grained marble specimens (data from this thesis and Attanasio *et al.,* 2006).

	Petrographic features	Trace elements features	anomaly	Isotopic values $\delta^{13}C$; $\delta^{18}O$
Carrara	Ho, polygonal mosaic structure with triple points	High Mg, Th content	Er anomaly in Gioia quarry	-1; -1.68 1.94;2.29
Paros	He, mortar microstructure	High Y content	Marked negative Ce anomaly	
Pentelicon	He irregular granoblastic microstructure with a anisotrope texture	High Pb content	Negative Ce anomaly	-5.36—7.46 2.36-2.78
Afyon	He, xenoblastic microstructure. No triple points	High Pb content, high Mn/Sr ratio		-3.32: -5.27 0.36; 2.46
Göktepe		High Sr and low Mn, Pb, Th, REE and Y content, low Mn/Sr ratio	Negative Er and Ce anomaly, positive Pr anomaly	

Coarse-grained marble

Previous provenance studies on Naxian, Thasian, Proconnesian and Thiountas marble have shown that these lithotypes are isotopically similar (Attanasio *et al.,* 2006). Marble from these locations can easily be misclassified through visual inspection as well as using analytical data, particularly where a single method is involved (Gorgoni *et al.,* 2002; Attanasio *et al.,* 2006; Antonelli and Lazzarini, 2015). In Fig. 5.23, the isotopic data ($\delta^{13}C$ *vs* $\delta^{18}O$) of medium to large grain-size marble from different sites have been plotted (Attanasio *et al.,* 2006). Some of the samples plotted in that diagram are considered in this thesis (*i.e.,* Naxos, Thasos and Proconnesos).

The different groups are distributed along the axis, and the samples with less negative $\delta^{13}C$ values (*i.e.,* Melanes and Kinidaros quarries from Naxos island) exhibit a superposition with marble from other areas (*i.e.,* Thasos, Proconnesos), resulting in an impossibility to define a distinct provenance.

In particular, Naxian marble is characterized by a large variability of its physico-chemical properties, mostly notable in the oxygen isotopic ratio (Attanasio, 2003).

Recently, the iclusion of several samples from Naxos highlights the fact that its quarrying districts (*i.e.,* Apollonas, Melanes, Kinidaros) span a considerably large area. An efficient discrimination is only possible for the Apollonas district of the Naxos site.

The Naxian microstructure, defined as mortar, differs from Thasian and Proconessian marbles, exhibiting a xenoblastic microstructure (Table 5.2). The high MGS values of Naxian specimens are often far from the other samples of coarse-grained marble, but such a parameter cannot be considered useful owing to its wide variability (standard deviation 1.43), which reduces its diagnostic value (Attanasio, 2003).

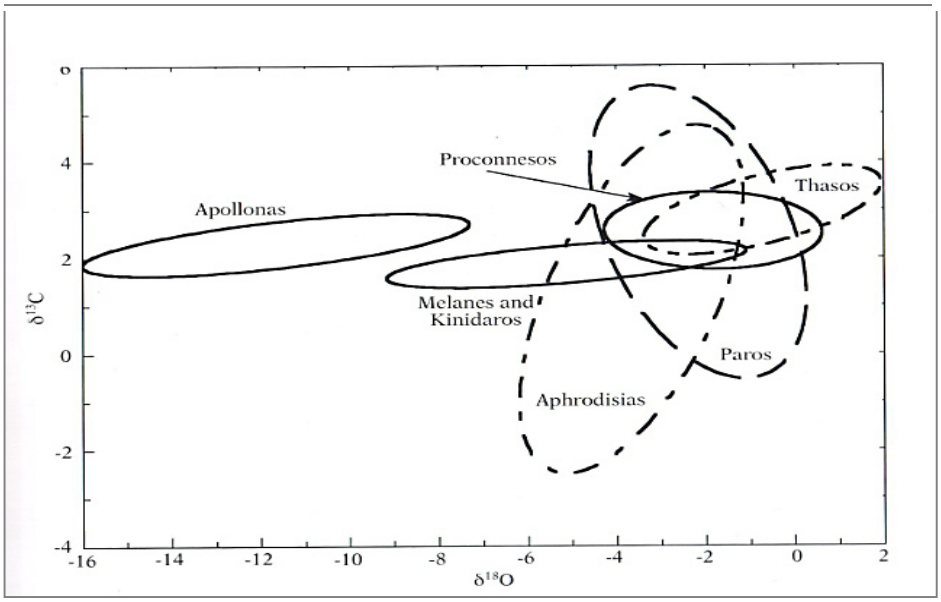

Fig.5.23: The graph compares Naxian isotopic data with the results obtained for other samples of medium to large grain-size marble from various sites. Isotopic analysis provides an efficient discrimination for Apollonas samples, extending in a highly negative region along the $\delta^{18}O$ axis. Samples with less strongly negative values (*i.e.,* Melanes and Kinidaros quarries) exhibit a superposition with other quarrying areas (*i.e.,* Paros, Thasos, Proconnesos, Aphrodisias) (Attanasio *et al.,* 2006).

The chondrite-normalized REE abundances in coarse-grained marble (Fig. 5.12) underlines a peculiar feature of this marble, which has a positive Ho anomaly not observed in marble from the other quarryareas.

Another problem concerns the hard isotopic discrimination between Proconnesos and Thasos, which commonly remains uncertain and unresolved.

The strong superposition of the stable isotopic data may be overcome by considering additional variables, as spectroscopic intensities. These two varieties show different EPR intensities (*e.g.,* Thasos and Proconnesos EPR intensities mean values are 1.3 and 0.0064 for Mn^{2+}, respectively). Actually, the most diagnostic property of

Proconnesian marble is the very low concentration of Mn^{2+} (Attanasio *et al.,* 2008).

Furthermore, the Proconnesian marble exhibits highly variable macroscopic features, such as grain size, from medium to large grain, strong sulphur odour upon scraping or grinding and, most notably, regular grey banding, and its identification is often considered a relatively simple task, not requiring sophisticated analyses and the subsequent statistical processing of data. These features form the basis for the correct identification of Proconnesos marble.

The specimens of Parian and Thasian marble also show similar macroscopic and microscopic characteristics, and the grey banding, undetectable on small samples, commonly turns into more complex and irregular patterns, common to other examples of famous Anatolian marble such as those from Aphrodisias.

The geochemical data reported in the present study confirm the difficulties encountered in the past in the study of this variety of marble, *i.e.,* Aphrodisias. Indeed, the trace elements in this marble present a wide range of concentrations, also intra-district variability (*e.g.,* Spilia' low and high level, Kokkinaras and Quarry I). Commonly, their trace-element content overlaps with the other medium to coarse-grained marble of other sites.

The most remarkable feature of the Proconnesian marble is its very low Mn content. It is characterized by a high Sr content, as reported above as also seem for the Thiountas samples (Fig. 5.27).

Furthermore, the low HREE content and the absence of a Ce anomaly may be useful to separate the two similar occurrences of marble, from Proconnesos and Thasos (characterized by a marked Ce negative anomaly), as shown in Figure 5.28.

The Thasos marble shows a marked negative Ce anomaly, whereas a positive Ho anomaly distinguishes the samples from Naxos.

The Turkish quarrying district of Thiountas seems to be distinguished from other occurrences of coarse-grained marble considered in this thesis on the basis of carbon and oxygen isotopes (Attanasio *et al.,* 2006). The rather homogeneous isotopic values overlap with other ancient sites (*e.g.,* Aphrodisias), however, and a detailed investigation of the geochemical composition is desirable, as stated by Attansio *et al.* (2006).

In this study, we observed that the Thiountas specimens are characterized by low LREE content (*i.e.,* La, Ce, Pr, Nd) and a positive Er anomaly, not shown by any other varieties of marble.

Finally, the case of the two dolomitic samples of Thasian marble (*i.e.,* samples MOUR5, MOUR) are described here. This case is extremely easy to solve, as dolomite is recognized without sophisticated techniques.

In antiquity, Thasos was the most important and almost unique source of dolomitic marbles

Other known examples of dolomitic marble are Villette, Crevola (French and Italian Alps, respectively; Attanasio *et al.,* 2006), and Malaga (Spain; Lapuente *et al.,* 2002). Materials from these quarries were used only locally. They can easily be distinguished from the Thasian variety owing to their macroscopic-microscopic features (*e.g.,* MGS, color).

The results of LA-ICP-MS analyses demonstrate that this dolomitic variety of white Thasian marble has the lowest content of Sr and does not show the Ce negative anomaly, unlike that occurring in the calcitic marble variety from Thasos.

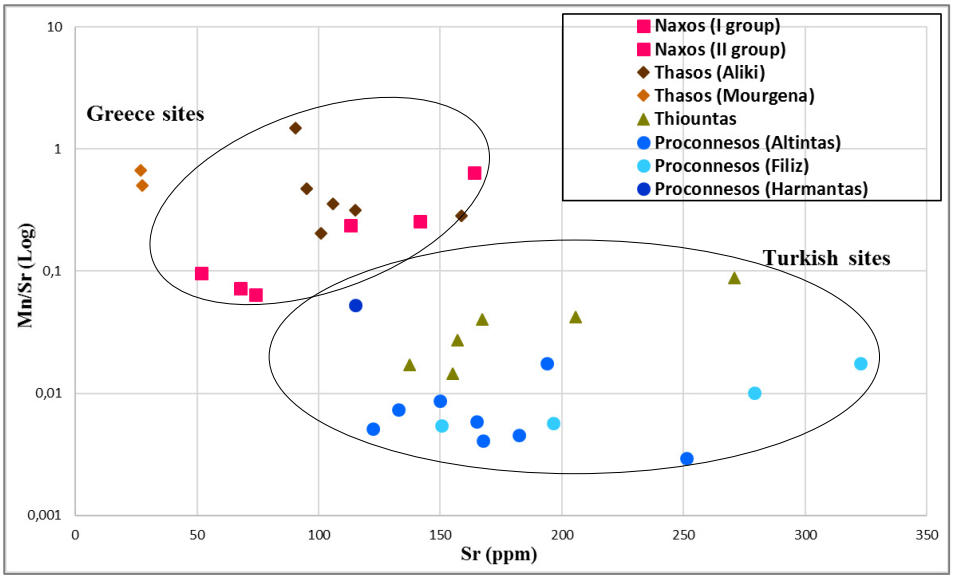

Fig. 5.27: The content of Sr and Mn separate the Turkish varieties of marble from those of Greece.

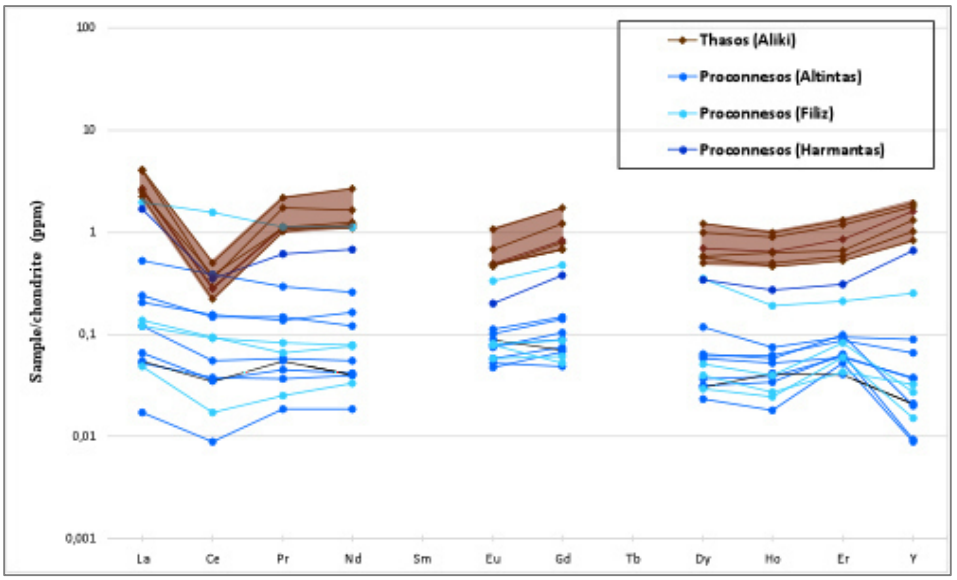

Fig. 5.28: The chondrite-normalized REE + Y diagram for coarse-grained specimens of marble from Thasos and Proconnesos.

Table 5.7: The main important features observed in the coarse-grained samples of marble in this Ph.D. thesis.

	Petrographic features	Trace elements features	Patterns	Isotopic values $\delta^{13}C$; $\delta^{18}O$
Naxos	HE, xenoblastic mortar microstructure		Positive Ho anomaly	
Thasos	HE, xenoblastic microstructure	High Y and Eu, LREE content	Marked negative Ce anomaly	-0.07 3.07
Thiountas	HE, mortar microstructure	Low LREE content	Positive Er anomaly	-3.58 1.78
Proconnesos	HE, xenoblastic microstructure			-0.97;-2.89 2.40;2.52
Greek sites		Low Sr, high Mn, High Y content		
Turkish site		High Sr, low Y and REE content, low Mn/Sr value		

Chapter 6

Conclusions

6. Conclusions

As shown here for trace elements, the LA-ICP-MS data allow one to explore the geochemical signatures of representative samples of white marble from the most important quarries of the Mediterranean area.

The goal of this work were twofold: 1) the establishment of a database gathering geochemical markers useful to discriminate different quarry districts, and 2) the determination of the abundances of a high number of trace elements in white marble of known provenance for their systematic geochemical characterization.

Furthermore, to test the proposed method, archaeological samples from the *Casa di Augusto* (an archaeological site of Rome) and from the *Musei Capitolini* (Rome) were also analyzed.

To achieve this goal, the LA-ICP-MS technique was adopted, after optical microscopy (OM) investigation.

A petrographic analysis of representative samples from Italy (Carrara), Greece (Pentelicon, Naxos, Paros and Thasos) and Turkey (Afyon, Thiuontas, Proconnesos and Göktepe) focused on the main features (*e.g.,* texture and the fabric, grain size and relationship among carbonate crystals). These results allow one to classify all marble samples into two subgroups, *i.e.,* fine - and coarse-grained marble, confirming the literature data.

The use of the LA-ICP-MS technique for the systematic acquisition of trace elements in white marble is the real novelty in approach in this thesis. Previous attempts are limited in terms of number of samples and trace elements sought. These results demonstrate, for the first time, the occurrence of numerous trace elements (commonly in the order of 0.1-1 ppm) useful to contribute to solve the provenance of fine-grained marble. In particular, the REE may yield the most typical fingerprints of the different quarry areas.

In the last decade, provenance investigation of Italian (Carrara, Colonnata and Torano districts), Greek (Pentelicon and Paros) and Turkish (Afyon) varieties resulted in controversy owing to their similar physico-chemical properties. However, the patterns of REE are different for Carrara and Greek samples, even if they have quite similar concentrations. Moreover, the REE content permits intra-site discrimination within Carrara marble; indeed, marble from Colonnata district shows a lower REE content (*i.e.,* quarries Gioia, Fossacava and Calagio) than those of the Torano district. Within the Colonnata district, the patterns of these elements provide evidence of a marked negative Er anomaly only in specimens from Gioia quarry. In addition, the Mg content distinguishes the Carrara marble (0.04‰-0.065‰) from two other fine-grain varieties, *i.e.,* Pentelic and Afyon marble (0.006-0.04‰ and 0.008-0.04‰, respectively). This result is very important, as these two lithotypes cannot be discriminated with oxygen and carbon isotopes, as they present an overlap of data.

The Greek varieties (*i.e.,* Pentelic and Paros) are characterized by a similar content of the REE compared to those from Turkey (*i.e.,* Afyon and Göktepe), and a marked negative Ce anomaly is not observed in the white marble from both Italian quarrying districts (*i.e.,* Colonnata and Torano) and Turkey (*i.e.,* Afyon). Moreover, the Paros marble presents the highest content of Y, and the Pentelic variety has the highest Pb content. Although the Pentelic districts (*i.e.,* Spilià low and high level, Kokkinaras and Quarry I) show highly marked intra-site superposition of the isotopic values, the trace-element concentrations seem to better discriminate among these. Quarry I samples are characterized by the lowest REE content, whereas the samples from the Kokkinaras quarry show a depletion in LREE compared to Spilià (high and low level quarries). Moreover, the Kokkinaras samples present a strong negative Ce anomaly, less

marked in the Spilià specimens and virtually absent in those from Quarry I.

The white marble that shows the most homogeneous content of trace elements is Göktepe. This group presents a very low content of REE (sum of REE 0.1-0.3 ppm), Pb (0.04-0.4 ppm), Th (0.002-0.01 ppm), Y (0.02-0.2 ppm) and Mn (0.95-4.47ppm), and the highest content of Sr (420-830 ppm). The patterns of the REE emphasize that this marble is also characterized by a marked negative Er and positive Pr anomaly.

Concerning the samples of the coarse-grained marbles, the abundance and patterns of REE provide evidence of some peculiarities for Greek (Naxos and Thasos) and Turkish quarries (Thiountas and Proconnesos). The Greek marble reveals an enrichment in HREE; in addition, the Naxos marble has a positive Ho anomaly, whereas Thasos presents a marked negative anomaly in Ce. The Turkish marble from Thiuontas shows low levels of LREE content and a positive Er anomaly, not observed in any other varieties. Concerning the common substitutes of Ca in the calcite structure, the Turkish specimens (Thiountas and Proconnesos) are characterized by a lower Mn content and a higher Sr content with respect to those from Greek (Naxos and Thasos).

The large variability in the physico-chemical properties of the Naxos marble does not permit one to distinguish this variety from the other coarse-grained specimens (*i.e.,* Thasos, Thiountas, Proconnesos). The LA-ICP-MS data in this thesis emphasized that these four coarse-grained varieties of marble differ in their enrichment in Y, HREE and Mn, and depletion in Sr. Although the REE concentrations of the two Greek sites Naxos and Thasos commonly overlap, they differ in their REE patterns and anomalies in Ce and Ho.

These LA-ICP-MS results will contribute to stimulate the debate on provenance sources of white marble in use in the Mediterranean

basin, and in turn can provide incentive in the acquisition of new data, thus improving the geochemical database for these rocks.

Further investigations will consist in implementing the number of geological samples in order to increase the quantity and quality of trace-element data, and the acquisition of the LA-ICP-MS data on a larger number of samples of archaeological interest to improve and test the method on white marble artifacts.

The main geochemical features of the white marble analyzed in this study can be shown schematically in flow charts (Fig. 6.1, Fig. 6.2).

Fig. 6.1: A flow chart for white fine-grained marble (MGS < 2 mm), with the discriminant parameters applied to Carrara, Paros, Pentelicon, Afyon, and Göktepe for purposes of provenance.

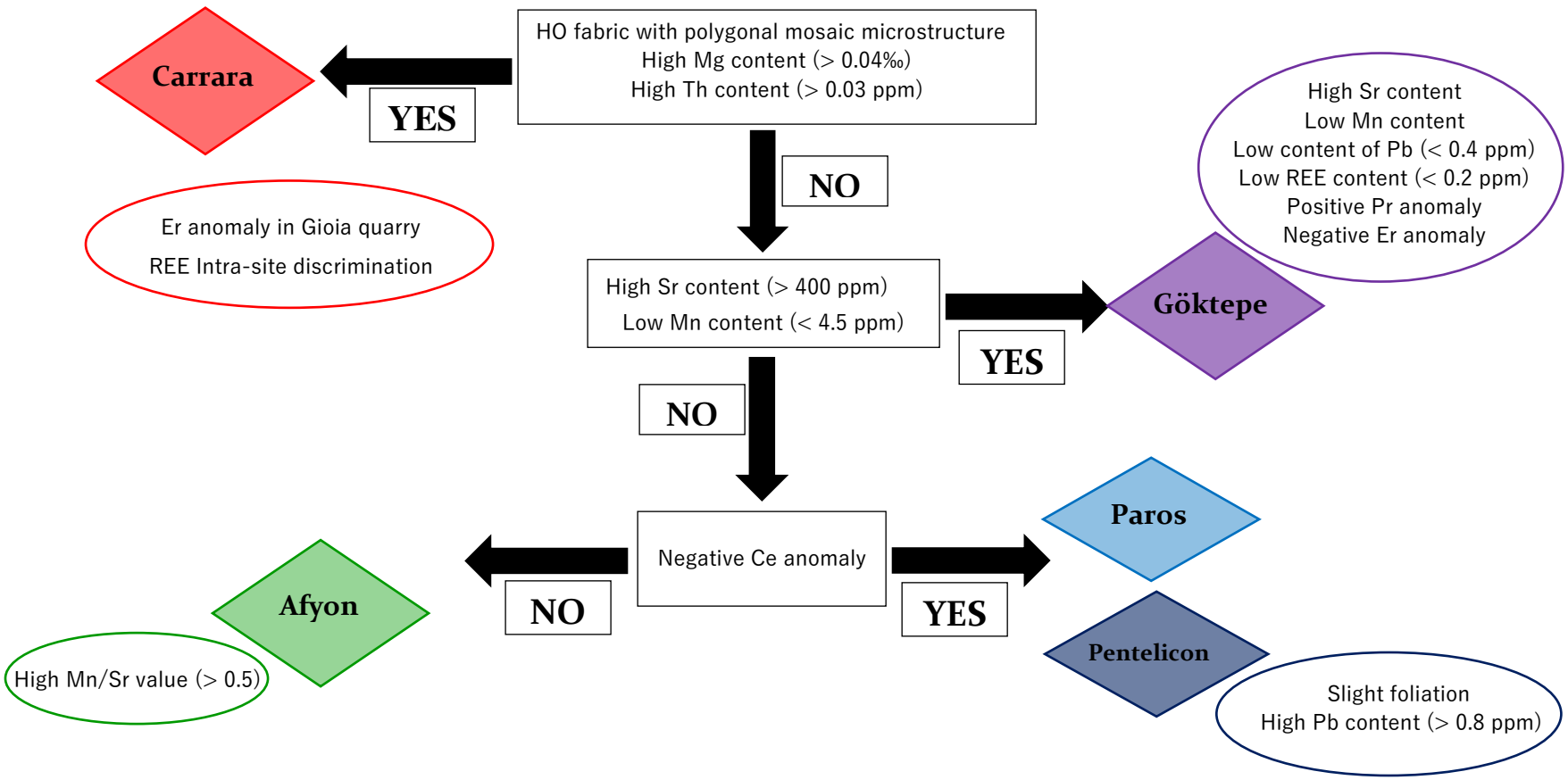

Fig. 6.2: A flow chart for the white coarse-grained marble (MGS > 2 mm), with the discriminant parameters applied to Naxos, Thasos, Thiountas, and Proconnesos for purposes of provenance.

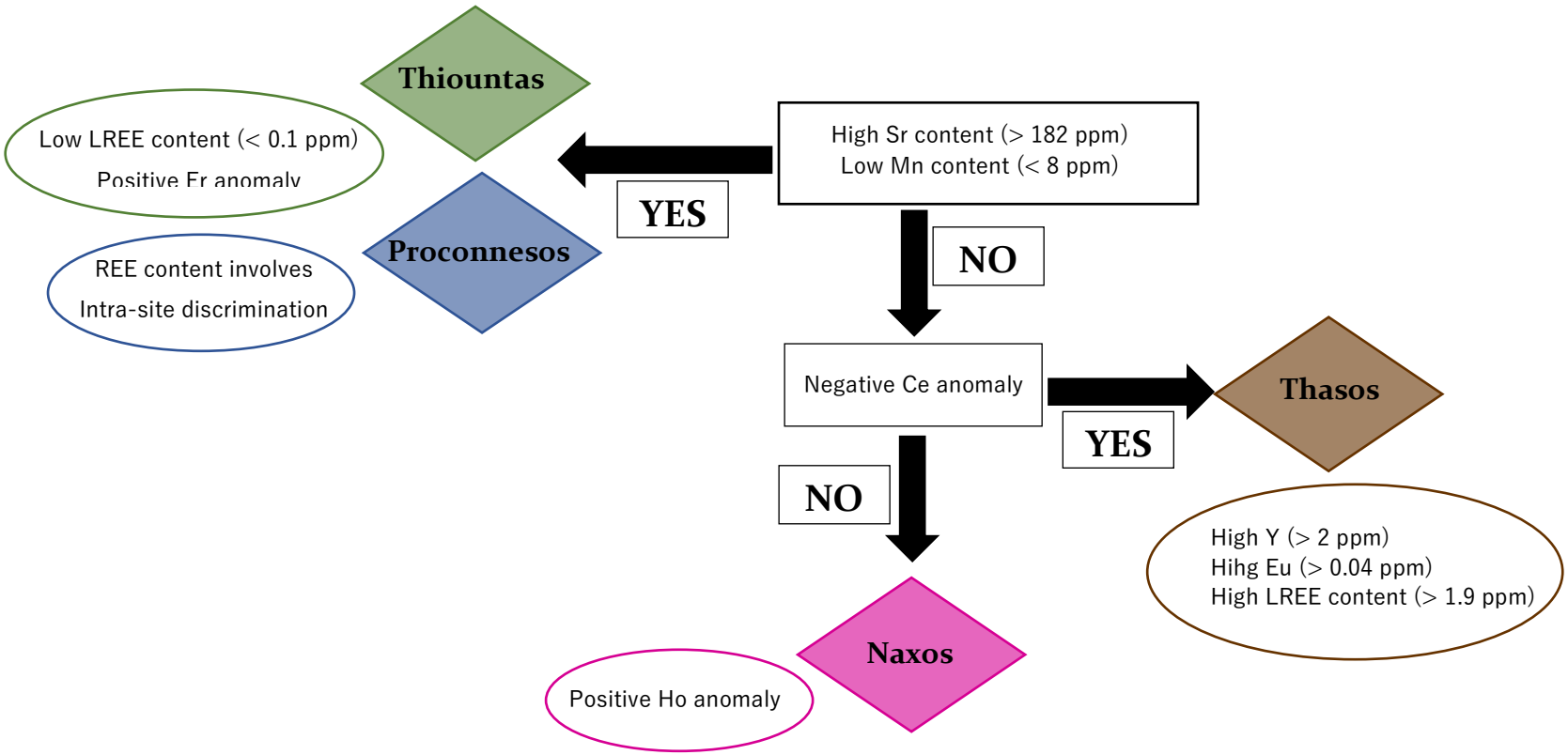

References

Aldanmaz E., Pearce J.A., Thirlwall M. F., Mitchel J.G., 2000, Petrogenetic evolution of late Cenozoic, post-collision volcanism in western Anatolia, Turkey, *Journal of Volcanology and Geothermal Research*, 102, 67-95.

Aksoy R., 1995, Stratigraphy of the Marmara Island and the Kapıdagı Peninsula, *TAPG (Turkish Association of Petroleum Geologists) Bulletin*, 7, 33–49.

Aksoy R., 1996, Mesoscopic tectonic features of the Marmara island and the Kapıdagı peninsula, NW Turkey, *Turkish Journal of Earth Sciences*, 5, 187–195.

Altherr R., Schliestedt M., Okrusch M., Seidel E., Kreuzer H., Harre W., Lenz H., Wendt I., Wagner G.A., 1979, Geochronology of high-pressure rocks on Sifnos (Cyclades, Greece), *Contrib. Mineral. Petrol.,* 70, 245–255.

Altherr R., Kreuzer H., Wendt I., Lenz H., Wagner G. A., Keller J., Harre W., Hohndorf A., 1982, A Late Oligocene/Early Miocene high temperature belt in the Anticycladic crystalline complex (SE Pelagonian, Greece), *Geol. Jahrb.,* 23, 97–164.

Altherr R., Siebel W., 2002, I-type plutonism in a continental back-arc setting: Miocene granitoids and monzonites from the central Aegean Sea, Greece, *Contrib. Mineral. Petrol.,* 143, 397–415.

Amadori M. L., Lazzarini L., Mariottini M., Pecoraro M., Pensabene P., 1998, Determinazione della provenienza dei marmi usati per alcuni monumenti antichi di Roma, in Marmi antichi, cave e tecnica di lavorazione, provenienze e distribuzione, ed. Pensabene P., L'Erma di Bretschneider, Roma, Studi Miscellanei, 31, 45-56.

Andriessen P. A. M., Boelrijk N. A. I. M., Hebeda E. H., Priem H. N. A., Verdurmen E. A. T., Verschure R. H., 1979, Dating the events of metamorphism and granitic magmatism in the Alpine Orogen of Naxos (Cyclades, Greece), *Contributions to Mineralogy and Petrology*, 69, 215–225.

Angelier J., Glaçon G., Muller C., 1978, Sur la présence et la position tectonique du Miocène inférieur marin dans l'archipel de Naxos (Cyclades, Grèce), *C. R. Acad. Sci., Paris,* 286, 21–24.

Antonelli F., Gentili G., Renzulli A., Amadori M. L., 2003, Provenance of the ornamental stones used in the baroque church of S. Pietro in Valle (Fano, Central Italy) and commentary on their state of conservation, *J. Cult. Herit*age, 4 (4), 299–312.

Antonelli F., Lazzarini L., 2013a, The use of white marble in the central and upper adriatic between Greece and Rome: Hellenistic Stelae from the necropolis of Ancona (Italy), *Camb Archaeol. J.,* 23 (2), 149–162.

Antonelli F., Lazzarini L., 2013b, White and coloured marbles of the Roman town of Urbs Salvia (Urbisaglia, Macerata, Marche, Italy), *Oxf. J. Archaeol.,* 32 (3), 293–317.

Antonelli F., Columbu S., Lezzerini M., Miriello D., 2014a, Petrographic characterization and provenance determination of the white marbles used in the Roman sculptures of Forum Semproni (Fossombrone, Marche, Italy), *Appl. Phys. A Mater Sci Process*, 115(3), 1033–1040.

Antonelli F, Lapuente MP, Dessandier D, Kamel S., 2014b, Petrographic characterization and provenance determination of the crystalline marbles used in the Roman city of Banasa (Morocco): new data on the import of Iberian marble in Roman North Africa, Archaeometry.

Antonelli F., Lazzarini L., 2015, An updated petrographic and isotopic reference database for white marbles used in antiquity*, Rend. Fis. Acc. Lincei,* 26, 399–413.

Armiento G., Attanasio D., Platania R., 1997, Electron spin resonance study of white marbles from Tharros Sardinia: A reappraisal of the technique, possibilities and limitations, *Archaeometry,* 39, 2, 309-319.

Asgari N., 1973, Roman and early Byzantine marble quarries of Proconnesus, The proceedings of the Xth International congress of Classical Archaeology (Ankara-Izmir), Vol. I-III, 23-30.

Asgari N., 1978, Roman and early Byzantine marble quarries of Proconnesos, in *X international congress of classical archaeology*, ed. E. Akurgal, 1–3, Türk Tarih Kurumu Basimevi, Ankara.

Ates A., Kayırana T., Sincer I., 2003, Structural interpretation of the Marmara region, NW Turkey, from aeromagnetic, seismic and gravity data, *Tectonophysics*, 367, 41– 99.

Attanasio D., 1999, The use of electron spin resonance spectroscopy for determining the provenance of classical marbles, *Applied magnetic resonance*, 16, 3, 383-402.

Attanasio D., Emanuele M. C., Platania R., 1999, ESR and petrographic determination of the provenance of classical marble: evaluation and assessment of the classification rules, in 2nd International Congress on Science and Technology for the Safeguard of Cultural Heritage in the Mediterranean Basin, Paris, 5-9 July 1999, Vol. 1.

Attanasio D., Armiento G., Brilli M., Emanuele M. C., Platania R., Turi B., 2000, Multi-method marble provenance determinations: the Carrara marbles as a case study for the combined use of isotopic, electron spin resonance and petrographic data, *Archaeometry*, 42, 2, 257-272.

Attanasio D., Platania R., 2000, ESR Spectroscopy as a Tool for Identifying Joining Fragments of Antique Marbles: The Example of a Pulpit by Donatello and Michelozzo, *Journal of Magnetic Resonance,* 144, 322- 329.

Attanasio D., 2003, Ancient white marbles: analysis and identification by paramagnetic resonance spectroscopy, ed. L'Erma di Bretschneider, Roma, pp. 283.

Attanasio D., Platania R., 2003, Refinement and assessment of the classification rule for an updated version of the EPR and petrographic marble database, in eds L. Lazzarini, *Interdisciplinary studies on ancient stone*, Bottega d'Erasmo, Padova, 149-155.

Attanasio D., Brilli M., Ogle N., 2006, The Isotopic Signature of Classical Marbles, L'Erma di Bretschneider eds, Roma.

Attanasio D., Brilli M., Bruno M., 2008a, The properties and identification of marble from Proconnesos (Marmara island, Turkey): a new database including isotopic, EPR and petrographic data, *Archaeometry*, 50, 5, 747–774.

Attanasio D., Bruno M., Yavuz A.B., Elçi, E., 2008b, Aphrodisias and the newly discovered quarries at Göktepe, in R.R.R. Smith and J.L. Lenaghan eds, *Roman Portraits from Aphrodisias*, 217–227, Istanbul, Yapı Kredi.

Attanasio D., Bruno M., Yavuz A.B., 2009, Quarries in the region of Aphrodisias: the black and white marbles of Göktepe (Mugˇ la, Turkey), *Journal of Roman Archaeology*, 22, 312–348.

Attanasio D., Bruno M., Yavuz A. B., Prochaska W., 2012b, Aphrodisian marble from Göktepe quarries: the Little Barbarians, Roman copies from Attalid Dedication in Athens, *Papers of the British School at Rome*, 80, 1-23.

Attanasio D., Bruno M., Prochaska W., Yavuz A. B., 2015, A multi-method database of the black and white marbles of Göktepe (Aphrodisias), including isotopic, EPR, trace and petrographic data, *Archaeometry*, 57, 217–245.

Avdis V., 1991, The effect of movement of high-angle faults on stratigraphy and structure: the Attico-Cycladic Massif, Greece, *Tectonophysics*, 192, 293-311.

Avigad D., Garfunkel Z., 1991, Uplift and exhumation of high pressure metamorphic terranes: the example of the Cycladic blueschists belt (Aegean Sea), *Tectonophysics,* 188, 357–372.

Avigad D., 1993, Tectonic juxtaposition of blueschists and greenschists in Sifnos Island (Aegean Sea) – implications for the structure of the Cycladic blueschist belt, *J. Struct. Geol.*, 15 (12), 1459-1469.

Avigad D., 1998, High-pressure metamorphism and cooling on SE Naxos (Cyclades, Greece), *European Journal of Mineralogy*, 10, 1309-1319.

Avigad D., Garfunkel Z., Jolivet L., Azanon J. M., 1997, Back arc extension and denudation of Mediterranean eclogites, *Tectonics*, 16(6), 924–41.

Aydin M., Sahintürk Ö., Serdar H. S., Özçelik Y., Akarsu I., Ungör A., Çokugras R., Kasar S., 1986, Ballidag-Çangaldag (Kastamonu) arasindaki bölgenin jeolojisi, *Geological Society of Turkey Bulletin*, 29, 1-16.

Bargnesi E. A., Stockli D. F., Mancktelow N., Soukis K., 2013, Miocene core complex development and coeval supra-detachment basin evolution of Paros, Greece, insights from (U–Th)/He thermochronometry, *Tectonophysics*, 595–596, 165–182.

Barberi F., Giglia G., 1965, La serie scistosa basale dell'autoctono delle Alpi Apuane, *Boll. Soc. Geol. It.*, 84, 41-92.

Barbin V., Ramseyer K., Decrouez D., Herb R., 1989, Marbres blancs: caractérisation par cathodoluminescence*, C.R.Acad Sci Paris*, 308, Série II, 865-866.

Barbin V., Burns S. J., Decrouez D., Oddone M., Zezza U., 1991, Cathodoluminescence, REE, and stable isotopes characterization of marbles from Crevola D'Ossola, Candoglia, Lasa (Italy) and Pteleos (Greece), in *The conservation of monuments in the Mediterranean basin*, D. Decrouez, J. Chamay, F. Zezza (eds), Genève, 47-62.

Barbin V., Ramseyer K., Decrouez D., Burns S. J., Chamay J., Maier J. L., 1992, Cathodoluminescence of white marbles: an overview, *Archaeometry,* 34 (2), pp. 175-183.

Barka A. A., 1992, The North Anatolian fault, *Annales Tectonicae*, 6, 164- 195.

Baroni C., RiboliniA., Bruschi G., Mannucci P., 2010, Geomorphological map and raised-relief model of the Carrara marble basins, Tuscany, Italy, *Geografia Fisica e Dinamica Quaternaria,* 33, 233-243.

Baxter M. J., 2006, A review of supervised and unsupervised pattern recognition in archaeometry, *Archaeometry*, 48 (4), 671–694.

Baxter M. J., 1999, Detecting multivariate outliers in artefact compositional data, *Archaeometry,* 41 (2), 321-338.

Baxter M. J., Buck C. E., 2000, Data handling and statistical analysis, in *Ciliberto Spoto*, 681-746.

Beck M. E., Schermer E. R., 1994, Aegean paleomagnetic inclination anomalies: is there a tectonic explanation?, *Tectonophysics*, 231, 281-292.

Bestmanna M., Kunzeb K., Matthews A., 2000, Evolution of a calcite marble shear zone complex on Thassos Island, Greece: microstructural and textural fabrics and their kinematic significance, *Journal of Structural Geology,* 22, 1789-1807.

Blake M.C., Bonneau M., Geyssant J., Kienast J.R., Lepvrier C., Maluski H. Papanikolaou D., 1981, A geological reconnaissance of the Cyclacic blueschist belt, Greece, *Bull. Geol. Soc. Am.* 92, 247–254.

Bonamici M., 1989, Il marmo lunense in epoca preromana, *Atti del Seminario il Marmo nella civiltà romana*, La produzione e il commercio, Carrara, Lucca, 83–113.

Bonneau M., 1982, Evolution géodynamique de l'arc égéen depuis le Jurassique Supérieur jusqu'au Miocène, *Bull. Soc. Géol. Fr.* 7, 229–242.

Bonneau M., Kienast J.R., 1982, Subduction, collision et schistes bleus: exemple de l'Egée, Grèce, *Bull. Soc. Géol. Fr.,* 7, 785–791.

Bonneau M., 1984, Correlation of the Hellenic nappes in the south-east Aegean and their tectonic reconstruction, in The Geological Evolution of the Eastern Mediterranean, in J. E. Dixon and A. H. F. Robertson, Editors, *Special Publication of the Geological Society ofLondon*, Blackwell Scientific Publications, Oxford, 517–527.

Bozkurt E., Mittwede S.K., 2001, Introduction to the Geology of Turkey - A Synthesis, *International Geology Review*, 43-7, 578-594.

Bradley F., 1991, Guida alle Cave di Marmo di Carrara, *Internazionale Marmi e Macchine Carrara*, pp. 91.

Brichau S., Ring U., Ketcham R. A., Carter A., Stockli D., Brunel M., 2006, Constraining the long-term evolution of the slip rate for a major extensional fault system in the central Aegean, Greece, using thermochronology, *Earth Planet. Sci. Lett.,* 241, 293–306.

Brichau S., Thomson S., Ring U., 2009, Thermochronometric constraints on the tectonic evolution of the Serifos detachment, Aegean Sea, Greece, *Int J Earth Sci,* 99, 379-393.

Brilli M., Giustini F., Pensabene P., 2015a, The beginning of the “Marmorization” process of the monumental buildings on the palatine hill in the Augustan Age: characterization of white marble objects from the temple of Apollo and the house of Augustus, *ASMOSIA XI International Conference*, Split, Croatia, 18-22 May 2015.

Brilli M., Giustini F., Conte A. M., Lapuente M., Quarta G., Plumed H. R., Scardozzi G., Belardi G., 2015b, Petrography, geochemistry, and cathodoluminescence of ancient white marble fromquarries in the southern Phrygia and northern Caria regions of Turkey: Considerations on provenance discrimination, *Journal of Archaeological Science: Reports*, 4, 124–142.

Bröcker M., 1990, Blueschist-to-greenschist transition in metabasites from Tinos island, Cyclade, Greece: compositional control or fluid infiltration, *Lithos,* 25, 25-39.

Bröcker M., Pidgeon R.T., 2007, Protolith ages of meta-igneous and metatuffaceous rocks from the Cycladic Blueschist Unit, Greece: results of a Reconnaissance U–Pb zircon study, *J. Geol.,* 115, 83-98.

Brunn J.H., Argyriadis I., Ricou L.E., Poisson A., Marcoux J., de Graciansky P.C., 1976, Eléments majeurs de liaison entre Taurides et Hellénides, *Bull. Soc. Géol. Fr.,* 18, pp. 481–497.

Bruno M., Cancelliere S., Conti L., Pensabene P., Lazzarini L., Pallante P., Turi B., 2002, Provenance and distribution of white marbles in temples and public buildings of Imperial

Rome, in *Interdisciplinary studies on ancient stone*, eds. J. J. Herrmann Jr, N. Herz, and R. Newman, 289–301, Archetype, London.

Bruno M., Attanasio D., Prochaska W., Yavuz A. B., 2015, An update on the use and distribution of white and black marbles from the 1st century AD to late antiquity, ASMOSIA X Conference, *Association for the study of Marble and other Stones in Antiquity*, Rome.

Bruschi G., Criscuolo A., Paribeni E., Zanchetta G., 2004, ^{14}C-dating from an old quarry waste dump of Carrara marble (Italy): evidence of pre-Roman exploitation, *Journal of Cultural Heritage*, 5, 3–6.

Buick I. S., 1991, The late alpine evolution of an extensional shear zone, Naxos, Greece, *J. Geol. Soc.,* 148, 93–103.

Buick I. S., Holland T. J. B., 1989, The P–T-t path associated with crustal extension, Naxos, Cyclades, Greece. In: J.S. Daly, Editor, *Evolution of metamorphic belts*, *Geol. Soc. Spec. Pub*, 43(1), pp. 365–369.

Burg J., Ivanov E., Ricou Z., Dimor L. E., Klain D., 1990, Implications of shear-sense criteria for the tectonic evolution of the Central Rhodope Massif, southern Bulgaria, *Geology*, 18, 451-454.

Candan O., Çetinkaplan M., Oberhansli R., Rimmele G., Akal C., 2005, Alpine high-P/low-T metamorphism of the Afyon Zone and implications for the metamorphic evolution of Western Anatolia, Turkey, *Lithos*, 84, 102-124.

Cantisani E., Fratini F., Malesani P., Molu G., 2005, Mineralogical and petrophysical characterization of white Apuan marble, *Per. Mineral.*, 74, 2, 117-140.

Cao S., Neubauer F., Bernroider M., Liu J., 2013, The lateral boundary of a metamorphic core complex: the Moutsounas shear zone on Naxos, Cyclades, Greece, *Journal of Structural Geology*, 54, 103-128.

Capedri S., Venturelli G., Photiades A., 2004, Accessory minerals and δ^{18}O and δ^{13}C of marbles from the Mediterranean area, *Journal of Cultural Heritage*, 5, 27–47.

Carmignani L., Giglia G., Kligfield R., 1978, Structural evolution of the Apuane Alps; an example of continental margin deformation in the northern Apennines, Italy, *Journal of Geology*, 86, 487-504.

Carmignani L., Giglia G., Kligfield R., 1980, *Nuovi* dati sulla zona di taglio ensialica delle Alpi Apuane, *Mem. Soc. Geol. It.*, 21, 93-100.

Carmignani L., Kligfield R., 1990, Crustal extension in the Northern Apennines: the transition from compression to extension in the Alpi Apuane core complex, *Tectonics*, 9, 1275-1303.

Casey M. S., Rutter E. H. Schmid, S. M. Siddans, A. W. B. Whalley J. S., 1978, Texture development in experimentally deformed calcite rocks, in: Gottstein, G., Luècke, K. (Eds.), *5th International Conference on Textures of Materials*, Springer Verlag, 231-240.

Chen F., Siebel W., Satir M., Terzioğlu N., Saka K., 2002, Geochronology of the Karadere basement (NW Turkey) and implications for the geological evolution of the İstanbul Zone, *International Journal Earth Sciences,* 91, 469-481.

Chilingar G.V., Bissel H.J. and Fairbridge R.W., 1967, *Carbonate rocks-origin, occurrenceand classification*, Amsterdam.

Coli M., Fazzuoli M., 1992, Considerazioni sulla litostratigrafia e sull'evoluzione sedimentaria delle formazioni retico-liassiche del nucleo metamorfico apuano, *Atti Ticinensi di Scienze della Terra*, 35, 43-60.

Columbu S., Antonelli F., Lezzerini M., Miriello D., Adembri B., Blanco A., 2014, Provenance of marbles used in the Heliocaminus Baths of Hadrian's Villa (Tivoli, Italy), *J Archaeol Sci*, 49, 332–342.

Cordischi D., Monna D., Segre A. L., 1983, ESR analysis of marble samples from Mediterranean quarries of archaeological interest, *Archaeometry,* 25(1), 68-76.

Corsi F., 1845, Delle Pietre antiche, 3a ed., Puccinelli, Roma.

Covey-Crump S. P., 1997, The high temperature static recovery and recrystallization behavior of cold-worked Carrara marble, *Journal of Structural Geology*, 19, 225-241.

Craig H., Craig V., 1972, Greek marble determination of provenance by isotopic analysis, *Science*, 176, 401-403.

De Bresser J.H.P., 1991, Intracristalline deformation of calcite, *Geologica ultraiectina*, 79, pp. 191.

Del Moro A., Puxeddu M., Radicati di Brozolo F., Villa I. M., 1982, Rb-Sr and K-Ar ages on minerals at temperatures of 300-400 °C from deep wells in the Larderello geothermal field (Italy), *Contrib. Mineral. Petrol.*, 81, 340-349.

Dean W. T., Monod O., Rickards R. B., Demir O., Bultynck P., 2000, Lower Paleozoic stratigraphy and palaeontology, Karadere-Zira area, Pontus Mountains, northern Turkey, *Geological Magazine*, 137, 555-582.

Delaloye M., Bingöl E., 2000, Granitoids from western and northwestern Anatolia: Geochemistry and modelling of geodynamic evolution, *International Geology Review,* 42, 241-268.

Dermitzakis M., Papanikolaou D., 1980, The molasse of Paros Island, Aegean Sea, *Annalen des Naturhistorischen Museums Wien*, 83, 59–71.

Dewey J. F., Sengör, A. M. C., 1979, Aegean and surrounding regions: Complex multiplate and continuum tectonics in a convergent zone, *Geol. Soc. Am. Bull.*, 90, 84-92.

Di Pisa A., Franceschelli M., Leoni L., Meccheri M., 1985, Regional variation of the metamorphic temperatures across the Tuscanid 1 Unit and its implications on the alpine metamorphism (Apuan Alps, N-Tuscany), *Neues Jahrbuch fue' Mineralogie, Abhandlungen*, 151, 197-211.

Dinter D.A., Royden L., 1993, Late Cenozoic extension in northeastern Greece: Strymon Valley detachment system and Rhodope metamorphic core complex, *Geology*, 21, 45-48.

Dinter D. A., Macfarlane A., Hames W., Isachsen C., Bowring S., Royden L., 1995, U-Pb and $^{40}Ar/^{39}Ar$ geochronology of the Symvolon granodiorite: Implications for the thermal and structural evolution of the Rhodope metamorphic core complex, northeastern Greece, *Tectonics*, 14, 886-908.

Dinter D. A., 1998, Late Cenozoic extension of the Alpine collisional orogen, northeastern Greece: Origin of the north Aegean basin, *Geological Society of America Bulletin*, 110 (9), 1208-1230.

Dolci E., 1985, I marmi lunensi: tradizione, produzione, applicazioni, *Centro Studi Lunensi Quaderni*, 11, 405–463.

Doust H., Arıkan Y., 1974, The geology of the Thrace Basin, in: Okay, H., Dilekoz, E. (Eds.), The Association of Turkish Petroleum Geologists Bulletin, *Second Petroleum Congress of Turkey*, 119–136.

Doutsos T., Pe-Piper G., Boronkay K., Koukouvelas I., 1993, Kinematics of the central Hellenides, *Tectonics,* 12, 936–953.

Duchêne S., Aïssa R., Vanderhaeghe O., 2006, Pressure–temperature-time evolution of metamorphic rocks from Naxos (Cyclades, Greece): constraints from Thermobarometry and Rb/Sr dating, *Geodyn. Acta,* 19, 299–319.

Dürr St., 1986, Geologie von Griechenland, Ed. Jacobshagen, Gebrüder Borntraeger, 24, 116-149.

Ebert A., Gnos E., Ramseyer K., Spandler C., Fleitmann D., Bitzios D., Decrouez D., 2010, Provenance of marbles from Naxos based on microstructural and geochemical characterization, *Archaeometry* 52, 2, 209–228.

Elmas A., 1996a, The Late Oligocene nappe emplacement in the Southeast Anatolian orogenic belt, *Turkish Journal of Earth Sciences*, 5, 89-98.

Elmas A., 1996b, Geological evolution of northeastern Anatolia, *International Geology Review*, 38, 884-900.

Elmas A., Yigtbas E., 2001, Ophiolite emplacement by strike-slip tectonics between the Pontide Zone and the Sakarya Zone in northwestern Anatolia, Turkey, *International Journal of Earth Sciences*, 90, 257- 269.

Engel M., Reischmann T., 1998, Single zircon geochronology of orthogneisses from Paros, Greece, *Bulletin of the Geological Society of Greece*, 32, 91–99.

Erdogan B., 1990, Stratigraphic features and tectonic evolution of the Izmir-Ankara Zone in the region between Izmir and Seferihisar, *Turkish Association of Petroleum Geologists Bulletin*, 2, 1-20.

Erentoz C., Pamir H. N., 1964, 1/2,000,000 Geological Map of Turkey, Maden Tetkik ve Arama Enstitu su, Ankara.

Ergun M., Ozel E., 1995, Structural relationship between the Sea of Marmara Basin and the North Anatolian Fault Zone, *TerraNova*, 7, 278–288.

Ersoy M., 2013, The role of occupational safety measures on reducing accidents in marble quarries of Iscehisar region, *Safety Science*, 57, 293–302.

Evelpidou N., 2002, GIS Database for the Geomorphological Study of Paros Island, *Cartography*, 31, 1, 45-53.

Fant J. C., 1984, Seven unedited quarry inscriptions from Docimium (İscehisar, Turkey), in *Zeitschrift für Papyrologie und Epigraphik*, 54, 171-182.

Fant, J. C., 1987, Three seasons of epigraphical survey at the Roman imperial quarries at Docimium (Iscehisar), 1983-1985.

Faure M., Bonneau M. Pons J., 1991, Ductile deformation and syntectonic granite emplacement during the late Miocene extension of the Aegean (Greece), *Bull. Soc.Géol. France* 162, pp. 3–12.

Forster M. A., Lister G. S., 2005, Several distinct tectono-metamorphic slices in the Cycladic eclogite–blueschist belt, Greece, *Contributions to Mineralogy and Petrology*, 150(5), 523-545.

Foster M. A., Lister G. S., 2009, Core-complex-related extension of the Aegean lithosphere initiated at the Eocene–Oligocene transition, *Journal of Geophysical Research: Solid Earth*, Vol. 114.

Franceschelli M., Leoni, L., Memmi M., Puxeddu M., 1986, Regional distribution of Al-silicates and metamorphic zonation in the low-grade Verrucano metasediments from the Northern Apennines, Italy, *Journal of Metamorphic Geology*, 4, 309-321.

Franceschelli M., Memmi I., Carcangiu G., Gianelli G., 1997, Prograde and retrograde chloritoid zoning in low temperature metamorphism, Alpi Apuane, Italy, *Schweizerische Mineralogische und Petrographische Mitteilungen*, 77, 41-50.

Fredrich J.T., Evans B., Wong T.F., 1989, Micromechanics of the brittle to plastic transition in Carrara marble, *Journal of Geophysical Research*, 94, 4129-4145.

Fryer B. J., Jackson S. E., Longerich H. P., 1995, The design, Operation and Role of the Laser.Ablation Microprobe Coupled with an Inductively Coupled Plasma.Mass Spectrometer (LAM-ICP-MS) in the Earth Sciences, *The Canadian Mineralogist*, Vol. 33, pp. 303-312.

Gautier P., Brun J. P., Jolivet L., 1993, Structure and kinematics of upper Cenozoic extensional detachment on Naxos and Paros (Cyclades Islands, Greece), *Tectonics,* 12, 1180–1194.

Gautier P., Brun J. P., 1994a, Crustal-scale geometry and kinematics of late-orogenic extension in the central Aegean (Cyclades and Evvia island), *Tectonophysics*, 238, 399-424.

Gautier P., Brun J. P., 1994b, Ductile crust exhumation and extensional detachments in the central Aegean (Cyclades and Evvia islands), *Geodin. Acta,* 7, 57–85.

Gautier P., Brun J. P., Moriceau R., Sokoutis D., Martinod J., Jolivet L., 1999, Timing, kinematics and cause of Aegean extension: a scenario based on a comparison with simple analogue experiments, *Tectonophysics*, 315(1–4), 31–72.

Genç S. C., Yilmaz Y., 1995, Evolution of the Triassic continental margin, northwest Anatolia, *Tectonophysics*, 243, 193-207.

Genova N., Meloni S., Oddone M., Mello E., 1986, Provenance studies of archaeological marbles by neutron activation analysis and data reduction, in Papers accepted for presentation at the *7th internat+ional conference MTAA*.

Germann K., Gruben G., Knoll H., Valis V., Winkler F. J., 1988, Provenance characteristics of Cycladic (Paros and Naxos) Marbles. A multivariate geological approach, In *Classical Marble: Geochemistry, Technology, Trade*, N. Herz, M. Waelkens (eds.), 153, 251-262.

Giacchero M., 1974, Edictum Diocletiani et collegarum de pretiis rerum venalium, ed. Giacchero, Genova.

Giglia G., Radicati di Brozolo F., 1970, K/Ar age of metamorphism in the Apuane Alps (Northern Tuscany), Bollettino della Società Geologica Italiana, 89, 485-497.

Gnoli R., 1988, Marmora romana, ed. *Edizioni dell'Elefante*, Roma, 261-262.

Goette H. R., Polykreti K., Vacoulis T., Maniatis Y., 1995, Investigation of the greyish-blue marble of Pentelikon and Hymettus, in *Archéomatériaux: marbres et autres roches*, ed. Schvoerer, 83-90.

Göncüoglu M. C., Dirik K., Kozlu H., 1996-1997, Pre-Alpine and Alpine terranes in Turkey: Explanatory notes to the terrane map of Turkey, *Annales Géologiques des Pays Helléniques*, 37, 515-536.

Göncüoglu M. C., Turhan N., Sentürk K., Özcan A., Uysal S., Yaliniz M. K., 2000, A geotraverse across northwestern Turkey: Tectonic units of the Central Sakarya region and their tectonic evolution, in Bozkurt E., Winchester J. A., Piper J. D. A., eds. *Tectonics and magmatism in Turkey and the surrounding area: Geological Society of London*, Special Publication, 173, 139-161.

Gorgoni C., Kokkinakis I., Lazzarini L., Mariottini M., 1992, Geochemical and petrographic characterization of «rosso antico»and other white-grey marbles of Mani (Greece). In: *ASMOSIA 2, Ancient Stones: quarrying, trade and provenance, Acta Archaeologica Lovaniensia*, Mon. 2, M. Waelkens, N. Herz, L. Moens (eds.), Leuven, 155-165.

Gorgoni C., Lazzarini L., Pallante P., Turi B., 2002, An updated and detailed mineropetrographic and C-O stable isotopic reference database for the main Mediterranean marbles used in antiquity. In: J. Herrmann, N. Herz & R. Newman (eds.): *ASMOSIA 5, Interdisciplinary Studies on Ancient Stone – Proceedings of the Fifth International Conference of the Association for the Study of Marble and Other Stones in Antiquity, Museum of Fine Arts, Boston, June 1998,* Archetype Publications, London, 110-131.

Görür N., Monod O., Okay, A. I., Sengör A. M. C., Tüysüz O., Yigtba E., Sakinç M., Akkök R., 1997, Palaeogeographic and tectonic position of the Carboniferous rocks of the western Pontides (Turkey) in the frame of the Variscan belt, *Bulletin de la Societé Géologique de France*, 168, 197-205.

Grasemann B., Petrakakis K., 2007, Evolution of the Serifos Metamorphic Core Complex. In: G. Lister and M. Foster (Editors), Inside the Aegean Core Complexes, *Journal of the Virtual Explorer*, Electronic Edition.

Green W.A., Young S.M.M., Van Der Merve N.J., Herrmann J.J., 2002, Source tracing of marble: trace element analysis with inductively coupled plasma-mass spectrometry, in *ASMOSIA 5, Interdisciplinary Studies on Ancient Stone*, J.J. Herrmann, N. Herz, R. Newton (eds.), London, 132-142.

Günther D, Hattendorf B., 2005, Solid sample analysis using laser ablation inductively coupled plasma mass spectrometry. *Trends in Analytical Chemistry*, Vol. 24, 3, 255-265.

Guillong M., Horn I., Günther D., 2003, Comparison of the ablation behavior of 266 nm Nd5YAG and 193 nm ArF excimer lasers for LA-ICP-MS analysis, *J. Anal. At. Spectrom.*, 18, 1224–1230.

Hagdorn H., Göncüoglu M.C., 2007, Early-Middle Triassic echinoderm remains from the Istranca Massif, Turkey, *N. Jb. Geol. Paläont. Abh.*, 246, 235-245.

Hannappel A., Reischmann T., 2005, Rhyolitic dykes of Paros Island, Cyclades, in: Fytikas M., Vougioukalakis G.E. (Eds.), *The South Aegean Active Arc: Present Knowledge and Future Perspectives*, Elsevier, Amsterdam, 305–328.

Harre W., Kockel F., Kreuzer H., Lenz H., Miiller E., Walther H.W., 1968, Ober Rejuvenationen im Serbo-Mazedonischen Massif (Deutung radiometrischer Altersbestimmungen), *Geol. Palaeontol.*, 2, 193-194.

Harris N.B.W., Kelley S.P., OkayA.I., 1994, Post-collision magmatism and tectonics in northwest Turkey, *Contribution to Mineralogy and Petrology*, 117, 241-252.

Helvaci C., 1995, Stratigraphy, mineralogy and genesis of the Bigadiç Borate deposits, western Turkey, *Economic Geology*, 90, 1237-1260.

Hejl E., Riedl H., Soulakellis N., Van Den Haute P., Weingartner H., 2003, Young Neogene tectonics and relief development on the Aegean islands of Naxos, Paros and Ios (Cyclades, Greece), *Mitteilungen. Österreichische Geologische Gesellschaft*, 93, 105–127.

Henjes-Kunst F., Altherr R., Kreuzer H., Hansen B.T., 1988, Disturbed U–Th–Pb systematics of young zircons and uranothorites: the case of the Miocene Aegean granitoids (Greece), *Chem. Geol.* 73, 125–145.

Herz N., 1955, Petrofabrics and classical archaeology, *American Journal of Science,* 253, 299-305.

Herz N., 1987b, Classical marble quarries of Thasos, in *Antike edel-und Buntmetallgewinnung auf Thasos*, Bochum, pp. 232-240.

Herz N., 1988a, The oxygen and carbon isotopic database for classical marble*,* in *Classical marble: geochemistry, technology, trade*, N. Herz, M. Waelkens (eds.), Dordrecht, 305-314.

Herz N., 1988b, Classical marble quarries of Thasos, in Wagner G.A, Weisgerber G., *Antike Edel- und Bunt-metallgewinning auf Thasos*, Deutsches Bergbau-Museum, Bochum.

Herz N., 2000, The Classical Marble Quarries of Paros: Paros-1, Paros-2, and Paros-3, in *Paria Lithos: Parian Quarries, Marble, and Workshops of Sculpture*, ed. Schilardi D., Katsarou S., Katsonopoulou D., Mckinney Brenner C., Archaeological and Historical Studies, Athens, 27-34.

Herz N., Pritchett W., 1953, Marble in Attic Epigraphy, *American Journal of Archaeology*, 57 (2), 71-83.

Herz N., Dean N. E., 1986, Stable isotopes and archaeological geology: the Carrara marble, northern Italy*, Applied Geochemistry*, 1, 139-151.

Herz N., Garrison E. G., 1998, Geological methods for archaeology, *Oxford University Press*, Oxford.

Higgins M. D., Higgins R., 1996, A Geological Companion to Greece and the Aegean, *Duckworth Publishers*, London.

Huet B., Labrousse L., Jolivet L., 2009, Thrust or detachment? Exhumation processes in the Aegean: insight from a field study on Ios (Cyclades, Greece), *Tectonics*, Vol. 28 (3).

Iglseder C., Grasemann B., Schneider D. A., Petrakakis K., Miller C., Klötzli U. S., Thöni M., Zámolyi A., Rambouseka C., 2009, I and S-type plutonism on Serifos (Cyclades, Greece), *Tectonophysics*, 473, 69–83.

IşikV., Tekeli O., Seyitoğlu G., 2004, The $^{40}Ar/^{39}Ar$ age of extensional ductile deformation and granitoid intrusion in the northern Menderes core complex: implications for the initiation of extensional tectonics in western Turkey, *Journal of Asian Earth Sciences*, 23, 555-566.

Jacobshagen V., Dürr S., Kockel F., Kopp K. O., Kowalczyk G., Berckhemer H., Büttner D., 1978, Structure and geodynamic evolution of the Aegean region. In: H. Cloos, D. Roeder and K. Schmidt, Editors, *Alps, Apennines, Hellenides*, IUGG, Stuttgart, 537–564.

Jackson J. A., McKenzie D., 1984, Active tectonics of the Alpine–Himalayan belt between western Turkey and Pakistan, *Geophys. J. R. Astron. Soc.,* 77, 185–264.

Jansen J. B. H., 1973, Geological map of Naxos (1/50 000), *Nation. Inst. Geol. Mining Res.*, Athens.

Jansen J. B. H., 1977, The geology of Naxos, *Geology and Geophysical Research Athens, Greece, 19*, 1-100.

Jansen J. B. H., Schuiling R. D., 1976, Metamorphism on Naxos; petrology and geothermal gradients, *American Journal of Science*, 276 (10), 1225–1253.

Jeffries T. E., Jackson S. E., Longerich H. P., 1998, Application of a frequency quintupled Nd5YAG source (λ=213 nm) for laser ablation inductively coupled plasma mass spectrometric analysis of Minerals. *Journal of Analytical Atomic Spectrometry*, Vol. 13, 935–940.

Jolivet L., Brun J. P., Gautier P., Lallemant S., Patriat M., 1994, 3-D kinematics of extension in the Aegean from the Early Miocene to the present, insight from the ductile crust, *Bull. Soc. Géol. Fr.,* 165, 195–209.

Jolivet L., Patriat M., 1999, Ductile extension and the formation of the Aegean Sea, in: B. Durand, L. Jolivet, F. Horvàth and M. Séranne, Editors, *The Mediterranean Basins: Tertiary Extension within the Alpine Orogen. Geological Society Special Publication*, Geological Society, London, 427–456.

Jolivet L., Faccenna C., 2000, Mediterranean extension and the Africa–Eurasia collision, *Tectonics*, 19, 1095–1106.

Jolivet L., Rimmelé G., Oberhänsli R., Goffé B., Candan O., 2004a, Correlation of syn-orogenic tectonic and metamorphic events in the Cyclades, the Lycian Nappes and the Menderes massif, geodynamic implications, *Bull. Soc. Geol. Fr.*, 175, 217–238.

Jolivet L., Famin V., Mehl C., Parra T., Aubourg C., Hébert R., Philippot P., 2004b, Progressive strain localisation, boudinage and extensional metamorphic complexes, the

Aegean Sea case, in: D.L. Whitney, C. Teyssier and C.S. Siddoway, Editors, *Gneiss Domes in Orogeny*, *Geological Society of America Special Paper,* 380, 185–210.

Jolivet L., Lecomte E., Huet B., Denèle Y., Lacombe O., 2010, The North Cycladic Detachment System, *Earth and Planetary Science Letters*, Elsevier, 289, 87-104.

Jolivet L., Brun J. P., 2010, Cenozoic geodynamic evolution of the Aegean region, *Int. J. Earth Sci (Geol Rundsch)*, 99 (1), 109–138.

Jones C. E., Tarney J., Barreiro B., 1994, The make-up and melting of a subduction-accretion complex: generation of S and I-type granitoids, *8th Int. Conf. Geochronology, Cosmochronology and Isotope Geology*, U.S.G.S. Circular, 1107.

Kaliampakos D. C., Mavrikos A. A., 2006, Introducing a new aspect in marble quarry rehabilitation in *Greece, Environ Geol.*, 50, 353–359

Karagianni E. E., Papazachos C. B., Panagiotopoulos D. G., Suhadolc P., Vuan A., Panza G. F., 2005, Shear velocity structure in the Aegean area obtained by inversion of Rayleigh waves, *Geophys. J. Int.,* 160, 127–143.

Katsikatsos G., 1977, La structure tectonique d'Attique et de l'île d'Eubée, *Proceedings of the 6th Colloquium of the Geology of the Aegean Region.*, Vol. 1.

Katsikatsos G., Migiros G., Triantaphyllis M., Mettos A., 1986, Geological structure of the Internal Hellenides (E. Thessaly S.W. Macedonia, Euboea -Attica - Northern Cycylades Islands and Lesvos), *Geology and Geophysical Research*, special issue, 191-212.

Keay S., Lister G., Buick, I., 2001, The timing of partial melting, Barrovian metamorphism and granite intrusion in the Naxos metamorphic core complex, Cyclades, Aegean Sea, Greece, *Tectonophysics*, 342, 275–312.

Keiter M., Piepjohn K., Ballhaus C., Lagos M. Bode M., 2004, Structural development of high-pressure metamorphic rocks on Syros island (Cyclades, Greece), *J. Struct. Geol.,* 26, 1433–1445.

Ketin I., 1966, Tectonic units of Anatolia, *Maden Tetkik ve Arama Bulletin*, 66, 23-34.

Kilias A., Falalakis G., & Mountrakis D., 1999, Cretaceous–Tertiary structures and kinematics of the Serbomacedonian metamorphic rocks and their relation to the exhumation of the Hellenic hinterland (Macedonia, Greece), *International Journal of Earth Sciences,* 88 (3), 513-531.

Klapisch-Zuber C., 1973, Carrara e i maestri del marmo, *Poligrafico Artioli*, Modena.

Kligfield R., Hunziker J., Dallmeyer R.D., Schamel S., 1986, Dating of deformation phases using K-Ar and $^{40}Ar/^{39}Ar$ techniques; results from the Northern Apennines, *Journal of Structural Geology*, 8, 781-798.

Köber L., 1929, Beiträgezur Geologie von Attika, *Akad. Wiss. Mat. –Nat*, 138, 299-327.

Kolocotroni C., Dixon J. E., 1991, The origin and emplacement of the Vrondou granite, Serres, NE Greece, *Geol. Soc. Greece Bull.*, 25, 469-483.

Korres M., 1990, The geologic factor in ancient Greek architecture, Marinos, *Engineering Geology of Ancient Works, Monuments and Historical Sites: Preservation and Protection*, 4, 1779-1793.

Korres M., 1995, From Pentelicon to the Parthenon: the ancient quarries and the story of a half-worked column capital of the first marble Parthenon, *Melissa Publishing House*.

Kozur H. W., Aydin M., Demir O., Yakar H., Göncüoglu M. C, Kuru F., 2000, New stratigraphic and palaeogeographic results from the Paleozoic and Early Mesozoic of the Middle Pontides (Northern Turkey) in the Azdavay, Devrakani, Küre, and Inebolu areas: Implications for the Carboniferous-Early Cretaceous geodynamic evolution and some related remarks to the Karakaya oceanic rift basin, *Geologica Croatica*, 53, 209-268.

Kozel T., 1988, Les carrières des époques grecque, romaine et byzantine: techniques et organisation, in *Ancient Marble Quarrying and Trade*, ed. J.C. Fant, BAR International Series 453, London.

Kruckenberg S. C., Vanderhaeghe O., Ferré E.C., Teyssier C., Whitney D.L., 2011, Flow of partially molten crust and the internal dynamics of a migmatite dome, Naxos, Greece, *Tectonics*, 30.

Kuhlemann J., Frisch W., Dunkl I., Kázmér M., Schmiedl G., 2004, Miocene siliciclastic deposits of Naxos Island: geodynamic and environmental implications for the evolution of the southern Aegean Sea (Greece), in Bernet, M., Spiegel, C., Detrital Thermochronology — Provenance Analysis, Exhumation, and Landscape Evolution of Mountain Belts, *Geological Society of America Special Paper*, 378, 51–65.

Lapuente M. P., Turi B., Blanc P., 2000, Marbles from Roman Hispania: stable isotope and cathodoluminescence characterization, *Applied Geochemistry,* 15, 1469-1493.

Lapuente P., Leòn P., Nogales T., Royo H., Preite Martinez M., Blanc Ph., 2012, White sculptural materials from Villa Adriana: study of provenance, in Interdisciplinary studies on ancient stone: *proceedings of the IX ASMOSIA Conference* (eds. A. Gutiérrez Garcia, P. Lapuente and I. Rodà), Institut Català d'Arqueologia Clàssica, Tarragona, 364–75.

Lazzarini L., 2004, Archaeometric aspects of white and coloured marbles used in antiquity: the state of the art, *Per. Mineral.*, 73, 113-125.

Lazzarini L., Moschini G., Stievano B. M., 1980a, A contribution to the identification of Italian, Greek and Anatolian marbles through a petrological study and the evaluation of Ca/Sr ratio, *Archaeometry,* 22, 173-182.

Lazzarini L., Moschini G., Stievano B. M., 1980b, Alcuni esempi di identificazione di marmi antichi mediante uno studio petrografico e la determinazione del rapporto Ca/Sr, *Quaderni della Soprintendenza ai beni Artistici e Storici di Venezia*, 9, 34-58.

Lazzarini L., Ponti G., Preite Martinez M., Rockwell P., Turi B., 2002, Historical, technical, petrographic and isotopic features of Aphrodisian marble, in *ASMOSIA 5: Interdisciplinary Studies on Ancient Stone,* J.J. Herrmann, N. Herz, R. Newton (eds.), London, 163-168.

Lazzarini L., Antonelli F., 2003, Petrographic and isotopic characterization of the marble of the island of Tinos (Greece), *Archaeometry*, 45 (4), 541-552.

Le Pichon X., Angelier J., 1979, The Hellenic arc and trench system: a key to the neotectonic evolution of the eastern Mediterranean area, *Tectonophysics,* 60, 1–42.

Le Pichon X., Angelier J., 1981, Aegean Sea, *Philos. Trans.R. Soc. Lond.,* 300, 357–372.

Lee J., Lister G. S., 1992, Late Miocene ductile extension and detachment faulting, Mykonos, Greece, *Geology,* 20, 121–124.

Leleu M., Neumann M., 1969, L'âge des formations d'Attique: du paléoziqueau mésozoique, *C. R. Acad. Sciences*, 268, 1361-1363.

Lepsius R., 1890, *Griechische marmorstudien,* Berlin.

Lepsius G.R, 1893, *Geologie von Attika*, Berlin.

Liati A., Kreuzer H., 1990, K-Ar dating of metamorphic and magmatic rocks from the Xanthi and Drama areas, Greek part of the Rhodope zone, *Ber. Dtsch. Mineral. Ges. Beih*., 1 2, 161.

Liati A., Mposkos E., 1990, Evolution of the eclogites in the Rhodope Zone of northern Greece, *Lithos*, 25, 89-99.

Lisans Y., 2002, *Marmara adasi antik Mermer ocaklari*, Master Thesis, Istanbul Teknik Universitesi.

Lister G. S., Banga G., Feenstra A., 1984, Metamorphic core complexes of Cordilleran type in the Cyclades, Aegean Sea, Greece, *Geology*, 12, 221-225.

Lister G. S., Baldwin S. L., 1993, Plutonism and the origin of metamorphic core complexes, *Geology*, 21, 607-610.

Lister G. S., Forster M. A., 1996, Inside the Aegean core complexes, Australian Crustal Research Centre, *Technical Publ.,* 45, pp. 101.

Lloyd R. V., Smith P. W., Haskell H. W., 1988, Evaluation of the manganese ESR method of marble characterization, *Archaeometry*, 27 (1), 108-116.

Maltezou F., Brooks M., 1989, A geophysical investigation of post-Alpine granites and Tertiary sedimentary basins in northern Greece, *Journal of the Geological Society,* 146(1), 53-59.

Manfra L., Masi U., Turi B., 1975, Carbon and oxygen isotope ratios of marbles from some ancient quarries of Western Anatolia and their archaeological significance*, Archaeometry,* 17*,* 215-221*.*

Maniatis Y., Mandi V., Nikolau A., 1988, Provenance investigation of marbles from Delphi with ESR spectroscopy, in N. Herz & M. Waelkens, *Classical marble: geochemistry, technology, trade. Kluwer Publications, Dordrecht*, 443-452.

Maniatis Y., Polikreti K., 1998, Provenance of white marble with EPR spectroscopy: further developments, in *Proc. of the V ASMOSIA Conference,* Boston, June 1998.

Maniatis, Y. Polikreti, K., 2000, The characterization and discrimination of Parian marbles in the Aegean region, in *Paria lithos* (eds. D. U. Schilardi and D. Katsonopoulou), 575–84, The Paros and Cycladic Institute of Archaeology, Athens.

Mannoni T., 1990, Analisi petrografica dei marmi etruschi di Pietrasanta, *Etruscorum ante quam Ligurum*, 168–187.

Marc J.Y., 1995, Who owned the marble quarries of Thasos during the Imperial period, in *The study of marble and other stones used in the antiquity*, eds. Maniatis Y., Herz N., Basiakos Y., Archetype Publ., London, 33-37.

Marinos G., Petrascheck W. E., 1956, *Laurium. Geol. geoshys. Research*, 4, 1-247.

Marinos G., 1973, The Athens schist formation II: Stratigraphy and structure, Annales Géologiques des Pays Helléniques, 25, 439-444.

Martin L., Duchêne S., Deloule E., Vanderhaeghe O., 2006, The isotopic composition of zircon and garnet: a record of the metamorphic history of Naxos, Greece, *Lithos,* 87, 174–192.

Martin L. A. J., Duchêne S., Deloule E., Vanderhaeghe O., 2008, Mobility of trace elements and oxygen in zircon during metamorphism: consequences for geochemical tracing, *Earth and Planetary Science Letters*, 267, 161-174.

Matthews K. J., Leese M. N., Hughes M. J., Herz N., Bowman S. G. E., 1995, Establishing the provenance of marble using statistical combinations of stable isotope and neutron activation data, in Y. Maniatis, N. Herz & Y. Basiakos (eds.), *The study of marble and other stones used in the antiquity*, Archetype Publisher, London, 181-186.

Matthews K. J., 1997, The establishment of a data base of neutron activation analyses of white marble*, Archaeometry*, 39, 321-332.

Mehl C., Jolivet L., Lacombe O., Labrousse L., Rimmelé G., 2007, Structural evolution of Andros island (Cyclades, Greece): a key to the behavior of a flat detachment within an extending continental crust, in T. Taymaz, Y. Dilek and Y. Ylmaz, Editors, *The Geodynamics of the Aegean and Anatolia, Special Publications*, Geological Society, London, 291 (1), 41-73.

Mello E., 1983, Studio della provenienza di marmi bianchi mediante analisi degli elementi in tracce e uso della, in Marmo restauro, Situazione e prospettive, Atti del convegno, carrara 31 maggio 1983, *Internazionale marmi e machine,* 150-162).

Mello E., Donna D., Oddone M., 1988, Discriminating sources of Mediterranean marbles: A pattern recognition approach, *Archaeometry*, 30 (1), 102-108.

Meloni S., Oddone M., Zezza U., 1995, Rare-earth element patterns of white marbles from ancient quarries in Carrara (Italy), in: *The study of marble and other stones used in antiquity*, Y. Maniatis, N. Herz, Y. Basiakos (eds), London, 181-186.

Miller C., Zanetti A., Thöni M., Konzett J., Klötzli U., 2012, Mafic and silica-rich glasses in mantle xenoliths from Wau-en-Namus, Libya: Textural and geochemical evidence for peridotite–melt reactions, *Lithos,* 128, 11-26.

Moens L, Roos P, De Rudder J, De Paepe P, Van Hende J, Marechal R, Waelkens M., 1988, A multi-method approach to the identification of white marbles used in antique artifacts. In: Herz N, Waelkens M (eds) Classical marble: geochemistry, technology, trade. Kluwer Academic Publishers, Dordrecht, 243–250.

Moens L., Roos P., De Paepe P., Lunsingh Scheurleer R., 1992, Provenance determination of white marble sculptures from the Allard Pierson Museum in Amsterdam, based on chemical, microscopic and isotopic criterias, in: M. Waelkens, N. Herz & L. Moens (eds.) *Ancient stones: quarrying, trade and provenance: interdisciplinary studies on stones and stone technology in Europe and Near East from the prehistoric to the early Christian period*, Leuven University Press, Leuven, 269-276.

Molli G., Heilbronner Panozzo R., Wittensoldener V., 1997, Microstructural features of naturally deformed Alpi Apuane marbles: an introduction, *Conference on deformation mechanism in nature and experiment*, Basel, 17-19 March, 45-46.

Molli G., Giorgetti G., 1999, Meso, microstructural and petrological contraints on the tectono-metamorphic evolution of the Alpi Apuane Complex (NW Tuscany, Italy), Exhumation of metamorphic terranes, *Bollettino della Società geologica italiana*, 121 (1) 789-800.

Molli G., Heilbronner P. R., 1999, Microstructures associated with static and dynamic recrystallization of Carrara marble (Alpi Apuane, NW Tuscany Italy), *Geologie en Mijnbouw*, 78, 119-126.

Molli G., Conti P., Giorgetti G., Meccheri M., Oesterling N., 2000, Microfabric study on the deformational and thermal history of the Alpi Apuane marbles (Carrara marbles), Italy, *Journal of Structural Geology*, 22, 1809-1825.

Monna D., Pensabene P., 1977, Marmi dell'Asia Minore, *Consiglio Nazionale delle Ricerche*, Roma.

Monna D., Pensabene P., Sodini J. P., 1993, L'identification des marbres: sa nécessité, ses méthodes, ses limites, in *Marmi Antichi: problemi d'impiego, di restauro e d'identificazione*, ed. Pensabene P., L'Erma di Bretschneider, Roma, Studi Miscellanei, 26, 15-34.

Moore W.J., Mckee E. H., Akinci Ö., 1980, Chemistry and chronology of plutonic rocks in the Pontid Mountains, northern Turkey, *European Copper Deposits*, 1, 209-216.

Monod O., Kozlu H., Ghienne J. F., Dean W. T., Günay Y., Herisse A. L., Paris F., Robardet, M., 2003, Late Ordovician glaciation in southern Turkey, *Terra Nova*, 15, 249-257.

Mposkos E., Wawrzenitz N., 1995, Metapegmatites and pegmatites bracketing the time of HP-metamorphism in polymetamorphic rocks of the E-Rhodope, N-Greece, 15th Congr. Carpatho-Balcan Geological Association, Sept. 95, Athens, *Geol. Soc. Greece*, Spec. Publ. 4, 602-608.

Negris P., 1912, Sur l'âges des schistes d'Athènes, *C. R. Acad. Sciences*, 154, 1838-1840.

Negris P., 1915, Roches cristallophylliennes et tectonique de la Grèce, Athenes.

Oddone M., Meloni S., Mello E., 1985, Provenance studies of the white marble of the cathedral of Como by neutron activation analysis and data reduction, *Journal of radioanalytical and nuclear chemistry*, 90 (2), 373-381.

Oesterling N, Heilbronner R., Stünitz H., Barnhoorn A, Molli G., 2007, Strain dependent variation of microstructure and texture in naturally deformed Carrara marble, *Journal of Structural Geology*, 29, 681-696.

Okay A. I., 1984, Distribution and characteristics of the northwest Turkish blueschists, in J.E. Dixon & A.H.F. Robertson, eds. *The Geological Evolution of the Eastern Mediterranean. Geol. Soc. London*, Spec. Publ., 17, 455-466.

Okay A. I., 1989a, Tectonic units and sutures in the Pontides, northern Turkey, in Sengör A. M. C., ed. Tectonic *evolution of the Tethyan region: Dordrecht*, Netherlands, Kluwer Academic Publishing, 109-116.

Okay A. I., Satir M., Maluski H., Siyako M., Monie P., Metzger R., Akyüz S.,1996, Paleo- and Neo-Tethyan events in northwest Turkey: Geological and geochronological constraints, in A. Yin & M. Harrison eds., *Tectonics of Asia*, Cambridge University Press, 420-441.

Okay A. I., Monié P., 1997, Early Mesozoic subduction in the Eastern Mediterranean: Evidence from Triassic eclogite in northwest Turkey, *Geology*, 25, 595-598.

Okay A. I., Sahintürk Ö., 1997, Geology of the Eastern Pontides, in Robinson, A., ed. Regional and petroleum geology of the Black Sea and surrounding region, *American Association of Petroleum Geologists Memoir*, 68, 291-311.

Okay A. I., Tüysüz, O., 1999, Tethyan sutures of northern Turkey, *in* Durand B., Jolivet, L., Horváth D., Séranne M., eds. The Mediterranean basins: Tertiary extension within the Alpine Orogen, *Geological Society of London*, Special Publication, 156, 475-515.

Okay A.I., 2000, Was the Late Triassic orogeny in Turkey caused by the collision of an oceanic plateau?, in Bozkurt E., Winchester J.A., J.A.D. Piper, eds. *Tectonics and Magmatism in Turkey and Surrounding Area. Geological Society*, London, Special Publication, 173, 25-41.

Okay A. I., Kaslilar-Ozcan A., Imren C., Boztepe-Guney A., Demirbag E., Kuscu I., 2000, Active faults and evolving strike-slip basins in the Marmara Sea, northwest Turkey: a multichannel seismic reflection study, *Tectonophysics*, 32, 189– 218.

Okay A. I., Satir M., 2000, Coeval plutonism and metamorphism in a latest Oligocene metamorphic core complex in northwest Turkey, *Geological Magazine*, 137, 495-516.

Okay A. I., Tansel I., Tuysiiz 0., 2001, Obduction, subduction and collision as reflected in the Upper Cretaceous- Lower Eocene sedimentary record of western Turkey, *Geological Magazine*, 138, 117-142.

Okay A. I., Monod O., Monié P., 2002, Triassic blueschists and eclogites from northwest Turkey: vestiges of the Paleo-Tethyan subduction, *Lithos*, 64, 155-178.

Okay A. I., Tüysüz O., Satir M., Özkan-altiner S., Altiner D., Sherlock S., & Eren R. H., 2006, Cretaceous and Triassic subduction-accretion, HP/LT metamorphism and continental growth in the Central Pontides, Turkey, *Geological Society of America Bulletin*, 118, 1247-1269.

Okay A. I., 2008, Geology of Turkey: A Synopsis, *Anschnitt*, 21, 19-42.

Okay A. I., Bozkurt E., Satir M., Yiğitbaş E., Crowley Q.G., Shang C.K., 2008, Defining the southern margin of Avalonia in the Pontides: geochronological data from the Late Proterozoic and Ordovician granitoids from NW Turkey, *Tectonophysics*, 461(1), 252-264.

Özcan A., Göncüoglu M. C, Turan N., Uysal S., Sentürk K., Isik A., 1988, Late Palaeozoic evolution of the Kütahya-Bolkardag belt, *METU Journal of Pure and Applied Science*, 21, 211-220.

Pandolfi D., Pandolfi O., 2003, La Cava 3, *Media Print*, Livorno, 36-78.

Papadeas G., 1970, Zurstratigraphie und Altersstellung der metamorphen Serien NE von Athen (Marathon), *PraktikaAkad. Athinon*, 44, 10-18.

Papp M., 2007, Geology and kinematics of detachment faulting on NE Paros Island in Greece, Unpublished diploma thesis, *ETH Zürich*.

Papageorgakis J., 1968b, The presence of marine Miocene on the island of Paros, *Praktika Akademia Athinon*, 43, 368–376.

Papanikolaou D. J., 1977, Contribution to the geology of the Aegean Sea: the island of Andros, *Ann. Geol. Pays Hell.,* 29, 477–553.

Papanikolaou D. J., 1980, Contribution to the geology of Aegean Sea: the island of Paros, *Annal. Géol. Pays Helldniques,* 30 (1), 65-96.

Papanikolaou D. J., 1984, The three metamorphic belts of the Hellenides: a review and a kinematic interpretation, in: Dixon, J.E. Robertson, A.H.F. (Eds.), Geological Evolution of the Eastern Mediterranean, *Geol. Soc. London*, Spec. Publ. 17, 551-556.

Papanikolaou D., 1987, Tectonic evolution of the Cycladic blueschist belt (Aegean Sea, Greece). In: H.C. Helgeson, Editor, *Chemical Transport in Metasomatic Processes*, D. Reidel Publishing Company, Dordrecht, 429–450.

Papanikolaou, D. J., 1979, Geological Map of Paros, Ca. 1: 150 000: IN TEXT: Papanikolaou D. J., Contribution to the Geology of the Aegean Sea: The Island of Paros, *Annales Geologiques des Pays Helleniques*, 1e Serie Tome XXX/1, University of Milan (Italy), Institute of Geological Sciences.

Paribeni E., Fabiani F., Pallecchi P., 1999, Acheronticae columellae, Cippi funerari della Versilia etrusca, *Officina Michelangelo*, Pietrasanta.

Parra T., Vidal O., Jolivet L., 2002, Relation between deformation and retrogression in blueschist metapelites of Tinos island (Greece) evidenced by chlorite-mica local equilibria, *Lithos* 63, 41–66.

Pearce J. A., Bender J. F., De Long S. E., Kidd W. S. F., Low P. J., Güner Y., Saroglu F., Yilmaz Y., Moorbath S., Mitchell J. G., 1990, Genesis of collision volcanism in Eastern Anatolia, Turkey, *Journal of Volcanology and Geothermal Research*, 44, 189-229.

Pensabene P., Lazzarini L., Soligo M., Bruno M., Turi B., 2000, The Parian marble blocks of the Fossa Traina, in D.U. Schilardi and D. Katsonopoulou eds, *Paria Lithos: Parian Quarries, Marble and Workshops of Sculpture*, 527–536, Athens, Paros and Cyclades Institute of Archaeology.

Pensabene P., Antonelli F., Lazzarini L., Cancelliere S., 2012, Provenance of marble sculptures and artifacts from the so-called Canopus and other buildings of ‘‘Villa Adriana’’ (Hadrian’s villa—Tivoli, Italy), *J Archaeol Sci,* 37, 994–1005.

Pentia M., Herz N., Turi B., 2002, Provenance determination of classical marbles: a statistical test based on 87Sr/86Sr, 18O/16O and 13C/12C isotopic ratios, in *ASMOSIA VI, proceedings of the Sixth International Conference of The Association for the Study of Marble and Other Stones in Antiquity*, Venice, June 15–18, 2000, 219-26.

Perinçek D., 1990, Hakkari ili ve dolayının stratigrafisi, Güneydoğu Anadolu, Türkiye, *Türkiye Petrol Jeologları Derneği Bülteni*, 2, 21-68.

Peterek A., Polte M., Wölf C., Bestmann M., Lemtis O., 1994, Zur jungtertiaÈren geologischen Entwicklung im SW der Insel Thassos (S Rhodope, Nordgriechenland), *Erlanger Geologische Abhandlungen*, 124, 29-59.

Pickett E. A., Robertson A. H. F., 1996, Formation of the Late Paleozoic-Early Mesozoic Karakaya Complex and related ophiolites in NW Turkey by Paleotethyan subduction accretion, *Journal of the Geological Society London*, 153, 995-1009.

Pike S., 1999, Preliminary results of a systematic characterization study of Mount Pentelicon, Attica, Greece, in *Archéomatériaux: marbres et autres roches*, ed. Schvoerer, 165-170.

Plinius, Naturalis Historia, *Liber XXXVI*, VII, Les Belles Lettres, Paris.

Pollini J., 2000, The marble type of the statue of Augustus from Prima Porta: facts and 93 fallacies, lithic power and ideology, color and color Symbolism in roman art, in *Paria Lithos: Parian Quarries, Marble, and Workshops of Sculpture*, ed. Schilardi D., Katsarou S., Katsonopoulou D., Mckinney Brenner C., Archaeological and Historical Studies, Athens, 237-252.

Reinecke T., Altherr R., Hartung B., Hatzipanagiotou K., Kreuzer H., Harre W., Klein H., Keller J., Geenen E., Böger H., 1982, Remnants of a late Cretaceous high temperature bet on the island of Anafi (Cyclades, Greece), *N. Jb. Miner. Abh,* 145, 157–182.

Reischmann T., 1998, Pre-Alpine origin of tectonic units from the metamorphic core complex of Naxos, Greece, identified by single zircon Pb/Pb dating, *Bulletin of the Geological Society of Greece*, 32, 101-111.

Renfrew C., Springer P.J., 1968, Aegean marble: a petrological study, *Annual of the British School at Athens* 63, 45-66.

Rigo De Righi M., Cortesini A., 1964, Gravity tectonics in foothills structure belt of southeast Turkey, *American Association of Petroleum Geologists Bulletin*, 48, 1911-1937.

Ring U., Layer P.W., Reischmann T., 2001, Miocene high-pressure metamorphism in the Cyclades and Crete, Aegean Sea, Greece: evidence for large-magnitude displacement on the Cretan detachment, *Geology,* 29, 395–398.

Ring W., Layer P. W., 2003, High-pressure metamorphism in the Aegean, eastern Mediterranean: Under plating and exhumation from the Late Cretaceous until the Miocene to Recent above the retreating Hellenic subduction zone, *Tectonics*, 22(3), 1-23.

Ring U., Glodny J., Will T., Thomson S., 2007a, An Oligocene extrusion wedge of blueschists-facies nappes on Evia, Aegean Sea, Greece: implications for the early exhumation of high-pressure rocks, *J. Geol. Soc. London* 164, 637–652.

Ring U., Will T., Glodny J., Kumerics C., Gessner K., Thomson S., Güngör T., Monie P., Okrusch M., Drüppel K., 2007b, Early exhumation of high-pressure rocks in extrusion wedges: Cycladic blueschist unit in the eastern Aegean, Greece, and Turkey, *Tectonics,* 26 (2).

Robert E., 1982, Contribution á l'étude géologique des Cyclades (Greece): l'ile de Paros, *thése de Doctorat*, pp 103, Paris-Sud (Orsay).

Robertson A. H. F., Grasso M., 1995, Overview of the Late Tertiary tectonic and palaeo-envrionmental development of the Mediterranean region, *Terra Nova*, 7, 114-127.

Robertson A. H. F., 1998, Mesozoic-Tertiary tectonic evolution of the Eastern Mediterranean area: Integration of marine and land evidence, in Robertson A. H. F., Emeis K.-C., Richter C., and Camerlenghi A., eds. *Proceedings of the Ocean Drilling Program, Scientific Results*, 160, 723-782.

Robinson A. G., Banks C. J., Rutherford M. M., Hirst, J. P. P., 1995, Stratigraphic and structural development of the Eastern Pontides, Turkey, *Journal of the Geological Society, London,* 152, 861-872.

Röder J., 1971, Marmor Phrygium. Die Antiken Marmorbrüche von Iscehisar in Westanatolien, *Jahrbuch des Deutschen Archäologischen Institute*, 86, 251-321.

Roesler G., 1978, Relics of non-metamorphic sediments on Central Aegean islands, in Alps, Apennines, Hellenides, edited by H. Closs *et al., IUCG Sci. Rep.*, 38, 480-481.

Rojay F. B., Altiner D., 1998, Middle Jurassic-Lower Cretaceous biostratigraphy in the central Pontides (Turkey): Remarks on paleogeography and tectonic evolution, *Rivista Italiana Paleontologia e Stratigrafia*, 104, 167-180.

Rutter E. H., 1972, The influence of interstitial water on the rheological behavior of calcite rocks, *Tectonophysics*, 14, 13-33.

Rutter E. H., 1995, Experimental study of the influence of stress, temperature, and strain on the dynamic recrystallization of Carrara marble, *Journal of Geophysical Research*, 100, 24651-24663.

Sakellariou D., 1989, Geologie des Serbomazedonischen Massivs in der nordoestlichen Chalkidiki, N-Griechenland–Deformation und Metamorphose, Nat. and Kapodistrian Univ. of Athens, *Geol. Monogr.*, 2, pp. 164.

Sánchez-Gómez M., Avigad D., Heimann A., 2002, Geochronology of clasts in allochthonous Miocene sedimentary sequence on Mykonos and Paros Islands: implications for backarc extension in the Aegean Sea, *Journal of the Geological Society of London*, 159, 45–60.

Schermer E., 1993, Geometry and kinematics of continental basement deformation during the Alpine orogeny, Mt. Olympos region, Greece, *J. Struct. Geol.*, 15, 571-592.

Schilardi D., Katsarou S., Katsonopoulou D., Mckinney Brenner C., 2000, Paria Lithos: Parian Quarries, Marble, and Workshops of Sculpture, *Archaeological and Historical Studies 1*.

Schliestedt M., Altherr R., Mathews A., 1988, Evolution of the Cycladic crystalline complex: petrology, isotope geochemistry and geochronology, in *Chemical Transport in Metasomatic*, eds. Processes H. C. Helgeson, eds. Springer, Netherlands, 389-428.

Schmid S. M., Paterson M. S., Boland J. N., 1980, High temperature flow and dynamic recrystallization in Carrara marble, *Tectonophysics*, 65, 245-280.

Schmid S.M., Panozzo R., Bauer S., 1987, Simple shear experiments on calcite rocks: rheology and microfabric, *Journal of Structural Geology*, 9, 747-778.

Schneider-Esquini E., 1972, La necropolis di Hierapolis in Frigia, in Monumenti antichi, *ser. Misc*. I-2, 48, Accademia Naz. Dei Lincei, Rome.

Schulz B., 1992, Syntectonic heating and loading-deduced from microstructures and mineral chemistry in micaschists and amphibolites of the Pangeon complex (Thassos island, Northern Greece), *Neues Jahrbuch für Geologie und Palaëontologie Abhandlungen*, 184, 181-201.

Sengör A. M. C., 1979a, Mid-Mesozoic closure of Permo-Triassic Tethys and its implications, *Nature*, 279, 590-593.

Sengör A. M. C., Yilmaz Y., 1981, Tethyan evolution of Turkey: A plate tectonic approach, *Tectonophysics*, 75, 181-241

Sengör A. M. C, Görür N., Saroglu F., 1985, Strike slip faulting and related basin formation in zones of tectonic escape: Turkey as a case study, in Biddle, K. T., and Christie-Blick, N., eds. *Strike-slip faulting and basin formation: Society of Economic Paleontologists and Mineralogists*, Special Publication, 37, 227-264.

Sengör A. M. C., 1987, Tectonics of the Tethysides: Orogenic collage development in a collisional setting, *Annual Review of Earth and Planetary Sciences*, 15, 213- 244.

Şengör A. M. C., Tüysüz O., İmren C., Sakinç M., Eyidoğan H., Görür N., Le Pichon X., Rangin C., 2005, The North Anatolian Fault: a new look, *Annual Review of Earth and Planetary Sciences*, 33, 37-112.

Seward D., Vanderhaeghe O., Siebenaller L., Thomson S., Hibsch C., Zingg A., Holzner P., Ring U., Duchêne S., 2009, Cenozoic tectonic evolution of Naxos Island a multi-faceted approach of fission-track analysis, *Geological Society,* London, Special Publications, 321(1), 179-196.

Sheedy, K., 2000, Archaic Parian Coinage and Parian Marble, in *Paria Lithos: Parian Quarries, Marble, and Workshops of Sculpture*, ed. Schilardi D., Katsarou S.,

Katsonopoulou D., Mckinney Brenner C., Archaeological and Historical Studies, Athens, 1117-121.

Sidiropoulos D., 1980, Geologie der Griechischen Tertiäirbecken Nestos-Prinos und Xanthi-Komotini, Geol. Inst. Kö1n, Veröff, 39, pp. 158.

Sherlock S., Kelley S.P., Inger S., Harris N., Okay A.I., 1999, ^{40}Ar-^{39}Ar and Rb-Sr geochronology of high-pressure metamorphism and exhumation history of the Tavsanli Zone, NW Turkey, *Contributions to Mineralogy and Petrology,* 137, 46-58.

Smith L. I., 2002, A tutorial on Principal Components Analysis, Cornell University, USA.

Sokoutis D., Brun J. R, van den Driessche J., Pavlides S., 1993, A major Oligo-Miocene detachment in southern Rhodope controlling north Aegean extension, *J. Geol. Soc. London*, 150, 243-246.

Sotiropoulos S., Kamberis E., Triantaphyllou M. V., Doutsos T., 2003, Thrust sequences in the central part of the External Hellenides, *Geol. Mag.* 140, 661–668.

Spiers C. J., 1979, Fabric development in calcite polycrystals deformed at 400-degrees-c, *Bulletin de Minéralogie*, 102, 282-289.

Stampfli G. M., 2000, Tethyan oceans, in Bozkurt, E., Winchester J. A., Piper J. D. A., eds. Tectonics and magmatism in Turkey and the surrounding area, *Geological Society of London*, Special Publication, 173, pp. 1-23.

Stampfli G. M., Borel, G. D., 2002, A plate tectonic model for the Paleozoic and Mesozoic constrained by dynamic plate boundaries and restored synthetic oceanic isochrones, *Earth and Planetary Science Letters*, 196(1), 17-33.

Steinmann G., 1890, Einigefossilreste aus Griechenland, *Zeitschr. d. Deutsch. Geol. Gesel*, 42, 764-771.

Strumpf N., 1997, Das Kernkristallin von Naxos (Kykladen, Griechenland), *Schriftenreihe für Geowissenschaften,*5, pp. 1-140.

Sunal G., Natalin B., Satir M., Toraman E., 2006, Paleozoic magmatic events in the Strandja Masif, NW Turkey, *Geodinamica Acta*, 19, 283-300.

Székely B., Zöldföldi J., 2009, Fractal analysis and quantitative fabric analysis database of West Anatolian white marbles, in *ASMOSIA VII, Proceedings of the 7th International Conference of Association for the Study of Marble and Other Stones in Antiquity*, Athenes: École française d'Athènes, pp. 719-734.

Taylor S. R., McLennan S. M., 1985, The continental crust: its composition and evolution.

Taymaz T., J. Jackson, McKenzie D., 1991, Active tectonics of the north and central Aegean Sea, *Geophys. J. Int.* 106, 433–490.

Tiepolo M., Bottazzi P., Palenzona M., Vannucci R., 2003, A laser probe coupled with ICP-double focusing sector-field mass spectrometer from in situ analysis of geological samples and U-Pb dating of zircon, *Can. Mineral.*, 41, 259–272.

Tirel C., Brun J. P., Burov E., 2004a, Thermo-mechanical modeling of extensional gneiss domes. In: D.L. Whitney, C. Teyssier and C.S. Siddoway, Editors, *Gneiss Domes in Orogeny, Geological Society of America Special Paper,* 67–78.

Tirel C., Gueydan F., Tiberi C., Brun J.P., 2004b, Aegean crustal thickness inferred from gravity inversion. Geodynamical implications, *Earth Planet. Sci. Lett.*, 228, 267–280.

Tykot R.H., 2004, *Scientific methods and applications to archaeological provenance studies*. In Physics Methods in Archaemotry (Proceedings of the International School of Physics "Enrico Fermi", Martini, Milazzo and Piacentini Ed., IOS Press, Amsterdam.

Tykot R. H., Ramage M. H., 2002, On the importation of monumental marble to Sardis, Herrmann J. J., Herz N., Newton R., *ASMOSIA*, 5, 335-339.

Topuz G., Altherr R., Kalt A., Satir M., Werner O., Schwartz W.H., 2004, Aluminous granulites from the Pulur Complex, NE Turkey: a case of partial melting, efficient melt extraction and crystallization, *Lithos*, 72, 183-207.

Topuz G., Altherr R., Schwartz W.H., Dokuz A., Meyer H-P., 2007, Variscan amphibolites-facies rocks from the Kurtoğlu metamorphic complex (Gümüşhane area, Eastern Pontides, Turkey), *International Journal of Earth Sciences*, 96, 861-873.

Trotet F., Vidal O., Jolivet L., 2001, Exhumation of Syros and Sifnos metamorphic rocks (Cyclades, Greece). New constraints on the P–T paths, *European Journal of Mineralogy,* 13 (5), 901–920.

Trotet F., Jolivet L., Vidal O., 2001, Tectono-metamorphic evolution of Syros and Sifnos islands (Cyclades, Greece), *Tectonophysics* 338, 179–206.

Turgut S., Turkaslan M., Perincek D., 1991, Evolution of the Thrace sedimentary basin and its hydrocarbon prospectivity, in Spencer, A.M. (Ed.), Generation Accumulation and Production of Europe's Hydrocarbons. Spec. *Publ. European Assoc. Petrol. Geoscientists*, vol. 1, 415– 437.

Urai J. L., Schuiling R. D., Jansen B. H., 1990, Alpine deformation on Naxos (Greece), in *Deformation mechanisms, rheology and tectonics*, eds. R. J. Knipe and E. H. Rutter, 509–22, Special Publications, Geological Society, London.

Ustaömer T., RobertsonA. H. F., 1999, Geochemical evidence used to test alternative plate tectonic models for pre-Jurassic (palaeotethyan) units in the central Pontides, N Turkey, *Geological Journal*, 34, 25-554.

Ustaömer P.A., Mundil R., Renne P.R., 2005, U/Pb and Pb/Pb zircon ages for arc-related intrusions of the Bolu Massif (W Pontides, NW Turkey): evidence for Late Precambrian (Cadomian) age, *Terra Nova*, 17, 215-223.

Uysal I. T., Mutlu H., Altunel E., Karabacak V., Golding S. D., 2006, Clay mineralogical and isotopic (K–Ar, $\delta^{18}O$, δD) constraints on the evolution of the North Anatolian Fault Zone, Turkey, *Earth and Planetary Science Letters*, 243, 181-194.

Vanderhaeghe O., Teyssier C., 2001, Crustal-scale rheological transitions during late-orogenic collapse, *Tectonophysics,* 335, 211–228.

Vanderhaeghe O., Hibsch C., Siebenaller L., Duchêne S., Kruckenberg S., Fotiadis A., Martin L., de Saint Blanquat M., 2007., Penrose conference — extending a continent — Naxos Field guide. Journal of the Virtual Explorer, 28, Paper 4.

Varti Matarangas M., Matarangas D., Lazzarini L., 2009, The marbles of Ikaria and Samos: quarries and characterization, in LEUKOS LITHOS – *Marbres et autres roches de la Méditerranée antique: études interdisciplinaires*, 31-48.

Vigner A., 2002 Images sismiques par réflexions verticals et grand-angle de la croûte en contexte extensif: les Cyclades et le Fossé Nord-Egéen. Thèse de doctorat Thesis, Institut de Physique du Globe, Paris, 269 pp.

Vinogradov A. P., Ronov A. B., Ratynski V. M., 1952, *Changes of chemical composition of carbonate rock of the Russian platform*, Izv. Akad. Nauk, *SSSR Geological Service*, 1, 33-50.

Waelkens M., 1982, Carrières de marbre en Phrygie (Turquie), *Bulletin des Musées d'Art et d'Histoire*, 53, 33-54.

Walker S., 1988, From west to east: evidence for a shift in the balance of trade in white marbles, in *Classical marble geochemistry, technology, trade,* eds. N. Herz and M. Waelkens, 187–95, NATO ASI Ser E, 153, Kluwer Dordrecht.

Washington H. S., 1898, The identification of the marbles used in Greek sculpture, *American journal of Archaeology*, 2, 1-18.

Wawrzenitz N., 1994, Ein miozäner metamorpher Kernkomplex in Nordgriechenland (Insel Thassos, Rhodope-Massiv)-Variszische Vorgeschichte und alpine Geschichte der Versenkung und Exhumierung mittelkrustaler Gesteine, *Erlanger Geol. Abh.*, 124, 61-75.

Wawrzenitz N., Krohe A., 1998, Exhumation and doming of the Thassos metamorphic core complex (S Rhodope, Greece): structural and geochronological constraints, *Tectonophysics*, 285, 301-332.

Weiss L. E., 1954, Fabric analysis of some Greek marbles and its applications to archaeology, *Am. J. Sci.*, 252, 641-662.

Wenk H. R., Takeshita T., Bechler E., Erskine B.G., Matthies S., 1987, Pure shear and simple shear calcite textures, Comparision of experimental, theoretical and natural data, *Journal of Structural Geology*, 9, 731-745.

Wijbrans J. R., McDougall I., 1986, $^{40}Ar/^{39}Ar$ dating of white micas from an alpine high-pressure metamorphic belt on Naxos (Greece); the resetting of the argon isotopic system, *Contrib. Mineral. Petrol.* 93, 187–194.

Wijbrans J. R., McDougall I., 1988, Metamorphic evolution of the Attic Cycladic Metamorphic Belt on Naxos (Cyclades, Greece) utilizing 40Ar/39Ar age spectrum measurements, *J. Metamorph. Geol.* 6, 571–594.

Wong H. K., Ulug A., Ludmann T., Ozel E., 1990, Neotectonic structure of the Sea of Marmara, *Mitt. Geol.-Palaont. Inst. Univ. Hamb.*, 69, 99– 116.

Yavuz A. B., Turk N., Koca M. Y., 2005a, Geological parameters affecting the marble production in the quarries along the southern flank of the Menderes Massif, in SW Turkey, *Engineering geology*, 80 (3), 214-241.

Yavuz A. B., Turk N., Koca M. Y., 2005b, Material properties of the Menderes massif marbles from SW Turkey, *Engineering geology*, 82 (2), 91-106.

Yavuz A. B., Attanasio D., Elçi H., Brilli M., Bruno M., 2009, Discovery of preliminary investigation of the Göktepe marble quarries (Mugla, Turkey): an alternative source of Aphrodisias marbles, in P. Jockey ed., *Marbres et autres roches de la Méditerranée antique: ėtudes interdisciplinaires*, 93–109, Paris, Maisonneuve & Larose.

Yiğitbaş E., Yilmaz Y., 1996, New evidence and solution to the Maden complex controversy of the Southeast Anatolian orogenic belt (Turkey), *Geologische Rundschau*, 85, 250-263.

Yilmaz Y., 1993, New evidence and model on the evolution of the Southeast Anatolian orogen, *Geological Society of America Bulletin*, 105, 251-271.

Yilmaz Y., Genç S. C., Yigtbas E., Bozcu M., Yilmaz K., 1995, Geological evolution of the Late Mesozoic continental margin of northwestern Anatolia, *Tectonophysics*, 243, 155-172.

Yilmaz Y., Yildirim M., 1996, Geology and evolution of the nappe region (the metamorphic massifs) of the southeast Anatolian orogenic belt, *Turkish Journal of Earth Science*, 5, 21-38.

Yilmaz Y., Genç Ş. C., Karacik Z., Altunkaynak Ş., 2001, Two contrasting magmatic associations of NW Anatolia and their tectonic significance, *Journal of Geodynamics*, 31, 243-271.

Young W.J., Ashmole B., 1968, The Boston relief and the Ludovisi Throne, *Bulletin of the Museum of Fine Arts* 66, 124-166.

Zaccagna D., 1905, Condizioni geologiche ed industriali degli agri marmiferi della regione del Canal Bianco e del Murlungo, in *Rassegna Mineraria e della Industria Chimica*, 23, 1-19.

Zachos S., 1982, Geological map of the Island of Thasos, 1:50,000, *Institute of Geology and Mineral Exploration (IGME)*, Athens.

Zapheiropoulou P., 1988, Naxos: Monuments and Museum, *Krene* Editions.

Zattin M., Okay A. I., Cavazza W., 2005, Fission-track evidence for late Oligocene and mid-Miocene activity along the North Anatolian Fault in south-western Thrace, *Terra Nova,* 17, 95-101.

Zöldföldi J., Satir M., 2003, Provenance of white marble building stones in the monuments of the ancient Troia, in G.A. Wagner, E. Pernicka & H.P. Uerpmann (eds.), *Troia and the Troad,* Springer, Berlin, 203-223.

Zöldföldi J., Székely B., 2003, A case study of combining quantitative fabric analysis (QFA) and fractal analysis (FA) on white marbles with conventional analytical techniques for provenance analysis, in R. Snethlage & J. Meinhardt-Degen (eds.), *Proceedings of the 13th Workshop of EU 496 EUROMARBLE*, Bavarian State Department of Historical Monuments Munich, 141-149.

Zöldföldi J., Székely B., 2004b, Interdisciplinary data base of historically relevant marble material for archaeometric, art historian and restoration use, in G. Grassegger-Schön & G. Patitz (eds.), *Natursteinsanierung Stuttgart 2004,* Neue Natursteinsanierungsergebnisse und messtechnische Erfassungen, Siegl, München, 79-86.

Zöldföldi J., Székely B., 2005a, Provenance of Roman and Greek marble building stones of Troy. Proceedings of the 33rd International Symposium on Archaeometry, 22-26 April 2002, Amsterdam, *Geoarchaeological and Bioarchaeological Studies* 3, pp. 123-129.

Zöldföldi J., Székely B., 2005b, Quantitative Fabric Analysis (QFA) and Fractal Analysis (FA) on Marble from West-Anatolia and Troy, in *Proceedings of the 33rd International Symposium on Archaeometry*, 22-26 April 2002, Amsterdam, *Geoarchaeological and Bioarchaeological Studies*, 113-119.

Appendix

A second challenge of this thesis was a geochemical study of archaeological artworks, aiming to compare and test the LA-ICP-MS data with those previously obtained on geological samples of known provenance.

The comparison of geochemical data on marble derived from both the geological and archaeological artifacts can be useful for attribution of provenance of raw materials involved in the manufacturing process.

In this way, depending on the types of artifacts and the archaeometric issues, it may be possible to confirm or contradict some attributions of museum catalogues and to suggest or ascribe the provenance of some objects.

Generally, the adopted protocol for the artifacts consists in a preliminary study aiming to collect a large number of available information about these items.

The second step consists in the acquisition of the concentrations of trace elements by means of the Laser-Ablation - Inductively Coupled Plasma – Mass Spectrometry (LA-ICP-MS) in the Laboratory of Inorganic Chemistry of Eidgenössische Technische Hochschule (ETH) of Zürich.

The third step involves a comparison of the identified geochemical markers on geological samples with those of archaeological ones.

Artifacts from the "Casa di Augusto" site

The sampling

The complex of Augustus on the Palatine Hill (Rome, Italy) was the subject of many recent studies with the aim of reconstructing the changes made to the first house of Augustus, also known as the house of Octavian (41-36 BC), and the renovation of the whole area at the time of the construction of the Temple of Apollo (36-28 BC).

The archaeological objects of the *domus* of Augustus, most of them in white marble found during the archaeological excavations of Carettoni (1957-1974 approx.), revealed the presence of four groups based on their features and uses.

A first group is made up of hundreds of fragments of statues; many of them, despite their small size, have been attributed to the great statue of Apollo Palatinus, placed inside the *cella* of the temple. Historical sources reported that Octavian brought this statue to Rome after the victory of Actium, and attribute it to the sculptor Skopas, also called "the Parian" (Brilli *et al.,* 2015).

A second group, consisting of the architectural elements of the high temple, includes fragments of Corinthian capitals, cornices and numerous fragments from gigantic fluted columns.

The third group is related to a few large fragments of fluted columns in "*giallo antico*" (an antique sedimentary rock) and large fragments of Ionic capitals attributed to the Portico of the Danaids.

Finally, the fourth group, consisting of architectural elements, is characterized by mixed Corinthian-Doric architectural items attributed to the facade of the house of Octavian. These latter elements are of smaller size than those of the temple and the Portico.

Previous study

A selection of white marble objects from each of the groups mentioned were studied by Brilli *et al.* (2015) in order to reconstruct the use of marble in private or public contexts, *i.e.,* fragments from the house of Octavian, from the Temple of Apollo and the Portico of the Danaids.

In particular, Brilli *et al.* (2015) applied a multi-analytical approach for provenance investigation; these authors involved petrographic and isotopic characterization along with X-ray diffraction on a selection of samples of white marbles from the Augustus complex.

The whole dataset revealed that all marble specimens from the architectural elements have a high likelihood to come from the Carrara quarries. Two samples collected from fragments, probably belonging to a statue of Apollo, are with a high probability composed of Pentelic marble.

In addition, Brilli *et al.* (2015) reported that the gigantic blocks involved in the construction of the temple of Apollo, since the first Augustan period, were extracted from Luni (Carrara marble). As for the temple of Apollo, this attribution was reported before in some historical sources. This allowed them to contend the existence of a state-controlled organization of the Carrara quarries ever since.

Regarding the statue of Apollo, the remarkable result of their work seems to confirm the reuse of raw material from ancient Greek monument, probably statue in Pentelic marble from the temple of Apollo at Rhamnus in Attica.

The samples analyzed in this Ph.D. thesis are shown in Fig. A1, whereas petrographic and isotopic results are reported in Tab. A1.

Tab.A.1: The petrographic and isotopic results (Brilli *et al.,* 2015).

Sample	Description	Color	Calcite	Texture	Fabric	Calcite crystal boundaries	MGS	$\delta^{13}C$	$\delta^{18}O$
CA_2	Fragment of statue	white	only	HE	Lineated	Curved, embayed	0.7	2.68	-4.77
CA_3	Ceiling slab	white	only	HE	Polygonal mosaic	Curved, straight, triple junctions	0.9	1.96	-2.74
CA_7	Imitation of opus sectile	white	only	HO	Polygonal mosaic	Curved, straight, frequent triple junctions	0.5	2.15	-1.13
CA_9	Erratic	white	only	HE	Polygonal mosaic	Polygonal with triple junctions, straight	0.8	2.17	2.03

Fig. A1: The white marble items sampled for this Ph.D. thesis.

References

Brilli M., Giustini F., Pensabene P., 2015, The beginning of the "Marmorization" process of the monumental buildings on the Palatine Hill in the Augustan Age: characterization of white marble objects from the temple of Apollo and the house of Augustus, *ASMOSIA XI International Conference*, Split, Croatia, 18 – 22 May 2015.

Geochemical composition using LA-ICP-MS

Fragments of the archaeological specimens shown in figure A1 were analyzed by means of Laser-Ablation - Inductively Coupled Plasma - Mass Spectrometry (LA-ICP-MS) in order to acquire the concentrations of trace elements. For each sample, five spot analyses were analyzed, and the concentrations of 47 trace elements were measured.

In the multi-elemental diagrams concentrations of the trace elements detected on the archaeological samples (*i.e.,* CA_2, CA_5, CA_7 and CA_9) were reported.

The chondrite-normalized multi-elemental diagram (Fig. A.2), shows a homogeneous enrichment in Sr and a scattered pattern of Rb, Ba, and K data points. In addition, all samples are enriched in U and depleted in Th and Ti.

In the same diagram (Fig. A.2), sample CA_2, *i.e.,* a marble fragment of the statue of Apollo, shows an enrichment of REE. This is confirmed by the diagram in Fig. A.3, the REE + Y diagram in which the highest REE content is recorded in CA_2 specimen, and a more marked negative Ce anomaly allows one to discriminate this sample from the other specimens (i.e., CA_3, CA_7 CA_9). The enrichment concerns both the LREE and HREE, as shown in Fig. A.4.

Also, the content of the transition metals, *i.e.,* Fe, Mn, is higher in the CA_2 sample than in the other samples, forming once again a separate cluster.

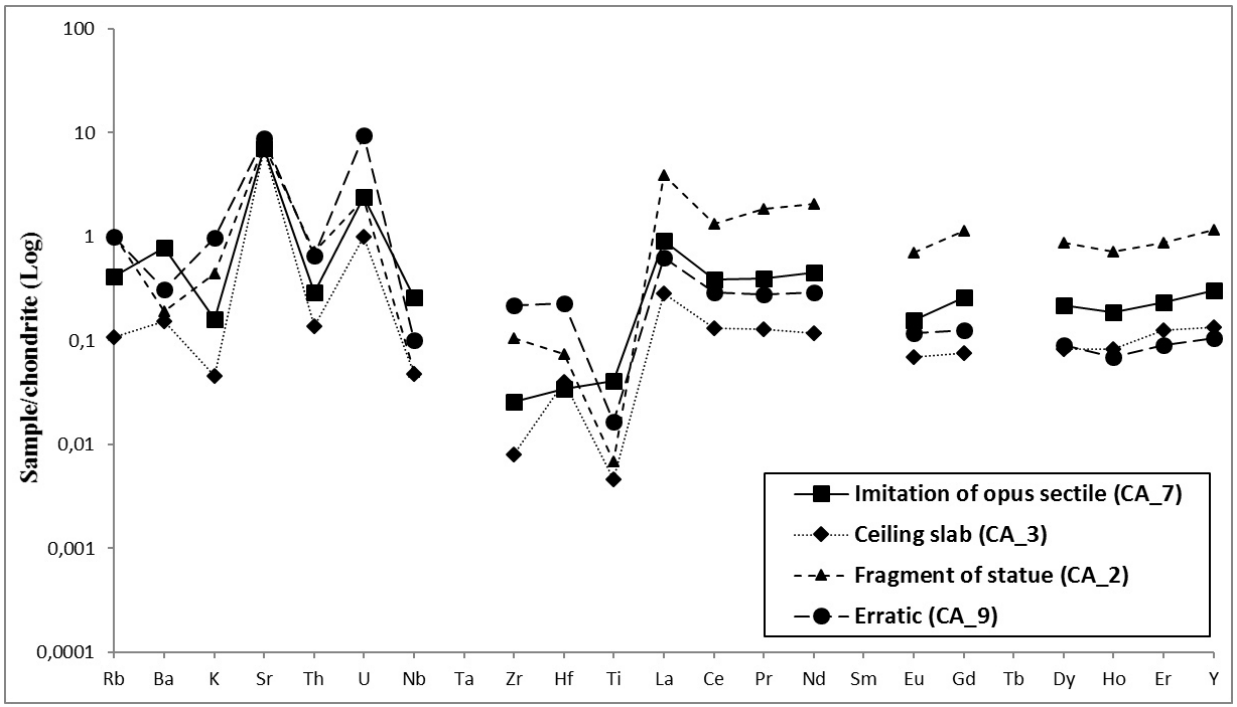

Fig. A.2: Patterns of trace elements in calcite of white archaeological samples from Casa di Augusto site (Italy). The specimens are displayed using different symbols and lines: continuous line and square symbol is used for opus sectile (CA_7); dot line and rhombus symbol for ceiling slab (CA_3); thin dash line and triangle symbol for fragment of the statue (CA_2); dash line and circle symbol for erratic (CA_9). The LA-ICP-MS concentrations are normalized to chondrite (Sun and McDonough (1989))

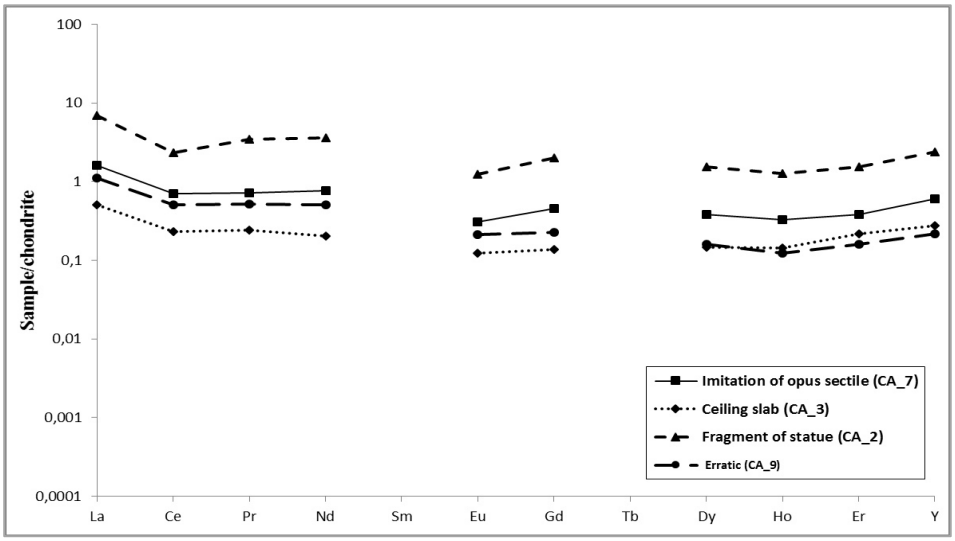

Fig. A.3: Patterns of REE + Y in calcite of white archaeological samples from Casa di Augusto site (Italy). The specimens are displayed using different symbols and lines: continuous line and square symbol for opus sectile (CA_7); dot line and rhombus symbol for ceiling slab (CA_3); thin dash line and triangle symbol for fragment of the statue (CA_2); dash line and circle symbol for erratic (CA_9). The LA-ICP-MS concentrations are normalized to chondrite (Taylor and McLennan (1985)).

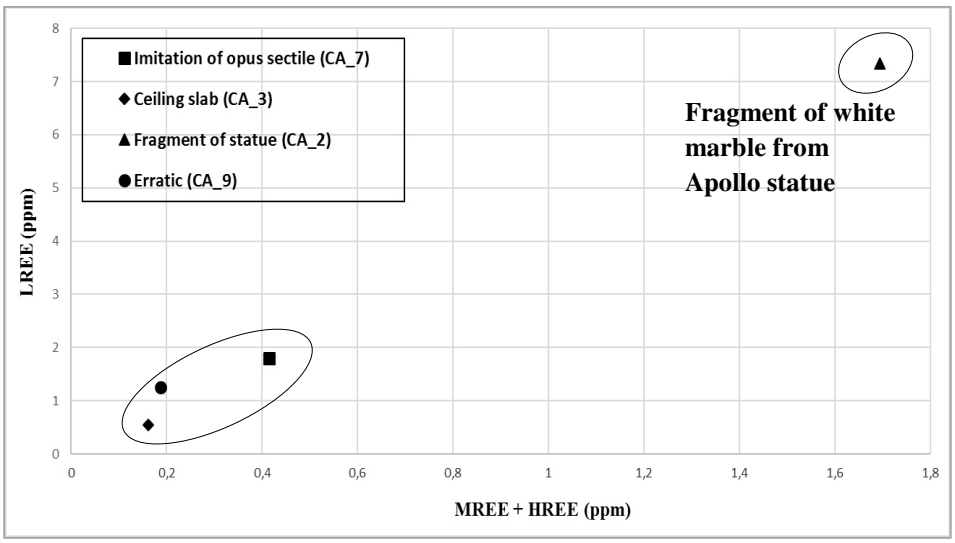

Fig. A.4: LREE *vs* MREE + HREE content. The lowest REE content in CA_3, CA_7, CA_9 samples separates these samples from CA_2 samples.

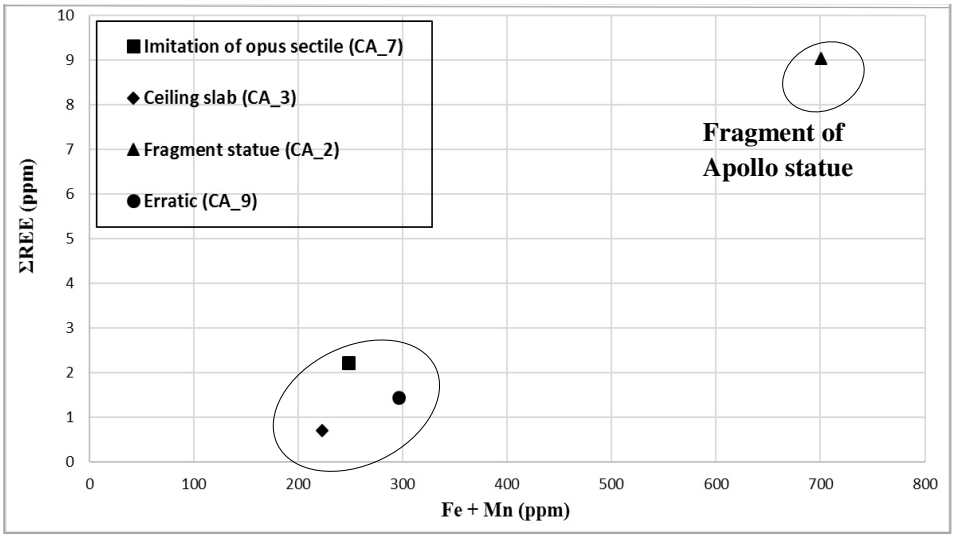

Fig. A.5: The content of Fe+Mn is higher in CA_2 sample than that of the other specimens.

Archaeological vs geological white marble

In this section, the trace-element concentrations of archaeological samples are compared with those of geological samples.

In Fig. A.6, the diagram Fe + Mn *vs* REE content shows that the sample from the statue of Apollo (CA_2) falls close to Pentelic samples, whereas the other three specimens are concentrations similar to those of the Carrara marble.

Figure A.7 shows the REE patterns of Casa di Augusto samples (CA_3, CA_7 and CA_9) compared with those of Carrara and Pentelic marble. In the archaeological samples, the concentrations and patterns close to those in Carrara specimens, whereas CA_2 has patterns similar to Pentelic specimens (*e.g.,* marked negative Ce anomaly) with slightly higher concentrations.

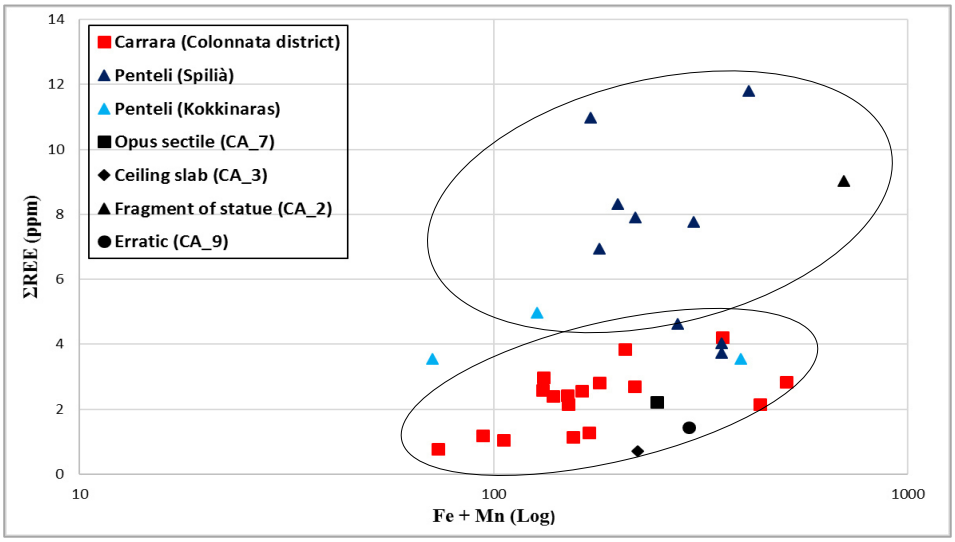

Fig. A.6: Fe+Mn *vs* REE content in archaeological samples compared to those of geological samples from Carrara and Mount Pentelicon.

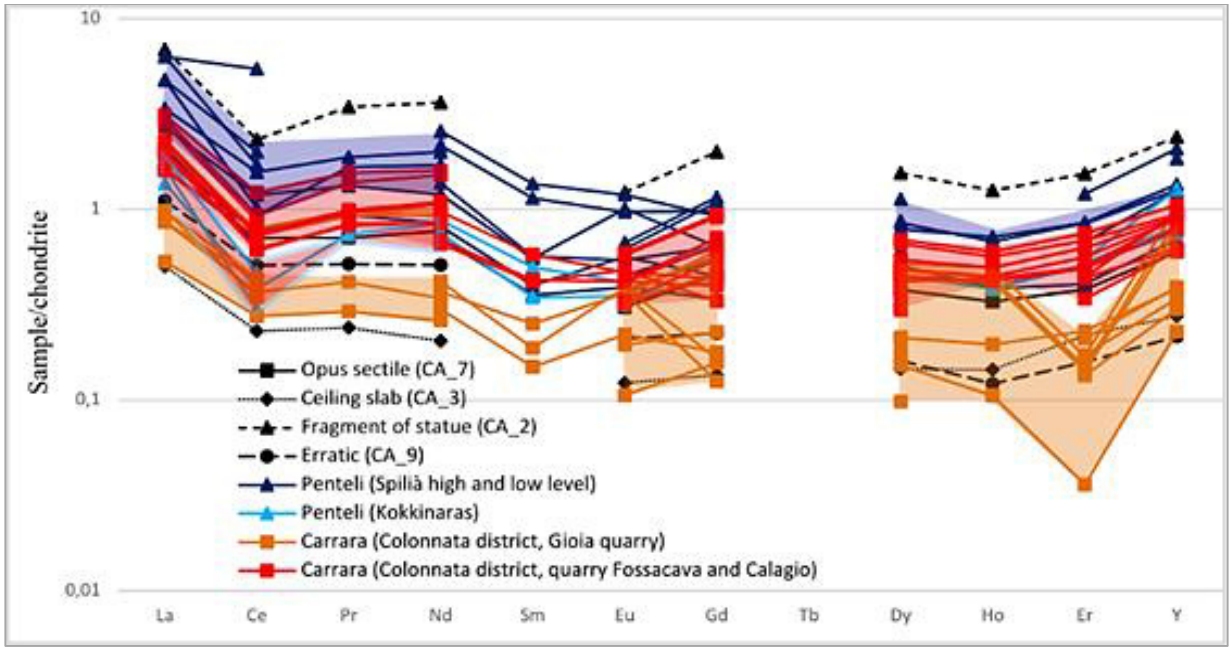

Fig. A.8: Patterns of REE + Y in calcite of archaeological samples from Casa di Augusto site (Italy) and geological samples from Carrara and Penteli. The specimens are displayed using different symbols and lines: continuous line and square symbol for opus sectile (CA_7); dot line and rhombus symbol for ceiling slab (CA_3); thin dashed line and triangle symbol for fragment of the statue (CA_2); dashed line and circle symbol for erratic (CA_9); dark blue continuous line and dark blue triangle for Pentelic marble (Spilià high and low level); light blue continuous line and light blue tringle symbol for Pentelic rocks; red continuous line and red square symbol for Carrara marble. The LA-ICP-MS concentrations are normalized to chondrite (Taylor and McClennan, 1985)

Discussion and conclusion

The summary of the previous study (Brilli *et al.,* 2015) on the artifacts (presented in Table A.1) and the geochemical markers identified using the LA-ICP-MS lead to some conclusions.

In the previous chapter, the Carrara marble was shown to have a high content of Mg compared to the other fine-grained specimens. The Pentelic samples contain a higher content of REE than those of Carrara and a more strongly negative Ce anomaly. A summary of the identified markers and a suggested provenance for the analyzed objects are presented in Table A.2.

Particular attention is directed to some Carrara specimens, collected from the Gioia quarry. These samples show a negative Er anomaly not observed in other Carrara samples and in those from the Casa di Augusto site.

In the principal component analysis (PCA), the concentrations of those parameters that seemed to be more discriminating for these two samples of white marble (*i.e.,* the Mg, Ce content and the sum of REE and Fe + Mn) were used. In this context, the geochemical markers previously identified for the quarrying districts were used in the PC analysis. The PCA chart (Fig. A.9) shows that the samples CA_3, CA_7 and CA_9 fall close to Carrara samples, as also confirmed in the previous study (Brilli *et al.,* 2015). The sample CA_2 falls completely away from Carrara specimens, thus excluding the provenance of this marble from the same site of the other three specimens. It is possible to infer a provenance of the raw material from Pentelic quarry, having concentrations and patterns similar to Pentelic samples.

Tab. A.2: Summary of the results of the “Casa di Augusto” marble, with an indication of its provenance

Artworks	Identified markers	Provenance
CA_3 Ceiling slab	Mg, REE, Fe+Mn content	Carrara
CA_7 Opus sectile	Mg, REE, Fe+Mn content	Carrara
CA_9 Erratic	Mg, REE, Fe+Mn content	Carrara
CA_2 fragment of statue	Mg, REE, Fe+Mn content, marked negative Ce anomaly	Pentelicon

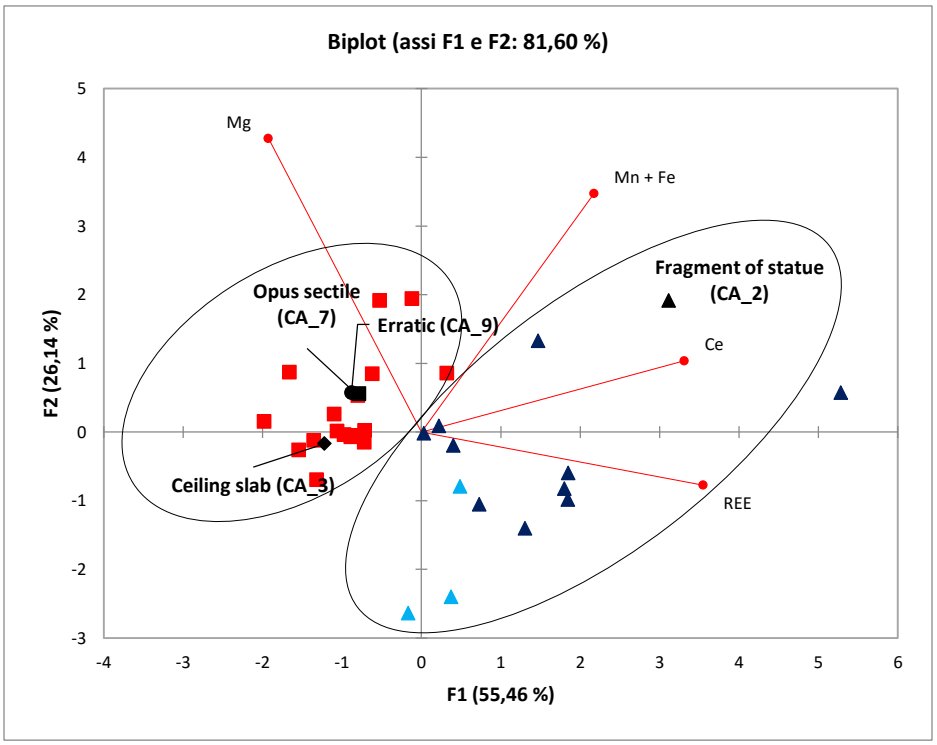

Fig. A.9: PCA chart of Casa di Augusto artifacts and marble from Carrara and Mount Pentelicon.

Appendix B

Artifacts from Musei Capitolini collection

The sampling and previous studies

The four precious samples here presented were collected from some of the most famous masterpieces of the Musei Capitolini in Rome, such as the statue of Colossus of Constantine (313-324 A.D.) and the statue of Mars (Fig. B.1).

Many fragments of the so-called Colossus are exposed in the court of "*Palazzo dei Conservatori*" (Rome).

It was argued that the Colossus was seated because of the pose of the left foot, but now it is doubtful whether all fragments belong to the same statue.

In particular, an archaeological problem, for which an assessment of provenance is of crucial importance, concerns the statue of Colossus of Constantine.

As reported by Mattei *et al.* (1997) and already noted by Stuart-Jones (1926), the various parts of the statue were made of marble of different origins (Head of Constantine: Pentelic marble; right hand and right arm: Luni marble; right leg and knee: Grechetto; calf of left leg and right leg: Pentelic marble; left foot: Parian marble).

The study of Mattei *et al.* (1997) concerns the chemical characterization of two fragments from the left hand and the left arm. The authors concluded that the provenance of the white marble was Carrara and Paros marble, respectively. These results confirm the possible use of marble from different sources, and it is well known that the utilization of marble in the late Empire in Rome was a very common practice.

Fig. B.1: a) The statue of Colossus of Constantine (313-324 A.D.); b) the statue of Mars. The fragments were collected the Musei Capitolini, Rome.

Geochemical composition of the fragments using LA-ICP-MS

The concentration of trace elements on marble fragments from the Musei Capitolini specimens were acquired by means the Laser-Ablation - Inductively Coupled Plasma - Mass Spectrometry (LA-ICP-MS); for each sample five spot analyses were made, for a total of 47 trace-element determinations.

The spider diagram shown as Fig. B.2 highlights a Sr enrichment and K depletion among the LIL elements. The samples of the Colossus of Constantine (MC35, MC36) have a higher Sr content than those collected from the Mars statue (MC43, MC44). The HFS elements present heterogeneous concentrations; in particular, Th and Ti are depleted, and U and Hf enriched.

The content of REE is homogeneous in the Mars statue fragments, whereas in the Colossus samples, the content of REE of the knee (MC35) is higher than that of the right hand (MC36).

In the REE+Y diagram (Fig. B.3), the patterns are homogeneous for both groups of samples. The Colossus statue shows a negative Ce and Ho anomaly, whereas the Mars statue has a slightly positive Ho anomaly.

The sample MC35 shows REE enrichment for both LREE and HREE (Fig. B.4).

The high content of Fe+Mn and REE (Fig. B.5) separates sample MC35 (knee) from the other, which shows a similar content of these trace elements. The MC36 sample (right hand of Colossus statue) has the lowest content of the REE.

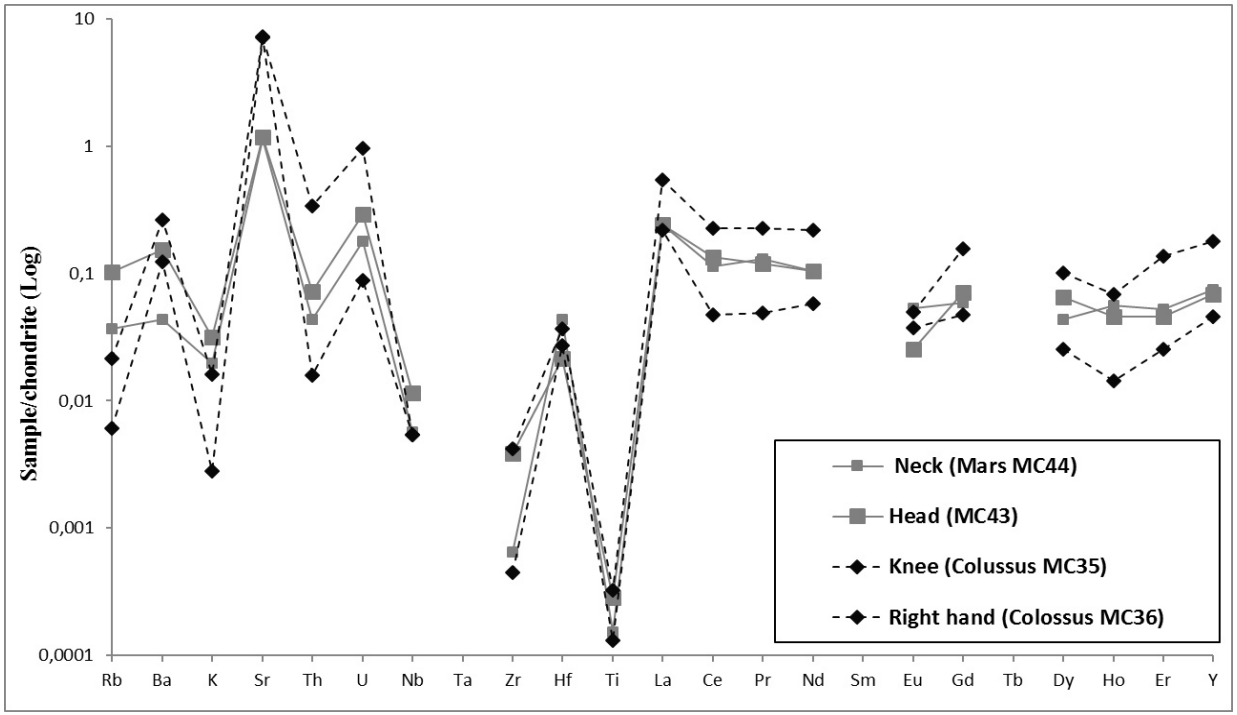

Fig. B.2: Patterns of trace elements in white archaeological samples from Musei Capitolini (Italy). The specimens are displayed using different symbols and lines: continuous line and square symbol for Colossus statue of Constantine (MC35, MC 36); dashed line and rhombus symbol for the Mars statue (MC44, MC43). The concentrations of trace elements are normalized to chondrite (Sun and McDonough (1989)).

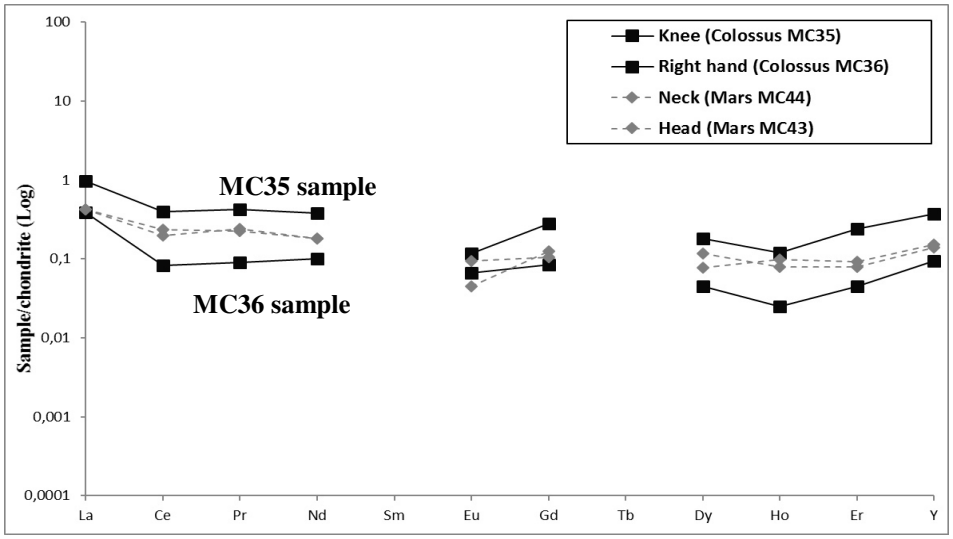

Fig. B.3: Patterns of REE + Y in archaeological samples from Musei Capitolini (Italy). The specimens are displayed using different symbols and lines: continuous line and square symbol for Colossus statue of Constantine (MC35, MC 36); dashed line and rhombus symbol for the Mars statue (MC44, MC43). The concentrations of trace elements are normalized to chondrite (Taylor and McLennan, 1985).

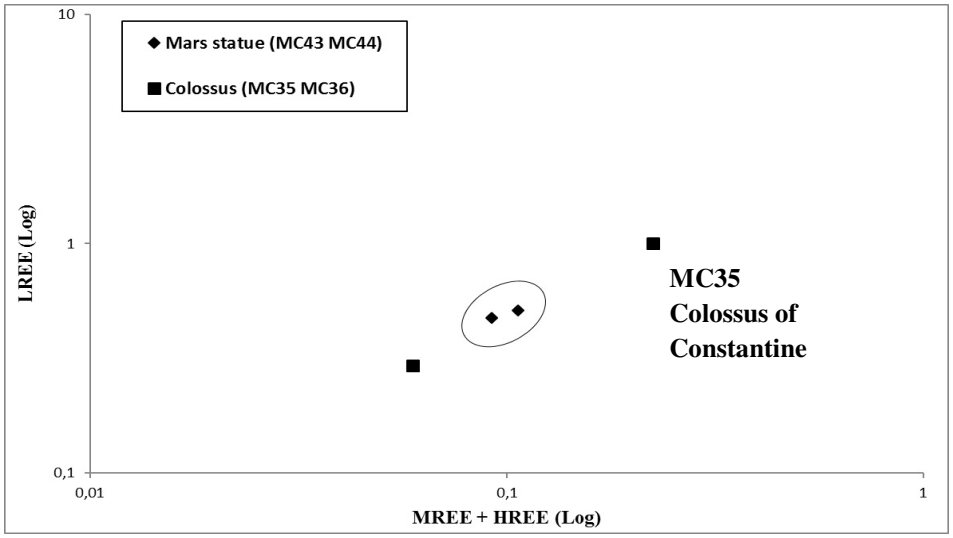

Fig. B.4: MREE+HREE *vs* LREE content in archaeological samples from Musei Capitolini. The MC35 sample (knee of the Colossus statue of Constantine) has enriched in LREE and HREE.

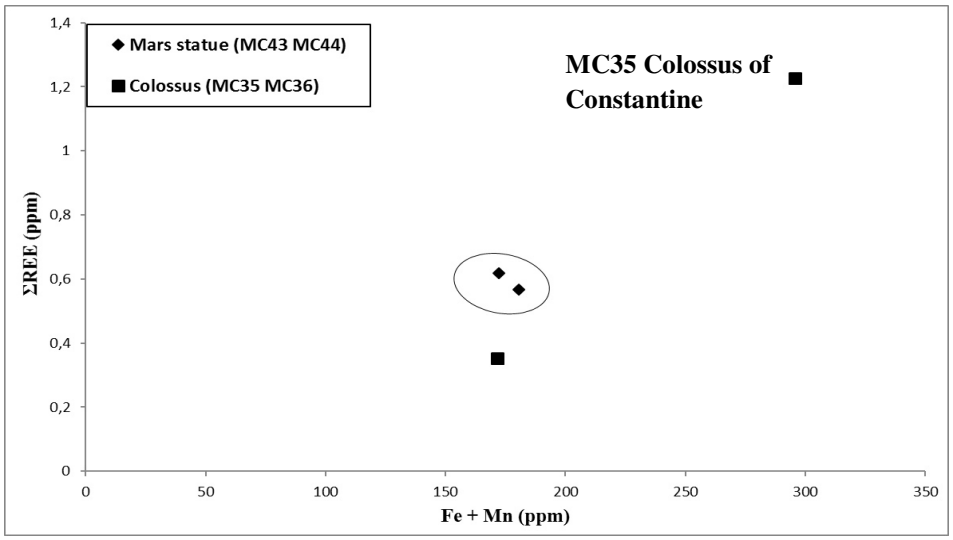

Fig. B.5: Fe+Mn *vs* REE content in samples from Musei Capitolini. The MC35 (knee of the Colossus statue of Constantine) is completely separate from the other three samples.

Archaeological and geological samples

In this section, the content of trace elements in the archaeological samples are compared with that of the geological samples.

In detail, the MC36 sample (right hand of Colossus) has the lowest REE concentrations in comparison with those of geological samples (*i.e.,* Carrara, Paros and Pentelicon) and the other archaeological specimens.

The content of REE of the MC35 sample falls in the range of Carrara marble. In this case, the absence of a negative anomaly of Ce seems to exclude the provenance of the raw material from Paros and Pentelic quarries.

In the PCA chart, the geological and archaeological samples from the Musei Capitolini have been considered (Fig. B.7). The MC 35 sample falls close to Carrara marble, whereas sample MC36 falls farther than the MC35, but completely separate from Paros and Penteli specimens. That finding suggests that the right hand (MC36) marble could come from other districts not considered in this study (*e.g.,* Miseglia or Tornano district).

The sample of the Mars statue exhibits lower REE concentrations than those of geological samples considered here (*i.e.,* Carrara, Paros and Pentelic white marble). The PCA chart highlights that these samples fall far from Carrara, Paros and Pentelicon specimens. The comparison of these data with those of other fine-grained marble, as Göktepe and Afyon specimens, indicates that these samples are not included in any provenance cluster of the PCA chart (Fig. B.8).

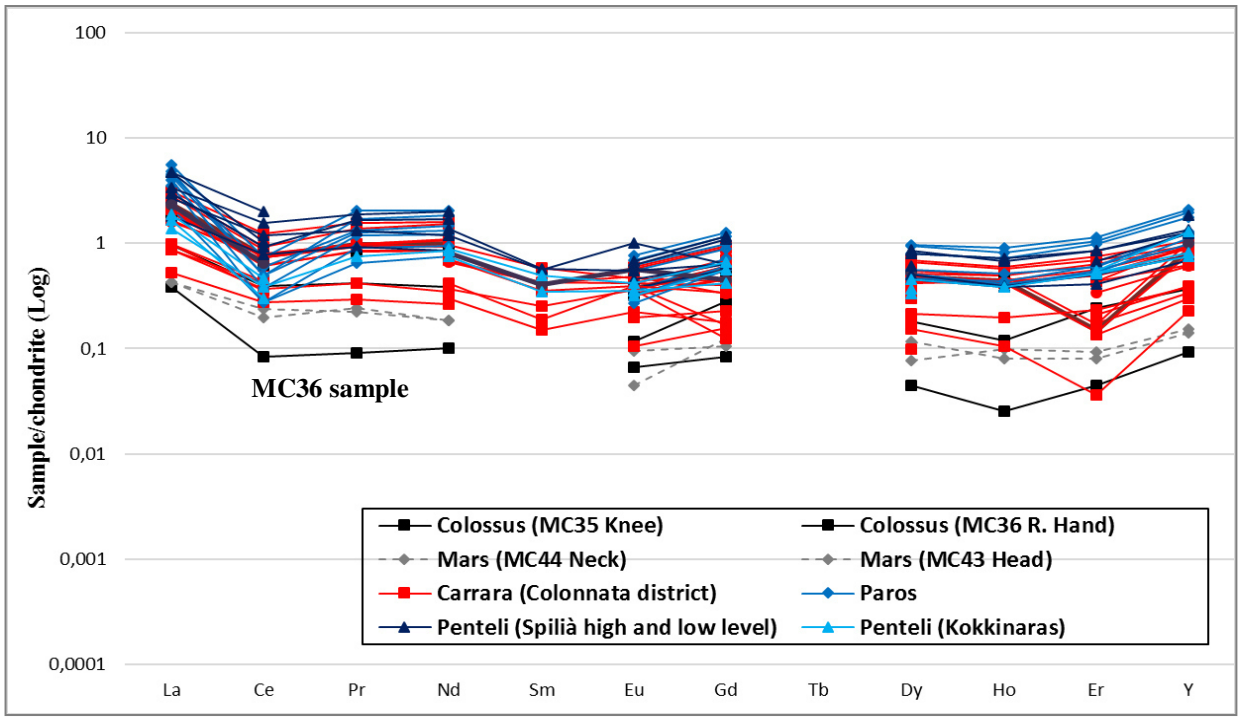

Fig. B.6: Patterns of REE + Y in archaeological samples from Musei Capitolini (Rome) and geological samples from Carrara and Paros districts. The specimens are displayed using different symbols and lines: continuous line and square symbol for Colossus statue of Constantine (MC35, MC 36); dashed line and rhombus symbol for the Mars statue (MC44, MC43); red line and red square symbols for Carrara specimens and light blue line and light blue rhombus for Paros specimens. The concentrations of trace elements are normalized to chondrite (Taylor and McLennan (1985)).

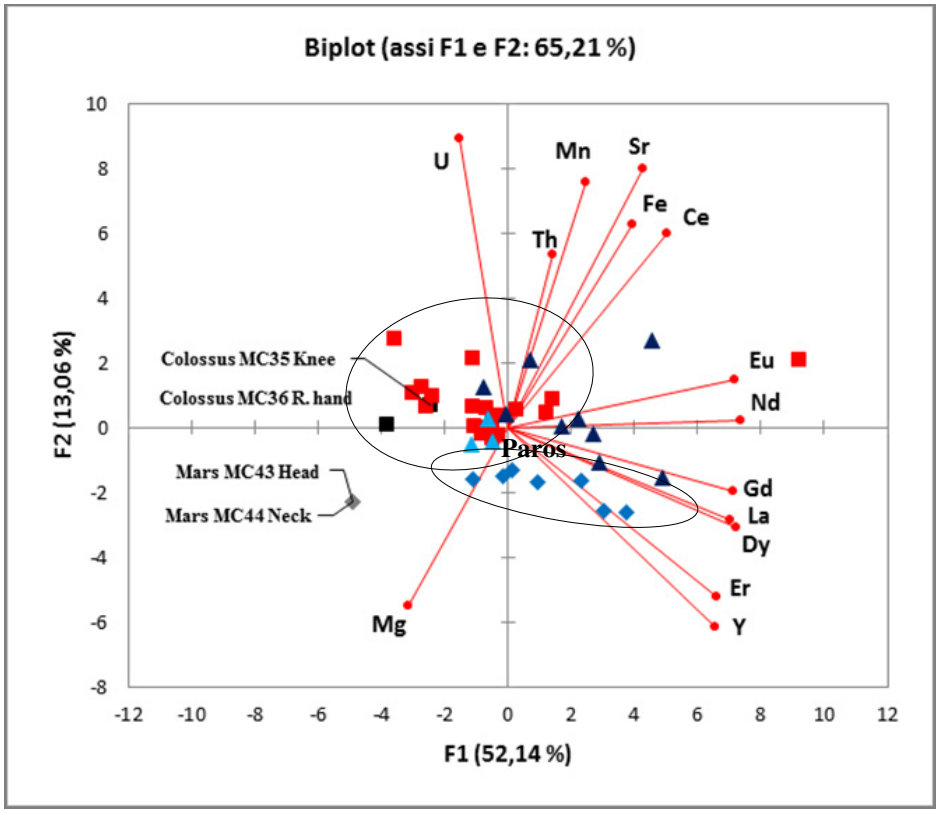

Fig. B.7: PCA chart of geological (Carrara, Paros and Pentelicon) and archaeological samples (Musei Capitolini, Rome). The symbols are: red square, Carrara specimens, light blue rhombus, Paros, dark blue triangle, Pentelicon.

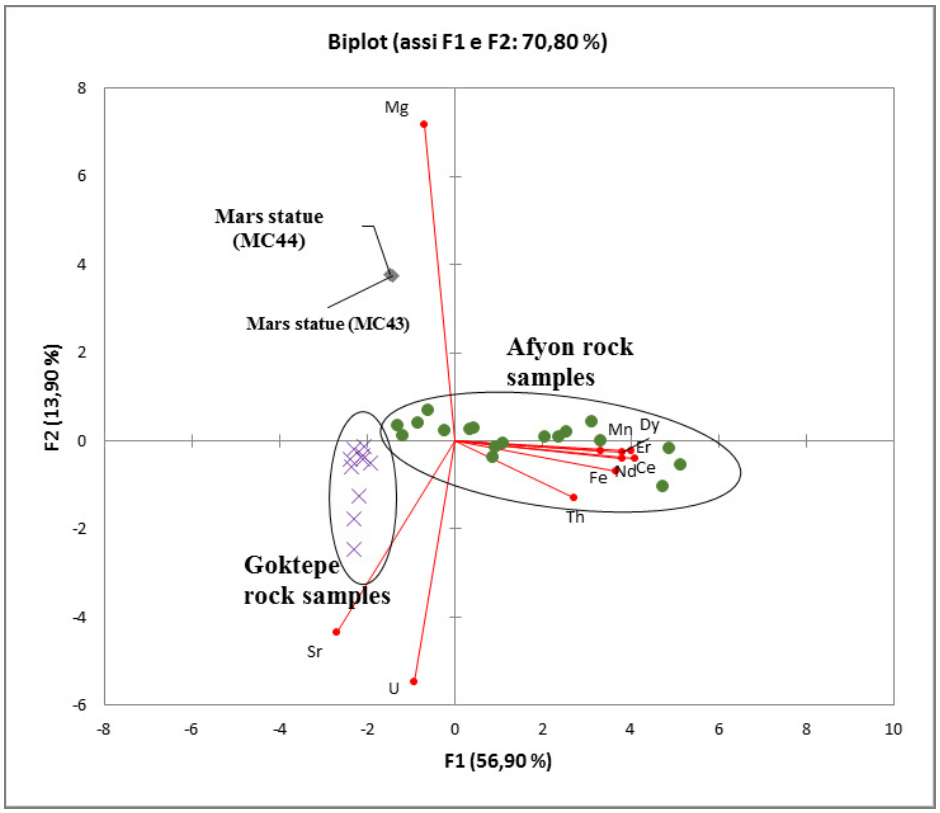

Fig. B.8: PCA chart of Afyon and Göktepe samples and Mars statue specimens (MC43, MC44). The symbols are: green circle for Afyon samples, purple cross for Göktepe specimens.

Future developments and expectations

In this Ph.D. thesis, the use of LA-ICP-MS was applied to archeological samples of an important collection. The present work aimed to test the results of this analytical technique, measuring also the concentrations of the trace elements in archaeological white marble.

What emerges from this research is the need to increase the number of both archaeological and geological samples to be analyzed.

The future development should include a systematic acquisition of LA-ICP-MS data on samples from all Mediterranean quarries active in the past in order to create of a robust and rich database of trace-element composition.

To date, it appears even clearer that a single technique is not able to solve the debated topic of the provenance of white marble. Only the use of more parameters plotted in different diagrams and more variables combined together can provide compositional markers (*e.g.,* trace-element concentrations, patterns of distribution) that allow the comparison of geological samples with those obtained by sampling of ancient white marble artifacts.

This study has shown how a deep understanding of the geochemical composition of the white marble can be helpful to investigate the quarrying sites of white marble.

The trace-element concentration in these rocks becomes a fundamental tool for provenance investigation of artifacts, as shown in this study.

Reference

Mattei M., Lazzarini L., Pensabene P., Turi B., 1997, The provenance of the marble of the late Republican and Imperial sculptures in the Musei Capitolini – Rome, In 4th International Symposium on the Conservation of Monuments in the Mediterranean.

Tab. C1: Trace-element content (ppm) of rock samples from Carrara, district of Colonnata (Gioia and Calagio quarries).

	Gioia								Calagio	
	G5	G6	G7	G8	G16	G 17	G19	G22	CL2	CL6
Li	0.47	0.84	0.11	0.12	0.56	0.14	0.09	0.11	0.15	0.08
B	0.77	1.80	0.64	0.76	0.86	1.08	0.59	0.44	0.76	0.58
Na	6.35	12.58	11.47	341.75	19.53	4.44	12.74	6.13	17.13	6.29
Mg	3978.42	6532.23	5893.33	5492.00	5420.54	4917.50	4722.00	4766.72	6224.00	4752.00
Al	173.15	389.78	6.97	439.72	392.82	20.19	6.21	25.83	13.43	3.53
Si	226.94	728.18	26.51	1079.72	751.11	130.83	69.72	216.24	72.42	61.36
P	8.01	10.06	17.81	10.80	6.88	9.96	10.75	13.67	24.69	32.80
K	123.82	272.02	7.63	19.44	269.56	35.62	9.65	46.60	12.36	5.44
Sc	0.29	0.32	0.05	0.13	0.42	0.19	0.10	0.30	0.27	0.18
Ti	8.16	7.65	0.54	2.71	16.39	4.59	1.59	10.50	4.94	0.41
V	1.07	1.48	0.37	2.25	1.16	0.49	0.70	0.57	1.17	0.98
Cr	1.45	2.16	1.81	1.65	3.80	1.49	0.91	1.74	1.49	1.38
Mn	24.52	30.56	17.37	18.08	16.79	22.23	11.46	14.67	35.42	25.38
Fe	69.64	139.36	56.15	201.00	134.83	109.25	151.60	117.02	172.20	154.60
Co	1.11	1.29	0.06	0.08	1.48	0.05	0.05	1.47	0.1	0.04
Ni	0.32	0.46	0.33	0.38	0.60	0.31	0.30	0.59	0.46	0.3
Cu	0.14	0.13	0.06	0.09	0.27	0.20	0.10	0.15	0.12	0.1
Zn	3.57	4.69	0.97	3.56	3.82	3.11	2.99	5.15	7.23	2.55
Ga	0.11	0.16	0.02	0.12	0.16	0.04	0.03	0.05	0.04	0.02
As	0.51	0.66	0.27	0.08	0.45	0.09	0.09	0.28	0.08	0.05
Rb	0.28	0.69	0.03	0.05	0.72	0.05	0.03	0.09	0.04	0.01
Sr	147.38	140.63	169.50	150.40	178.35	146.00	150.80	152.44	146.80	151.20
Zr	0.74	0.37	0.06	0.83	0.20	0.33	0.10	0.54	0.14	0.12
Nb	0.05	0.04	0.01	0.01	0.07	0.03	0.01	0.09	0.03	0.003
Mo	0.18	0.29	0.14	0.03	0.16	0.05	0.05	0.15	0.053	0.028
Cd	0.26	0.31	0.46	0.44	0.25	0.45	0.48	0.39	0.35	0.28
Sb	0.06	0.04	0.02	0.02	0.05	0.02	0.02	0.04	0.02	0.015
Cs	0.01	0.01	0.01	0.01	0.04	0.005	0.01	0.005	0.007	0.04
Ba	2.67	2.36	3.19	2.00	2.64	1.57	1.50	1.52	1.8	2.29
Hf	0.03	0.02	0.04	0.15	0.02	0.16	0.13	0.02	0.02	0.01
W	0.03	0.04	0.03	0.02	0.04	0.04	0.02	0.02	0.04	0.02
Pb	0.27	0.27	0.18	0.47	0.52	0.45	0.40	0.53	1.59	0.50
Bi	0.03	0.07	0.02	0.02	0.06	0.02	0.01	0.03	0.02	0.004
Th	0.02	0.03	0.01	0.04	0.03	0.03	0.03	0.03	0.04	0.02
U	0.09	0.05	0.21	0.05	0.04	0.02	0.01	0.04	0.1	0.01

Tab. C2: Trace-element content (ppm) of rock samples from Carrara, district of Colonnata. (Fossacava quarries) and Torano district.

	Fossacava							*Torano*
	F01	FO 3	FO7	F08	F09	FO10	FO11	TR 8
Li	0.39	0.23	0.12	0.12	0.07	0.14	1.07	0.12
B	0.92	0.98	0.38	0.60	0.64	0.57	1.61	0.9
Na	25.64	6.73	19.32	24.10	12.63	26.31	30.68	67.7
Mg	5922.00	5078.00	4781.25	4651.25	4880	4920	6359.9	5064
Al	13.58	95.95	35.49	26.82	2.05	62.80	510.95	214.4
Si	80.60	198.26	117.63	103.84	69.26	191.48	910.96	486.8
P	20.50	10.06	9.51	10.79	10.96	34.43	9.30	24.6
K	16.99	72.15	30.25	24.73	4.16	45.70	414.55	86.0
Sc	0.22	0.10	0.20	0.06	0.12	0.31	0.32	0.42
Ti	2.09	4.47	1.69	2.69	0.28	8.05	14.58	25.40
V	0.72	1.01	1.21	0.89	0.30	1.03	2.15	0.42
Cr	1.16	3.16	1.27	1.57	0.96	2.05	1.61	1.57
Mn	32.86	35.38	21.06	25.15	25.38	28.05	30.29	51.12
Fe	476.00	103.90	84.34	130.38	125.20	328.00	408.64	1188.00
Co	0.28	0.07	1.27	0.08	0.11	0.15	1.22	0.30
Ni	1.63	0.32	0.42	0.43	0.41	0.68	0.45	0.70
Cu	0.17	0.12	0.49	0.11	0.11	0.07	0.18	0.14
Zn	1.34	1.63	2.38	1.72	1.47	2.99	6.05	4.16
Ga	0.03	0.04	0.07	0.04	0.03	0.06	0.16	0.1
As	0.10	0.10	0.29	0.32	0.07	0.08	0.81	0.12
Rb	0.04	0.16	0.11	0.10	0.02	0.10	1.08	0.22
Sr	142.20	146.00	153.58	144.38	163.20	105.75	143.83	235.60
Zr	0.77	0.24	0.41	0.18	0.03	0.35	0.28	1.6
Nb	0.01	0.02	0.03	0.01	0.003	0.04	0.04	0.12
Mo	0.14	0.05	0.13	0.10	0.04	0.04	0.24	0.06
Cd	0.25	0.51	0.31	0.39	0.47	0.35	0.44	0.300
Sb	0.02	0.02	0.03	0.04	0.02	0.02	0.05	0.023
Cs	0.01	0.01	0.01	0.03	0.003	0.004	0.04	0.007
Ba	1.09	1.32	1.21	1.72	1.01	2.82	1.65	1.58
Hf	0.02	0.02	0.02	0.01	0.01	0.02	0.02	0.04
W	0.02	0.03	0.02	0.05	0.02	0.03	0.03	0.03
Pb	0.42	0.39	0.31	0.41	0.31	0.63	0.54	2.35
Bi	0.01	0.01	0.02	0.08	0.01	0.01	0.02	0.010
Th	0.02	0.02	0.01	0.03	0.02	0.10	0.06	0.04
U	0.05	0.02	0.07	0.04	0.004	0.06	0.10	0.06

Tab. C3: REE+Y content (ppm) of rock samples from Carrara, district of Colonnata (Gioia and Calagio quarries).

	Gioia								*Calagio*	
	G5	G6	G7	G8	G16	G 17	G19	G22	CL2	CL6
La	0.32	0.36	0.19	0.85	0.61	0.71	0.81	1.03	1.10	0.84
Ce	0.40	0.41	0.26	0.72	0.67	0.76	0.70	0.83	0.89	0.70
Nd	0.26	0.30	0.19	0.71	0.49	0.66	0.67	0.69	1.08	0.76
Eu	0.03	0.03	0.01	0.03	0.04	0.03	0.03	0.04	0.05	0.04
Gd	0.04	0.05	0.05	0.18	0.12	0.19	0.14	0.13	0.28	0.20
Dy	0.08	0.07	0.06	0.18	0.11	0.20	0.17	0.14	0.26	0.17
Er	0.04	0.05	0.01	0.04	0.11	0.04	0.04	0.11	0.19	0.12
Y	0.71	0.82	0.48	1.83	1.32	2.16	1.65	2.03	2.22	1.66

Tab. C4: REE +Y content (ppm) of rock samples from Carrara, district of Colonnata (Fossacava quarry) and Torano district.

	Fossacava							*Torano*
	F01	FO 3	FO7	F08	F09	FO10	FO11	TR 8
La	0.73	0.75	0.36	0.32	0.71	1.15	0.59	2.40
Ce	0.71	0.58	0.33	0.35	0.60	1.17	0.74	2.74
Nd	0.78	0.61	0.21	0.24	0.60	1.13	0.47	2.64
Eu	0.04	0.03	0.02	0.02	0.03	0.05	0.04	0.13
Gd	0.22	0.14	0.05	0.07	0.17	0.29	0.10	0.60
Dy	0.21	0.16	0.04	0.08	0.19	0.25	0.12	0.50
Er	0.16	0.12	0.03	0.06	0.14	0.17	0.08	0.31
Y	1.91	1.91	0.63	0.81	1.86	1.98	1.27	4.19

Tab. C5: Trace-element content (ppm) of rock samples from Paros Island.

	Paros								*PAROS1*
	CYPA3	CYPA 5	CYPA11	CYPA12	CYPA14	CYPA25	CYPA26	CYPA28	PAROS 1
Li	0.05	0.12	0.05	0.06	0.05	0.05	0.06	0.05	0.10
B	0.41	1.50	0.52	0.69	0.64	1.02	0.48	0.54	0.86
Na	4.11	8.38	4.20	3.34	2.89	8.06	2.28	3.48	44.74
Mg	1932.50	2590	2030	6100	3664	2016	2516	3896	3390
Al	0.10	0.94	0.84	0.17	0.17	0.36	0.30	0.12	638.31
Si	59.83	83.62	55.82	57.36	52.12	51.40	42.46	40.64	1766.83
P	10.25	11.11	8.82	9.65	8.13	8.05	7.90	7.79	11.98
K	0.66	4.13	1.79	1.13	1.22	1.65	0.52	0.81	774.16
Sc	0.21	0.17	0.08	0.18	0.07	0.12	0.08	0.08	0.12
Ti	0.16	0.29	0.21	0.22	0.20	0.20	0.19	0.17	0.41
V	0.06	0.06	0.04	0.09	0.08	0.09	0.07	0.05	0.84
Cr	0.65	0.68	0.58	0.52	0.79	0.69	0.71	0.59	2.71
Mn	8.61	11.24	6.03	18.02	5.33	6.78	12.08	11.26	31.38
Fe	147.25	89.52	127.80	152.60	132.60	138.40	143.40	143.40	223.00
Co	0.04	0.03	0.06	0.04	0.05	0.05	0.05	0.04	0.03
Ni	0.18	0.18	0.24	0.25	0.28	0.24	0.20	0.20	0.25
Cu	0.09	0.48	0.12	0.11	0.07	0.10	0.08	0.09	0.16
Zn	0.58	0.69	0.45	1.19	0.93	0.38	0.44	0.66	1.03
Ga	0.03	0.06	0.02	0.03	0.03	0.02	0.02	0.02	0.09
As	0.10	0.24	0.07	0.36	0.23	0.09	0.10	0.09	0.13
Rb	0.005	0.02	0.01	0.01	0.01	0.01	0.00	0.01	1.87
Sr	113.25	142.6	82.44	181.40	140.80	124.60	111.00	134.40	130.93
Nb	0.003	0.01	0.002	0.003	0.004	0.004	0.002	0.003	0.01
Mo	0.03	0.05	0.03	0.04	0.03	0.04	0.03	0.03	0.08
Cd	0.23	0.30	0.22	0.22	0.14	0.16	0.10	0.13	0.17
Sb	0.02	0.03	0.02	0.02	0.02	0.02	0.02	0.01	0.04
Cs	0.002	0.004	0.002	0.004	0.003	0.002	0.01	0.003	0.09
Ba	1.60	1.16	0.85	1.60	1.08	1.16	0.72	0.72	7.99
Hf	0.01	0.02	0.01	0.01	0.01	0.01	0.01	0.01	0.02
W	0.02	0.04	0.02	0.02	0.02	0.02	0.01	0.02	0.16
Pb	0.32	0.42	0.36	1.61	1.22	0.58	0.32	0.32	0.39
Bi	0.01	0.02	0.005	0.02	0.02	0.01	0.004	0.01	0.02
Th	0.003	0.01	0.02	0.01	0.01	0.01	0.01	0.01	0.06
U	0.002	0.01	0.002	0.004	0.01	0.00	0.004	0.01	0.08

Tab. C6: REE +Y content (ppm) of rock samples from Paros Island.

	Paros								*PAROS1*
	CYPA3	CYPA 5	CYPA11	CYPA12	CYPA14	CYPA25	CYPA26	CYPA28	PAROS 1
La	5.09	2.06	0.79	1.60	1.30	1.77	1.64	1.47	0.44
Ce	0.52	0.70	0.26	0.48	0.27	0.48	0.57	0.36	0.61
Pr	0.58	0.28	0.09	0.17	0.12	0.23	0.18	0.16	0.08
Nd	3.37	1.47	0.53	0.94	0.68	1.32	1.05	0.85	0.36
Eu	0.14	0.07	0.02	0.05	0.03	0.06	0.05	0.03	0.02
Gd	0.94	0.39	0.17	0.30	0.19	0.36	0.27	0.22	0.07
Dy	0.85	0.37	0.17	0.30	0.18	0.36	0.21	0.20	0.06
Ho	0.17	0.08	0.03	0.06	0.04	0.07	0.04	0.04	0.01
Er	0.60	0.28	0.14	0.24	0.15	0.26	0.15	0.13	0.04
Y	8.96	4.43	2.08	3.67	2.71	4.12	2.67	2.36	0.58

Tab. C7: Trace-element content (ppm) of rock samples from Mt Pentelicon, Splià district (quarry 13-15, quarry 6-8).

	Quarry 13-15 Spilià - Low level						*Quarry 6-8 Spilià - High level*			
	SML 1.1	SML2.4	SML13	SML14	SML33	SML42	SMH 1.3	SMH1.9	SMH2.18	SMH2.21
Li	0.38	0.16	0.24	0.13	0.25	0.21	0.22	0.23	0.25	0.09
B	1.47	1.66	1.06	0.65	1.38	0.78	1.33	0.69	0.69	0.46
Na	87.83	100.42	13.51	63.11	78.69	60.86	47.04	33.08	49.12	5.96
Mg	3685.00	2126.00	2105.72	3512.42	2869.25	4059.99	2875.00	3954.02	2347.46	2960.00
Al	69.87	595.72	3.35	10.73	1.02	0.60	0.20	0.69	4.02	0.36
Si	183.07	633.74	232.60	131.79	221.00	149.53	74.60	189.66	2042.26	119.25
P	9.14	9.06	14.17	7.69	18.14	9.86	9.01	8.57	10.55	19.29
K	52.26	189.44	6.75	11.00	7.06	7.05	3.36	5.29	10.20	1.06
Sc	0.09	0.07	0.48	0.32	0.54	0.34	0.10	0.37	0.42	0.08
Ti	0.58	1.49	3.17	3.01	2.76	1.96	0.37	2.02	1.97	0.21
V	0.17	0.20	0.54	0.45	0.59	0.34	0.15	0.36	0.42	0.14
Cr	0.83	0.93	1.75	1.31	2.57	1.81	0.71	1.92	1.81	0.72
Mn	149.75	42.66	63.12	120.41	142.64	54.47	53.70	38.30	72.60	66.10
Fe	478.00	261.60	136.03	234.38	271.14	224.04	126.25	132.98	147.34	289.00
Co	0.04	0.07	1.50	1.18	1.44	1.44	0.04	1.61	1.53	0.17
Ni	0.37	0.32	0.66	0.38	0.63	0.43	0.30	0.58	0.53	0.36
Cu	0.12	0.11	1.06	0.27	0.59	0.14	0.13	0.12	4.09	0.09
Zn	2.86	3.30	7.62	4.75	8.38	2.74	1.67	4.76	3.45	3.06
Ga	0.05	0.10	0.12	0.08	0.14	0.13	0.03	0.08	0.10	0.03
As	0.15	0.06	0.81	0.62	1.07	0.50	0.11	0.45	0.41	0.13
Rb	0.15	0.43	0.14	0.09	0.12	0.08	0.01	0.07	0.08	0.01
Sr	176.50	150.20	154.52	158.29	175.70	171.59	143.25	187.65	162.77	156.00
Zr	0.06	0.46	0.28	0.10	0.07	0.05	0.53	0.03	0.07	0.23
Nb	0.01	0.01	0.06	0.03	0.07	0.04	0.01	0.03	0.03	0.01
Mo	0.05	0.04	0.37	0.23	0.46	0.15	0.07	0.22	0.19	0.43
Cd	0.18	0.14	0.71	0.38	0.63	0.30	0.20	0.37	0.32	0.21
Sb	0.02	0.02	0.06	0.07	0.06	0.04	0.05	0.06	0.04	0.03
Cs	0.02	0.01	0.01	0.02	0.01	0.02	0.01	0.02	0.01	0.01
Ba	1.12	1.20	0.49	0.38	0.20	0.44	0.64	0.61	0.61	0.75
Hf	0.02	0.02	0.02	0.01	0.03	0.01	0.02	0.02	0.01	0.01
W	0.03	0.02	0.07	0.04	0.04	0.03	0.03	0.03	0.03	0.02
Pb	3.82	2.38	2.58	2.33	1.45	1.66	1.21	1.78	1.36	2.79
Bi	0.01	0.01	0.06	0.03	0.30	0.08	0.01	0.05	0.05	0.01
Th	0.01	0.03	0.01	0.01	0.01	0.01	0.09	0.01	0.01	0.004
U	0.01	0.02	0.01	0.01	0.005	0.01	0.03	0.002	0.01	0.01

Tab. C8: Trace-element content (ppm) of rock samples from Mt Pentelicon, Kokkinaras district and quarry I.

	Kokkinaras			*Quarry I*	
	K3	K5	K7	I-1	I-2
Li	0.09	0.27	0.09	0.09	0.08
B	0.57	0.76	0.63	1.02	0.74
Na	1.70	6.25	8.86	11.07	11.40
Mg	484.68	566.71	1515.00	2522.50	4286.00
Al	3.06	0.99	0.70	0.45	1.00
Si	138.53	203.95	99.82	85.55	98.04
P	6.24	17.98	9.95	9.69	41.80
K	5.07	7.86	1.62	5.38	4.23
Sc	0.27	0.40	0.14	0.04	0.04
Ti	1.73	1.96	0.19	0.23	0.25
V	0.30	0.41	0.15	0.03	0.03
Cr	1.61	3.16	0.82	1.27	1.16
Mn	8.54	28.12	82.32	25.13	22.00
Fe	62.44	99.32	312.60	81.65	148.00
Co	1.39	1.54	0.09	0.07	0.08
Ni	0.52	0.93	0.27	0.28	0.39
Cu	0.10	0.21	0.12	0.19	0.30
Zn	13.74	2.85	1.33	0.94	1.39
Ga	0.07	0.09	0.02	0.02	0.02
As	0.32	0.52	0.12	1.91	0.10
Rb	0.06	0.09	0.01	0.02	0.02
Sr	163.70	131.27	136.20	136.25	178.40
Zr	0.04	0.23	0.01	0.04	0.04
Nb	0.03	0.04	0.003	0.01	0.003
Mo	0.17	0.25	0.04	0.06	0.03
Cd	0.20	0.40	0.16	0.16	0.11
Sb	0.04	0.05	0.02	0.03	0.02
Cs	0.002	0.01	0.005	0.004	0.01
Ba	0.58	1.27	1.85	1.47	0.72
Hf	0.01	0.03	0.01	0.02	0.01
W	0.02	0.04	0.03	0.03	0.02
Pb	2.58	0.53	1.25	0.42	1.06
Bi	0.02	0.05	0.01	0.01	0.01
Th	0.01	0.02	0.01	0.01	0.01
U	0.01	0.05	0.01	0.004	6.71

Tab. C9: REE +Y content (ppm) of rock samples from from Mt Pentelicon, Splià district (quarry 13-15. quarry 6-8).

	Quarry 13-15 Spilià - Low level						*Quarry 6-8 Spilià - High level*			
	SML 1.1	SML2.4	SML13	SML14	SML33	SML42	SMH 1.3	SMH1.9	SMH2.18	SMH2.21
La	1.02	1.24	1.75	0.77	2.32	0.85	1.10	2.33	1.75	0.62
Ce	1.18	1.50	0.97	0.72	5.22	0.62	0.89	1.63	1.92	0.71
Nd	0.87	1.42	0.85	0.50	1.83	0.58	1.22	1.53	0.98	0.58
Eu	0.03	0.06	0.09	0.03	0.10	0.05	0.05	0.08	0.05	0.04
Gd	0.18	0.35	0.20	0.10	0.28	0.14	0.33	0.30	0.20	0.19
Dy	0.17	0.32	0.33	0.13	0.23	0.20	0.30	0.43	0.23	0.18
Er	0.10	0.21	0.25	0.08	0.09	0.09	0.21	0.30	0.17	0.13
Y	1.48	2.65	3.87	1.40	1.71	2.11	2.83	4.37	2.62	1.58

Tab. C10: REE +Y content (ppm) of rock samples from Mt Pentelicon, Kokkinaras district and quarry I.

	Kokkinaras			*Quarry I*	
	K3	K5	K7	I-1	I-2
La	0.60	0.69	0.50	0.16	0.18
Ce	0.29	0.45	0.37	0.15	0.21
Nd	0.53	0.62	0.60	0.11	0.12
Eu	0.03	0.04	0.03	0.01	0.01
Gd	0.13	0.20	0.17	0.04	0.02
Dy	0.13	0.14	0.17	0.03	0.02
Er	0.13	0.14	0.13	0.03	0.01
Y	1.71	2.68	1.58	0.36	0.22

Tab. C11: Trace-element content (ppm) of rock samples from Afyon, Bacakale and Roder districts.

	Quarry I Bacakale				*Quarry II Roder*					
	D2A	D9A	D11A	D14 A	D26A	D 27A	D28 A	D34A	D36A	D37A
Li	0.16	0.07	0.05	0.05	0.18	0.11	0.15	0.06	0.24	0.25
B	0.58	0.47	0.47	0.79	0.58	1.16	1.04	0.38	0.73	0.70
Na	12.33	5.90	3.43	2.67	1.77	3.74	5.25	5.16	7.17	11.84
Mg	1370.4	1396.4	1586	771.6	976.8	1696	1837.5	2890	2503.12	2725.02
Al	6.56	1.91	0.55	2.55	4.72	3.25	0.70	7.68	0.54	13.27
Si	152.81	61.74	61.78	48.42	202.25	113.24	52.88	53.98	194.46	259.24
P	11.27	26.82	13.62	15.19	11.13	120.22	22.30	14.93	18.11	25.43
K	9.10	3.32	2.78	2.28	8.19	1.97	0.76	3.06	5.00	13.21
Sc	0.34	0.05	0.09	0.03	0.32	0.05	0.11	0.07	0.35	0.43
Ti	2.22	1.11	0.19	0.40	2.57	0.62	0.18	0.30	2.82	2.73
V	0.48	0.50	0.17	0.14	0.63	0.37	0.70	0.44	0.48	0.52
Cr	1.36	0.74	0.71	1.14	1.78	1.09	0.95	1.00	2.15	2.32
Mn	82.64	48.58	85.70	163.12	139.01	141.00	118.75	189.40	93.56	138.39
Fe	467.91	295.60	358.80	264.80	174.94	254.20	466.75	593.00	382.61	402.23
Co	1.38	0.08	0.09	0.08	1.60	0.36	0.27	0.60	1.86	1.98
Ni	0.59	0.27	0.35	0.38	0.49	0.72	0.54	2.50	1.19	2.94
Cu	0.18	0.48	0.23	0.18	0.61	0.81	2.08	0.09	6.82	2.22
Zn	5.40	1.87	2.74	0.75	3.06	1.91	1.75	4.16	6.73	7.17
Ga	0.10	0.03	0.02	0.02	0.08	0.03	0.05	0.02	0.08	0.08
As	0.51	0.10	0.06	0.07	0.49	0.12	0.07	0.06	0.48	0.55
Rb	0.10	0.01	0.01	0.01	0.08	0.01	0.01	0.02	0.08	0.11
Sr	91.96	69.34	44.74	46.62	99.41	128.28	111.65	122.80	128.42	123.62
Zr	0.63	0.24	0.07	0.07	0.28	0.08	0.15	0.48	1.40	0.38
Nb	0.04	0.01	0.002	0.004	0.03	0.01	0.004	0.003	0.04	0.04
Mo	0.27	0.04	0.03	0.12	1.58	0.10	0.04	0.03	1.49	0.22
Cd	0.30	0.19	0.26	0.22	0.38	0.24	0.33	0.35	0.66	0.54
Sb	0.06	0.02	0.02	0.01	0.07	0.03	0.02	0.02	0.06	0.04
Cs	0.01	0.01	0.003	0.004	0.004	0.01	0.01	0.01	0.01	0.01
Ba	0.31	0.36	0.24	1.29	0.68	0.60	0.37	0.54	0.34	0.74
Hf	0.01	0.01	0.01	0.01	0.02	0.02	0.01	0.01	0.02	0.02
W	0.04	0.02	0.02	0.02	0.04	0.03	0.02	0.02	0.04	0.05
Pb	0.76	0.43	0.46	0.68	1.64	0.98	1.04	1.40	0.95	1.38
Bi	0.03	0.01	0.01	0.02	0.23	0.03	0.03	0.01	0.19	0.05
Th	0.03	0.04	0.01	0.002	0.01	0.01	0.01	0.01	0.03	0.01
U	0.02	0.03	0.003	0.01	0.03	0.02	0.02	0.02	0.04	0.01

Tab. C12: Trace-element content (ppm) of rock samples from Afyon, Boluk Mermer and Mermer Isletmesi districts.

	Quarry V Boluk Mermer				*Quarry III-IV*			
	D38A	D39A	D40A	D43A	D59	D62	D64	D68
Li	0.07	0.11	0.09	0.13	0.20	0.19	0.11	0.14
B	0.32	0.46	0.80	0.54	0.77	0.56	0.54	0.50
Na	6.80	12.84	3.07	8.87	40.08	5.69	8.23	18.23
Mg	1704.00	3345.00	1938.00	2646.49	1335.16	4271.69	2824.00	2842.00
Al	89.84	15.54	12.67	1.77	2.93	0.66	18.75	12.19
Si	222.22	78.83	107.08	180.14	258.32	157.24	78.14	667.70
P	18.87	31.40	41.86	17.04	23.01	10.86	26.37	12.59
K	66.08	13.83	8.30	6.30	5.11	7.30	11.61	9.65
Sc	0.10	0.28	0.06	0.30	0.41	0.34	0.25	0.05
Ti	3.27	0.63	0.38	2.35	2.82	2.04	0.85	1.59
V	0.47	0.41	0.58	1.09	0.83	0.86	0.36	0.14
Cr	1.12	0.71	0.99	1.63	2.34	2.20	1.06	1.45
Mn	224.00	359.50	93.70	236.27	46.01	70.83	159.80	25.32
Fe	566.80	359.25	184.40	97.53	174.29	148.35	398.60	187.80
Co	0.27	0.48	0.15	1.76	1.64	1.74	0.09	0.12
Ni	0.80	0.86	0.59	0.50	0.68	0.46	0.35	0.36
Cu	0.52	2.30	1.09	1.12	13.96	0.16	0.20	0.17
Zn	1.92	2.44	3.35	3.69	4.64	3.30	1.49	1.17
Ga	0.05	0.05	0.03	0.07	0.10	0.09	0.04	0.02
As	0.07	0.17	0.11	0.38	0.51	0.44	0.08	0.05
Rb	0.15	0.05	0.03	0.08	0.11	0.08	0.04	0.04
Sr	110.80	129.25	186.60	154.89	450.14	272.46	137.80	174.20
Zr	0.42	2.56	0.68	0.14	0.08	0.05	0.38	0.25
Nb	0.01	0.003	0.01	0.04	0.04	0.04	0.01	0.01
Mo	0.04	0.29	0.30	0.18	0.28	0.27	0.05	0.03
Cd	0.29	0.46	0.28	0.32	0.36	0.43	0.37	0.13
Sb	0.01	0.05	0.02	0.03	0.06	0.05	0.02	0.02
Cs	0.01	0.01	0.004	0.01	0.01	0.01	0.01	0.01
Ba	2.03	0.97	1.36	0.94	0.87	1.05	0.57	1.26
Hf	0.06	0.02	0.01	0.01	0.03	0.02	0.01	0.01
W	0.02	0.04	0.03	0.04	0.03	0.02	0.02	0.01
Pb	1.21	2.83	3.07	1.24	1.50	0.43	0.59	0.29
Bi	0.01	0.02	0.02	0.05	0.06	0.01	0.01	0.01
Th	0.04	0.01	0.01	0.01	0.01	0.02	0.01	0.01
U	0.06	0.03	0.02	0.01	0.02	0.01	0.01	0.03

Tab. C13: REE +Y content (ppm) of rock samples from Afyon, Bacakale and Roder districts.

	Quarry I Bacakale				*Quarry II Roder*					
	D2A	D9A	D11A	D14 A	D26A	D 27A	D28 A	D34A	D36A	D37A
La	0.98	0.69	0.80	0.09	0.40	0.53	0.55	0.51	0.59	1.13
Ce	1.09	0.42	0.72	0.09	0.28	0.60	0.74	1.07	0.69	1.32
Nd	1.59	0.59	0.91	0.08	0.29	0.54	0.69	1.12	0.41	0.90
Eu	0.10	0.03	0.05	0.01	0.03	0.03	0.04	0.05	0.03	0.04
Gd	0.47	0.15	0.27	0.03	0.08	0.10	0.22	0.26	0.09	0.15
Dy	0.51	0.16	0.36	0.03	0.10	0.08	0.20	0.21	0.09	0.16
Er	0.24	0.11	0.28	0.02	0.05	0.05	0.14	0.13	0.05	0.13
Y	4.51	1.58	4.04	0.27	0.92	0.79	1.62	1.47	0.81	2.16

Tab. C14: REE +Y content (ppm) of rock samples from Afyon, Boluk Mermer and Mermer Isletmesi districts.

	Quarry V Boluk Mermer				*Quarry III-IV*			
	D38A	D39A	D40A	D43A	D59	D62	D64	D68
La	0.85	1.30	0.61	0.53	1.67	0.26	0.45	0.25
Ce	1.51	1.35	0.40	0.78	0.75	0.13	0.88	0.32
Nd	0.98	1.24	0.55	0.39	1.40	0.16	0.91	0.23
Eu	0.03	0.05	0.03	0.03	0.06	0.03	0.05	0.01
Gd	0.22	0.26	0.19	0.06	0.28	0.04	0.23	0.06
Dy	0.21	0.30	0.22	0.07	0.22	0.05	0.21	0.05
Er	0.15	0.23	0.17	0.05	0.14	0.03	0.12	0.03
Y	1.83	2.61	2.70	0.81	2.68	0.47	1.72	0.53

Tab. C15: Trace-element content (ppm) of rock samples from Göktepe.

	GT1	GT2	GT4	GT5	GT6	GT7	GT8	GT9	GT10	GT11	GT12
Li	0.05	0.10	0.17	0.15	0.06	0.09	0.08	0.07	0.12	0.18	0.25
B	0.66	1.28	5.79	0.59	0.55	0.94	0.60	1.19	1.22	1.64	4.04
Na	12.32	22.18	46.40	12.83	13.67	24.24	17.28	14.20	16.86	35.36	49.30
Mg	2250	3782.5	2236	2304	2146	2170	2382.5	2310	2480	2544	2792.5
Al	0.44	2.31	1.68	1.98	1.12	1.08	0.75	0.76	0.65	2.35	4.76
Si	50.83	39.35	91.66	49.36	40.38	49.00	44.68	44.90	82.60	114.62	217.18
P	10.35	9.57	10.42	14.32	13.14	9.43	8.10	10.74	14.00	23.40	28.13
Cl	129.00	145.00	158.60	119.00	113.26	122.75	123.75	154.25	147.25	158.20	163.00
K	10.57	1.47	29.99	1.24	1.28	2.90	1.38	27.45	26.56	49.37	70.60
Sc	0.04	0.04	0.05	0.05	0.04	0.05	0.04	0.04	0.05	0.05	0.05
Ti	0.21	0.20	0.26	0.23	0.20	0.26	0.21	0.23	0.22	0.27	0.32
V	0.26	6.78	0.62	0.36	0.31	0.25	0.30	0.25	0.26	0.37	0.65
Cr	0.66	2.69	1.05	1.12	0.86	0.79	1.03	0.85	0.78	1.06	1.20
Mn	1.68	1.14	1.45	1.46	1.88	1.87	1.35	0.95	2.24	2.96	4.47
Fe	159.75	166.75	170.60	184.00	161.80	172.25	160	167.25	166.75	174.80	179.00
Co	0.06	0.07	0.15	0.07	0.06	0.06	0.05	0.07	0.10	0.14	0.22
Ni	0.33	0.31	0.44	0.91	0.26	0.27	0.19	0.43	0.35	0.43	0.61
Cu	0.11	0.13	0.27	0.15	0.08	0.13	0.08	0.28	0.61	0.51	1.60
Zn	0.19	0.12	0.22	0.20	0.18	0.17	0.08	0.84	0.24	0.48	1.11
Ga	0.02	0.02	0.07	0.03	0.02	0.03	0.02	0.02	0.02	0.04	0.12
As	0.07	0.07	0.31	0.24	0.12	0.14	0.11	0.21	0.14	0.30	0.53
Rb	0.03	0.06	0.13	0.02	0.01	0.02	0.01	0.07	0.09	0.17	0.49
Sr	701	460	528.6	440.6	457.8	453.25	427.75	784.25	837	834.8	832.5
Zr	0.01	0.01	0.01	0.01	0.01	0.01	0.004	0.01	0.01	0.03	0.05
Nb	0.005	0.004	0.03	0.01	0.00	0.01	0.004	0.005	0.004	0.01	0.02
Mo	0.15	0.03	0.09	0.32	0.18	0.04	0.10	0.03	0.06	0.07	0.13
Cd	0.12	0.07	0.16	0.11	0.10	0.11	0.09	0.07	0.12	0.12	0.16
Sn	0.02	0.05	0.11	0.04	0.02	0.03	0.04	0.02	0.02	0.06	0.13
Sb	0.01	0.02	0.09	0.04	0.02	0.02	0.02	0.02	0.02	0.03	0.09
Cs	0.01	0.02	0.04	0.03	0.004	0.01	0.004	0.005	0.002	0.02	0.09
Ba	0.95	1.14	1.25	0.96	0.72	0.75	0.83	1.35	1.20	1.52	2.02
Hf	0.02	0.01	0.01	0.01	0.01	0.01	0.01	0.02	0.02	0.02	0.02
W	0.03	0.05	0.08	0.03	0.03	0.02	0.02	0.02	0.02	0.04	0.11
Pb	0.13	0.12	0.09	0.06	0.04	0.08	0.06	0.28	0.14	0.20	0.39
Bi	0.01	0.01	0.02	0.02	0.005	0.01	0.01	0.01	0.01	0.03	0.04
Th	0.00	0.00	0.01	0.01	0.003	0.002	0.003	0.003	0.004	0.003	0.01
U	0.01	0.14	0.07	0.04	0.04	0.02	0.04	0.01	0.01	0.01	0.07

Tab. C16: REE +Y content (ppm) of rock samples from Göktepe.

	GT1	GT2	GT4	GT5	GT6	GT7	GT8	GT9	GT10	GT11	GT12
La	0.02	0.09	0.04	0.03	0.02	0.02	0.03	0.02	0.02	0.03	0.06
Ce	0.02	0.09	0.09	0.03	0.02	0.02	0.02	0.02	0.02	0.04	0.11
Pr	0.003	0.02	0.02	0.02	0.004	0.004	0.01	0.004	0.003	0.01	0.04
Nd	0.02	0.07	0.04	0.03	0.02	0.02	0.02	0.02	0.02	0.02	0.06
Eu	0.01	0.02	0.01	0.01	0.01	0.02	0.01	0.003	0.01	0.01	0.02
Gd	0.02	0.02	0.02	0.03	0.02	0.03	0.03	0.02	0.02	0.03	0.03
Dy	0.01	0.02	0.01	0.02	0.02	0.01	0.02	0.01	0.01	0.02	0.02
Ho	0.004	0.004	0.005	0.004	0.003	0.003	0.005	0.003	0.003	0.051	0.004
Er	0.02	0.01	0.01	0.02	0.02	0.02	0.02	0.02	0.01	0.02	0.02
Y	0.03	0.16	0.04	0.05	0.04	0.03	0.06	0.04	0.04	0.04	0.04

Tab. C17: Trace-element content (ppm) of rock samples from Naxos Island.

	CY-NA70	CY-NA 72	CY-NA75	CYNA77	CYNA 78	CY-NA81
Li	0.03	0.10	0.44	0.70	0.09	0.04
B	0.37	1.40	0.67	0.57	0.67	0.47
Na	1.89	3.04	17.25	12.11	0.49	1.91
Mg	2856.67	4960	149300	149950	628	3970
Al	0.08	0.90	9.09	8.44	0.34	0.47
Si	52.93	92.10	55.68	43.30	97.15	68.18
P	8.32	14.52	8.67	8.04	10.04	9.72
K	0.81	1.89	1.21	0.59	1.64	0.90
Sc	0.09	0.07	0.03	0.05	0.04	0.18
Ti	0.15	0.32	0.13	0.14	0.24	0.16
V	0.02	0.04	12.35	11.53	1.33	0.19
Cr	0.55	0.77	0.93	0.98	0.99	0.68
Mn	36.13	26.73	4.92	4.73	5.02	105.23
Fe	138.00	58.15	98.13	108.25	50.75	241.25
Co	0.03	0.04	0.04	0.04	0.02	0.06
Ni	0.20	0.22	0.50	0.60	0.21	0.77
Cu	0.06	0.25	0.33	0.23	0.13	0.12
Zn	0.34	1.57	1.53	1.50	0.18	1.72
Ga	0.02	0.03	0.02	0.02	0.02	0.02
As	0.05	0.11	0.10	0.06	0.11	0.07
Rb	0.01	0.01	0.004	0.004	0.01	0.01
Sr	141.67	113.00	68.00	74.10	51.85	164.00
Zr	0.13	0.02	0.01	0.01	0.07	0.10
Nb	0.003	0.01	0.002	0.003	0.01	0.003
Mo	0.03	0.06	0.07	0.02	0.06	0.04
Cd	0.09	0.18	0.10	0.12	0.13	0.20
Sb	0.02	0.03	0.02	0.02	0.02	0.02
Cs	0.002	0.004	0.002	0.002	0.004	0.003
Ba	1.12	1.03	0.16	0.12	0.39	1.24
Hf	0.01	0.02	0.01	0.01	0.02	0.01
W	0.02	0.04	0.03	0.02	0.03	0.02
Pb	0.75	0.30	0.14	0.09	0.17	1.19
Bi	0.005	0.01	0.01	0.003	0.01	0.01
Th	0.001	0.005	0.01	0.01	0.01	0.003
U	0.01	0.004	0.03	0.004	0.01	0.01

Tab. C18: REE +Y content (ppm) of rock samples from Naxos Island.

	CY-NA70	CY-NA 72	CY-NA75	CYNA77	CYNA 78	CY-NA81
La	0.57	0.54	0.05	0.07	0.14	0.36
Ce	0.38	0.32	0.08	0.10	0.16	0.46
Nd	0.53	0.55	0.06	0.07	0.06	0.59
Eu	0.02	0.03	0.004	0.004	0.01	0.04
Gd	0.19	0.15	0.02	0.02	0.03	0.20
Dy	0.20	0.17	0.01	0.02	0.03	0.23
Er	0.14	0.11	0.01	0.02	0.03	0.16
Y	2.04	1.66	0.04	0.08	0.12	2.09

Tab. C19: Trace-element content (ppm) of rock samples from Thasos Island, calcitic TA1-TA8; dolomitic MOUR2 and MOUR5.

	TA1	TA 5	TA6	TA 7	TA8	TA22	MOUR 1	MOUR 5
Li	0.12	0.12	0.22	0.12	0.07	0.05	0.28	0.43
B	1.03	1.33	1.39	1.17	0.72	0.53	0.97	1.53
Na	26.04	3.44	47.03	19.44	13.57	13.42	6.16	16.53
Mg	3820	2856	11600	2580	3758	3622.5	115300	117666.7
Al	0.18	0.29	0.71	0.74	0.27	0.10	5.60	3.20
Si	95.26	99.28	64.30	87.38	78.00	77.73	83.68	80.30
P	11.40	10.53	9.34	14.57	9.36	68.63	9.99	16.67
Cl	141.20	125.40	137.33	129.20	122.00	125.75	103.96	123.00
K	10.15	1.43	7.30	2.28	3.05	1.79	2.33	4.80
Sc	0.15	0.08	0.23	0.15	0.15	0.31	0.14	0.09
Ti	0.18	0.41	0.20	0.26	0.18	0.16	0.47	0.23
V	0.17	0.23	0.39	0.65	0.22	0.15	1.06	0.95
Cr	0.60	0.89	0.71	1.06	0.57	0.79	0.88	0.86
Mn	45.16	45.22	133.67	36.42	20.52	37.55	13.84	17.83
Fe	163.40	57.26	138.67	72.88	138.40	157.50	282.00	207.00
Co	0.06	0.04	0.07	0.06	0.06	0.05	0.23	0.13
Ni	0.32	0.33	0.48	0.34	0.26	0.27	1.27	0.68
Cu	0.44	0.37	0.37	0.90	0.18	0.12	0.45	0.36
Zn	2.67	1.15	2.11	11.01	0.96	4.76	5.62	4.00
Ga	0.02	0.04	0.02	0.04	0.03	0.02	0.03	0.02
As	0.12	0.14	0.23	0.21	0.10	0.07	0.12	0.19
Rb	0.16	0.01	0.02	0.01	0.03	0.01	0.01	0.01
Sr	95.08	158.60	90.63	115.00	100.84	106.00	27.58	26.80
Zr	0.29	0.02	0.01	0.31	0.09	0.42	0.01	0.12
Nb	0.003	0.01	0.003	0.01	0.004	0.004	0.01	0.01
Mo	0.04	0.09	0.04	0.06	0.05	0.03	0.06	0.08
Cd	0.48	0.63	0.48	1.53	0.34	0.39	0.16	0.24
Sn	0.04	0.03	0.02	0.03	0.02	0.02	0.02	0.02
Sb	0.02	0.03	0.02	0.03	0.02	0.02	0.02	0.03
Cs	0.003	0.005	0.01	0.005	0.01	0.003	0.004	0.01
Ba	0.66	0.77	0.65	0.78	0.77	0.96	0.10	0.55
Hf	0.01	0.02	0.01	0.02	0.01	0.01	0.02	0.02
W	0.02	0.04	0.02	0.04	0.03	0.02	0.03	0.09
Pb	5.62	0.39	1.06	0.63	0.36	3.40	0.56	0.38
Bi	0.01	0.02	0.01	0.04	0.01	0.01	0.01	0.03
Th	0.03	0.02	0.02	0.05	0.01	0.004	0.01	0.02
U	0.01	0.005	0.01	0.02	0.01	0.01	0.004	0.004

Tab. C20: REE +Y content (ppm) of rock samples from Thasos Island, calcitic marble TA1-TA8; dolomitic marble MOUR2 and MOUR5.

	TA1	TA 5	TA6	TA 7	TA8	TA22	MOUR 1	MOUR 5
La	0.97	0.96	1.48	0.91	0.83	1.49	0.27	0.24
Ce	0.27	0.27	0.34	0.36	0.21	0.48	0.54	0.45
Pr	0.16	0.15	0.24	0.15	0.14	0.30	0.05	0.04
Nd	0.89	0.81	1.17	0.78	0.85	1.88	0.26	0.24
Eu	0.04	0.04	0.06	0.04	0.04	0.09	0.01	0.01
Gd	0.24	0.26	0.37	0.21	0.21	0.53	0.06	0.05
Dy	0.21	0.27	0.38	0.22	0.19	0.47	0.05	0.04
Ho	0.04	0.06	0.08	0.05	0.04	0.08	0.01	0.01
Er	0.13	0.21	0.30	0.16	0.14	0.32	0.04	0.03
Y	1.76	3.36	3.69	2.77	2.11	4.05	0.30	0.24

Tab. C21: Trace-element content (ppm) of rock samples from Thiountas.

	T 3	T 6	T8	T10	T17	T20
Li	0.28	0.16	0.08	0.05	0.05	0.06
B	1.12	1.17	0.56	0.37	0.61	0.27
Na	105.87	59.42	24.03	4.33	21.83	11.20
Mg	2978	4208	3935	3447.5	3886.7	5505
Al	0.62	1.51	1.07	1.12	1.05	1.02
Si	109.50	99.26	63.93	57.95	47.10	57.15
P	9.11	11.11	7.50	8.04	9.42	7.96
K	13.47	3.38	3.21	0.84	2.03	1.20
Sc	0.03	0.04	0.04	0.04	0.04	0.04
Ti	0.23	0.27	0.23	0.17	0.20	0.19
V	0.74	0.77	0.75	0.45	0.30	0.68
Cr	1.88	2.20	2.50	1.66	1.77	1.55
Mn	23.85	8.63	6.74	4.30	2.35	2.24
Fe	174.26	76.92	156.00	143.25	126.67	144.00
Co	0.03	0.02	0.04	0.05	0.06	0.06
Ni	0.23	0.22	0.27	0.26	0.28	0.28
Cu	0.45	0.52	0.13	0.07	0.07	0.06
Zn	1.42	0.30	0.61	0.17	0.27	0.27
Ga	0.02	0.03	0.02	0.02	0.02	0.01
As	0.63	0.27	0.29	0.07	0.08	0.06
Rb	0.05	0.02	0.01	0.005	0.01	0.005
Sr	271.00	205.60	167.25	157.00	137.33	155.00
Zr	0.02	0.02	0.26	0.01	0.01	0.003
Nb	0.01	0.01	0.003	0.004	0.003	0.003
Mo	0.06	0.07	0.04	0.04	0.02	0.02
Cd	0.15	0.17	0.09	0.12	0.07	0.09
Sb	0.06	0.02	0.03	0.02	0.02	0.01
Cs	0.01	0.01	0.002	0.003	0.003	0.002
Ba	3.78	0.80	0.85	0.72	1.14	1.12
Hf	0.02	0.02	0.01	0.01	0.01	0.01
W	0.04	0.03	0.03	0.02	0.02	0.01
Pb	4.59	0.78	1.11	0.61	0.81	0.51
Bi	0.02	0.02	0.01	0.01	0.01	0.003
Th	0.01	0.02	0.02	0.02	0.01	0.01
U	0.01	0.01	0.10	0.29	0.03	0.01

Tab. C22: REE +Y content (ppm) of rock samples from Thiountas.

	T 3	T 6	T8	T10	T17	T20
La	0.01	0.04	0.04	0.02	0.02	0.03
Ce	0.03	0.05	0.05	0.02	0.04	0.07
Pr	0.005	0.01	0.01	0.00	0.01	0.01
Nd	0.03	0.03	0.03	0.02	0.03	0.04
Eu	0.01	0.01	0.005	0.004	0.01	0.004
Gd	0.04	0.04	0.03	0.02	0.02	0.02
Dy	0.02	0.02	0.01	0.01	0.01	0.01
Ho	0.01	0.01	0.002	0.002	0.003	0.002
Er	0.03	0.02	0.02	0.01	0.02	0.01
Y	0.03	0.03	0.03	0.02	0.03	0.03

Tab. C23: Trace-element content (ppm) of rock samples from Proconnesos Island, Altintas, Filiz, and Harmatas districts.

	PRO14	PRO15	PRO 17	PR018	PRO25	PRO19	PRO22	OC 13_2	OC13/4	OC13/6	OC13/8	OC140	OC994/3	OBG1
Li	0.08	0.06	0.10	0.07	0.08	0.09	0.07	0.07	0.26	0.08	0.05	0.28	0.59	3.38
B	0.75	0.46	0.85	0.74	0.93	0.63	0.37	0.81	0.38	0.76	0.69	1.33	1.49	1.70
Na	11.86	7.25	6.18	7.88	16.13	9.25	4.72	6.39	14.00	14.50	9.44	42.05	23.60	18.90
Mg	3832.00	2857.50	2960	4950	2795	5440	2745	2640	12090	12466.7	3802	27076.7	23416.7	3142
Al	3.04	0.19	1.45	0.28	1.33	0.90	0.45	0.38	119.17	0.57	0.43	1.19	226.62	641.52
Si	61.20	55.08	93.04	77.80	59.78	61.85	56.35	65.18	267.37	52.33	51.30	57.55	273.40	1420.64
P	8.83	7.90	10.87	9.00	8.50	8.99	8.36	11.05	9.02	8.29	7.58	8.85	11.77	8.43
Cl	130.40	126.00	100.98	135.67	119.25	127.25	119.00	94.94	126.00	124.00	112.40	158.17	136.33	133.20
K	1.32	0.91	1.73	0.71	6.02	1.71	1.65	2.40	161.39	1.32	1.48	2.39	135.28	19.81
Sc	0.06	0.04	0.04	0.05	0.06	0.07	0.04	0.03	0.35	0.05	0.04	0.17	0.12	0.08
Ti	0.28	0.21	0.27	0.23	0.22	0.20	0.26	0.21	1.76	0.27	0.17	0.22	1.14	0.24
V	0.17	0.77	0.19	0.09	0.32	0.33	0.32	0.19	0.74	0.34	0.25	0.33	0.69	0.39
Cr	1.90	2.27	1.64	1.81	1.32	1.25	3.12	3.41	2.65	1.78	1.93	1.10	1.94	0.83
Mn	0.74	0.62	0.98	0.83	0.97	1.30	0.68	0.82	5.70	2.82	1.13	6.84	3.40	6.11
Fe	102	98.6	40.8	115	134.25	117.25	233.15	62.9	349.3	113.3	103.1	139.3	140	124.2
Co	0.05	0.05	0.03	0.05	0.07	0.05	0.06	0.03	0.05	0.03	0.04	0.06	0.04	0.05
Ni	0.22	0.31	0.26	0.24	0.62	0.23	0.99	0.28	0.40	0.21	0.25	0.42	0.44	0.28
Cu	0.14	0.25	0.23	0.07	0.14	0.09	0.08	0.10	0.20	0.13	0.05	0.38	0.18	0.13
Zn	0.42	0.14	0.38	0.22	1.20	0.57	0.19	1.00	3.60	0.41	0.50	2.24	2.20	1.19
Ga	0.03	0.02	0.02	0.02	0.02	0.02	0.02	0.02	0.06	0.02	0.01	0.03	0.08	0.36
As	0.13	0.08	0.10	0.09	0.08	0.10	0.06	0.11	0.10	0.09	0.06	0.45	0.08	0.11
Rb	0.01	0.01	0.01	0.005	0.02	0.04	0.01	0.01	0.49	0.01	0.01	0.01	0.33	0.04
Sr	251.20	122.25	132.80	182.33	165.00	149.75	167.50	150.40	322.67	279.00	196.60	124.17	193.67	115.20
Zr	0.01	0.003	0.02	0.01	0.004	0.01	0.07	0.21	0.02	0.03	0.01	0.01	0.01	0.02
Nb	0.005	0.003	0.01	0.004	0.002	0.003	0.003	0.01	0.003	0.003	0.003	0.004	0.003	0.003
Mo	0.03	0.03	0.05	0.04	0.03	0.04	0.04	0.05	0.03	0.04	0.03	0.04	0.03	0.03
Cd	0.15	0.12	0.20	0.11	0.14	0.17	0.12	0.29	0.28	0.12	0.10	0.15	0.15	0.17
Sn	0.04	0.03	0.02	0.01	0.02	0.03	0.02	0.02	0.03	0.02	0.01	0.02	0.02	0.02
Sb	0.02	0.02	0.03	0.03	0.01	0.03	0.02	0.02	0.02	0.02	0.01	0.10	0.02	0.02
Cs	0.004	0.003	0.004	0.004	0.004	0.01	0.002	0.003	0.04	0.003	0.003	0.01	0.004	0.005
Ba	0.67	0.53	0.76	0.71	0.75	0.78	0.67	0.56	1.13	0.85	0.58	0.83	1.35	0.81
Hf	0.02	0.01	0.02	0.01	0.01	0.01	0.01	0.01	0.01	0.01	0.01	0.01	0.01	0.01
W	0.02	0.02	0.03	0.04	0.02	0.02	0.01	0.03	0.02	0.02	0.01	0.10	0.02	0.02
Pb	0.13	0.10	0.06	0.24	0.12	0.12	0.09	0.25	0.39	0.13	0.10	0.60	0.25	0.27
Bi	0.03	0.02	0.01	0.01	0.01	0.01	0.01	0.01	0.01	0.01	0.00	0.01	0.01	0.00
Th	0.01	0.001	0.004	0.003	0.004	0.004	0.002	0.004	0.02	0.01	0.01	0.01	0.02	0.02
U	0.01	0.003	0.02	0.01	0.02	0.01	0.004	0.13	0.05	0.02	0.005	0.005	0.003	0.01

Tab. C24: REE +Y content (ppm) of rock samples from Proconnesos Island, Altintas, Filiz and Harmatas districts.

	PRO14	PRO15	PRO 17	PR018	PRO25	PRO19	PRO22	OC 13_2	OC13/4	OC13/6	OC13/8	OC140	OC994/3	OBG1
La	0.09	0.01	0.02	0.02	0.04	0.08	0.02	0.02	0.72	0.04	0.05	1.18	0.19	0.61
Ce	0.14	0.01	0.03	0.04	0.05	0.15	0.03	0.02	1.48	0.09	0.09	0.57	0.37	0.33
Pr	0.02	0.003	0.01	0.01	0.01	0.02	0.01	0.003	0.15	0.01	0.01	0.21	0.04	0.08
Nd	0.09	0.01	0.03	0.03	0.04	0.12	0.03	0.02	0.79	0.06	0.06	1.20	0.18	0.48
Eu	0.01	0.01	0.01	0.004	0.005	0.01	0.01	0.01	0.03	0.01	0.01	0.05	0.01	0.02
Gd	0.03	0.02	0.04	0.02	0.02	0.03	0.02	0.03	0.15	0.02	0.02	0.31	0.05	0.12
Dy	0.02	0.01	0.02	0.01	0.01	0.02	0.01	0.02	0.13	0.01	0.02	0.32	0.04	0.13
Ho	0.01	0.002	0.005	0.003	0.003	0.004	0.004	0.003	0.02	0.002	0.002	0.05	0.01	0.02
Er	0.02	0.01	0.02	0.02	0.02	0.01	0.01	0.02	0.05	0.02	0.01	0.23	0.02	0.08
Y	0.14	0.02	0.04	0.02	0.08	0.08	0.04	0.06	0.54	0.03	0.07	3.10	0.19	1.40

Acknowledgments

I would like to express my special appreciation and thanks to my advisor Dr. Caterina De Vito, you have been a tremendous mentor for me. I would like to thank you for encouraging my research and for allowing me to grow as a research scientist. I would also like to thank for your invaluable help, for teaching me to create a mental order that allowed me to never lose the final goal and your sixth sense that allowed me to overcome obstacles that often seemed insurmountable.

Besides my advisor, I would like to thank the rest of my thesis committee, for their insightful comments and encouragement, but also for the hard question, which incented me to widen my research from various perspectives.

Thank you Dr. Aida Maria Conte (Istituto di Geoscienze e Georisorse - CNR, U.O.S. of Rome, Italy), who with your suggestions and your teachings you gave me the opportunity to learn more about the rocks and their mechanisms and their nature so complex. Your perspectives on focus of study not only provided me with a number of challenging opportunities, but also encouraged me to produce a stronger and more coherent research endeavor.

Thanks Professor Alessandro Borghi (Department of Earth Sciences, University of Turin, Italy) for conveying to me the passion for petrography and more than ten years helps me to carry on my path. Your teachings are precious and essential.

Thanks Dr. Mauro Brilli (Istituto di Geologia Ambientale e Geoingegneria –CNR, Rome), your foresight on a topic so interesting and debated has meant that this project took off. Thank you for

providing me with the necessary material to carry out the research project and for conveying to me your knowledge.

My sincere thanks also goes to Professor Detlef Günther of Department of Chemistry and Applied Biosciences Laboratory of Inorganic Chemistry of ETH (Zurich), Dr. Alberto Zanetti of CNR-Istituto di Geoscienze e Georisorse, U.O.S. of Pavia, who provided me an opportunity to join their team, and who gave access to the laboratory and research facilities. Without they precious support it would not be possible to conduct this research.

I owe a lot Professor Gianni Andreozzi for his constant advice through the years of my PhD.

Thanks to the Department of Earth Sciences of the La Sapienza, University of Rome and the Department of Earth Sciences of the University of Turin. The collaboration between these departments has allowed that I was surrounded (squared) of a formidable group of people, very active in research. Thanks to Alessandra Marengo and Erica Bittarello for their expertise and for their advice.

A particular thank to my reviewers Dr. Robert F. Martin and Dr. Pilar Lapuente.

A special thanks to my family. Words cannot express how grateful I am to my mother, my father and my brother for all of the sacrifices that you've made on my behalf. I would also like to thank all of my friends who supported me in writing, and incented me to strive towards my goal. At the end I would like express appreciation to my best friends, in particular Laura and Simone who shared with me joy and grief of this pathway and they were always my support in the moments when there was no one to answer my queries.

Finally, I must express my gratitude to those who at the end of the day, and not only, allowed me to unload the tensions even after days where everything seemed still and inconclusive. “*Mens sana in corpore sano*” thanks to my coach Randolf and to my training partners Burby, Giova, Amalia, Dany&Danush, Podda.